



Universiteit
Leiden
The Netherlands

Chromatin modifiers in DNA repair and human disease

Helfricht, A.

Citation

Helfricht, A. (2016, November 1). *Chromatin modifiers in DNA repair and human disease*. Retrieved from <https://hdl.handle.net/1887/43800>

Version: Not Applicable (or Unknown)

License: [Licence agreement concerning inclusion of doctoral thesis in the Institutional Repository of the University of Leiden](#)

Downloaded from: <https://hdl.handle.net/1887/43800>

Note: To cite this publication please use the final published version (if applicable).

Cover Page



Universiteit Leiden



The handle <http://hdl.handle.net/1887/43800> holds various files of this Leiden University dissertation.

Author: Helfricht, A.

Title: Chromatin modifiers in DNA repair and human disease

Issue Date: 2016-11-01

Chromatin modifiers in DNA repair and human disease

Angela Helfricht



Cover design & layout: Angela Helfricht

Printing: Off Page, Amsterdam, the Netherlands
www.offpage.nl

ISBN: 978-94-6182-719-7

© Copyright 2016 by Angela Helfricht

All rights reserved. No parts of this thesis may be reprinted, reproduced or utilised in any form or by electronic, mechanical, or other means, now known or hereafter devised, including photocopying and recording in any information storage or retrieval system without the expressed, written consent of the author.

Chromatin modifiers in DNA repair and human disease

Proefschrift

ter verkrijging van de graad van Doctor aan de Universiteit Leiden,
op gezag van Rector Magnificus Prof.mr. C.J.J.M. Stolker,
volgens besluit van het College voor Promoties
te verdedigen op dinsdag 1 november 2016
klokke 13:45 uur

door

Angela Helfricht

geboren te Dresden, Duitsland
in 1984

Promotor: Prof.dr.ir. S. M. van der Maarel

Co-promotoren: Dr. H. van Attikum

Dr. A.C.O. Vertegaal

Leden promotiecommissie: Prof.dr. M. Tijsterman

Prof.dr. R. Kanaar (Erasmus MC)

Dr. M. v. d. Burg (Erasmus MC)

Willst du dich am Ganzen erquicken,
so musst du das Ganze im Kleinsten erblicken.

Johan Wolfgang von Goethe (1827)

TABLE OF CONTENTS

CHAPTER 1

General introduction	10
Aim of this study	37

CHAPTER 2

Identification of EHMT1 as a chromatin factor that negatively regulates 53BP1 accrual during the DNA double-strand break response	52
---	----

CHAPTER 3

Remodeling and spacing factor 1 (RSF1) deposits centromere proteins at DNA double-strand breaks to promote non-homologous end-joining	80
---	----

CHAPTER 4

Investigating DNA damage-induced RSF1 SUMOylation	108
---	-----

CHAPTER 5

Loss of ZBTB24, a novel non-homologous end-joining protein, impairs class-switch recombination in ICF syndrome	126
--	-----

CHAPTER 6

Perspectives	168
--------------	-----

CHAPTER 7

Appendix: English summary	182
Nederlandse samenvatting	184
Deutsche Zusammenfassung	186
Curriculum vitae	188
List of publications	189
Acknowledgements	190



GENERAL INTRODUCTION

1

GENERAL INTRODUCTION

DNA is the macromolecule that encodes the genetic information of life. It defines the structure, organization and function of each cell and therefore it is crucial to preserve the integrity of the DNA during lifespan. However, the DNA is constantly exposed to various genotoxic threats that lead to around 1.000 to 1.000.000 lesions per cell each day (Lindahl, 1993). If these lesions are repaired incorrectly or left unrepaired, genetic alterations (mutations) occur that can lead to cell death and/or genome instability, and consequently to human diseases such as neurodegeneration and cancer.

DNA organization

In eukaryotes chromosomal DNA is organized into a highly condensed structure called chromatin. The basic unit of chromatin is the nucleosome, which is composed of ~147 base pairs of DNA that is wrapped around histone octamers in two left-handed superhelical turns. Each histone octamer contains two copies of each of the four conserved core histones H2A, H2B, H3 and H4. However, several histone variants can be incorporated that can affect nucleosome or higher-order chromatin structure. In addition, the binding of non-histone proteins can add to the degree of chromatin compaction. Very condensed chromatin is called heterochromatin, whereas very open and transcriptionally active DNA structures are referred to as euchromatin.

DNA damage response

The packaging of DNA into chromatin does not protect DNA from the constant attacks by various exogenous and endogenous DNA damage-inducing agents causing a large variety of structural different DNA lesions. Fortunately, cells have evolved sophisticated mechanisms that can sense DNA damage. Subsequently, a multi-step signaling cascade is triggered to transduce the DNA damage signal and to promote the recruitment and/or activation of effector proteins that can mediate DNA damage repair, change the chromatin composition, adjust the transcriptional program and pause cell cycle progression if necessary. However, if the occurred DNA damage is beyond repair, a cell can also enter programmed cell death called apoptosis. These events are collectively referred to as the DNA damage response (DDR) and take place simultaneously with the ultimate goal to maintain DNA integrity. Thus, although discussed separately below, the signaling and repair of DNA damage operate in chorus and several proteins actually function within both parts of the DDR.

Since the DDR maintains the stability of the genome in cells, it is extremely important for human health. It is therefore not surprising that inactivating mutations in DDR genes cause rare hereditary genetic disorders like Xeroderma Pigmentosum and Ataxia Telangiectasia (De Boer and Hoeijmakers, 2000; McKinnon, 2012). Patients that suffer from such disorders are often not able to effectively respond to DNA damage, and hence display a highly increased risk to develop DNA damage related disease such as cancer. AT patients additionally present with defective brain development and a weakened immune system.

DNA damage response upon DNA double-strand breaks

One of the most toxic forms of DNA damage is the DNA double-strand break (DSB), which is due to the menacing information loss on both DNA strands when a DSB occurs. Replication fork stalling or collapse as well as the covalent attachment of a protein such as SPO11 during meiosis can lead to DSB induction. Additionally, the exposure to ionizing radiation (IR), the

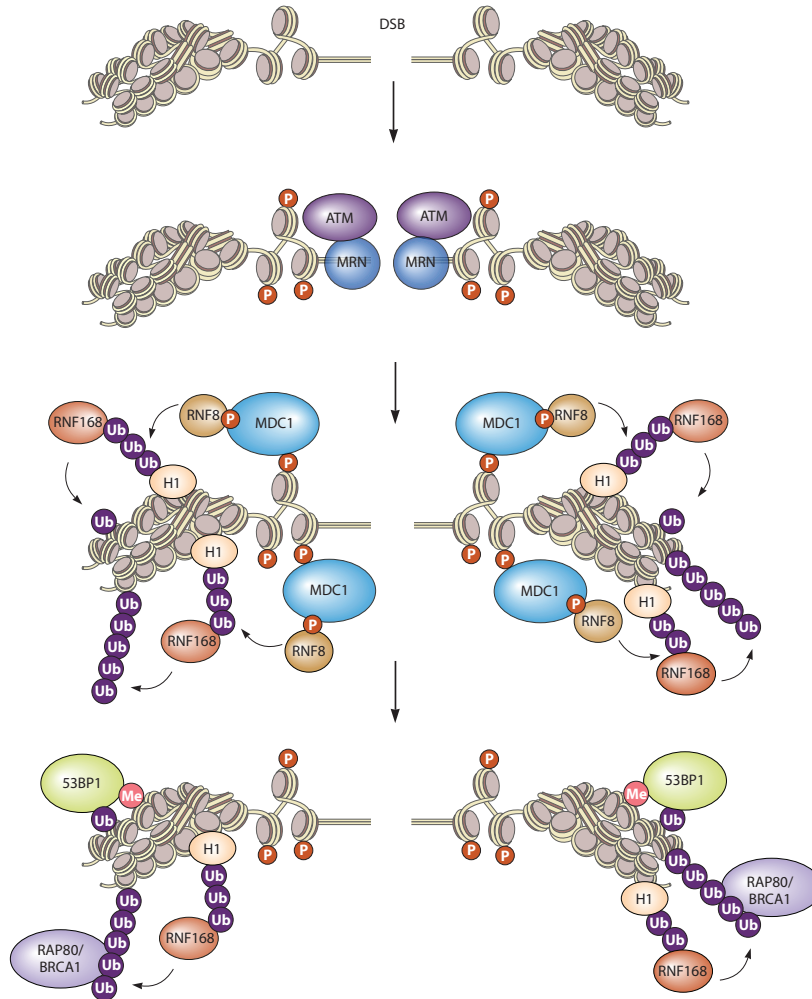


Figure 1. Overview of the signaling response to DSBs. DSBs are sensed by the MRN complex that directly recruits the ATM kinase to the lesion. The subsequent ATM-dependent phosphorylation of histone H2AX (called γ H2AX) in DSB flanking chromatin facilitates the binding of MDC1 nearby the site of DNA damage. MDC1 functions as a binding platform for the RNF8 E3 ubiquitin ligase. RNF8 initiates an ubiquitin-dependent cascade by ubiquitylating histone H1. The formed poly-ubiquitin chains are subsequently bound by the E3 ubiquitin ligase RNF168, which targets H2A(X). These events eventually culminate in monoubiquitin-dependent accrual of 53BP1, that is simultaneously reliant on the availability of methylated histone H4 (H4K20me is a pre-existing methylation mark and thus not DNA-damage induced, however it is not shown in all panels for clarity reasons.), and agglomeration of poly-ubiquitylated H2A(X), that for instance attracts the RAP80-BRCA1 complex.

treatment with chemicals such as camptothecin or the occurrence of several DNA lesions within a relatively small region can also result in DSB formation. When a DSB is inflicted, a fine-tuned DDR is triggered that coordinates cell cycle progression and DNA repair (Ciccia and Elledge, 2010; Jackson and Bartek, 2009; Smeenk and van Attikum, 2013). A key feature of the DDR is the assembly of signaling and repair factors in the vicinity of DSBs (Bekker-Jensen and Mailand, 2010; Huen and Chen, 2010). Initially, DSBs are sensed by the Mre11-Rad50-Nbs1 (MRN) complex (Petrini and Stracker, 2003), which directly attracts the PIKK

kinase ATM at the lesion and assists in phosphorylation dependent ATM activation (p-ATM); subsequently, p-ATM phosphorylates all three members of the MRN complex to initiate downstream signaling. Phosphorylation of histone H2AX (called γ H2AX) by ATM in DSB flanking chromatin culminates in the binding of MDC1 nearby the site of DNA damage. The subsequent binding of the RNF8 E3 ubiquitin ligase to MDC1 in turn triggers a ubiquitin-dependent cascade, involving the recruitment of the E3 ligase RNF168 to poly-ubiquitylated histone H1, the subsequent ubiquitylation of histone H2A/H2AX by RNF168, as well as the ubiquitin-dependent accrual of 53BP1 and the RAP80-BRCA1 complex (Fig. 1) (Doil et al., 2009; Lok et al., 2012; Stewart et al., 2009; Thorslund et al., 2015; Wang and Elledge, 2007).

Double-strand break repair - Homologous recombination

Two major pathways facilitate the repair of DSBs namely homologous recombination (HR) and non-homologous end-joining (NHEJ). HR mediates the error-free repair of DNA breaks during the S or G2 phase of the cell cycle by using the sequence information from an undamaged, homologous template, usually the sister chromatid (San Filippo et al., 2008). In more detail, MRN facilitates short-range degradation of the broken DNA ends together with CtIP to create 3' single stranded DNA (ssDNA) overhangs. This is followed by long range end-resection mediated by either EXO1 alone or the concerted action of the nuclease DNA2 with the BLM helicase (Liu et al., 2014). The ssDNA overhangs are bound and stabilized by RPA to prevent degradation and the formation of secondary structure. Simultaneously, the Partner and localizer of BRCA2 (PALB2) is recruited in a BRCA1-dependent manner and the retention of PALB2 at chromatin is mediated by its Chromatin Association Motif (ChAM) (Bleuyard et al., 2012; Zhang et al., 2009b; Zhang et al., 2009a). PALB2 also comprises a WD40 domain that facilitates its interaction with BRCA2, an event that is crucial for BRCA2 recruitment to DSBs (Sy et al., 2009; Xia et al., 2006). Subsequently, BRCA2 promotes RPA displacement and loading of the RAD51 recombinase, forming an ssDNA-containing nucleoprotein filament. Once bound to ssDNA, RAD51 can search for and invade a homologous duplex DNA template. Subsequently, restoration of the original DNA sequence is achieved by DNA synthesis and ligation (Fig. 2) (Liu et al., 2014).

Double-strand break repair - Non-homologous end-joining

Classical NHEJ (c-NHEJ) is the dominant pathway for DSB repair in mammalian cells. It re-joins the broken DNA ends and is active throughout the whole cell cycle. However, c-NHEJ has no inherent mechanism to ensure the restoration of the original DNA sequence in the vicinity of DSBs and can therefore be either error-free or error-prone. During c-NHEJ repair, the DNA ends are bound and held in close proximity by a single molecule of the heterodimer Ku70/Ku80, which attracts the DNA-dependent kinase DNA-PKcs to form the DNA-PK complex. DNA-PKcs mainly undergoes autophosphorylation, but also displays activity towards other NHEJ factors. A subset of DSBs requires DNA end-processing before re-joining can occur. In that case, the endonuclease Artemis can resect the broken DNA ends upon interaction with DNA-PKcs. On the contrary, the DNA polymerases μ and λ can add nucleotides to fill in remaining gaps. These events are subsequently followed by DNA ligation, a process that is facilitated by the DNA ligase IV, XRCC4 and XLF/Cernunnos complex (Fig. 3) (Kakarougkas and Jeggo, 2014; Lieber, 2010; Liu et al., 2014).

Noteworthy, a second NHEJ repair pathway has been discerned and is referred to as alternative NHEJ (alt-NHEJ). While c-NHEJ, as described above, is the only DSB repair pathway that can operate during all phases of the cell cycle, alt-NHEJ mainly operates during

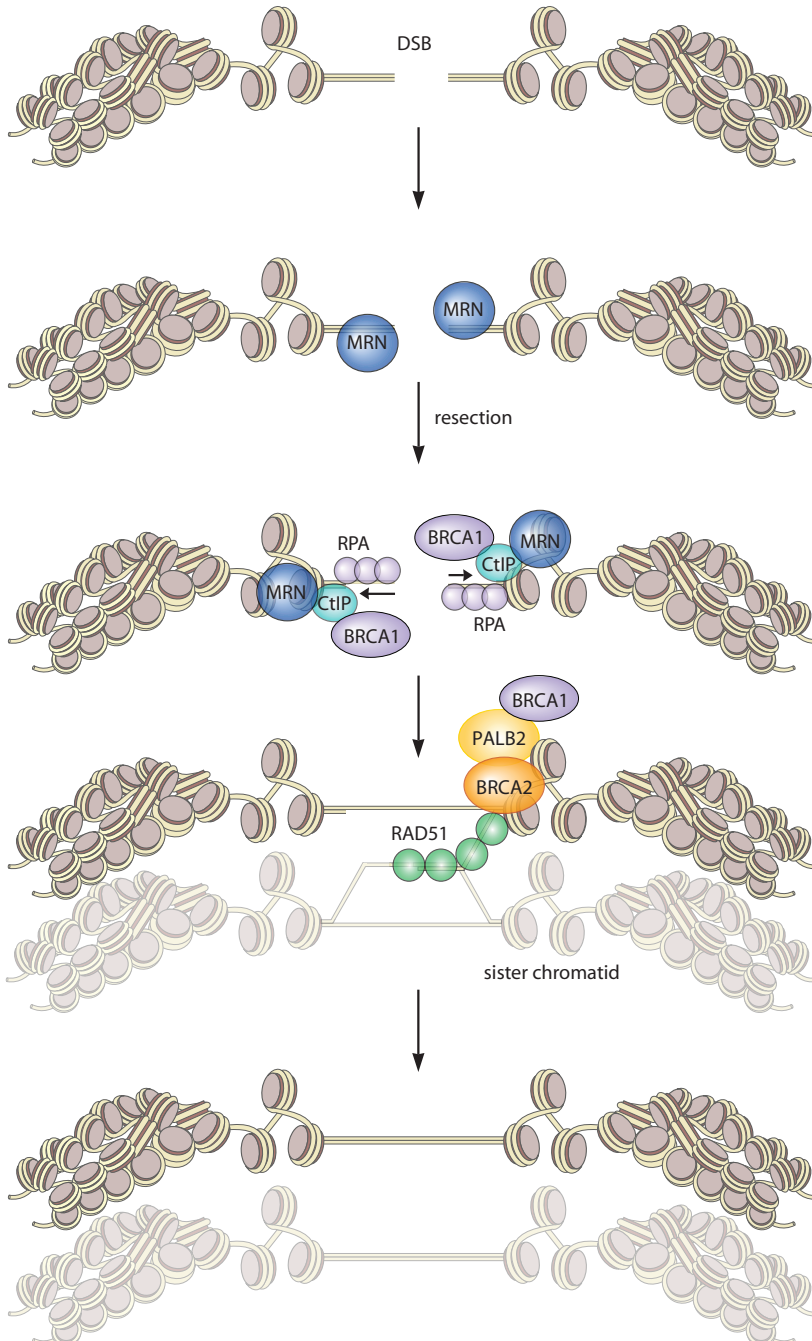


Figure 2. Overview of DSB repair by the homologous recombination (HR) pathway. 5'–3' DNA end resection is initiated by the MRN complex together with CtIP and the 3' ssDNA is coated by RPA. BRCA1 and CtIP physically interact at DSBs, while BRCA1 also recruits and binds PALB2, which in turn facilitates the accrual of BRCA2. Eventually, RPA is exchanged for RAD51 by BRCA2. The RAD51 filaments mediate the search for a homologous sequence and invasion of the homologous strand. Upon DNA synthesis, the formed DNA structures are resolved and the DNA strand is restored in an error-free fashion.

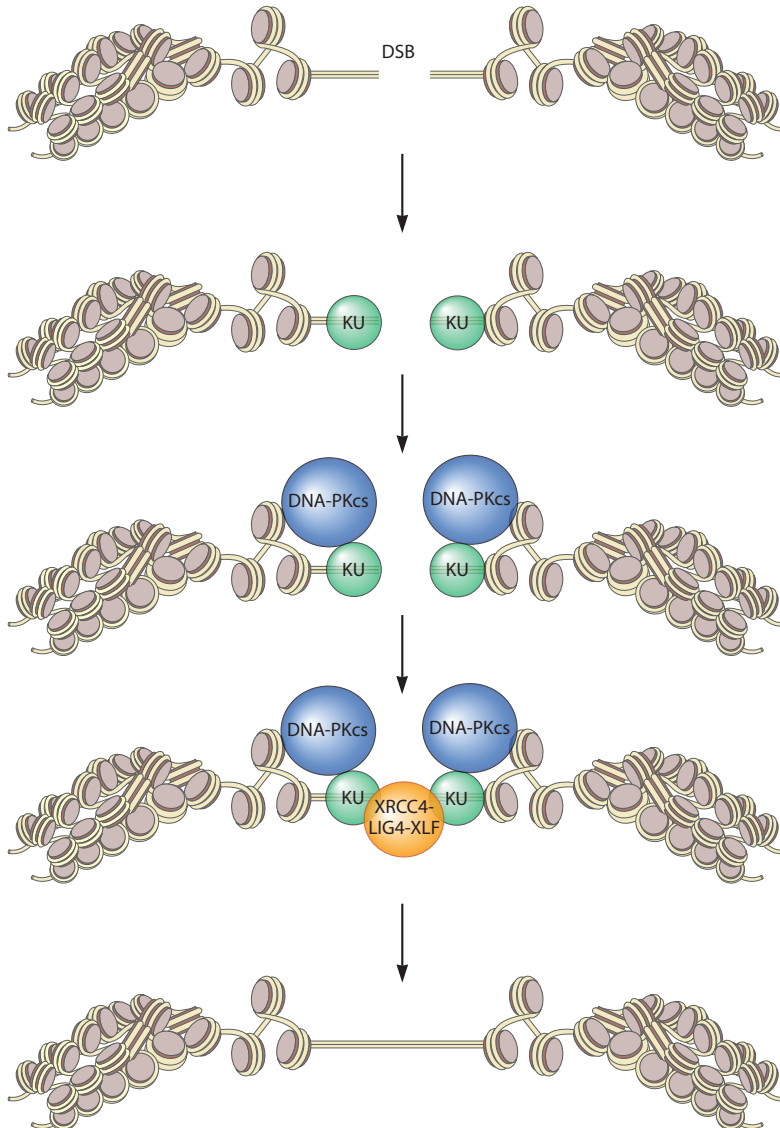


Figure 3. Overview of the Non-homologous end-joining (NHEJ) pathway. The Ku70/80 dimer binds DNA ends and recruits DNA-PKcs that undergoes activation. End-processing enzymes are attracted, which modify the DNA ends. The accumulation of the XRCC4-LIG4-XLF complex results in the ligation of the broken DNA ends.

S-phase and only if classical NHEJ is not functional i.e. when proteins like Ku70/80, DNA-PKcs or XRCC4/LigaseIV are unavailable or inactive (Lieber, 2010). This alternate pathway is initiated through the binding of PARP1 to the DSB, which can be in competition with Ku-binding (Wang et al., 2006). Next, the end-processing enzymes MRN, CtIP and BRCA1 assemble to facilitate DSB end resection. Alt-NHEJ occurs if micro-homologies of 5-25 bp are exposed upon end resection that enable the DNA single strands to anneal. Due to the use of micro-homology to stabilize the DSB ends, alt-NHEJ is also frequently referred to as micro-homology mediated end-joining (MMEJ) (Liu et al., 2014). Finally, the ligation of the broken ends involves either the LigaseIII/XRCC1 complex or DNA LigaseI in mammalian cells (Fig. 4).

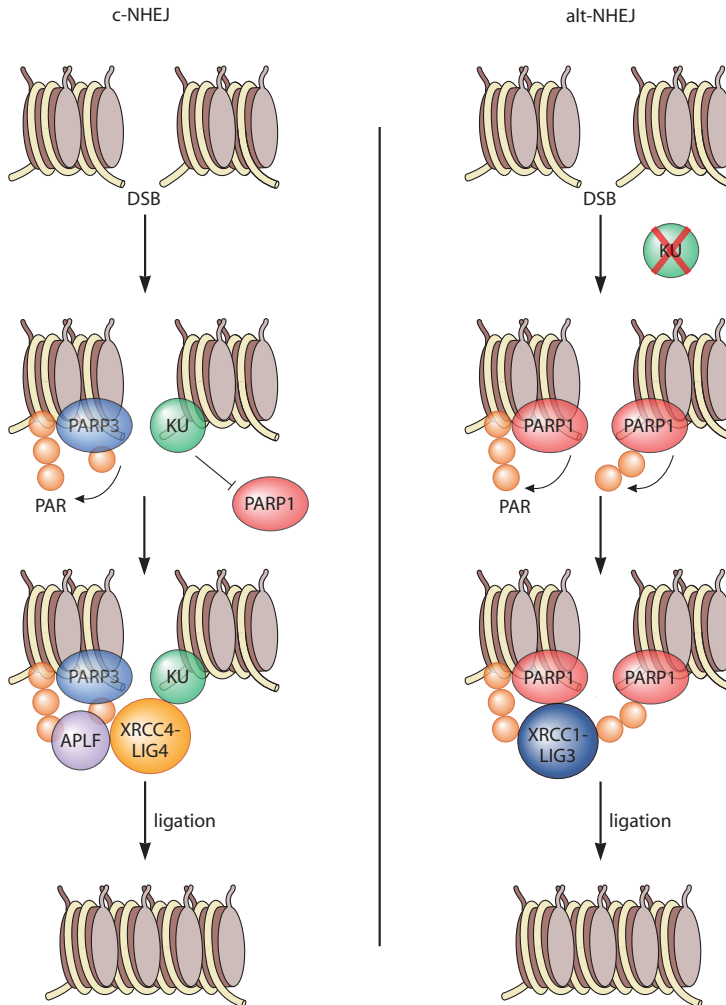


Figure 4. Classical versus alternative NHEJ and the role of PARP1. DSBs are mainly repaired through rapid classical NHEJ. However, in the absence of Ku, PARP1 binds efficiently to DSBs, which leads to its activation, resulting in auto-poly(ADP-ribosyl)ation. The synthesis of poly(ADP-ribosyl) (PAR) chains initiates the recruitment of the XRCC1-LIG3 complex leading to a slow sealing of the DSB in an XRCC4-LIG4 independent manner.

Since deletions regularly occur upon DSB end processing during alt-NHEJ, this pathway is considered to be an error-prone pathway.

NHEJ also has an essential role during the somatic gene rearrangement process V(D)J recombination and throughout the process of immunoglobulin (Ig) gene-diversification called class-switch recombination (CSR). These processes take place at the immunoglobulin heavy chain (IgH) locus that comprises the variable (V), diversity (D) and joining (J) gene segment and the constant region (C) (Fig. 5). During V(D)J recombination the RAG1/2 complex deliberately generates sequence-specific DSBs. One segment of each V, D and J region is subsequently joined through c-NHEJ and together these regions encode for the variable domain of the Ig that defines the antigen specificity (Fig. 5). In maturing B and T lymphocytes, V(D)J occurs in a multistep rearrangement process at the Ig or T cell receptor locus respectively, leading to the generation of a diverse repertoire of Igs and T cell receptors.

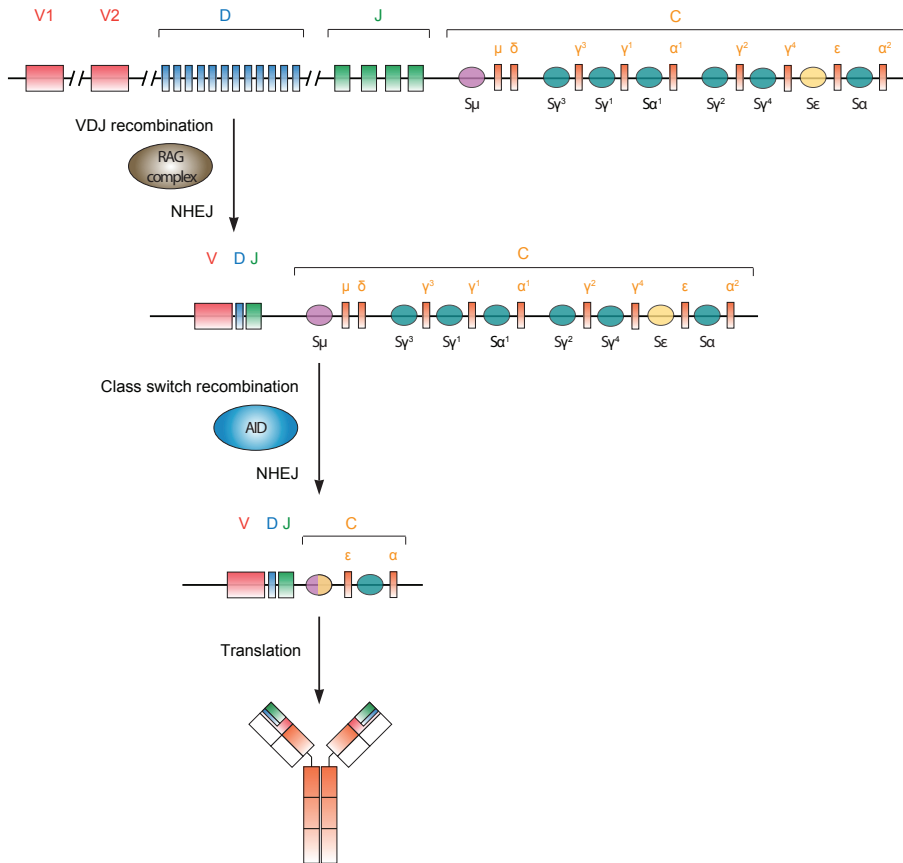


Figure 5. Variable (V), diversity (D) and joining (J) recombination and class switch recombination (CSR) of the IgH locus. Rearrangements of the IgH locus depend on the deliberate induction of either sequence-specific DSBs by the RAG complex during V(D)J recombination or on the induction of base mismatches by the deaminase AID that eventually lead to DSB formation throughout CSR. The formed DSBs are re-joined through classical NHEJ, a possibly error-prone process that can allow functional rearrangements to occur. The switch from IgM to IgE is depicted. Once the final transcript is generated, RNA is produced from the newly arranged IgH locus and translated into a specific immunoglobulin. These processes contribute to the variety of immunoglobulin species within the immune system. Figure adapted from (Mani and Chinnaiyan, 2010).

CSR on the other hand changes the production of Igs in B cells from one type to another when facilitating the exchange of the constant region of the IgH gene locus by a set of constant-region genes located further downstream within the same locus. Here the deaminase AID converts cytidines (C) preceded by W(A/T)R(A/G) dinucleotides to an uracil (U) within the switch regions (S μ - α) located upstream of the different constant region genes (C μ - α) (Fig. 5). This leads to the generation of mismatches, which can subsequently transform into single strand breaks (SSBs) when excision repair pathways attempt to repair these lesions. Due to the high density of AID motifs within the switch regions and the induction of numerous SSBs, DSBs ultimately arise during CSR. Upon DSB repair via c-NHEJ, different constant regions can be ligated together and subsequent transcription will determine the B-cell immunoglobulin isotype to which the cell will switch (Chaudhuri and Alt, 2004). The effector function of the Ig is changed during such a CSR event, but the V(D)J-mediated antigen specificity of the Ig remains unaltered.

Double-strand break repair pathway choice

How DSB pathway choice is determined during the cell cycle has been subject of numerous investigations. A combination of factors seems responsible, such as the availability of DNA repair proteins, cell cycle stage, chromatin environment and DNA damage complexity. Ku70-Ku80 has high affinity for DSB ends and thus accumulates within seconds encircling the DNA at both DSB ends in a sequence-independent manner. Ku thereby forms the scaffold for downstream c-NHEJ repair factors and mediates the fast repair of DSBs through c-NHEJ, while inhibiting other DSB pathways (Wang et al., 2006). This makes c-NHEJ the first choice DSB repair pathway. However, if re-joining of a DSB is delayed due to the absence of crucial c-NHEJ factors or because the DSB ends require major DNA end processing, either alt-NHEJ or HR can take over.

53BP1 is an important regulator of DSB repair pathway choice, which promotes NHEJ. Upon DSB induction, 53BP1 binds to nucleosomes that are both di-methylated at H4K20 and mono-ubiquitylated at H2AK15 (Fradet-Turcotte et al., 2013) (the subsequent modifications will be discussed in more detail below). Its binding affinity proximal to DSBs is mediated through histone acetyltransferase TIP60/TRRAP-induced acetylation of histone H4 on lysine (K) 16 (H4K16ac) upon damage induction that blocks 53BP1 binding to the neighbouring H4K20 methylation mark and inhibits DSB repair via HR. However, the antagonizing deacetylation of H4K16 by histone deacetylase 1 (HDAC1) and HDAC2 is then required for efficient 53BP1 binding to H4K20me2 (Hsiao and Mizzen, 2013; Tang et al., 2013). 53BP1 nucleosome binding is followed by its ATM-dependent phosphorylation, that is required to recruit RIF1 and PTIP to DSBs. RIF1 functions as the effector protein of 53BP1 in the G1 phase of the cell cycle and inhibits DNA end resection. In G2/S phase, RIF1 recruitment is suppressed by BRCA1 and its interacting protein CtIP, providing a switch to DSB repair via HR (Chapman et al., 2013; Escribano-Diaz et al., 2013; Zimmermann et al., 2013). PTIP also counteracts resection upon direct binding to ATM-phosphorylated 53BP1 and Artemis via its BRCT domains. Artemis thereby seems to function as downstream effector and limits DNA end resection at DSBs (Callen et al., 2013; Wang et al., 2014).

If rapid re-joining of the DSB via NHEJ does not ensue, HR can also be the DSB resolving pathway during S or G2 phase of the cell cycle (Shibata et al., 2011). If necessary, a switch from NHEJ to HR is mediated by BRCA1 and the deubiquitylating enzyme POH1, which belongs to the proteasomal machinery. BRCA1 recruits POH1 to DSBs, which promotes RPA-mediated resection through the removal of RAP80 from ubiquitin conjugates. The latter is required, since RAP80 blocks ubiquitin proteolysis and thus has a protective role towards ubiquitin. However, in the absence of RAP80, ubiquitin chains are degraded leading to the loss of 53BP1 in damaged chromatin and initiation of DNA end resection (Butler et al., 2012; Kakarougkas et al., 2013). CtIP is of great importance for this process, because it stimulates DSB repair via HR by promoting end-resection. Activation of CtIP is regulated on the one hand through its cell-cycle dependent expression, being up-regulated during S/G2 phase, and on the other hand by the p-ATM dependent recruitment of CtIP to DNA damage. Also the DSB-induced deacetylation as well as MRE11-CDK2-dependent phosphorylation of CtIP both regulate its action and promote its binding to BRCA1 (Buis et al., 2012; Kaidi et al., 2010; You et al., 2009). Thus, a multitude of interactions and posttranslational modifications (PTMs) mediate the local chromatin environment of DSBs and the key players regulate the cells' choice for a particular DSB repair pathway during the cell cycle.

Chromatin structure changes through histone posttranslational modifications and chromatin remodeling

Various regulatory mechanisms control the folding-state of DNA to provide access to proteins involved in DNA-based metabolic processes including transcription, DNA replication and DNA repair. First, histones can be posttranslationally modified through the action of enzymes that covalently modify residues at their inner core or at their N- and C-terminal tails. In that way not only the physical properties of the chromatin, but also the binding of non-histone proteins to chromatin can be altered. Besides phosphorylation, histones can also be ubiquitylated, SUMOylated, methylated, acetylated and poly(ADP-ribosyl)ated; the combinatorial nature of these modifications forms what is called the 'histone code' (Jenuwein and Allis, 2001).

Alternatively, ATPase-containing multi-subunit chromatin remodeling complexes can change the biophysical properties of chromatin through sliding nucleosomes along the DNA, evicting histone dimers or octameres and exchanging core histones or histone dimers with histone variants (Clapier and Cairns, 2009) such as H2A.Z (Xu et al., 2012) (discussed in more detail below).

Previous studies have shown that histone modifiers (Luijsterburg and van Attikum, 2011) and ATP-dependent chromatin remodelers are involved in the human DDR (Luijsterburg and van Attikum, 2011; Smeenk and van Attikum, 2013). In the following section more information on our current understanding of the role of chromatin modifications and chromatin remodelling in the DSB response is presented.

Posttranslational modifications during the DSB response

Phosphorylation

Upon phosphorylation, a phosphate group is attached to an acceptor protein at a serine (S) or threonine (T) residue. Among the huge number of phosphorylated proteins, hundreds of proteins have been found to contain SQ/TQ motifs, which can undergo DNA damage dependent phosphorylation by kinases from the phosphatidylinositol-3 kinase (PIKK)-family including ATM, ATR and DNA-PKcs (Matsuoka et al., 2007). Phosphorylation can thereby facilitate phospho-specific interactions with one of the many DDR factors that contain phospho-binding motifs, such as the Breast-cancer C-terminal (BRCT) domain or the Forkhead associated (FHA) domain (Mohammad and Yaffe, 2009). Also histones are phosphorylated upon DNA damage induction with the phosphorylation of the histone H2A variant H2AX on serine S139 (γ H2AX) as a key example. H2AX differs from H2A by an additional SQ(EY) motif at the C-terminus and engulfs about 10-15% of the H2A pool in higher organisms (Stucki and Jackson, 2006). ATM is the primary kinase that phosphorylates H2AX at DSBs (Burma et al., 2001) but acts in a redundant fashion with DNA-PKcs (Stiff et al., 2004). Conversely upon UV damage or replication stress, H2AX becomes phosphorylated primarily by ATR (Ward and Chen, 2001).

γ H2AX spreads over more than 20 megabases of chromatin surrounding the DSB (Fig. 1) (Iacovoni et al., 2010) and interacts with MDC1 through the BRCT domain of the latter. γ H2AX maintenance and MDC1-binding is regulated by the Williams syndrome transcription factor (WSTF), also called BAZ1B, which has kinase activity and was found to phosphorylate histone H2AX on tyrosine T142 independently from DNA damage. While WSTF is not directly involved in the DNA damage-induced phosphorylation of H2AX on Ser139, it does help to maintain γ H2AX levels following DNA damage (Barnett and Krebs, 2011; Xiao et al., 2009). Furthermore, the antagonizing activity of the EYA1/3 phosphatases

is required to dephosphorylate H2AX T142 following DNA damage, thereby promoting the chromatin assembly of MDC1 and counteracting an apoptotic response driven by T142 phosphorylation (Cook et al., 2009; Krishnan et al., 2009). MDC1 then provides a binding platform for several downstream DDR factors at DSBs (Stucki and Jackson, 2006). The formation of γ H2AX is further required to arrest cell cycle progression upon exposure to low doses of IR (Fernandez-Capetillo et al., 2002). Another crucial role of γ H2AX in the DDR is the MDC1-mediated recruitment of the E3 ubiquitin ligases RNF8 and RNF168 to DSBs, which facilitate the accumulation of 53BP1 and BRCA1 through the formation of ubiquitin conjugates on several H1 and H2A residues (discussed below) (Doil et al., 2009; Huen et al., 2007; Kolas et al., 2007; Mailand et al., 2007; Stewart et al., 2009; Thorslund et al., 2015; Wang and Elledge, 2007).

A different, but important event during the DSB response is the ATM-mediated phosphorylation of KAP1 on serine S824 in heterochromatic regions (Goodarzi et al., 2008; Lee et al., 2010b; Noon et al., 2010; Ziv et al., 2006). Heterochromatin comprises about 10-25% of total DNA within a cell, dependent on age, cell type as well as species. Importantly, heterochromatin forms a barrier for efficient DSB repair that is overcome by ATM-dependent KAP1 phosphorylation. Phosphorylated KAP1 interferes with the SUMO-dependent interaction between KAP1 and the nucleosome remodeler CHD3, leading to CHD3 dispersal from DSBs in heterochromatic regions (Goodarzi et al., 2011). Additionally, the chromatin remodelers SMARCA5 and ACF1 are recruited by RNF20/40 to heterochromatic DSBs and induce Artemis-dependent chromatin relaxation. This leads to a transient and local increase in the accessibility of the heterochromatin and enables the repair of the damaged DNA (Klement et al., 2014).

Apart from kinases, a number of dephosphorylating enzymes (phosphatases), including PP2A α , PP2A β , PP4C, PP6C and WIP1 have been linked to the DSB response and were shown to be involved in γ H2AX dephosphorylation (Cha et al., 2010; Chowdhury et al., 2008; Douglas et al., 2010; Keogh et al., 2006; Macurek et al., 2010; Moon et al., 2010; Nakada et al., 2008). The absence of either of these phosphatases leads to defective γ H2AX removal from DSBs and impairs the completion of DSB repair rendering cells hypersensitive towards IR. This shows the importance of a tight regulation of the phosphorylation events during the response to DSBs.

Ubiquitylation

Ubiquitin is a small protein of 76 amino acids (8.5 kDa) that is essential and highly conserved throughout evolution. The versatile cellular signals given by various types of ubiquitin modifications control a large variety of biological processes including protein degradation and DNA repair. Ubiquitin is expressed in cells as a precursor protein, which requires cleavage for its activation upon which a carboxyl-terminal di-glycine motif is exposed. Ubiquitin can then be covalently conjugated onto a target protein in a three-step enzymatic process that facilitates the binding of the ubiquitin carboxyl-terminus to a ϵ -amino group of a lysine within a substrate. This process requires an E1- (activating), an E2- (conjugating) and an E3- (ligase) enzyme. The latter type of enzymes thereby belongs to one of the three main families: HECT-domain E3 ligases, RBR E3 ligases and RING E3 ligases. The HECT and RBR E3 ligases contain an active cysteine to which ubiquitin is transferred from the E2 before it is conjugated onto the substrate. In contrast, RING E3 ligases do not bind ubiquitin directly, but rather bind the ubiquitin-charged E2 and the substrate simultaneously (Brown and Jackson, 2015).

Interestingly, no consensus motif exists for ubiquitin conjugation, hence substrate specificity is determined by the E3 ligase, its interacting partners and the substrate itself (Mattioli and Sixma, 2014). Ubiquitin can be conjugated as single molecule on one or more lysine residues of a substrate but also in chains due to the presence of 7 lysine residues (K6, K11, K27, K29, K33, K48 and K63) within the ubiquitin amino acid sequence that can undergo autoubiquitylation. Ubiquitin chains are named after the ubiquitylated lysine linking the ubiquitin molecules. The regulatory role of ubiquitylation differs according to its type of linkage: monoubiquitylation can for instance affect transcription and chromatin remodeling, while polyubiquitylation by means of K48-linked ubiquitin chain formation can target proteins for proteasomal degradation. Moreover, K63-linked ubiquitin chains are required for a proper response to DSBs and provide a binding platform for several DSB signaling proteins when generated in the vicinity of these lesions (Panier and Durocher, 2009).

At the vicinity of DSBs RNF8 binds to phosphorylated MDC1 via its FHA domain and initiates the ubiquitin signaling cascade (Huen et al., 2007; Kolas et al., 2007; Mailand et al., 2007) providing an important link between the two PTMs. Together with the E2 enzyme UBC13, RNF8 creates K63-linked ubiquitin chains on histone H1 within DSB-flanking chromatin (Fig. 1) (Doil et al., 2009; Pinato et al., 2011; Stewart et al., 2009; Thorslund et al., 2015). Furthermore, RNF8 also attracts the polycomb protein BMI1, which has been shown to monoubiquitylate H2A and H2AX at K119 and K120 in cooperation with other components of the polycomb repressive complex 1 (PRC1) like E3 ligase RNF2 (Facchino et al., 2010; Ginjala et al., 2011; Ismail et al., 2010; Pan et al., 2011; Wu et al., 2011). Moreover, the RING E3 ligase RNF168 is recruited through binding of the RNF8-induced K63-linked ubiquitin chains on histone H1 via its tandem ubiquitin interacting motifs (UIMs) (Doil et al., 2009; Stewart et al., 2009; Thorslund et al., 2015). RNF168 then generates more K63-linked ubiquitin chains and monoubiquitylates H2A/H2AX at K13-15 (Mattioli et al., 2012). Interestingly, RNF168 was recently found to also induce K27-linked ubiquitin chain formation on H2A and H2AX (Gatti et al., 2015). These K27- and K63-linked ubiquitin chains form the basis for the recruitment of 53BP1 by means of H2AK15ub, to which 53BP1 binds with an ubiquitylation-dependent recruitment motif (Fradet-Turcotte et al., 2013). Also the assembly of the BRCA1-A complex to DSBs is facilitated by this ubiquitin conjugate formation (Fig. 1) (Gatti et al., 2015; Mattioli et al., 2012).

BRCA1 dimerizes with the BRCA1-associated RING domain protein BARD1, which together function as an E3 ubiquitin ligase (referred to as BRCA1 core complex) (Baer and Ludwig, 2002; Hashizume et al., 2001; Ruffner et al., 2001; Wu et al., 1996). When ABRAXAS, BRCC36, MERIT40 and RAP80, interact with this BRCA1 core complex the so called BRCA1-A complex is formed (Shao et al., 2009; Wang and Elledge, 2007). RAP80 has been shown to directly bind K63-linked ubiquitin chains through its UIMs (Sato et al., 2009) as well as K27-linked ubiquitin chains (Gatti et al., 2015). In that way, RAP80 targets the BRCA1-A complex to the damaged DNA in a manner dependent on K63-linked ubiquitin conjugate formation by RNF8 together with UBC13 and RNF168 (Fig. 1) (Thorslund et al., 2015; Wang and Elledge, 2007). The assembly of BRCA1 within the BRCA1-A complex might simultaneously restrict the amount of BRCA1-CtIP and BRCA1-PALB2 complex formation and consequently DNA end-resection and BRCA2-RAD51 loading at DSBs, respectively (Coleman and Greenberg, 2011; Hu et al., 2011; Typas et al., 2015).

Besides RAP80, also 53BP1, RNF168 and RNF169 interact directly with K27- and K63-linked ubiquitin (Gatti et al., 2015). RNF169 thereby is an RNF168-related ubiquitin

ligase that provides an interesting example for negative regulation of the DDR by simply competing with 53BP1 and the BRCA1-A complex for binding to ubiquitylated chromatin and limiting their recruitment to DSBs (Chen et al., 2012a; Poulsen et al., 2012).

The HECT domain containing protein HERC2 provides an additional regulatory level to the ubiquitin cascade by controlling the ubiquitin-dependent retention of DDR factors (53BP1 and BRCA1) on damaged chromatin. It has been shown that upon exposure to IR, HERC2 interacts with RNF8 in a manner dependent on its phosphorylation at threonine Thr4827 (Bekker-Jensen et al., 2010). Moreover, the RNF8-dependent SUMOylation of HERC2 by the E3 SUMO ligase PIAS4 is also required for the HERC2-RNF8 interaction (Danielsen et al., 2012). Mechanistically, HERC2 is thought to facilitate the assembly of the RNF8-UBC13 complex, which promotes K63-linked polyubiquitylation and simultaneously restricts the interaction of RNF8 with other E2 conjugating enzymes. HERC2 also stabilizes RNF168 and its absence severely affects ubiquitin conjugate-formation and the recruitment of downstream repair factors like 53BP1 and BRCA1 (Bekker-Jensen et al., 2010).

Besides H2A, also H2B has been reported to be a target for monoubiquitylation when DNA damage is induced. H2B ubiquitylation is facilitated by the E3 ubiquitin ligase RNF20-RNF40, which form a heterodimer. This E3 ligase is recruited to DSBs upon ATM-dependent phosphorylation and is important for the timely repair of DSBs. Furthermore, RNF20 has been shown to promote the accumulation of NHEJ as well as HR repair factors and, interestingly, also the accrual of chromatin remodeler SMARCA5/SNF2h which facilitates repair (discussed below) (Moyal et al., 2011; Nakamura et al., 2011).

The tight control of the ubiquitylation cascade by ubiquitin ligases and the indirect contribution of chromatin remodeling enzymes entails yet another important level of regulation that is mediated by the group of deubiquitylating enzymes, shortly termed DUBs. Five distinct families subdivide approximately 90 potential DUBs encoded by the human genome: ovarian tumor proteases (OTUs), ubiquitin-specific proteases (USPs), ubiquitin carboxy-terminal hydrolases (UCHs), Machado-Joseph disease enzymes (MJDs) and JAB1/MPN/MOV34 metalloenzymes (JAMMs). OTUB1 binds directly to and inhibits the E2 enzyme UBC13, preventing the interaction of UBC13 with RNF168. This subsequently suppresses the RNF168-dependent ubiquitylation of DSB-containing chromatin (Nakada et al., 2010). Other DUBs that have roles within the DDR are USP44 and USP3, which both antagonize the RNF8/168-dependent ubiquitin conjugation on H2A and in the latter case also (γ) H2AX (Mosbech et al., 2013; Sharma et al., 2014). Moreover, a recent genetic screen identified hitherto unknown DUBs to be potentially involved in the DDR (Nishi et al., 2014), while a similar screen in our lab identified USP26 and USP37 as DUBs that are critical for the DDR. Both DUBs actively degrade RNF168-induced ubiquitin conjugates at DSBs, which averts BRCA1 sequestration via the BRCA1-A complex and reverses the RAP80-inhibitory effect on DSB repair via HR. Hence, this may subsequently promote the assembly of BRCA1 with PALB2-BRCA2-RAD51 to regulate HR (Typas et al., 2015).

SUMOylation

The small ubiquitin-like modifier (SUMO) has been implicated in the modification of a vast variety of proteins and the regulation of many cellular processes, including transcription, chromatin remodeling and DNA repair (Flotho and Melchior, 2013; Hickey et al., 2012; Jackson and Durocher, 2013). Like ubiquitin, SUMO is synthesized as a precursor protein and requires processing by SUMO-specific proteases (Fig. 6A). The subsequent exposure of the di-glycine motif that is needed for SUMO conjugation functions via a 3-step enzymatic

1

cascade as described for ubiquitin. The dimeric E1 activating enzyme is SUMO-Activating Enzyme Subunit 1 and 2 (SAE1/SAE2), while Ubiquitin Carrier Protein 9 (UBC9) forms the E2 conjugating enzyme (Bernier-Villamor et al., 2002; Desterro et al., 1999; Schulman and Harper, 2009). The combined action of E1 and E2 is only sufficient for a few target proteins to become efficiently SUMOylated, instead, a series of E3 SUMO ligases is required to enhance SUMO conjugation specificity and efficiency (Flotho and Melchior, 2013; Hay, 2005; Johnson, 2004; Nagy and Dikic, 2010) (Fig. 6A). SUMO is mainly conjugated to lysines, which are part of a SUMO consensus motif comprised of a large hydrophobic residue (ψ) that is followed by the SUMO acceptor lysine (K) and a glutamic acid (E) two positions downstream of the SUMOylated lysine [ψ KxE] (Hendriks et al., 2014; Matic et al., 2010).

Three different SUMO modifiers can be distinguished in human cells: SUMO-1, SUMO-2 and SUMO-3. SUMO-2 and SUMO-3 are nearly identical as these two modifiers differ in only three amino acids within the N-terminus and can therefore only be distinguished experimentally with great difficulty. On the contrary, the amino acid sequences of SUMO-2 and SUMO-3 only match for ~45% with that of SUMO-1 (Wang and Dasso, 2009). While SUMO-2/3 comprise an internal SUMOylation site that provides the possibility for polymeric SUMO-chain formation, SUMO-1 lacks this and consequently serves as a SUMO-chain terminator when conjugated (Matic et al., 2008; Tatham et al., 2001; Vertegaal, 2010) (Fig. 6B). Poly-SUMO chains have vital roles during proteasome-mediated protein turnover, the cell cycle regulation, DNA replication and DNA repair (Vertegaal, 2010).

SUMO can be bound by SUMO-interacting motifs (SIMs), which are formed by a stretch of hydrophobic amino acids, or a specific ZZ zinc finger (Danielsen et al., 2012; Song et al., 2004; Vertegaal, 2010). Like all PTMs, SUMOylation is reversible and SUMO conjugates can be removed from target proteins by SUMO-specific proteases (Li et al., 2010b; Mukhopadhyay and Dasso, 2007) thus providing a dynamic response mechanism for cells to react on external and internal conditions and stimuli.

SUMOylation has been implicated in the response to different types of DNA damage (Bergink and Jentsch, 2009). All components of the 3-step SUMO conjugation cascade i.e. SAE1, UBC9, the SUMO E3 ligases PIAS1 and PIAS4 as well as SUMO -1 and SUMO-2/3 have been shown to accumulate at sites of DNA damage (Galanty et al., 2009; Morris et al., 2009). While SUMO-1 requires only PIAS4 for its recruitment, conjugation of SUMO-2/3 is apparently catalysed by both SUMO ligases PIAS1 and PIAS4 in the proximity of DSB induced by laser radiation (Galanty et al., 2009). Moreover, the PIAS4-dependent recruitment of RNF168 and the abrogated ubiquitin conjugate formation in PIAS1- and PIAS4-depleted cells indicate substantial cross-talk between the ubiquitin cascade and the SUMOylation-mediated response to DSBs (Galanty et al., 2009; Morris et al., 2009). The underlying mechanism is thought to involve the PIAS4-mediated SUMOylation of HERC2, which promotes RNF8-UBC13 binding and K63-linked ubiquitin chain formation, of which the latter is required for RNF168 accrual. However, RNF168 itself is also SUMOylated by PIAS4, which might positively regulate its stability (Danielsen et al., 2012). Furthermore, 53BP1 recruitment appeared to be merely dependent on PIAS4, while both PIAS1 and PIAS4 are necessary for the accumulation of the BRCA1-A complex at sites of DNA damage (Galanty et al., 2009; Morris et al., 2009). Besides its UIMs, RAP80 also contains a SUMO-2/3-specific SIM, which is required for its recruitment. Consequently, at DSBs RAP80 probably binds to K63-linked ubiquitin chains and SUMO simultaneously, as was suggested by an in vitro binding assay with a Rap80 SIM-UIM-UIM fragment (Hu et al., 2012). The SUMO moiety for RAP80-binding thereby most likely is conjugated onto MDC1 (Hu et al., 2012; Luo et al.,

2012; Strauss and Goldberg, 2011; Yin et al., 2012). Remarkably, while RNF8 and RNF168 are dispensable for PIAS1 and PIAS4 accumulation at DSBs, they still promote the accrual of SUMO-1 and SUMO-2/3, probably by serving as SUMO targets as described above. The recruitment of PIAS1 and PIAS4 is dependent on their SAP domains and while both PIAS1 and PIAS4 are important for the efficient association of BRCA1 with DSBs, the recruitment of RNF168 and 53BP1 only requires PIAS4. Thus it is not surprising, that PIAS1 and PIAS4 have been implemented in the efficient repair of DSBs via NHEJ and HR as well as cell cycle progression (Galanty et al., 2009; Morris et al., 2009).

SUMO has also been implicated in DSB repair by regulating the disassembly of repair complexes at sites of DNA damage. The recruitment of the SUMO-targeted ubiquitin E3 ligase (StUbl) RNF4 relies on its SIM domains, PIAS1 and PIAS4 as well as a number of DDR proteins like MDC1 and BRCA1. When being SUMOylated, these proteins seem to function as binding targets for RNF4 (Galanty et al., 2012; Vyas et al., 2013; Yin et al.,

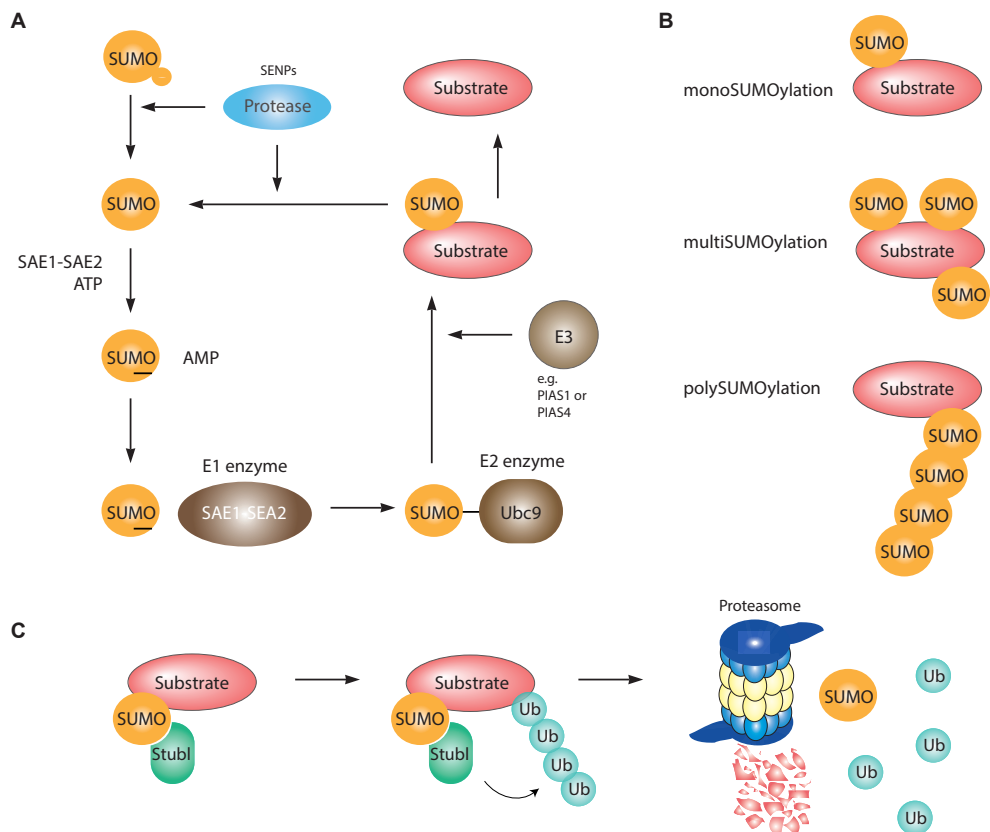


Figure 6. SUMOylation of proteins. (A) The SUMO cycle. Precursor SUMO is cleaved by SUMO specific proteases (SENPs). Via an ATP-dependent cascade involving the activating E1 enzyme SEA1/2, the conjugating E2 enzyme UBC9 and if required a catalytic E3 enzyme, mature SUMO is conjugated onto a lysine of a substrate protein. SUMOylation is a reversible process, because SUMO proteases can deconjugate SUMO from substrate proteins. (B) Substrate proteins can be modified by SUMO by means of monoSUMOylation, multiSUMOylation or polySUMOylation. (C) SUMOylated substrate proteins can be targeted for proteasomal degradation by a SUMO targeted ubiquitin ligase (StUbl). Figure adapted from (Schimmel et al., 2014).

2012). RNF4 promotes the efficient assembly of ubiquitin conjugates at DSBs and that lead to proteasomal degradation of DDR proteins (Fig. 6C), which in turn stimulates DSB repair via both DSB repair pathways, NHEJ and HR. While it is still questionable whether RNF4 mediates NHEJ through the regulation of the rapid turnover of MDC1, RNF4 has been shown to restrict RPA accumulation to DSBs and thus facilitates efficient loading of the HR machinery including RAD51 (Galanty et al., 2012; Luo et al., 2012; Vyas et al., 2013; Yin et al., 2012).

In conclusion, DNA damage triggers a SUMOylation wave that leads to the modification of various DSB repair proteins. It recently has been proposed, that only the simultaneous abrogation of SUMOylation of multiple DSB repair proteins results in a significant defect in DSB repair by HR (Psakhye and Jentsch, 2012). Thus, only the coinciding deSUMOylation of several proteins will lead to detectable phenotypes during the DDR.

Acetylation

Acetylation encompasses the addition of an acetyl group (-COCH₃) to the ε-amino group of a target lysine of a protein. This modification is catalysed onto histones by histone acetyltransferases (HATs) and removed by histone deacetylases (HDACs). Through the neutralization of the positive charge of lysine residues, acetylation can weaken the nucleosomal interactions within chromatin. Acetylated histones are therefore associated with an open chromatin state in which transcription can be active. In general, acetylation is seen as a regulator of higher-order chromatin structure and is important for various cellular processes such as transcription regulation and DNA damage repair.

Upon exposure to IR, both HATs and HDACs accumulate at DNA damage. A well-studied example is the HAT TIP60 that is probably recruited as part of the Nucleosome acetyltransferase of H4 (NuA4) complex. The recruitment of this complex is not sufficient to trigger its activation as only the local transient release of the heterochromatin 1 protein (HP1) upon DSB induction can initiate TIP60 activation. The release of HP1 unmasks the abundant tri-methylated H3K9 mark, to which TIP60 binds with its chromodomain (Sun et al., 2009). ATM activity is subsequently enhanced through TIP60-mediated acetylation and leads to the phosphorylation of numerous downstream targets (Kaidi and Jackson, 2013; Sun et al., 2005). At DSBs TIP60 also acetylates H2AX at K5, which is required for H2AX ubiquitylation at K119 and efficient DSB signaling (Ikura et al., 2007).

Apart from H2AX, also other core histones are targeted for acetylation. Accordingly, TIP60 together with its NuA4 co-factor TRRAP acetylates H4K16 in response to DSBs. The H4K16ac mark mediates the effective accrual of the DSB repair proteins MDC1, 53BP1, BRCA1 and RAD51 and promotes efficient HR (Doyon and Cote, 2004; Murr et al., 2006).

In addition to HR, histone acetylation also plays an important role during NHEJ. The recruitment of CBP and p300 to DSBs induces the acetylation of a number of H3 (K18) and H4 (K5, K8, K12 and K16) residues and promotes the recruitment of the heterodimer Ku70-Ku80 as well as the catalytic subunit of the SWI/SNF chromatin remodeling complex BRM (discussed below) (Ogiwara et al., 2011). Moreover, other labs reported on additional acetylation activity of CBP, p300 and GCN5 on H3K56 and the deacetylation of this mark by the Sirtuin proteins SIRT2 and SIRT3 (Das et al., 2009; Tjeertes et al., 2009; Vempati et al., 2010), showing that the acetylation status of chromatin is dynamically regulated.

Yet another important histone acetylation target is H3K14. Its acetylation has been described to globally increase in cells exposed to IR and to depend on the nucleosome-binding protein HMGN1. Depletion of HMGN1 resulted in decreased ATM-autophosphorylation upon

IR and thus insufficient activation of ATM-targets, while chromatin relaxation induced by HDAC inhibitors bypassed the need for HMGN1-mediated ATM activation (Kim et al., 2009). HMNG1 therefore promotes decompaction of chromatin in the vicinity to DSBs and protects cells from the disastrous effects of IR and UV (Birger et al., 2005).

The acetylation of H4K16A has a central role in the regulation of the DDR, which is linked to releasing higher order chromatin structure (Shogren-Knaak and Peterson, 2006). MOF (or MYST1) is the major HAT that catalyses H4K16 acetylation and its loss causes reduced H4K16ac levels and defects in IR-induced DSB signaling and repair (Li et al., 2010a; Sharma et al., 2010). In more detail, MOF depletion does not affect γ H2AX formation, but is required for the recruitment of MDC1 as well as the downstream factors 53BP1 and BRCA1. This suggests that H4K16ac is crucial for DSB-induced binding of MDC1 to γ H2AX. Interestingly, upon IR-exposure the absence of MOF leads to severe cell cycle arrest at the G2/M border and gives rise to chromosomal aberrations most likely due to severe defects in DSB repair by NHEJ as well as HR (Gupta et al., 2014; Li et al., 2010b; Sharma et al., 2010).

Furthermore, an important role in the DDR has been assigned to HDACs. HDAC1 and HDAC2 are known to rapidly recruit to sites of DSBs, where they deacetylate H3K56. Cells depleted from HDAC1 and HDAC2 show sustained DNA damage signaling, defective DSB repair predominantly by NHEJ and are hypersensitive to IR (Miller et al., 2010). Besides H3K56ac levels, also global H3K9ac decreases upon DNA damage induction in an HDAC-dependent manner (Tjeertes et al., 2009). Furthermore, H4K16ac levels decrease similarly at first through HDAC activity, but increase at later time points during the DSB response in a MOF-dependent manner. Thus H4K16 acetylation has a bi-phasic character during the DDR (Li et al., 2010a; Miller et al., 2010). In addition, HDAC-mediated deacetylation was shown to promote efficient DSB repair via NHEJ (Miller et al., 2010) by the effective disassembly of Ku70 and Artemis from DSBs.

Methylation

Methylation denotes the addition of a methyl group to a lysine or an arginine of a protein. Histone methyltransferases facilitate this reaction on histone proteins through their catalytic SET domain and can either mono-, di- or tri-methylate histones. Proteins harbouring a chromo or a tudor domain are able to bind to these methyl moieties. Similar to other PTMs, histone methylation is a reversible process due to the activity of histone demethylases.

Condensed chromatin displays high levels of H3K9 trimethylation (H3K9me3) rendering the DNA inaccessible for repair proteins and transcriptionally inactive. The histone methyltransferase SUV39H establishes the H3K9me3 mark, to which HP1 directly binds (via its chromodomains) and contributes to the maintenance of heterochromatin (Cheutin et al., 2003). Very recently, scientists found SUV39H to be recruited to DSBs in association with KAP1 and HP1 SUV39H, which thereby locally increases H3K9me3 levels and creates more binding positions for HP1 and subsequently more KAP1-HP1-SUV39H complex. The H3K9me3 mark eventually also becomes available for TIP60 binding mediating acetylation and activation of ATM (Sun et al., 2005; Sun et al., 2009) and rapid phosphorylation of KAP1. These events are followed by the release of the repressive KAP1-HP1-SUV39H complex from damaged chromatin and thus describe a negative feedback loop for the activation of ATM. The transient formation of repressive chromatin might thereby be important for stabilizing the damaged chromatin and might generate a suitable template for DNA repair proteins (Ayrapetov et al., 2014).

Another important methylation mark is H4 dimethylated at lysine 20 (H2K20me2).

This mark, together with RNF168-ubiquitylated H2AK15 is critical for the recruitment of 53BP1 to DNA damage, demonstrating that 53BP1 is a bivalent PTM reader. Hence, only the recognition of nucleosomes comprising both marks leads to actual 53BP1 binding at DSBs involving H4K20me2 with its Tudor domain and H2AK15ub with its ubiquitylation-dependent recruitment (UDR) motif (Botuyan et al., 2006; Fradet-Turcotte et al., 2013; Mattioli et al., 2012). While it is clear, how H2AK15ub is formed during the DDR, quite some debate prevails within the field about H4K20 methylation and the responsible methyltransferase(s). Pei and colleagues have shown that the histone methyltransferase MMSET is recruited to DNA damage in a γ H2AX-MDC1-ATM-dependent manner and that it increases local H4K20me2/3 levels at DSBs to facilitate 53BP1 recruitment in human cells (Pei et al., 2011). Additionally, the activity of the H4K20 monomethyltransferase SET8 (or PR-SET7) was shown to be required for 53BP1 foci formation in human cells (Dulev et al., 2014; Hartlerode et al., 2012). In contrast to these findings, MMSET and the H4K20 dimethyltransferase SUV420H were not requisites for 53BP1 recruitment in mouse embryonic fibroblasts (MEFs) (Hartlerode et al., 2012). This implies that the function of these methyltransferases might not be conserved from mice to humans.

Alternatively, it has been suggested that 53BP1 assembles onto H4K20me2 established in a DNA damage-independent fashion, since H4K20me2 is a very abundant histone mark. This would argue against the involvement of these methyltransferases within the DSB response and proposes that H4K20me2 could rather represent an additional binding interface for 53BP1, which is important for its stable association to damaged chromatin. Interestingly, 53BP1 binding to H4K20me2 can be perturbed by other proteins that have affinity for this histone mark in the absence of DNA damage, such as the Polycomb protein L3MBTL1 and the demethylase JMJD2A (or KDM4A) (Acs et al., 2011; Mallette et al., 2012). Both proteins are ubiquitylated by RNF168 upon DNA damage induction. L3MBTL1 is subsequently removed from chromatin by proteosomal degradation (Butler et al., 2012; Mallette et al., 2012), while JMJD2A gets evicted from the histone mark by the ATPase activity of VCP (or p97) (Acs et al., 2011; Meerang et al., 2011). These processes thus unmask the H4K20me2 marks locally in the vicinity of DSBs and could also enable 53BP1 binding at damaged chromatin.

Another methylation mark that is involved in the response to DSBs is dimethylated H3K36, which is generated upon DSB induction by the methyltransferase Metnase (also named SETMAR). The accrual of NBS1 and Ku70 is stimulated upon Metnase-mediated H3K36me2 formation at damaged chromatin and specifically promotes DSB repair via NHEJ (Fnu et al., 2011).

Poly(ADP-ribosyl)ation

The process by which a linear or multibranched polymer of ADP-ribose units is attached to a target is termed PARylation for Poly(ADP-ribose)ylation. These polymers can be conjugated onto a glutamate, aspartate or lysine residue of an acceptor protein. PAR is catalysed by poly(ADP-ribose) polymerases (PARPs) that belong to a 17 members counting PARP superfamily, which is further divided into four groups dependent on their domain architecture. One subfamily is formed by the DNA-dependent PARPs: PARP1, PARP2 and PARP3 (Schreiber et al., 2006). These PARPs form the most relevant group for the work presented in this thesis as they have been implicated in the DDR (Pines et al., 2013). PAR-chain synthesis is mediated by PARP, but PAR-chains have a short turnover time due to their rapid degradation by poly(ADP-ribose) glycohydrolase (PARG). PARG functions in a

coordinated manner together with PARPs to regulate various cellular processes. Hence, the amount of PAR-chains is kept in a tight equilibrium to fine tune protein function and cellular processes. PARP1 has been shown to be important during the response to SSBs and DSBs (El-Khamisy et al., 2003; Masson et al., 1998). Proteins are not only PARylated, but can also bind to PAR via several PAR-binding modules: the PAR-binding motif, WWE domains containing a Trp-Trp-Glu motif, PAR-binding zinc fingers and macrodomains that bind to the terminal ADP-ribose of PAR (Gibson and Kraus, 2012).

PARP1 is the main catalyst of PAR and gets activated by binding to DNA damage through its zinc finger domains (Langelier et al., 2010). An essential step in this process is the autoPARylation of PARP1 at the PAR-acceptor sites K498, K521 and K524 (Altmeyer et al., 2009). PARP1 can also PARylate many other targets, including histone proteins (Mortusewicz et al., 2007; Poirier et al., 1982). Histone H2AK13, H2BK30, H3K27, H3K37 as well as H4K16 have all been identified as ADP-ribose acceptor sites and their PARylation might contribute to the rapid recruitment of PAR-binding proteins to DNA lesions. Interestingly, H4K16ac inhibits H4K16 PARylation by PARP1 and thus provides another indication for the existence of functional crosstalk between the different histone tail modifications (Messner et al., 2010). Moreover, the PARylation of nucleosomes has been shown to induce chromatin relaxation and PARP1 activity facilitates expansion of damaged chromatin and the spreading of DDR factors within the damaged chromatin compartment (Poirier et al., 1982; Smeenk et al., 2013).

The chromatin remodeler Amplified in Liver Cancer (ALC1) binds PAR-molecules with its macrodomain at sites of laser-induced DNA damage and thus is an example for a PAR-binding protein. This subsequently leads to its activation and is followed by nucleosome remodeling (Ahel et al., 2009; Gottschalk et al., 2009). Worth mentioning is also the histone chaperone APLF, which incorporates the histone variant MacroH2A1.1 at sites of DNA damage (Mehrotra et al., 2011). Both macroH2A1.1 and APLF bind to PAR-chains through a macrodomain and PAR-binding zinc finger domain, respectively (Ahel et al., 2008; Timinszky et al., 2009). MacroH2A1.1 transiently compacts chromatin and negatively regulates the recruitment of the NHEJ factors Ku70-Ku80 (Timinszky et al., 2009), while APLF promotes NHEJ complex assembly and functions as a scaffold for XRCC4-LIG4-XLF recruitment at DSBs (Ahel et al., 2008; Iles et al., 2007; Kanno et al., 2007; Rulten et al., 2008).

The chromodomain helicase DNA-binding protein CHD4 is the ATPase subunit of the NuRD complex and its recruitment to DNA damage has been shown to be partially dependent on PARP. Remarkably, CHD4 can bind to PAR *in vitro*, despite the lack of any known PAR-binding consensus sites or PAR binding domains (Polo et al., 2010). Another example is the chromatin remodeler SMARCA5 (or SNF2h), which is also recruited in a partially PARP-dependent manner. Upon DSB-induction, RNF168 gets PARylated and interacts with SMARCA5 in a PAR-dependent fashion, contributing to its accrual to DSBs. On the other hand, SMARCA5 supports RNF168 recruitment to DSBs, thereby regulating the RNF168-driven ubiquitin cascade (Smeenk et al., 2013). Hence, the distribution of SMARCA5 and factors involved in this ubiquitin cascade within laser-damaged chromatin compartments was mediated by the activity of PARP. It was suggested that PARP spatially organizes the ubiquitin cascade in response to DNA damage at the level of SMARCA5 as well as RNF168 recruitment, and thereby contributes to efficient ubiquitin conjugate formation and subsequent BRCA1 assembly (Smeenk et al., 2013).

PARP1 can also be activated in the absence of DNA by the mono(ADP-ribosyl)ase PARP3. In contrast to PARP1, PARP3 can auto-ADP-ribosylate without DNA-binding and

the reported interaction of PARP1 and PARP3 seems to be unrelated to repair of at least single strand DNA breaks (Loseva et al., 2010). In line with these findings is the observation that PARP1^{-/-}/PARP3^{-/-} mice are more sensitive to IR compared to the single mutant mice. PARP1 and PARP3 might therefore function synergistically within the DDR (Boehler et al., 2011). However, recent reports suggest that PARP3 also accelerates NHEJ through the ADP-ribosylation of the Ku dimer and histone H1. As such they provide a platform for the PAR-binding protein APLF, which promotes the retention of the XRCC4/LIG4 complex at damaged chromatin (Fig. 4) (Beck et al., 2014; Rulten et al., 2011). These findings thus rather suggest an epistatic role for PARP1 and PARP3 within the DDR.

PTM crosstalk shapes epigenetic environment of DSBs

From the previous sections on PTMs one might start wondering, why there are so many different PTMs and how they relate to each other during the response to DNA damage. PTMs alter protein interactions and influence their translocation or degradation and therefore provide opportunities to regulate and control the activities of distinct proteins like those involved in the DDR. Since there are several different PTMs that can influence protein function, processes can be mediated in a very precise way through numerous different modifications. However, we are just beginning to understand the immense crosstalk of PTMs occurring in the vicinity of DNA damage and its complexity. One interesting finding so far is that the recruitment of several proteins to DNA damage depends on a multiple interaction strategy. 53BP1 is a notable example of a bivalent binding factor, since it binds ubiquitylated and methylated histones in order to robustly enrich and remain at DSBs (Fradet-Turcotte et al., 2013). Moreover, the ubiquitin ligases RNF168 (Mattioli and Sixma, 2014) and RNF4 (Grocock et al., 2014) bind to either ubiquitin or SUMO conjugates, respectively, while they additionally need to interact with chromatin for stable association in close vicinity to the lesion.

Thus, the signaling and repair of DSBs is an extremely fine-tuned multi-step process, where the composition of all PTMs shape the epigenetic chromatin environment of DSBs.

ATP-dependent chromatin remodeling during the DSB response

Chromatin remodelers use the energy from ATP hydrolysis to alter chromatin structure. As previously mentioned, they can do so by sliding nucleosomes along the DNA, exchanging or ejecting histone dimers, or disassembling nucleosomes by ejecting octamers. Originally described in yeast, the sucrose nonfermenting (SNF2) family of chromatin remodelers comprises an ATPase catalytic subunit as well as a helicase domain. The SNF2 family members are further categorized into four subgroups, each group containing different additional functional domains (Fig. 7), which will be addressed per group below. These ATPases often form the catalytic subunit of multi-subunit complexes, in which they assemble together with varying subunits that all contribute to the remodeling activity and/or the functionality of the complex.

SWI/SNF

The catalytic subunit of the Switching defective/sucrose nonfermenting (SWI/SNF) family of chromatin remodelers characteristically comprises an additional helicase SANT-associated (HSA) domain and an C-terminal bromodomain (Fig. 6), the latter is capable to bind acetylated histone tails (Clapier and Cairns, 2009). The SWI/SNF family contains two catalytic subunits, BRM (also SMARCA2) and BRG1 (SMARCA4), and each forms a multi-subunit complex with

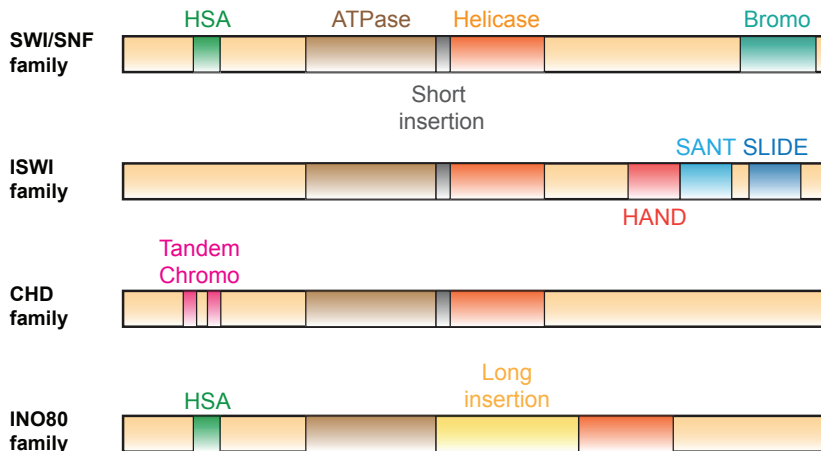


Figure 6. Schematic representation of the SWI2/SNF2 chromatin remodeling superfamily. Next to the catalytic ATPase and helicase domain, all SNF2 family members contain additional domains, by which they are classified into the four subfamilies: SWI/SNF, ISWI, CHD and INO80. The SWI/SNF family comprises a helicase-SANT-associated (HSA) domain, which facilitates the binding to nuclear actin-related proteins, and a bromodomain that is capable of binding acetylated lysines. ISWI chromatin remodelers are equipped with an HAND, SANT and SLIDE domain that can mediate interactions with proteins and DNA. The CHD family members contain an N-terminal tandem chromodomain, which enables these chromatin remodelers to bind methylated lysines. In contrast to the other subfamilies, INO80-related enzymes have a longer insertion between the ATPase and helicase domain as well as an HAS domain within the N-terminal part.

8 - 10 BRM- or BRG1-associated factors (BAFs). Both remodelers can facilitate nucleosome repositioning, dimer or octamer ejection and nucleosome unwrapping (Kasten et al., 2011).

SWI/SNF has been implicated in the DSB response: a positive feedback loop has been described for γ H2AX formation at DSBs, constituting the rapid and transient phosphorylation of BRG1 on Ser-721 by activated ATM. This stimulates the binding of BRG1 through its bromodomain to acetylated H3 in chromatin comprising γ H2AX-containing nucleosomes and the phosphorylation of H2AX by ATM through the remodeling activity of BRG1. Simultaneously, the HAT GCN5 is recruited to DNA damage in a γ H2AX-dependent manner and acetylates H3 within the chromatin surrounding the lesion. This subsequently induces the recruitment of additional BRG1 and facilitates the spreading of the γ H2AX signal, as well as DNA damage signaling and repair (Kwon et al., 2015; Lee et al., 2010a; Park et al., 2006). Furthermore, BRG1 has just recently been suggested to function in the HR pathway, while NHEJ efficiency was normal in BRG1-depleted cells (Qi et al., 2015). This study showed that BRG1 regulates HR through the exchange of RPA with RAD51 at DSBs.

SWI/SNF has also been shown to be regulated by BRIT1 (or MCPH1), which associates with core subunits of the SWI/SNF complex in an ATM-/ATR-dependent manner and promotes the recruitment and binding of SWI/SNF at DSBs (Peng et al., 2009). Probably through the interaction with SWI/SNF and indirectly γ H2AX, BRIT1 attracts DDR response factors like NBS1, p-ATM, MDC1 and 53BP1 (Rai et al., 2006; Wood et al., 2007). Thus, consistent with BRIT1 contributing to early DSB signaling, the absence of BRIT1 resulted in a G2/M checkpoint defect and abrogated DSB repair via HR and NHEJ (Lin et al., 2005; Peng et al., 2009). Interestingly, defects in BRIT1 were also shown to promote tumor development and underlie primary microcephaly, a neural development disorder characterized by reduced brain size (Chaplet et al., 2006).

ISWI

Thus far, seven different complexes of the mammalian Imitation SWItch (ISWI) family have been described (Erdel and Rippe, 2011; Toto et al., 2014). Two ATPase subunits built the core of these complexes: SMARCA5 (or SNF2H) and SMARCA1 (or SNF2L). In addition to their ATPase domain located within the N-terminus, both ATPases possess a HAND, SANT and SLIDE domain within their C-terminus (Fig. 6) (Grune et al., 2003).

SMARCA1 has been found in the CERF (Banting et al., 2005) and NURF (Barak et al., 2003) complexes, which function within the central nervous system during neurulation or neuronal development, respectively. However, to our knowledge a function for these factors in the DDR has not yet been established. In contrast, SMARCA5 has been implicated in the DDR. In fact, we and others have recently shown that upon DSB induction the RNF8/RNF168-induced ubiquitylation response is tightly controlled by the chromatin remodeler SMARCA5 and PARP (Lan et al., 2010; Smeenk et al., 2013). PARP thereby regulates the distribution of SMARCA5 and factors of the RNF168 signaling cascade throughout the damaged chromatin compartment of a cell, which subsequently leads to the efficient formation of ubiquitin conjugates at and the assembly of BRCA1 to the lesion (Smeenk et al., 2013). However, the recruitment of SMARCA5 is also mediated by the histone H3K56 deacetylase SIRT6 (Toiber et al., 2013) and the RNF20-RNF40 ubiquitin ligase, which ubiquitylates H2B to promote the assembly of HR repair factors (Nakamura et al., 2011; Oliveira et al., 2014). The depletion of RNF20 or SMARCA5 renders cells defective in DNA end resection and unable to recruit BRCA1 and RAD51 to DSBs. Interestingly, RNF20 also facilitates DSB-induced chromatin relaxation in heterochromatin downstream of KAP1 phosphorylation and the dispersal of CHD3 in an SMARCA5-dependent fashion, which is favourable for the repair of DSBs via an Artemis-dependent NHEJ pathway (Klement et al., 2014). Thus, SMARCA5 is important for the proper execution of the two DSB repair pathways HR and NHEJ (Lan et al., 2010; Smeenk et al., 2013). Remarkably, SMARCA5 resides in several different complexes, including WICH (SMARCA5 and WSTF), ACF (SMARCA5 and ACF1), CHRAC (SMARCA5, ACF1, CHRAC15 and CHRAC17) and RSF (SMARCA5 and RSF1) (Wang et al., 2007) that contain one or more auxiliary factors in addition to SMARCA5. Thus far, each of these factors has been implicated in the DDR and will be briefly discussed below.

The WSTF kinase and its role in H2AX T142 phosphorylation have been described in the 'Phosphorylation' section. The SMARCA5-complex partner ACF1, also known as BAZ1A, protects cells from various types of DNA damage and facilitates activation of the G2/M checkpoint upon DNA damage induction (Sanchez-Molina et al., 2011). In addition, ACF1 promotes efficient DSB repair by both HR and NHEJ. ACF1 physically associates with the key NHEJ factor Ku70, thereby recruiting the Ku70/Ku80 heterodimer to sites of DNA damage and initiating DSB repair (Lan et al., 2010). The histone fold proteins CHRAC15 and CHRAC17 also facilitate DSB repair by HR and NHEJ although the precise mechanisms are unclear (Lan et al., 2010). The role of the histone chaperone RSF1 during the DDR remains enigmatic and has been investigated in chapters 3 and 4.

CHD

The catalytic subunits of the Chromodomain Helicase DNA-binding (CHD)-type remodelers are characterized by a tandem chromodomain at their N-terminus enabling these remodelers to bind to methylated histones (Fig. 6). Nine different CHD catalytic subunits exist that have various additional DNA- or protein-binding motifs, by which they are discriminated. So far, two CHD proteins, CHD3 and CHD4, were described to mediate the DDR. They are

both mutually exclusive catalytic subunits of the Nucleosome Remodeling and Deacetylase (NuRD) complex. Several of the NuRD subunits were shown to accumulate at sites of DNA damage, including CHD3 and CHD4, HDAC1 and HDAC2, the regulatory subunits MTA1 and MTA2 as well as the methylated DNA-binding protein MBD3 (Chou et al., 2010; Goodarzi et al., 2011; Larsen et al., 2010; Luijsterburg et al., 2012; Polo et al., 2010; Smeenk et al., 2010). Besides chromatin remodeling, the different NuRD complexes also facilitate histone deacetylation through HDAC1 and HDAC2, and have both inhibitory (CHD3) and stimulatory (CHD4) effects on the progression of DSB repair as described below.

The nucleosome remodeler CHD3 possess a small SIM domain, which mediates its binding to SUMOylated KAP1 within undamaged heterochromatin. Upon DSB induction, however, KAP1 becomes phosphorylated by ATM and this modification interferes with the SIM-SUMO interaction between CHD3 and KAP1. This results in the dispersal of CHD3 from heterochromatin surrounding DSBs, local chromatin relaxation and subsequently efficient DSB repair (Goodarzi et al., 2011). Interestingly, since CHD4-depletion did not affect chromatin condensation, only CHD3 seems to collaborate with KAP1 in maintaining heterochromatin compaction (Goodarzi et al., 2011).

A role of CHD4 in DDR has been implicated by several labs. The protein is recruited in a PARP-dependent fashion and physically associates with the FHA domain of RNF8 to promote RNF8-dependent chromatin unfolding and ubiquitin conjugation. These steps are then followed by the assembly of downstream signaling and repair factors, such as RNF168 and BRCA1. Hence, CHD4 was shown to be important for the proper execution of DSB repair (Chou et al., 2010; Goodarzi et al., 2011; Larsen et al., 2010; Luijsterburg et al., 2012; Polo et al., 2010; Smeenk et al., 2010).

The chromatin remodeler ALC1, often referred to as Chromodomain Helicase DNA binding protein 1 like (CHD1L), is related to the CHD family, but contains a C-terminal macrodomain that facilitates PAR-binding (Ahel et al., 2009; Gottschalk et al., 2009). Nonetheless, its exact mode of action during the response to DSBs remains enigmatic.

INO80

ATPases of the INO80 family of chromatin remodelers are divergent from other families by their longer spacer region between the ATPase and helicase domains (Clapier and Cairns, 2009). They also feature an HSA domain which mediates the assembly of actin and actin-related proteins (ARP) to the complex (Fig. 6) (Szerlong et al., 2008). In the human INO80 complex subunits INO80, SRCAP, TIP60/TRRAP with ATPase p400 and SMARCAD1 are unique to the complex, whereas several other subunits are known to be part of different multi-subunit complexes.

Human INO80 accumulates at laser inflicted DNA damage in a manner that is dependent on its subunit ARP8, but independent from γ H2AX (Kashiwaba et al., 2010). In contrast, the recruitment of yeast Ino80 relies on the interaction of the subunit Arp4 with γ H2AX, as well as the on other subunits like Arp8 and Nhp10 (Downs et al., 2004; Kashiwaba et al., 2010; Morrison et al., 2004). Several studies in yeast have described a role for Ino80 in DNA end resection and DSB repair mediated through the removal of H2A.Z/H2B histone dimers from the DNA in the vicinity of DSBs (Chambers and Downs, 2012). This nucleosome remodeling activity contributes to enhanced accessibility of DSBs for repair proteins and ultimately the maintenance of genome stability. Consistently, also mammalian INO80 has recently been suggested to support efficient DSB repair by mediating the 5' to 3' resection of DSB ends (Gospodinov et al., 2011). In more detail, INO80 removes H2A.Z from chromatin

flanking DSBs together with the histone chaperone ANP32E and thereby promotes DNA end resection and DSB repair via HR (Alatwi and Downs, 2015).

The two other human ATPases that belong to the INO80 family are Snf-2-related CREB-binding protein activator protein (SRCAP) and p400. These are part of the SRCAP and TIP60/TRRAP (also NuA4) chromatin remodeling complexes, respectively. Whereas both ATPases have been implemented in the deposition of histone variant H2A.Z in nucleosomes, only p400 additionally incorporates H2A.Z in the vicinity of DSBs (Ruhl et al., 2006; Wong et al., 2007; Xu et al., 2012). Incorporation of H2A.Z promotes an open chromatin configuration through stimulation of H4 acetylation via TIP60 and p400, ubiquitin conjugate formation via RNF8 and subsequent BRCA1 loading. On the other hand, the presence of H2A.Z restricts DNA end resection and loads the Ku70-80 dimer onto DSBs (Xu et al., 2012). Hence, INO80-dependent removal of H2A.Z from damaged chromatin rather promotes end resection and DSB repair via HR (Alatwi and Downs, 2015), as mentioned above. Interestingly, p400 itself has also been described to promote HR through the recruitment of RAD51 (Courilleau et al., 2012), while SRCAP facilitates efficient DSB repair via HR through its DNA damage-induced interaction with CtIP that promotes its recruitment and that of RPA and RAD51 (Dong et al., 2014).

SMARCAD1

The yeast Snf2-related chromatin remodeler FUN30 forms a homodimer in cells and its ATPase activity is stimulated by the presence of DNA (Awad et al., 2010). Fun30 has been implicated in the maintenance of the chromatin structure through the inhibition of euchromatin assembly at heterochromatic regions (Stralfors et al., 2011). Three separate studies showed the recruitment of Fun30 to DNA damage and implicated a role for FUN30 in long-range DNA end resection (Chen et al., 2012b; Costelloe et al., 2012; Eapen et al., 2012). The closest human homolog of Fun30 is SMARCAD1, which similarly promotes the 5' to 3' degradation of DSB ends and facilitates RPA/RAD51 loading onto chromatin (Costelloe et al., 2012). SMARCAD1 thus has an evolutionary conserved role in DSB repair and in the maintenance of genome stability in the context of chromatin.

DDR AND DISEASE

As described in the previous paragraphs, the DNA damage-mediated posttranslational modifications of chromatin and chromatin-associated proteins are crucial for the efficient and timely recruitment of DDR proteins involved in chromatin remodeling, DNA damage signaling, DNA repair (pathway choice), cell cycle progression or transcription, at DNA lesions. The attracted histone modifiers and chromatin remodelers dynamically shape the chromatin environment around these lesions by controlling chromatin organization and the binding of DDR factors to the lesion. In this manner, these chromatin-modifying enzymes regulate the crosstalk between DNA damage signaling and repair as well as other nuclear processes such as replication, transcription and cell cycle regulation (Kruhlak et al., 2007; Shanbhag et al., 2010; Solovjeva et al., 2007; Ui et al., 2015). Consequently, loss of such enzymes can have detrimental effects on genome stability, one of the major hallmarks of cancer. In addition, on the organismal level their loss can cause embryonic lethality, neurodegeneration and premature aging. Thus, it is of great importance to gain further insight in the exact roles of chromatin modifying enzymes during the spatiotemporal organization in diverse cellular processes, including the DDR, in order to understand how and which diseases are caused by their functional loss. Even though our knowledge of the DDR has tremendously increased

over the last decades, novel factors, which often include chromatin modifiers, are still being identified. It is therefore challenging to implement the large number of identified DDR factors in one general model describing their roles during the cellular response to DNA damage. Moreover, parameters like the cell type, the differentiation state of cells and the compaction status of the chromatin surrounding the DNA damage, as well as the type of DNA damage have to be taken into account when trying to get an integrated view on all aspects of the DDR. Future work should therefore focus on mechanistic analysis of each of the identified players in the context of the DDR network in a defined cellular model upon the induction of defined types of DNA damage in order to obtain a more detailed understanding of the complexity of the DDR in the context of chromatin.

Several monogenic diseases are caused by defects in DDR factors and often display pleiotropic clinical phenotypes. For example, mutations in the gene encoding NBS, which together with MRE11 and RAD50 keeps the broken DNA ends in close proximity and activates the ATM kinase (Paull, 2015), lead to Nijmegen Breakage Syndrome. NBS patients display a typical facial appearance, growth retardation, microcephaly, immunodeficiency, IR-sensitivity and predisposition to (lymphoid) malignancies (Chrzanowska et al., 2012; Gladkowska-Dura et al., 2008; Weemaes et al., 1981). Another example represents mutations in ATM, which cause the disorder Ataxia Telangiectasia (AT). AT patients are radiosensitive, display a high incidence of cancer (leukemia, lymphoma) and suffer from immunodeficiency (Staples et al., 2008). The phenotypic manifestation varies in severity with the type of mutation and accordingly with the residual amount of functional ATM kinase present in cells (Verhagen et al., 2012). Finally, mutations in the E3 ubiquitin ligase RNF168 involved in the ubiquitin-dependent signaling of DSBs can give rise to a human disease. Patients with either homozygous or compound heterozygous mutations in RNF168 suffer from RIDDLE syndrome and display immunodeficiency, radiosensitivity, learning difficulties, as well as dysmorphic features (Devgan et al., 2011; Stewart et al., 2009).

Primary immunodeficiencies in patients have been described to originate from mutations in NHEJ genes, which are important for the repair of DSBs. Interestingly, these mutations also hamper the development of B- and T-cells via V(D)J recombination and CSR within the bone marrow, since NHEJ is required for these processes to repair the deliberately induced DNA breaks. The first patient with classical severe combined immunodeficiency (SCID), comprising defective precursor B-cell development and IR sensitivity, was described in 2009 (van der Burg et al., 2009). Mutations in Artemis and members of the LIG4-XRCC4-XLF NHEJ ligation complex have also been linked with such clinical phenotypes. LIG4-deficient patients are sensitive to IR, but dependent on the mutation patients show slightly different additional clinical features such as growth anomalies or immunodeficiency with varying severity (Woodbine et al., 2014). Furthermore, Lig4 is essential in mice, since Lig4 knockout mice are embryonic lethal. In line with this observation, LIG4 deficient patients suffer from tolerable hypomorphic mutations (Barnes et al., 1998; Frank et al., 1998; Gao et al., 1998). In contrast to the LIG4 deficient patients, the immunological phenotype of XLF deficient patients is very severe and these patients additionally display microcephaly, growth retardation as well as sensitivity towards IR (Ahnesorg et al., 2006; Buck et al., 2006; Dai et al., 2003; Dutrannoy et al., 2010). Also a few patients carrying XRCC4 mutations have been described. While they phenotypically showed developmental alterations, no immunological defect was documented for this group of patients, despite the fact that patient-derived cells actually did display defects in NHEJ (de Bruin et al., 2015; Guo et al., 2015; Rosin et al., 2015; Shaheen et al., 2014).

As mentioned above, the aberrant expression of chromatin-modifying enzymes can also lead to various diseases. For example, mutations in several components of the SWI/SNF chromatin remodeling complexes have recently been found in patients with intellectual disability syndromes i.e. Coffin-Siris and Nicolaides-Baraitser (Santen et al., 2012a; Schrier et al., 2012; Van Houdt et al., 2012). On the other hand, expression of the SWI/SNF ATPases BRG1 and BRM is frequently lost in several human tumors, with one or both genes being silenced (Reisman et al., 2009). Moreover, the ISWI chromatin remodeler SMARCA5 (Table 1), which associates with RNF168 and helps to execute the RNF168-mediated DSB response (Smeenk et al., 2013), was found to be either overexpressed or mutated in several different tumors (Cetin et al., 2008; Gigek et al., 2011; Stopka et al., 2000; Sumegi et al., 2011). For an overview of these and other chromatin remodelers that have been causally linked to various diseases due to aberrant expression or mutations, I refer to Table 1.

DDR AND THERAPY

In the last few decades scientists tried to gain more detailed knowledge on the events taking place during the DDR with the purpose to better diagnose and subsequently develop treatments for DDR-associated diseases. To improve the current treatment opportunities of for instance cancer, mechanistic insights in the organization of the DDR are exploited by means of developing small molecule inhibitors for targeted cancer therapies. This form of patient treatment is tailored according to the genetic alterations in their tumor cells, which often have defects in one or more DDR pathway(s). Consequently, the tumor cells are increasingly reliant on the remaining DDR pathways to restore damaged DNA. The concept of synthetic lethality takes advantage of this fact: the targeted deactivation of one DNA repair pathway in combination with a cancer-specific defect in at least one other DNA repair pathway leads to cell death, whereas the deficiency in only one of these repair pathways does not. This approach is very promising since it specifically targets a defect in cancer cells. The PARP1 enzyme has been described to be involved in a number of DNA repair pathways such as SSB repair, base excision repair, nucleotide excision repair and DSB repair (Pines et al., 2013). Its inhibition suppresses DNA repair and sensitizes cells to the cytotoxic effects of DNA damaging agents (Durrant and Boyle, 1982; Nduka et al., 1980). Recently, inhibitors of PARP appeared to have clinical impact on the treatment of cancers lacking functional HR. The best studied example represents BRCA1/2-deficient (breast and ovarian) cancer cells, which proved highly sensitive to PARP inhibitors. The current view is that inhibitor-inactivated PARP becomes trapped at single-strand DNA breaks, which are converted into deleterious DSBs upon DNA replication. Repair of these DSBs normally requires HR (Helleday, 2011; Murai et al., 2012). However, BRCA1/2-deficient cancer cells, when treated with PARP inhibitor, fail to repair these DSBs. This leads to the accumulation of unrepaired DNA breaks till over multiple rounds of replication the level of genomic instability becomes non-viable and eventually causes tumor cells to die (Fong et al., 2010). Recent clinical trials with the PARP inhibitor Olaparib have established the therapeutic potential of PARP inhibitors for BRCA1/2-deficient cancer patients (Feng et al., 2015) and this inhibitor was recently approved for clinical use.

Promising candidates for this PARP-dependent synthetic lethality approach are chromatin remodelers that have recently been linked to DSB repair by HR and to tumorigenesis. For instance, cells depleted of the chromatin remodeling ATPase SMARCA5 are defective in HR and highly sensitive to PARP inhibitor treatment (Smeenk et al., 2013). Furthermore, loss of functional SMARCA5 was found in various cancer cell types (Cetin et

al., 2008; Sumegi et al., 2011), raising the opportunity to treat these cancer cells with PARP inhibitor to induce their cell death. Additionally, loss of the chromatin remodeler CHD4 has also been shown to give rise to significant sensitivity to PARP inhibition as a consequence of defective HR repair (Pan et al., 2012). Remarkably, the expression of CHD4 is lost in about 50% of investigated gastric cancers (Kim et al., 2011), which may sensitize these cancer cells towards PARP inhibitor treatment.

Furthermore, also histone modifiers have recently been identified as promising candidates for PARPi treatment. USP26 and USP37 are two DUBs that regulate RAP80-dependent BRCA1 assembly by reversing RNF168-induced histone H2A(X) ubiquitylation at sites of DNA damage (Typas et al., 2015). Decreased and increased expression of these DUBs lead to defective HR (Typas et al., 2015), and accordingly knockdown of either DUB renders cells sensitive to PARP inhibition. Interestingly, numerous cancer cell lines with decreased or excessive expression of one of these DUBs exist as published in the COSMIC database. As such, these tumors may display defects in HR and sensitivity towards PARP inhibitors. However, since USP37 depletion only results in moderate PARP sensitivity (Typas et al., 2015) patient benefits could be modest with regard to tumor cell death. In this respect it is interesting to note that USP26-deficient cells are almost as sensitive to PARP inhibitor treatment as BRCA1/2-deficient cells (Typas et al., 2015), suggesting that targeting USP26-defects rather than USP37-defects by using PARP inhibitor treatment may be a more promising strategy.

Remarkably, also aberrant levels of epigenetic chromatin modifications have been linked to the development and maintenance of cancer. These (primarily histone) modifications can determine phenotypic characteristics of diseases in a manner that is independent of the patient's genotype. The reversible nature of such epigenetic alterations can provide opportunities for pharmacologically targeted cancer therapies that employ small-molecule inhibitors. Reversing the enzymatic activity of such histone-modifiers can for instance (re-)direct transcriptional processes and (re)activate epigenetically silenced genes in cancer cells. Accordingly, research has focussed on the application of inhibitors of HATs, HDACs, histone methyltransferases and demethylases in cancer therapy (Biancotto et al., 2010). Promising compounds have been found of which some received approval for patient treatment by the US Food and Drug Administration. However, in spite of this achievement it is important to note that clinical responses appeared to be pleiotropic when inhibiting a whole class of enzymes (such as HDACs) (Biancotto et al., 2010) causing unwanted side-effects. Consequently, the development of more specific inhibitors of epigenetic modifiers is a high priority in research. This has been fruitful for instance in the case of HDAC inhibitors, from which an effective anticancer drug (Romidepsin) to cutaneous T-cell lymphomas was generated. Upon Romidepsin-mediated inhibition of HDACs in these cells, acetylation levels of histones and non-histone proteins are maintained, which promote transcriptionally active DNA. The latter can lead to the restoration of gene expression of silenced genes and subsequently inhibited cancer progression (Barbarotta and Hurley, 2015). Furthermore, HDAC inhibitors can induce cell cycle arrest as well as apoptosis and suppress DNA repair through the acetylation or down regulation of DDR genes. The latter effect can be further exploited to increase the lethal effect of HDAC inhibitors on cancer cells when combining the HDAC inhibitor treatment with chemotherapy or radiation (Lakshmaiah et al., 2014).

Specific inhibitors targeting chromatin modifiers can nowadays be used for a cancer treatment approach referred to as personalized medicine, which thrives to identify the genetic background of a patient and unravel the altered biology of their tumor. This information will help clinicians to customize the treatment to each patient's needs and although this

approach sounds very promising, a few drawbacks are still to be overcome. Deciphering the genetic variation(s) in patient tumor cells via genotyping and the subsequent treatment are for example still rather expensive. In addition and more importantly, despite the amount of available genetic information gathered in the last decades, we still lack knowledge of the consequences of (the identified) mutations in cancer cells. Since a significant portion of such mutations have been found in histone modifiers and chromatin remodelers involved in the DDR, mechanistic apprehension of their function can help to define the effect of mutations. We and others are investigating the role of chromatin modifiers in the DDR upon suppression of gene expression, which is a well-defined experimental setting and the easiest to imitate in cell culture. However, whether a mutation in a histone modifier or chromatin remodeler causes complete loss of gene activity in tumor tissue remains questionable and requires further investigation. Eventually, this knowledge will contribute to our understanding of the DDR and could explain the cause of diseases arising from aberrant activity of chromatin modifiers due to (epi-)genetic defects. This fundamental research should eventually contribute to the identification of appropriate targets for future therapies and the development of novel treatment approaches for various human diseases such as cancer.

AIMS AND OUTLINE OF THIS THESIS

Upon the induction of DNA damage, cells initiate a protective response, referred to as the DNA damage response (DDR), to repair DNA damage and maintain genome integrity. This response is driven and regulated by posttranslational protein modifications and chromatin remodeling events. Mutations or aberrant expression of chromatin modifying proteins not only impacts on the DDR, but also causes human diseases with severe clinical phenotypes, illustrating the importance of these proteins for genome stability maintenance and human health. Largely unclear is, however, which and how chromatin modifying enzymes control the complex DDR pathways and in this manner prevent the onset of disease. To this end, we employed cross-disciplinary approaches that combined cell biological, biochemical and microscopic methods to identify histone modifying enzymes, chromatin remodelers as well as other DDR proteins and elucidate their mechanistic role in the response to DNA double-strand breaks (DSBs) and disease prevention.

Chapter 1 comprises a general introduction and reviews the current knowledge on DDR pathways, in particular pathways that respond to DSBs and the role of chromatin modifying enzymes therein. In **Chapter 2**, I introduce the set-up of a siRNA-based screening approach that I used to identify novel chromatin regulators involved in the DSB response. This screen identified the histone methyltransferase EHMT1 as a negative regulator of 53BP1 recruitment to sites of DNA breaks and presents the first evidence for a role in DSB repair by HR and NHEJ. **Chapter 3** addresses the role of the Remodeling and spacing factor 1 (RSF1) during DSB repair via NHEJ. RSF1 deposits the centromeric proteins CENP-S and CENP-X at DSBs. These factors subsequently promote the recruitment of XRCC4 and consequently efficient NHEJ. Additionally, the DNA damage-dependent SUMOylation of RSF1 is presented in **Chapter 4**. The so far obtained data suggests that SUMOylated RSF1 regulates XRCC4 recruitment and possibly NHEJ. In **Chapter 5** I show that ZBTB24, which is mutated in Immunodeficiency, facial anomalies and centromeric instability 2 (ICF2), interacts with key factors of the NHEJ pathway, namely PARP1 and DNA-PKcs. Moreover, I demonstrate that ZBTB24 promotes XRCC4/LIG4 binding, most likely to PARP1 by binding and protecting PARP1-associated PAR chains, facilitating DSB repair via NHEJ. Importantly, ZBTB24's role in NHEJ is required for NHEJ-mediated immunoglobulin class switch recombination (CSR) in B cells, which provides a molecular basis for the immunodeficiency in ICF2 syndrome. Finally, in **Chapter 6**, I generally discuss the implications of the presented studies described in this thesis.

REFERENCES

1. Acs, K., Luijsterburg, M.S., Ackermann, L., Salomons, F.A., Hoppe, T., and Dantuma, N.P. (2011). The AAA-ATPase VCP/p97 promotes 53BP1 recruitment by removing L3MBTL1 from DNA double-strand breaks. *Nat. Struct. Mol. Biol.* 18, 1345-1350.
2. Ahel, D., Horejsi, Z., Wiechens, N., Polo, S.E., Garcia-Wilson, E., Ahel, I., Flynn, H., Skehel, M., West, S.C., Jackson, S.P., Owen-Hughes, T., and Boulton, S.J. (2009). Poly(ADP-ribose)-dependent regulation of DNA repair by the chromatin remodeling enzyme ALC1. *Science* 325, 1240-1243.
3. Ahel, I., Ahel, D., Matsusaka, T., Clark, A.J., Pines, J., Boulton, S.J., and West, S.C. (2008). Poly(ADP-ribose)-binding zinc finger motifs in DNA repair/checkpoint proteins. *Nature* 451, 81-85.
4. Ahnesorg, P., Smith, P., and Jackson, S.P. (2006). XLF interacts with the XRCC4-DNA ligase IV complex to promote DNA nonhomologous end-joining. *Cell* 124, 301-313.
5. Alatwi, H.E. and Downs, J.A. (2015). Removal of H2A.Z by INO80 promotes homologous recombination. *EMBO Rep.* 16, 986-994.
6. Altmeyer, M., Messner, S., Hassa, P.O., Fey, M., and Hottiger, M.O. (2009). Molecular mechanism of poly(ADP-ribosylation) by PARP1 and identification of lysine residues as ADP-ribose acceptor sites. *Nucleic Acids Res.* 37, 3723-3738.
7. Awad, S., Ryan, D., Prochasson, P., Owen-Hughes, T., and Hassan, A.H. (2010). The Snf2 homolog Fun30 acts as a homodimeric ATP-dependent chromatin-remodeling enzyme. *J. Biol. Chem.* 285, 9477-9484.
8. Ayrapetov, M.K., Gursoy-Yuzugullu, O., Xu, C., Xu, Y., and Price, B.D. (2014). DNA double-strand breaks promote methylation of histone H3 on lysine 9 and transient formation of repressive chromatin. *Proc. Natl. Acad. Sci. U. S. A.* 111, 9169-9174.
9. Baer, R. and Ludwig, T. (2002). The BRCA1/BARD1 heterodimer, a tumor suppressor complex with ubiquitin E3 ligase activity. *Curr. Opin. Genet. Dev.* 12, 86-91.
10. Banting, G.S., Barak, O., Ames, T.M., Burnham, A.C., Kardel, M.D., Cooch, N.S., Davidson, C.E., Godbout, R., McDermid, H.E., and Shiekhattar, R. (2005). CECR2, a protein involved in neurulation, forms a novel chromatin remodeling complex with SNF2L. *Hum. Mol. Genet.* 14, 513-524.
11. Barak, O., Lazzaro, M.A., Lane, W.S., Speicher, D.W., Picketts, D.J., and Shiekhattar, R. (2003). Isolation of human NURF: a regulator of Engrailed gene expression. *EMBO J.* 22, 6089-6100.
12. Barbarotta, L. and Hurley, K. (2015). Romidepsin for the Treatment of Peripheral T-Cell Lymphoma. *J. Adv. Pract. Oncol.* 6, 22-36.
13. Barnes, D.E., Stamp, G., Rosewell, I., Denzel, A., and Lindahl, T. (1998). Targeted disruption of the gene encoding DNA ligase IV leads to lethality in embryonic mice. *Curr. Biol.* 8, 1395-1398.
14. Barnett, C. and Krebs, J.E. (2011). WSTF does it all: a multifunctional protein in transcription, repair, and replication. *Biochem. Cell Biol.* 89, 12-23.
15. Beck, C., Boehler, C., Guirouilh, B.J., Bonnet, M.E., Illuzzi, G., Ronde, P., Gauthier, L.R., Magroun, N., Rajendran, A., Lopez, B.S., Scully, R., Boussin, F.D., Schreiber, V., and Dantzer, F. (2014). PARP3 affects the relative contribution of homologous recombination and nonhomologous end-joining pathways. *Nucleic Acids Res.* 42, 5616-5632.
16. Bekker-Jensen, S. and Mailand, N. (2010). Assembly and function of DNA double-strand break repair foci in mammalian cells. *DNA Repair (Amst)* 9, 1219-1228.
17. Bekker-Jensen, S., Rendtlew, D.J., Fugger, K., Gromova, I., Nerstedt, A., Lukas, C., Bartek, J., Lukas, J., and Mailand, N. (2010). HERC2 coordinates ubiquitin-dependent assembly of DNA repair factors on damaged chromosomes. *Nat. Cell Biol.* 12, 80-86.
18. Bergink, S. and Jentsch, S. (2009). Principles of ubiquitin and SUMO modifications in DNA repair. *Nature* 458, 461-467.
19. Bernier-Villamor, V., Sampson, D.A., Matunis, M.J., and Lima, C.D. (2002). Structural basis for E2-mediated SUMO conjugation revealed by a complex between ubiquitin-conjugating enzyme Ubc9 and RanGAP1. *Cell* 108, 345-356.
20. Biancotto, C., Frige, G., and Minucci, S. (2010). Histone modification therapy of cancer. *Adv. Genet.* 70, 341-386.
21. Birger, Y., Catez, F., Furusawa, T., Lim, J.H., Prymakowska-Bosak, M., West, K.L., Postnikov, Y.V., Haines, D.C., and Bustin, M. (2005). Increased tumorigenicity and sensitivity to ionizing radiation upon loss of chromosomal protein HMG1. *Cancer Res.* 65, 6711-6718.
22. Bleuyard, J.Y., Buisson, R., Masson, J.Y., and Esashi, F. (2012). ChAM, a novel motif that mediates PALB2 intrinsic chromatin binding and facilitates DNA repair. *EMBO Rep.* 13, 135-141.
23. Boehler, C., Gauthier, L.R., Mortusewicz, O., Biard, D.S., Saliou, J.M., Bresson, A., Sanglier-Cianferani, S., Smith, S., Schreiber, V., Boussin, F., and Dantzer, F. (2011). Poly(ADP-ribose) polymerase 3 (PARP3), a newcomer in cellular response to DNA damage and mitotic progression. *Proc. Natl. Acad. Sci. U. S. A.* 108, 2783-2788.
24. Botuyan, M.V., Lee, J., Ward, J.M., Kim, J.E., Thompson, J.R., Chen, J., and Mer, G. (2006). Structural basis for the methylation state-specific recognition of histone H4-K20 by 53BP1 and Crb2 in DNA repair. *Cell* 127, 1361-1373.
25. Brown, J.S. and Jackson, S.P. (2015). Ubiquitylation, neddylation and the DNA damage response. *Open. Biol.* 5.
26. Buck, D., Malivert, L., de Chasseval, R., Barraud, A., Fondaneche, M.C., Sanal, O., Plebani, A., Stephan, J.L., Hufnagel, M., le Deist, F., Fischer, A., Durandy, A., de Villartay, J.P., and Revy, P. (2006). Cernunnos, a novel nonhomologous end-joining factor, is mutated in human immunodeficiency with microcephaly. *Cell* 124, 287-299.
27. Buis, J., Stoneham, T., Sphelski, E., and Ferguson, D.O. (2012). Mre11 regulates CtIP-dependent double-strand break repair by

- interaction with CDK2. *Nat. Struct. Mol. Biol.* 19, 246-252.
28. Burma,S., Chen,B.P., Murphy,M., Kurimasa,A., and Chen,D.J. (2001). ATM phosphorylates histone H2AX in response to DNA double-strand breaks. *J. Biol. Chem.* 276, 42462-42467.
 29. Butler,L.R., Densham,R.M., Jia,J., Garvin,A.J., Stone,H.R., Shah,V., Weekes,D., Festy,F., Beesley,J., and Morris,J.R. (2012). The proteasomal de-ubiquitinating enzyme POH1 promotes the double-strand DNA break response. *EMBO J.* 31, 3918-3934.
 30. Callen,E., Di,V.M., Kruhlik,M.J., Nieto-Soler,M., Wong,N., Chen,H.T., Faryabi,R.B., Polato,F., Santos,M., Starnes,L.M., Wesemann,D.R., Lee,J.E., Tubbs,A., Sleckman,B.P., Daniel,J.A., Ge,K., Alt,F.W., Fernandez-Capetillo,O., Nussenzweig,M.C., and Nussenzweig,A. (2013). 53BP1 mediates productive and mutagenic DNA repair through distinct phosphoprotein interactions. *Cell* 153, 1266-1280.
 31. Cetin,E., Cengiz,B., Gunduz,E., Gunduz,M., Nagatsuka,H., Bekir-Beder,L., Fukushima,K., Pehlivan,D., MO,N., Nishizaki,K., Shimizu,K., and Nagai,N. (2008). Deletion mapping of chromosome 4q22-35 and identification of four frequently deleted regions in head and neck cancers. *Neoplasma* 55, 299-304.
 32. Cha,H., Lowe,J.M., Li,H., Lee,J.S., Belova,G.I., Bulavin,D.V., and Fornace,A.J., Jr. (2010). Wip1 directly dephosphorylates gamma-H2AX and attenuates the DNA damage response. *Cancer Res.* 70, 4112-4122.
 33. Chambers,A.L. and Downs,J.A. (2012). The RSC and INO80 chromatin-remodeling complexes in DNA double-strand break repair. *Prog. Mol. Biol. Transl. Sci.* 110, 229-261.
 34. Chaplet,M., Rai,R., Jackson-Bernitsas,D., Li,K., and Lin,S.Y. (2006). BRIT1/MCPH1: a guardian of genome and an enemy of tumors. *Cell Cycle* 5, 2579-2583.
 35. Chapman,J.R., Barral,P., Vannier,J.B., Borel,V., Steger,M., Tomas-Loba,A., Sartori,A.A., Adams,I.R., Batista,F.D., and Boulton,S.J. (2013). RIF1 is essential for 53BP1-dependent nonhomologous end joining and suppression of DNA double-strand break resection. *Mol. Cell* 49, 858-871.
 36. Chaudhuri,J. and Alt,F.W. (2004). Class-switch recombination: interplay of transcription, DNA deamination and DNA repair. *Nat. Rev. Immunol.* 4, 541-552.
 37. Chen,J., Feng,W., Jiang,J., Deng,Y., and Huen,M.S. (2012a). Ring finger protein RNF169 antagonizes the ubiquitin-dependent signaling cascade at sites of DNA damage. *J. Biol. Chem.* 287, 27715-27722.
 38. Chen,T.J., Huang,S.C., Huang,H.Y., Wei,Y.C., and Li,C.F. (2011). Rsf-1/HBXAP overexpression is associated with disease-specific survival of patients with gallbladder carcinoma. *APMIS* 119, 808-814.
 39. Chen,X., Cui,D., Papusha,A., Zhang,X., Chu,C.D., Tang,J., Chen,K., Pan,X., and Ira,G. (2012b). The Fun30 nucleosome remodeller promotes resection of DNA double-strand break ends. *Nature* 489, 576-580.
 40. Cheng,W., Su,Y., and Xu,F. (2013). CHD1L: a novel oncogene. *Mol. Cancer* 12, 170.
 41. Chenier,S., Yoon,G., Argiropoulos,B., Lauzon,J., Laframboise,R., Ahn,J.W., Ogilvie,C.M., Lionel,A.C., Marshall,C.R., Vaags,A.K., Hashemi,B., Boisvert,K., Mathonnet,G., Tihy,F., So,J., Scherer,S.W., Lemyre,E., and Stavropoulos,D.J. (2014). CHD2 haploinsufficiency is associated with developmental delay, intellectual disability, epilepsy and neurobehavioural problems. *J. Neurodev. Disord.* 6, 9.
 42. Cheutin,T., McNairn,A.J., Jenuwein,T., Gilbert,D.M., Singh,P.B., and Misteli,T. (2003). Maintenance of stable heterochromatin domains by dynamic HP1 binding. *Science* 299, 721-725.
 43. Chou,D.M., Adamson,B., Dephoure,N.E., Tan,X., Nottke,A.C., Hurov,K.E., Gygi,S.P., Colaiacovo,M.P., and Elledge,S.J. (2010). A chromatin localization screen reveals poly (ADP ribose)-regulated recruitment of the repressive polycomb and NuRD complexes to sites of DNA damage. *Proc. Natl. Acad. Sci. U. S. A* 107, 18475-18480.
 44. Chowdhury,D., Xu,X., Zhong,X., Ahmed,F., Zhong,J., Liao,J., Dykxhoorn,D.M., Weinstock,D.M., Pfeifer,G.P., and Lieberman,J. (2008). A PP4-phosphatase complex dephosphorylates gamma-H2AX generated during DNA replication. *Mol. Cell* 31, 33-46.
 45. Chrzanowska,K.H., Gregorek,H., Dembowska-Baginska,B., Kalina,M.A., and Digweed,M. (2012). Nijmegen breakage syndrome (NBS). *Orphanet. J. Rare. Dis.* 7, 13.
 46. Ciccio,A. and Elledge,S.J. (2010). The DNA damage response: making it safe to play with knives. *Mol. Cell* 40, 179-204.
 47. Clapier,C.R. and Cairns,B.R. (2009). The biology of chromatin remodeling complexes. *Annu. Rev. Biochem.* 78, 273-304.
 48. Coleman,K.A. and Greenberg,R.A. (2011). The BRCA1-RAP80 complex regulates DNA repair mechanism utilization by restricting end resection. *J. Biol. Chem.* 286, 13669-13680.
 49. Cook,P.J., Ju,B.G., Telese,F., Wang,X., Glass,C.K., and Rosenfeld,M.G. (2009). Tyrosine dephosphorylation of H2AX modulates apoptosis and survival decisions. *Nature* 458, 591-596.
 50. Costelloe,T., Louge,R., Tomimatsu,N., Mukherjee,B., Martini,E., Khadaroo,B., Dubois,K., Wiegant,W.W., Thierry,A., Burma,S., van Attikum,H., and Llorente,B. (2012). The yeast Fun30 and human SMARCAD1 chromatin remodellers promote DNA end resection. *Nature* 489, 581-584.
 51. Courilleau,C., Chailleux,C., Jauneau,A., Grimal,F., Briois,S., Boutet-Robinet,E., Boudsocq,F., Trouche,D., and Canitrot,Y. (2012). The chromatin remodeler p400 ATPase facilitates Rad51-mediated repair of DNA double-strand breaks. *J. Cell Biol.* 199, 1067-1081.
 52. Dai,Y., Kysela,B., Hanakahi,L.A., Manolis,K., Riballo,E., Stumm,M., Harville,T.O., West,S.C., Oettinger,M.A., and Jeggo,P.A. (2003). Nonhomologous end joining and V(D)J recombination require an additional factor. *Proc. Natl. Acad. Sci. U. S. A* 100,

- 2462-2467.
53. Danielsen,J.R., Povlsen,L.K., Villumsen,B.H., Streicher,W., Nilsson,J., Wikstrom,M., Bekker-Jensen,S., and Mailand,N. (2012). DNA damage-inducible SUMOylation of HERC2 promotes RNF8 binding via a novel SUMO-binding Zinc finger. *J. Cell Biol.* 197, 179-187.
 54. Das,C., Lucia,M.S., Hansen,K.C., and Tyler,J.K. (2009). CBP/p300-mediated acetylation of histone H3 on lysine 56. *Nature* 459, 113-117.
 55. De Boer,J. and Hoeijmakers,J.H. (2000). Nucleotide excision repair and human syndromes. *Carcinogenesis* 21, 453-460.
 56. de Bruin,C., Mericq,V., Andrew,S.F., van Duyvenvoorde,H.A., Verkaik,N.S., Losekoot,M., Porollo,A., Garcia,H., Kuang,Y., Hanson,D., Clayton,P., van Gent,D.C., Wit,J.M., Hwa,V., and Dauber,A. (2015). An XRCC4 splice mutation associated with severe short stature, gonadal failure, and early-onset metabolic syndrome. *J. Clin. Endocrinol. Metab* 100, E789-E798.
 57. Desterro,J.M., Rodriguez,M.S., Kemp,G.D., and Hay,R.T. (1999). Identification of the enzyme required for activation of the small ubiquitin-like protein SUMO-1. *J. Biol. Chem.* 274, 10618-10624.
 58. Devgan,S.S., Sanal,O., Doil,C., Nakamura,K., Nahas,S.A., Pettijohn,K., Bartek,J., Lukas,C., Lukas,J., and Gatti,R.A. (2011). Homozygous deficiency of ubiquitin-ligase ring-finger protein RNF168 mimics the radiosensitivity syndrome of ataxia-telangiectasia. *Cell Death. Differ.* 18, 1500-1506.
 59. Doil,C., Mailand,N., Bekker-Jensen,S., Menard,P., Larsen,D.H., Pepperkok,R., Ellenberg,J., Panier,S., Durocher,D., Bartek,J., Lukas,J., and Lukas,C. (2009). RNF168 binds and amplifies ubiquitin conjugates on damaged chromosomes to allow accumulation of repair proteins. *Cell* 136, 435-446.
 60. Dong,S., Han,J., Chen,H., Liu,T., Huen,M.S., Yang,Y., Guo,C., and Huang,J. (2014). The human SRCAP chromatin remodeling complex promotes DNA-end resection. *Curr. Biol.* 24, 2097-2110.
 61. Douglas,P., Zhong,J., Ye,R., Moorhead,G.B., Xu,X., and Lees-Miller,S.P. (2010). Protein phosphatase 6 interacts with the DNA-dependent protein kinase catalytic subunit and dephosphorylates gamma-H2AX. *Mol. Cell Biol.* 30, 1368-1381.
 62. Downs,J.A., Allard,S., Jobin-Robitaille,O., Javaheri,A., Auger,A., Bouchard,N., Kron,S.J., Jackson,S.P., and Cote,J. (2004). Binding of chromatin-modifying activities to phosphorylated histone H2A at DNA damage sites. *Mol. Cell* 16, 979-990.
 63. Doyon,Y. and Cote,J. (2004). The highly conserved and multifunctional NuA4 HAT complex. *Curr. Opin. Genet. Dev.* 14, 147-154.
 64. Dulev,S., Tkach,J., Lin,S., and Batada,N.N. (2014). SET8 methyltransferase activity during the DNA double-strand break response is required for recruitment of 53BP1. *EMBO Rep.* 15, 1163-1174.
 65. Durrant,L.G. and Boyle,J.M. (1982). Potentiation of cell killing by inhibitors of poly(ADP-ribose) polymerase in four rodent cell lines exposed to N-methyl-N-nitrosourea or UV light. *Chem. Biol. Interact.* 38, 325-338.
 66. Dutranoy,V., Demuth,I., Baumann,U., Schindler,D., Konrat,K., Neitzel,H., Gillessen-Kaesbach,G., Radszewski,J., Rothe,S., Schellenberger,M.T., Nurnberg,G., Nurnberg,P., Teik,K.W., Nallusamy,R., Reis,A., Sperling,K., Digweed,M., and Varon,R. (2010). Clinical variability and novel mutations in the NHEJ1 gene in patients with a Nijmegen breakage syndrome-like phenotype. *Hum. Mutat.* 31, 1059-1068.
 67. Eapen,V.V., Sugawara,N., Tsaabar,M., Wu,W.H., and Haber,J.E. (2012). The *Saccharomyces cerevisiae* chromatin remodeler Fun30 regulates DNA end resection and checkpoint deactivation. *Mol. Cell Biol.* 32, 4727-4740.
 68. El-Khamisy,S.F., Masutani,M., Suzuki,H., and Caldecott,K.W. (2003). A requirement for PARP-1 for the assembly or stability of XRCC1 nuclear foci at sites of oxidative DNA damage. *Nucleic Acids Res.* 31, 5526-5533.
 69. Erdel,F. and Rippe,K. (2011). Chromatin remodelling in mammalian cells by ISWI-type complexes--where, when and why? *FEBS J.* 278, 3608-3618.
 70. Escribano-Diaz,C., Orthwein,A., Fradet-Turcotte,A., Xing,M., Young,J.T., Tkac,J., Cook,M.A., Rosebrock,A.P., Munro,M., Canny,M.D., Xu,D., and Durocher,D. (2013). A cell cycle-dependent regulatory circuit composed of 53BP1-RIF1 and BRCA1-CTIP controls DNA repair pathway choice. *Mol. Cell* 49, 872-883.
 71. Facchino,S., Abdouh,M., Chato,W., and Bernier,G. (2010). BMI1 confers radioresistance to normal and cancerous neural stem cells through recruitment of the DNA damage response machinery. *J. Neurosci.* 30, 10096-10111.
 72. Feng,F.Y., de Bono,J.S., Rubin,M.A., and Knudsen,K.E. (2015). Chromatin to Clinic: The Molecular Rationale for PARP1 Inhibitor Function. *Mol. Cell* 58, 925-934.
 73. Fernandez-Capetillo,O., Chen,H.T., Celeste,A., Ward,I., Romanienko,P.J., Morales,J.C., Naka,K., Xia,Z., Camerini-Otero,R.D., Motoyama,N., Carpenter,P.B., Bonner,W.M., Chen,J., and Nussenzweig,A. (2002). DNA damage-induced G2-M checkpoint activation by histone H2AX and 53BP1. *Nat. Cell Biol.* 4, 993-997.
 74. Flotho,A. and Melchior,F. (2013). Sumoylation: a regulatory protein modification in health and disease. *Annu. Rev. Biochem.* 82, 357-385.
 75. Fnu,S., Williamson,E.A., De Haro,L.P., Brenneman,M., Wray,J., Shaheen,M., Radhakrishnan,K., Lee,S.H., Nickoloff,J.A., and Hromas,R. (2011). Methylation of histone H3 lysine 36 enhances DNA repair by nonhomologous end-joining. *Proc. Natl. Acad. Sci. U. S. A* 108, 540-545.
 76. Fong,P.C., Yap,T.A., Boss,D.S., Carden,C.P., Mergui-Roelvink,M., Gourley,C., De Greve,J., Lubinski,J., Shanley,S., Messiou,C., A'Hern,R., Tutt,A., Ashworth,A., Stone,J., Carmichael,J., Schellens,J.H., de Bono,J.S., and Kaye,S.B. (2010). Poly(ADP-ribose) polymerase inhibition: frequent durable responses in BRCA carrier ovarian cancer correlating with platinum-free interval. *J.*

- Clin. Oncol. 28, 2512-2519.
77. Fradet-Turcotte, A., Canny, M.D., Escrbano-Diaz, C., Orthwein, A., Leung, C.C., Huang, H., Landry, M.C., Kitevski-LeBlanc, J., Noordermeer, S.M., Sicheri, F., and Durocher, D. (2013). 53BP1 is a reader of the DNA-damage-induced H2A Lys 15 ubiquitin mark. *Nature* 499, 50-54.
 78. Frank, K.M., Sekiguchi, J.M., Seidl, K.J., Swat, W., Rathbun, G.A., Cheng, H.L., Davidson, L., Kangaloo, L., and Alt, F.W. (1998). Late embryonic lethality and impaired V(D)J recombination in mice lacking DNA ligase IV. *Nature* 396, 173-177.
 79. Galanty, Y., Belotserkovskaya, R., Coates, J., and Jackson, S.P. (2012). RNF4, a SUMO-targeted ubiquitin E3 ligase, promotes DNA double-strand break repair. *Genes Dev.* 26, 1179-1195.
 80. Galanty, Y., Belotserkovskaya, R., Coates, J., Polo, S., Miller, K.M., and Jackson, S.P. (2009). Mammalian SUMO E3-ligases PIAS1 and PIAS4 promote responses to DNA double-strand breaks. *Nature* 462, 935-939.
 81. Gao, Y., Sun, Y., Frank, K.M., Dikkes, P., Fujiwara, Y., Seidl, K.J., Sekiguchi, J.M., Rathbun, G.A., Swat, W., Wang, J., Bronson, R.T., Malynn, B.A., Bryans, M., Zhu, C., Chaudhuri, J., Davidson, L., Ferrini, R., Stamoto, T., Orkin, S.H., Greenberg, M.E., and Alt, F.W. (1998). A critical role for DNA end-joining proteins in both lymphogenesis and neurogenesis. *Cell* 95, 891-902.
 82. Gatti, M., Pinato, S., Maiolica, A., Rocchio, F., Prato, M.G., Aebersold, R., and Penengo, L. (2015). RNF168 promotes noncanonical K27 ubiquitination to signal DNA damage. *Cell Rep.* 10, 226-238.
 83. Gibson, B.A. and Kraus, W.L. (2012). New insights into the molecular and cellular functions of poly(ADP-ribose) and PARPs. *Nat. Rev. Mol. Cell Biol.* 13, 411-424.
 84. Gigeck, C.O., Lisboa, L.C., Leal, M.F., Silva, P.N., Lima, E.M., Khayat, A.S., Assumpcao, P.P., Burbano, R.R., and Smith, M.A. (2011). SMARCA5 methylation and expression in gastric cancer. *Cancer Invest* 29, 162-166.
 85. Ginjala, V., Nacerddine, K., Kulkarni, A., Oza, J., Hill, S.J., Yao, M., Citterio, E., van Lohuizen, M., and Ganesan, S. (2011). BMI1 is recruited to DNA breaks and contributes to DNA damage-induced H2A ubiquitination and repair. *Mol. Cell Biol.* 31, 1972-1982.
 84. Gladkowska-Dura, M., Dzierzanowska-Fangrat, K., Dura, W.T., van Krieken, J.H., Chrzanowska, K.H., van Dongen, J.J., and Langerak, A.W. (2008). Unique morphological spectrum of lymphomas in Nijmegen breakage syndrome (NBS) patients with high frequency of consecutive lymphoma formation. *J. Pathol.* 216, 337-344.
 85. Goodarzi, A.A., Kurka, T., and Jeggo, P.A. (2011). KAP-1 phosphorylation regulates CHD3 nucleosome remodeling during the DNA double-strand break response. *Nat. Struct. Mol. Biol.* 18, 831-839.
 86. Goodarzi, A.A., Noon, A.T., Deckbar, D., Ziv, Y., Shiloh, Y., Lobrich, M., and Jeggo, P.A. (2008). ATM signaling facilitates repair of DNA double-strand breaks associated with heterochromatin. *Mol. Cell* 31, 167-177.
 87. Gospodinov, A., Vaissiere, T., Krastev, D.B., Legube, G., Anachkova, B., and Herceg, Z. (2011). Mammalian Ino80 mediates double-strand break repair through its role in DNA end strand resection. *Mol. Cell Biol.* 31, 4735-4745.
 88. Gottschalk, A.J., Timinsky, G., Kong, S.E., Jin, J., Cai, Y., Swanson, S.K., Washburn, M.P., Florens, L., Ladurner, A.G., Conaway, J.W., and Conaway, R.C. (2009). Poly(ADP-ribosyl)ation directs recruitment and activation of an ATP-dependent chromatin remodeler. *Proc. Natl. Acad. Sci. U. S. A.* 106, 13770-13774.
 89. Grocock, L.M., Nie, M., Prudden, J., Moiani, D., Wang, T., Cheltsov, A., Rambo, R.P., Arvai, A.S., Hitomi, C., Tainer, J.A., Luger, K., Perry, J.J., Lazzarini-Denchi, E., and Boddy, M.N. (2014). RNF4 interacts with both SUMO and nucleosomes to promote the DNA damage response. *EMBO Rep.* 15, 601-608.
 90. Grune, T., Brzeski, J., Eberharter, A., Clapier, C.R., Corona, D.F., Becker, P.B., and Muller, C.W. (2003). Crystal structure and functional analysis of a nucleosome recognition module of the remodeling factor ISWI. *Mol. Cell* 12, 449-460.
 92. Guo, C., Nakazawa, Y., Woodbine, L., Bjorkman, A., Shimada, M., Fawcett, H., Jia, N., Ohyama, K., Li, T.S., Nagayama, Y., Mitsutake, N., Pan-Hammarstrom, Q., Gennery, A.R., Lehmann, A.R., Jeggo, P.A., and Ogi, T. (2015). XRCC4 deficiency in human subjects causes a marked neurological phenotype but no overt immunodeficiency. *J. Allergy Clin. Immunol.*
 93. Gupta, A., Hunt, C.R., Hegde, M.L., Chakraborty, S., Chakraborty, S., Udayakumar, D., Horikoshi, N., Singh, M., Ramnarain, D.B., Hittelman, W.N., Namjoshi, S., Asaithamby, A., Hazra, T.K., Ludwig, T., Pandita, R.K., Tyler, J.K., and Pandita, T.K. (2014). MOF phosphorylation by ATM regulates 53BP1-mediated double-strand break repair pathway choice. *Cell Rep.* 8, 177-189.
 94. Hartlerode, A.J., Guan, Y., Rajendran, A., Ura, K., Schotta, G., Xie, A., Shah, J.V., and Scully, R. (2012). Impact of histone H4 lysine 20 methylation on 53BP1 responses to chromosomal double strand breaks. *PLoS. One.* 7, e49211.
 95. Hashizume, R., Fukuda, M., Maeda, I., Nishikawa, H., Oyake, D., Yabuki, Y., Ogata, H., and Ohta, T. (2001). The RING heterodimer BRCA1-BARD1 is a ubiquitin ligase inactivated by a breast cancer-derived mutation. *J. Biol. Chem.* 276, 14537-14540.
 96. Hay, R.T. (2005). SUMO: a history of modification. *Mol. Cell* 18, 1-12.
 97. Helleday, T. (2011). The underlying mechanism for the PARP and BRCA synthetic lethality: clearing up the misunderstandings. *Mol. Oncol.* 5, 387-393.
 98. Hendriks, I.A., D'Souza, R.C., Yang, B., Verlaan-de Vries, M., Mann, M., and Vertegaal, A.C. (2014). Uncovering global SUMOylation signaling networks in a site-specific manner. *Nat. Struct. Mol. Biol.* 21, 927-936.
 99. Hickey, C.M., Wilson, N.R., and Hochstrasser, M. (2012). Function and regulation of SUMO proteases. *Nat. Rev. Mol. Cell Biol.* 13, 755-766.
 100. Hsiao, K.Y. and Mizzen, C.A. (2013). Histone H4 deacetylation facilitates 53BP1 DNA damage signaling and double-strand break repair. *J. Mol. Cell Biol.* 5, 157-165.

101. Hsu,P., Ma,A., Barnes,E.H., Wilson,M., Hoefsloot,L.H., Rinne,T., Munns,C., Williams,G., Wong,M., and Mehr,S. (2015). The Immune Phenotype of Patients with CHARGE Syndrome. *J. Allergy Clin. Immunol. Pract.*
102. Hu,X., Paul,A., and Wang,B. (2012). Rap80 protein recruitment to DNA double-strand breaks requires binding to both small ubiquitin-like modifier (SUMO) and ubiquitin conjugates. *J. Biol. Chem.* 287, 25510-25519.
103. Hu,Y., Scully,R., Sobhian,B., Xie,A., Shestakova,E., and Livingston,D.M. (2011). RAP80-directed tuning of BRCA1 homologous recombination function at ionizing radiation-induced nuclear foci. *Genes Dev.* 25, 685-700.
104. Huen,M.S. and Chen,J. (2010). Assembly of checkpoint and repair machineries at DNA damage sites. *Trends Biochem. Sci.* 35, 101-108.
105. Huen,M.S., Grant,R., Manke,I., Minn,K., Yu,X., Yaffe,M.B., and Chen,J. (2007). RNF8 transduces the DNA-damage signal via histone ubiquitylation and checkpoint protein assembly. *Cell* 131, 901-914.
106. Iacovoni,J.S., Caron,P., Lassadi,J., Nicolas,E., Massip,L., Trouche,D., and Legube,G. (2010). High-resolution profiling of gammaH2AX around DNA double strand breaks in the mammalian genome. *EMBO J.* 29, 1446-1457.
107. Ikura,T., Tashiro,S., Kakino,A., Shima,H., Jacob,N., Amunugama,R., Yoder,K., Izumi,S., Kuraoka,I., Tanaka,K., Kimura,H., Ikura,M., Nishikubo,S., Ito,T., Muto,A., Miyagawa,K., Takeda,S., Fishel,R., Igarashi,K., and Kamiya,K. (2007). DNA damage-dependent acetylation and ubiquitination of H2AX enhances chromatin dynamics. *Mol. Cell Biol.* 27, 7028-7040.
108. Iles,N., Rulten,S., El-Khamisy,S.F., and Caldecott,K.W. (2007). APLF (C2orf13) is a novel human protein involved in the cellular response to chromosomal DNA strand breaks. *Mol. Cell Biol.* 27, 3793-3803.
109. Ismail,I.H., Andrin,C., McDonald,D., and Hendzel,M.J. (2010). BMI1-mediated histone ubiquitylation promotes DNA double-strand break repair. *J. Cell Biol.* 191, 45-60.
110. Jackson,S.P. and Bartek,J. (2009). The DNA-damage response in human biology and disease. *Nature* 461, 1071-1078.
111. Jackson,S.P. and Durocher,D. (2013). Regulation of DNA damage responses by ubiquitin and SUMO. *Mol. Cell* 49, 795-807.
112. Jenuwein,T. and Allis,C.D. (2001). Translating the histone code. *Science* 293, 1074-1080.
113. Jin,Q., Mao,X., Li,B., Guan,S., Yao,F., and Jin,F. (2015). Overexpression of SMARCA5 correlates with cell proliferation and migration in breast cancer. *Tumour. Biol.* 36, 1895-1902.
114. Johnson,E.S. (2004). Protein modification by SUMO. *Annu. Rev. Biochem.* 73, 355-382.
115. Kaidi,A. and Jackson,S.P. (2013). KAT5 tyrosine phosphorylation couples chromatin sensing to ATM signalling. *Nature* 498, 70-74.
116. Kaidi,A., Weinert,B.T., Choudhary,C., and Jackson,S.P. (2010). Human SIRT6 promotes DNA end resection through CtIP deacetylation. *Science* 329, 1348-1353.
117. Kakarougkas,A., Ismail,A., Katsuki,Y., Freire,R., Shibata,A., and Jeggo,P.A. (2013). Co-operation of BRCA1 and POH1 relieves the barriers posed by 53BP1 and RAP80 to resection. *Nucleic Acids Res.* 41, 10298-10311.
118. Kakarougkas,A. and Jeggo,P.A. (2014). DNA DSB repair pathway choice: an orchestrated handover mechanism. *Br. J. Radiol.* 87, 20130685.
119. Kanno,S., Kuzuoka,H., Sasao,S., Hong,Z., Lan,L., Nakajima,S., and Yasui,A. (2007). A novel human AP endonuclease with conserved zinc-finger-like motifs involved in DNA strand break responses. *EMBO J.* 26, 2094-2103.
120. Kashiwaba,S., Kitahashi,K., Watanabe,T., Onoda,F., Ohtsu,M., and Murakami,Y. (2010). The mammalian INO80 complex is recruited to DNA damage sites in an ARP8 dependent manner. *Biochem. Biophys. Res. Commun.* 402, 619-625.
121. Kasten,M.M., Clapier,C.R., and Cairns,B.R. (2011). SnapShot: Chromatin remodeling: SWI/SNF. *Cell* 144, 310.
122. Keogh,M.C., Kim,J.A., Downey,M., Fillingham,J., Chowdhury,D., Harrison,J.C., Onishi,M., Datta,N., Galicia,S., Emili,A.,
123. Lieberman,J., Shen,X., Buratowski,S., Haber,J.E., Durocher,D., Greenblatt,J.F., and Krogan,N.J. (2006). A phosphatase complex that dephosphorylates gammaH2AX regulates DNA damage checkpoint recovery. *Nature* 439, 497-501.
124. Kim,M.S., Chung,N.G., Kang,M.R., Yoo,N.J., and Lee,S.H. (2011). Genetic and expressional alterations of CHD genes in gastric and colorectal cancers. *Histopathology* 58, 660-668.
125. Kim,Y.C., Gerlitz,G., Furusawa,T., Catez,F., Nussenzweig,A., Oh,K.S., Kraemer,K.H., Shiloh,Y., and Bustin,M. (2009). Activation of ATM depends on chromatin interactions occurring before induction of DNA damage. *Nat. Cell Biol.* 11, 92-96.
126. Klement,K., Luijsterburg,M.S., Pinder,J.B., Cena,C.S., Del,N., V, Wintersinger,C.M., Dellaire,G., van Attikum,H., and Goodarzi,A.A. (2014). Opposing ISWI- and CHD-class chromatin remodeling activities orchestrate heterochromatic DNA repair. *J. Cell Biol.* 207, 717-733.
127. Kolas,N.K., Chapman,J.R., Nakada,S., Ylanko,J., Chahwan,R., Sweeney,F.D., Panier,S., Mendez,M., Wildenhain,J., Thomson,T.M., Pelletier,L., Jackson,S.P., and Durocher,D. (2007). Orchestration of the DNA-damage response by the RNF8 ubiquitin ligase. *Science* 318, 1637-1640.
128. Krishnan,N., Jeong,D.G., Jung,S.K., Ryu,S.E., Xiao,A., Allis,C.D., Kim,S.J., and Tonks,N.K. (2009). Dephosphorylation of the C-terminal tyrosyl residue of the DNA damage-related histone H2A.X is mediated by the protein phosphatase eyes absent. *J. Biol. Chem.* 284, 16066-16070.
129. Kruhlak,M., Crouch,E.E., Orlov,M., Montano,C., Gorski,S.A., Nussenzweig,A., Misteli,T., Phair,R.D., and Casellas,R. (2007). The ATM repair pathway inhibits RNA polymerase I transcription in response to chromosome breaks. *Nature* 447, 730-734.
130. Kwon,S.J., Park,J.H., Park,E.J., Lee,S.A., Lee,H.S., Kang,S.W., and Kwon,J. (2015). ATM-mediated phosphorylation of the

- chromatin remodeling enzyme BRG1 modulates DNA double-strand break repair. *Oncogene* 34, 303-313.
131. Lakshmaiah,K.C., Jacob,L.A., Aparna,S., Lokanatha,D., and Saldanha,S.C. (2014). Epigenetic therapy of cancer with histone deacetylase inhibitors. *J. Cancer Res. Ther.* 10, 469-478.
 132. Lan,L., Ui,A., Nakajima,S., Hatakeyama,K., Hoshi,M., Watanabe,R., Janicki,S.M., Ogiwara,H., Kohno,T., Kanno,S., and Yasui,A. (2010). The ACF1 complex is required for DNA double-strand break repair in human cells. *Mol. Cell* 40, 976-987.
 133. Langelier,M.F., Ruhl,D.D., Planck,J.L., Kraus,W.L., and Pascal,J.M. (2010). The Zn3 domain of human poly(ADP-ribose) polymerase-1 (PARP-1) functions in both DNA-dependent poly(ADP-ribose) synthesis activity and chromatin compaction. *J. Biol. Chem.* 285, 18877-18887.
 134. Larsen,D.H., Poinson,C., Gudjonsson,T., Dinant,C., Payne,M.R., Hari,F.J., Rendtlew Danielsen,J.M., Menard,P., Sand,J.C., Stucki,M., Lukas,C., Bartek,J., Andersen,J.S., and Lukas,J. (2010). The chromatin-remodeling factor CHD4 coordinates signaling and repair after DNA damage. *J. Cell Biol.* 190, 731-740.
 135. Lee,H.S., Park,J.H., Kim,S.J., Kwon,S.J., and Kwon,J. (2010a). A cooperative activation loop among SWI/SNF, gamma-H2AX and H3 acetylation for DNA double-strand break repair. *EMBO J.* 29, 1434-1445.
 136. Lee,J.H., Goodarzi,A.A., Jeggo,P.A., and Paull,T.T. (2010b). 53BP1 promotes ATM activity through direct interactions with the MRN complex. *EMBO J.* 29, 574-585.
 137. Li,X., Corsa,C.A., Pan,P.W., Wu,L., Ferguson,D., Yu,X., Min,J., and Dou,Y. (2010a). MOF and H4 K16 acetylation play important roles in DNA damage repair by modulating recruitment of DNA damage repair protein Mdc1. *Mol. Cell Biol.* 30, 5335-5347.
 138. Li,Y.J., Stark,J.M., Chen,D.J., Ann,D.K., and Chen,Y. (2010b). Role of SUMO:SIM-mediated protein-protein interaction in non-homologous end joining. *Oncogene* 29, 3509-3518.
 139. Lieber,M.R. (2010). The mechanism of double-strand DNA break repair by the nonhomologous DNA end-joining pathway. *Annu. Rev. Biochem.* 79, 181-211.
 140. Lin,S.Y., Rai,R., Li,K., Xu,Z.X., and Elledge,S.J. (2005). BRIT1/MCPH1 is a DNA damage responsive protein that regulates the Brca1-Chk1 pathway, implicating checkpoint dysfunction in microcephaly. *Proc. Natl. Acad. Sci. U. S. A.* 102, 15105-15109.
 141. Lindahl,T. (1993). Instability and decay of the primary structure of DNA. *Nature* 362, 709-715.
 142. Liu,C., Srihari,S., Cao,K.A., Chenevix-Trench,G., Simpson,P.T., Ragan,M.A., and Khanna,K.K. (2014). A fine-scale dissection of the DNA double-strand break repair machinery and its implications for breast cancer therapy. *Nucleic Acids Res.* 42, 6106-6127.
 143. Lok,G.T., Sy,S.M., Dong,S.S., Ching,Y.P., Tsao,S.W., Thomson,T.M., and Huen,M.S. (2012). Differential regulation of RNF8-mediated Lys48- and Lys63-based poly-ubiquitylation. *Nucleic Acids Res.* 40, 196-205.
 144. Loseva,O., Jemth,A.S., Bryant,H.E., Schuler,H., Lehtio,L., Karlberg,T., and Helleday,T. (2010). PARP-3 is a mono-ADP-ribosylase that activates PARP-1 in the absence of DNA. *J. Biol. Chem.* 285, 8054-8060.
 145. Luijsterburg,M.S., Acs,K., Ackermann,L., Wiegant,W.W., Bekker-Jensen,S., Larsen,D.H., Khanna,K.K., van Attikum,H., Mailand,N., and Dantuma,N.P. (2012). A new non-catalytic role for ubiquitin ligase RNF8 in unfolding higher-order chromatin structure. *EMBO J.* 31, 2511-2527.
 146. Luijsterburg,M.S. and van Attikum,H. (2011). Chromatin and the DNA damage response: the cancer connection. *Mol. Oncol.* 5, 349-367.
 147. Luo,K., Zhang,H., Wang,L., Yuan,J., and Lou,Z. (2012). Sumoylation of MDC1 is important for proper DNA damage response. *EMBO J.* 31, 3008-3019.
 148. Macurek,L., Lindqvist,A., Voets,O., Kool,J., Vos,H.R., and Medema,R.H. (2010). Wip1 phosphatase is associated with chromatin and dephosphorylates gammaH2AX to promote checkpoint inhibition. *Oncogene* 29, 2281-2291.
 149. Mailand,N., Bekker-Jensen,S., Fastrup,H., Melander,F., Bartek,J., Lukas,C., and Lukas,J. (2007). RNF8 ubiquitylates histones at DNA double-strand breaks and promotes assembly of repair proteins. *Cell* 131, 887-900.
 150. Mallette,F.A., Mattioli,F., Cui,G., Young,L.C., Hendzel,M.J., Mer,G., Sixma,T.K., and Richard,S. (2012). RNF8- and RNF168-dependent degradation of KDM4A/JMJD2A triggers 53BP1 recruitment to DNA damage sites. *EMBO J.* 31, 1865-1878.
 151. Mani,R.S. and Chinnaiyan,A.M. (2010). Triggers for genomic rearrangements: insights into genomic, cellular and environmental influences. *Nat. Rev. Genet.* 11, 819-829.
 152. Mao,T.L., Hsu,C.Y., Yen,M.J., Gilks,B., Sheu,J.J., Gabrielson,E., Vang,R., Cope,L., Kurman,R.J., Wang,T.L., and Shih,I. (2006). Expression of Rsf-1, a chromatin-remodeling gene, in ovarian and breast carcinoma. *Hum. Pathol.* 37, 1169-1175.
 153. Masson,M., Niedergang,C., Schreiber,V., Muller,S., Menissier-de Murcia,J., and de Murcia,G. (1998). XRCC1 is specifically associated with poly(ADP-ribose) polymerase and negatively regulates its activity following DNA damage. *Mol. Cell Biol.* 18, 3563-3571.
 154. Matic,I., Schimmel,J., Hendriks,I.A., van Santen,M.A., van de Rijke,F., van Dam,H., Gnad,F., Mann,M., and Vertegaal,A.C. (2010). Site-specific identification of SUMO-2 targets in cells reveals an inverted SUMOylation motif and a hydrophobic cluster SUMOylation motif. *Mol. Cell* 39, 641-652.
 155. Matic,I., van Hagen,M., Macek,B., Ogg,S.C., Tatham,M.H., Hay,R.T., Lamond,A.I., Mann,M., and Vertegaal,A.C. (2008). In vivo identification of human small ubiquitin-like modifier polymerization sites by high accuracy mass spectrometry and an in vitro to in vivo strategy. *Mol. Cell Proteomics.* 7, 132-144.
 156. Matsuoka,S., Ballif,B.A., Smogorzewska,A., McDonald,E.R., III, Hurov,K.E., Luo,J., Bakalarski,C.E., Zhao,Z., Solimini,N.,

- Lerenthal,Y., Shiloh,Y., Gygi,S.P., and Elledge,S.J. (2007). ATM and ATR substrate analysis reveals extensive protein networks responsive to DNA damage. *Science* 316, 1160-1166.
157. Mattioli,F. and Sixma,T.K. (2014). Lysine-targeting specificity in ubiquitin and ubiquitin-like modification pathways. *Nat. Struct. Mol. Biol.* 21, 308-316.
158. Mattioli,F., Vissers,J.H., van Dijk,W.J., Ikpa,P., Citterio,E., Vermeulen,W., Marteiijn,J.A., and Sixma,T.K. (2012). RNF168 ubiquitinates K13-15 on H2A/H2AX to drive DNA damage signaling. *Cell* 150, 1182-1195.
159. McKinnon,P.J. (2012). ATM and the molecular pathogenesis of ataxia telangiectasia. *Annu. Rev. Pathol.* 7, 303-321.
160. Meerang,M., Ritz,D., Paliwal,S., Garajova,Z., Bosshard,M., Mailand,N., Janscak,P., Hubscher,U., Meyer,H., and Ramadan,K. (2011). The ubiquitin-selective segregase VCP/p97 orchestrates the response to DNA double-strand breaks. *Nat. Cell Biol.* 13, 1376-1382.
161. Mehrotra,P.V., Ahel,D., Ryan,D.P., Weston,R., Wiechens,N., Kraehenbuehl,R., Owen-Hughes,T., and Ahel,I. (2011). DNA repair factor APLF is a histone chaperone. *Mol. Cell* 41, 46-55.
162. Messner,S., Altmeyer,M., Zhao,H., Pozivil,A., Roschitzki,B., Gehrig,P., Rutishauser,D., Huang,D., Caflisch,A., and Hottiger,M.O. (2010). PARP1 ADP-ribosylates lysine residues of the core histone tails. *Nucleic Acids Res.* 38, 6350-6362.
163. Miller,K.M., Tjeertes,J.V., Coates,J., Legube,G., Polo,S.E., Britton,S., and Jackson,S.P. (2010). Human HDAC1 and HDAC2 function in the DNA-damage response to promote DNA nonhomologous end-joining. *Nat. Struct. Mol. Biol.* 17, 1144-1151.
164. Mohammad,D.H. and Yaffe,M.B. (2009). 14-3-3 proteins, FHA domains and BRCT domains in the DNA damage response. *DNA Repair (Amst)* 8, 1009-1017.
165. Moon,S.H., Lin,L., Zhang,X., Nguyen,T.A., Darlington,Y., Waldman,A.S., Lu,X., and Donehower,L.A. (2010). Wild-type p53-induced phosphatase 1 dephosphorylates histone variant gamma-H2AX and suppresses DNA double strand break repair. *J. Biol. Chem.* 285, 12935-12947.
166. Morris,J.R., Boutell,C., Keppler,M., Densham,R., Weekes,D., Alamshah,A., Butler,L., Galanty,Y., Pangon,L., Kiuchi,T., Ng,T., and Solomon,E. (2009). The SUMO modification pathway is involved in the BRCA1 response to genotoxic stress. *Nature* 462, 886-890.
167. Morrison,A.J., Highland,J., Krogan,N.J., Arbel-Eden,A., Greenblatt,J.F., Haber,J.E., and Shen,X. (2004). INO80 and gamma-H2AX interaction links ATP-dependent chromatin remodeling to DNA damage repair. *Cell* 119, 767-775.
168. Mortusewicz,O., Ame,J.C., Schreiber,V., and Leonhardt,H. (2007). Feedback-regulated poly(ADP-ribosylation) by PARP-1 is required for rapid response to DNA damage in living cells. *Nucleic Acids Res.* 35, 7665-7675.
169. Mosbech,A., Lukas,C., Bekker-Jensen,S., and Mailand,N. (2013). The deubiquitylating enzyme USP44 counteracts the DNA double-strand break response mediated by the RNF8 and RNF168 ubiquitin ligases. *J. Biol. Chem.* 288, 16579-16587.
170. Moyal,L., Lerenthal,Y., Gana-Weisz,M., Mass,G., So,S., Wang,S.Y., Eppink,B., Chung,Y.M., Shalev,G., Shema,E., Shkedy,D., Smorodinsky,N.I., van Vliet,N., Kuster,B., Mann,M., Ciechanover,A., Dahm-Daphi,J., Kanaar,R., Hu,M.C., Chen,D.J., Oren,M., and Shiloh,Y. (2011). Requirement of ATM-dependent monoubiquitylation of histone H2B for timely repair of DNA double-strand breaks. *Mol. Cell* 41, 529-542.
171. Mukhopadhyay,D. and Dasso,M. (2007). Modification in reverse: the SUMO proteases. *Trends Biochem. Sci.* 32, 286-295.
172. Murai,J., Huang,S.Y., Das,B.B., Renaud,A., Zhang,Y., Doroshow,J.H., Ji,J., Takeda,S., and Pommier,Y. (2012). Trapping of PARP1 and PARP2 by Clinical PARP Inhibitors. *Cancer Res.* 72, 5588-5599.
173. Murr,R., Loizou,J.I., Yang,Y.G., Cuenin,C., Li,H., Wang,Z.Q., and Hecceg,Z. (2006). Histone acetylation by Trrap-Tip60 modulates loading of repair proteins and repair of DNA double-strand breaks. *Nat. Cell Biol.* 8, 91-99.
174. Nagy,V. and Dikic,I. (2010). Ubiquitin ligase complexes: from substrate selectivity to conjugational specificity. *Biol. Chem.* 391, 163-169.
175. Nakada,S., Chen,G.I., Gingras,A.C., and Durocher,D. (2008). PP4 is a gamma H2AX phosphatase required for recovery from the DNA damage checkpoint. *EMBO Rep.* 9, 1019-1026.
176. Nakada,S., Tai,I., Panier,S., Al-Hakim,A., Iemura,S., Juang,Y.C., O'Donnell,L., Kumakubo,A., Munro,M., Sicheri,F., Gingras,A.C., Natsume,T., Suda,T., and Durocher,D. (2010). Non-canonical inhibition of DNA damage-dependent ubiquitination by OTUB1. *Nature* 466, 941-946.
177. Nakamura,K., Kato,A., Kobayashi,J., Yanagihara,H., Sakamoto,S., Oliveira,D.V., Shimada,M., Tauchi,H., Suzuki,H., Tashiro,S., Zou,L., and Komatsu,K. (2011). Regulation of homologous recombination by RNF20-dependent H2B ubiquitination. *Mol. Cell* 41, 515-528.
178. Nduka,N., Skidmore,C.J., and Shall,S. (1980). The enhancement of cytotoxicity of N-methyl-N-nitrosourea and of gamma-radiation by inhibitors of poly(ADP-ribose) polymerase. *Eur. J. Biochem.* 105, 525-530.
179. Nishi,R., Wijnhoven,P., Ie,S.C., Tjeertes,J., Galanty,Y., Forment,J.V., Clague,M.J., Urbe,S., and Jackson,S.P. (2014). Systematic characterization of deubiquitylating enzymes for roles in maintaining genome integrity. *Nat. Cell Biol.* 16, 1016-1018.
180. Noon,A.T., Shibata,A., Rief,N., Loblrich,M., Stewart,G.S., Jeggo,P.A., and Goodarzi,A.A. (2010). 53BP1-dependent robust localized KAP-1 phosphorylation is essential for heterochromatic DNA double-strand break repair. *Nat. Cell Biol.* 12, 177-184.
- Ogiwara,H., Ui,A., Otsuka,A., Satoh,H., Yokomi,I., Nakajima,S., Yasui,A., Yokota,J., and Kohno,T. (2011). Histone acetylation by CBP and p300 at double-strand break sites facilitates SWI/SNF chromatin remodeling and the recruitment of non-homologous

- end joining factors. *Oncogene* 30, 2135-2146.
181. Oliveira,D.V., Kato,A., Nakamura,K., Ikura,T., Okada,M., Kobayashi,J., Yanagihara,H., Saito,Y., Tauchi,H., and Komatsu,K. (2014). Histone chaperone FACT regulates homologous recombination by chromatin remodeling through interaction with RNF20. *J. Cell Sci.* 127, 763-772.
 182. Pan,M.R., Hsieh,H.J., Dai,H., Hung,W.C., Li,K., Peng,G., and Lin,S.Y. (2012). Chromodomain helicase DNA-binding protein 4 (CHD4) regulates homologous recombination DNA repair, and its deficiency sensitizes cells to poly(ADP-ribose) polymerase (PARP) inhibitor treatment. *J. Biol. Chem.* 287, 6764-6772.
 183. Pan,M.R., Peng,G., Hung,W.C., and Lin,S.Y. (2011). Monoubiquitination of H2AX protein regulates DNA damage response signaling. *J. Biol. Chem.* 286, 28599-28607.
 184. Panier,S. and Durocher,D. (2009). Regulatory ubiquitylation in response to DNA double-strand breaks. *DNA Repair (Amst)* 8, 436-443.
 185. Park,J.H., Park,E.J., Lee,H.S., Kim,S.J., Hur,S.K., Imbalzano,A.N., and Kwon,J. (2006). Mammalian SWI/SNF complexes facilitate DNA double-strand break repair by promoting gamma-H2AX induction. *EMBO J.* 25, 3986-3997.
 186. Paull,T.T. (2015). Mechanisms of ATM Activation. *Annu. Rev. Biochem.* 84, 711-738.
 187. Pei,H., Zhang,L., Luo,K., Qin,Y., Chesi,M., Fei,F., Bergsagel,P.L., Wang,L., You,Z., and Lou,Z. (2011). MMSET regulates histone H4K20 methylation and 53BP1 accumulation at DNA damage sites. *Nature* 470, 124-128.
 188. Peng,G., Yim,E.K., Dai,H., Jackson,A.P., Burgt,I., Pan,M.R., Hu,R., Li,K., and Lin,S.Y. (2009). BRIT1/MCPH1 links chromatin remodelling to DNA damage response. *Nat. Cell Biol.* 11, 865-872.
 189. Petrini,J.H. and Stracker,T.H. (2003). The cellular response to DNA double-strand breaks: defining the sensors and mediators. *Trends Cell Biol.* 13, 458-462.
 190. Pinato,S., Gatti,M., Scandiuzzi,C., Confalonieri,S., and Penengo,L. (2011). UMI, a novel RNF168 ubiquitin binding domain involved in the DNA damage signaling pathway. *Mol. Cell Biol.* 31, 118-126.
 191. Pines,A., Mullenders,L.H., van Attikum,H., and Luijsterburg,M.S. (2013). Touching base with PARPs: moonlighting in the repair of UV lesions and double-strand breaks. *Trends Biochem. Sci.* 38, 321-330.
 192. Poirier,G.G., de Murcia,G., Jongstra-Bilen,J., Niedergang,C., and Mandel,P. (1982). Poly(ADP-ribosyl)ation of polynucleosomes causes relaxation of chromatin structure. *Proc. Natl. Acad. Sci. U. S. A* 79, 3423-3427.
 193. Polo,S.E., Kaidi,A., Baskcomb,L., Galanty,Y., and Jackson,S.P. (2010). Regulation of DNA-damage responses and cell-cycle progression by the chromatin remodelling factor CHD4. *EMBO J.* 29, 3130-3139.
 194. Poulsen,M., Lukas,C., Lukas,J., Bekker-Jensen,S., and Mailand,N. (2012). Human RNF169 is a negative regulator of the ubiquitin-dependent response to DNA double-strand breaks. *J. Cell Biol.* 197, 189-199.
 195. Psakhye,I. and Jentsch,S. (2012). Protein group modification and synergy in the SUMO pathway as exemplified in DNA repair. *Cell* 151, 807-820.
 196. Qi,W., Wang,R., Chen,H., Wang,X., Xiao,T., Boldogh,I., Ba,X., Han,L., and Zeng,X. (2015). BRG1 promotes the repair of DNA double-strand breaks by facilitating the replacement of RPA with RAD51. *J. Cell Sci.* 128, 317-330.
 197. Rai,R., Dai,H., Multani,A.S., Li,K., Chin,K., Gray,J., Lahad,J.P., Liang,J., Mills,G.B., Meric-Bernstam,F., and Lin,S.Y. (2006). BRIT1 regulates early DNA damage response, chromosomal integrity, and cancer. *Cancer Cell* 10, 145-157.
 198. Reisman,D., Glaros,S., and Thompson,E.A. (2009). The SWI/SNF complex and cancer. *Oncogene* 28, 1653-1668.
 199. Rodriguez,D., Bretones,G., Quesada,V., Villamor,N., Arango,J.R., Lopez-Guillermo,A., Ramsay,A.J., Baumann,T., Quiros,P.M., Navarro,A., Royo,C., Martin-Subero,J.I., Campo,E., and Lopez-Otin,C. (2015). Mutations in CHD2 cause defective association with active chromatin in chronic lymphocytic leukemia. *Blood* 126, 195-202.
 200. Rosin,N., Elcioglu,N.H., Beleggia,F., Isguven,P., Altmuller,J., Thiele,H., Steindl,K., Joset,P., Rauch,A., Nurnberg,P., Wollnik,B., and Yigit,G. (2015). Mutations in XRCC4 cause primary microcephaly, short stature and increased genomic instability. *Hum. Mol. Genet.* 24, 3708-3717.
 201. Ruffner,H., Joazeiro,C.A., Hemmati,D., Hunter,T., and Verma,I.M. (2001). Cancer-predisposing mutations within the RING domain of BRCA1: loss of ubiquitin protein ligase activity and protection from radiation hypersensitivity. *Proc. Natl. Acad. Sci. U. S. A* 98, 5134-5139.
 202. Ruhl,D.D., Jin,J., Cai,Y., Swanson,S., Florens,L., Washburn,M.P., Conaway,R.C., Conaway,J.W., and Chrivia,J.C. (2006). Purification of a human SRCAP complex that remodels chromatin by incorporating the histone variant H2A.Z into nucleosomes. *Biochemistry* 45, 5671-5677.
 203. Rulten,S.L., Cortes-Ledesma,F., Guo,L., Iles,N.J., and Caldecott,K.W. (2008). APLF (C2orf13) is a novel component of poly(ADP-ribose) signaling in mammalian cells. *Mol. Cell Biol.* 28, 4620-4628.
 204. Rulten,S.L., Fisher,A.E., Robert,I., Zuma,M.C., Rouleau,M., Ju,L., Poirier,G., Reina-San-Martin,B., and Caldecott,K.W. (2011). PARP-3 and APLF function together to accelerate nonhomologous end-joining. *Mol. Cell* 41, 33-45.
 205. San Filippo,J., Sung,P., and Klein,H. (2008). Mechanism of eukaryotic homologous recombination. *Annu. Rev. Biochem.* 77, 229-257.
 206. Sanchez-Molina,S., Mortusewicz,O., Bieber,B., Auer,S., Eckey,M., Leonhardt,H., Friedl,A.A., and Becker,P.B. (2011). Role for hACF1 in the G2/M damage checkpoint. *Nucleic Acids Res.* 39, 8445-8456.

207. Santen,G.W., Aten,E., Sun,Y., Almomani,R., Gilissen,C., Nielsen,M., Kant,S.G., Snoeck,I.N., Peeters,E.A., Hilhorst-Hofstee,Y., Wessels,M.W., den Hollander,N.S., Ruivenkamp,C.A., van Ommen,G.J., Breuning,M.H., den Dunnen,J.T., van Haeringen,A., and Kriek,M. (2012a). Mutations in SWI/SNF chromatin remodeling complex gene ARID1B cause Coffin-Siris syndrome. *Nat. Genet.* 44, 379-380.
208. Santen,G.W., Kriek,M., and van Attikum,H. (2012b). SWI/SNF complex in disorder: SWItching from malignancies to intellectual disability. *Epigenetics.* 7, 1219-1224.
209. Sato,Y., Yoshikawa,A., Mimura,H., Yamashita,M., Yamagata,A., and Fukai,S. (2009). Structural basis for specific recognition of Lys 63-linked polyubiquitin chains by tandem UIMs of RAP80. *EMBO J.* 28, 2461-2468.
210. Schreiber,V., Dantzer,F., Ame,J.C., and de,M.G. (2006). Poly(ADP-ribose): novel functions for an old molecule. *Nat. Rev. Mol. Cell Biol.* 7, 517-528.
211. Schrier,S.A., Bodurtha,J.N., Burton,B., Chudley,A.E., Chiong,M.A., D'avanzo,M.G., Lynch,S.A., Musio,A., Nyazov,D.M., Sanchez-Lara,P.A., Shaley,S.A., and Deardorff,M.A. (2012). The Coffin-Siris syndrome: a proposed diagnostic approach and assessment of 15 overlapping cases. *Am. J. Med. Genet. A* 158A, 1865-1876.
212. Schulman,B.A. and Harper,J.W. (2009). Ubiquitin-like protein activation by E1 enzymes: the apex for downstream signalling pathways. *Nat. Rev. Mol. Cell Biol.* 10, 319-331.
213. Shaheen,R., Faqeh,E., Ansari,S., Abdel-Salam,G., Al-Hassnan,Z.N., Al-Shidi,T., Alomar,R., Sogaty,S., and Alkuraya,F.S. (2014). Genomic analysis of primordial dwarfism reveals novel disease genes. *Genome Res.* 24, 291-299.
214. Shanbhag,N.M., Rafalska-Metcalf,I.U., Balane-Bolivar,C., Janicki,S.M., and Greenberg,R.A. (2010). ATM-dependent chromatin changes silence transcription in cis to DNA double-strand breaks. *Cell* 141, 970-981.
215. Shao,G., Patterson-Fortin,J., Messick,T.E., Feng,D., Shanbhag,N., Wang,Y., and Greenberg,R.A. (2009). MERIT40 controls BRCA1-Rap80 complex integrity and recruitment to DNA double-strand breaks. *Genes Dev.* 23, 740-754.
216. Sharma,G.G., So,S., Gupta,A., Kumar,R., Cayrou,C., Avvakumov,N., Bhadra,U., Pandita,R.K., Porteus,M.H., Chen,D.J., Cote,J., and Pandita,T.K. (2010). MOF and histone H4 acetylation at lysine 16 are critical for DNA damage response and double-strand break repair. *Mol. Cell Biol.* 30, 3582-3595.
217. Sharma,N., Zhu,Q., Wani,G., He,J., Wang,Q.E., and Wani,A.A. (2014). USP3 counteracts RNF168 via deubiquitinating H2A and gammaH2AX at lysine 13 and 15. *Cell Cycle* 13, 106-114.
218. Sheu,J.J., Choi,J.H., Guan,B., Tsai,F.J., Hua,C.H., Lai,M.T., Wang,T.L., and Shih,I. (2013). Rsf-1, a chromatin remodelling protein, interacts with cyclin E1 and promotes tumour development. *J. Pathol.* 229, 559-568.
219. Shibata,A., Conrad,S., Birraux,J., Geuting,V., Barton,O., Ismail,A., Kakarougkas,A., Meek,K., Taucher-Scholz,G., Loblrich,M., and Jeggo,P.A. (2011). Factors determining DNA double-strand break repair pathway choice in G2 phase. *EMBO J.* 30, 1079-1092.
220. Shogren-Knaak,M. and Peterson,C.L. (2006). Switching on chromatin: mechanistic role of histone H4-K16 acetylation. *Cell Cycle* 5, 1361-1365.
221. Smeenk,G. and van Attikum,H. (2013). The chromatin response to DNA breaks: leaving a mark on genome integrity. *Annu. Rev. Biochem.* 82, 55-80.
222. Smeenk,G., Wiegant,W.W., Marteiijn,J.A., Luijsterburg,M.S., Sroczynski,N., Costelloe,T., Romeijn,R.J., Pastink,A., Mailand,N., Vermeulen,W., and van Attikum,H. (2013). Poly(ADP-ribosyl)ation links the chromatin remodeler SMARCA5/SNF2H to RNF168-dependent DNA damage signaling. *J. Cell Sci.* 126, 889-903.
223. Smeenk,G., Wiegant,W.W., Vrolijk,H., Solari,A.P., Pastink,A., and van Attikum,H. (2010). The NuRD chromatin-remodeling complex regulates signaling and repair of DNA damage. *J. Cell Biol.* 190, 741-749.
224. Solovjeva,L.V., Svetlova,M.P., Chagin,V.O., and Tomilin,N.V. (2007). Inhibition of transcription at radiation-induced nuclear foci of phosphorylated histone H2AX in mammalian cells. *Chromosome. Res.* 15, 787-797.
225. Song,J., Durrin,L.K., Wilkinson,T.A., Krontiris,T.G., and Chen,Y. (2004). Identification of a SUMO-binding motif that recognizes SUMO-modified proteins. *Proc. Natl. Acad. Sci. U. S. A* 101, 14373-14378.
226. Staples,E.R., McDermott,E.M., Reiman,A., Byrd,P.J., Ritchie,S., Taylor,A.M., and Davies,E.G. (2008). Immunodeficiency in ataxia telangiectasia is correlated strongly with the presence of two null mutations in the ataxia telangiectasia mutated gene. *Clin. Exp. Immunol.* 153, 214-220.
227. Stephens,P.J., Tarpey,P.S., Davies,H., Van,L.P., Greenman,C., Wedge,D.C., Nik-Zainal,S., Martin,S., Varela,I., Bignell,G.R., Yates,L.R., Papaemmanuil,E., Beare,D., Butler,A., Cheverton,A., Gamble,J., Hinton,J., Jia,M., Jayakumar,A., Jones,D., Latimer,C., Lau,K.W., McLaren,S., McBride,D.J., Menzies,A., Mudie,L., Raine,K., Rad,R., Chapman,M.S., Teague,J., Easton,D., Langerod,A., Lee,M.T., Shen,C.Y., Tee,B.T., Huimin,B.W., Broeks,A., Vargas,A.C., Turashvili,G., Martens,J., Fatima,A., Miron,P., Chin,S.F., Thomas,G., Boyault,S., Mariani,O., Lakhani,S.R., van de Vijver,M., van 't Veer,L., Foekens,J., Desmedt,C., Sotiriou,C., Tutt,A., Caldas,C., Reis-Filho,J.S., Aparicio,S.A., Salomon,A.V., Borresen-Dale,A.L., Richardson,A.L., Campbell,P.J., Futreal,P.A., and Stratton,M.R. (2012). The landscape of cancer genes and mutational processes in breast cancer. *Nature* 486, 400-404.
228. Stewart,G.S., Panier,S., Townsend,K., Al-Hakim,A.K., Kolas,N.K., Miller,E.S., Nakada,S., Ylanko,J., Olivarius,S., Mendez,M., Oldreive,C., Wildenhain,J., Tagliaferro,A., Pelletier,L., Taubenheim,N., Durandy,A., Byrd,P.J., Stankovic,T., Taylor,A.M., and Durocher,D. (2009). The RIDDLE syndrome protein mediates a ubiquitin-dependent signaling cascade at sites of DNA damage. *Cell* 136, 420-434.

229. Stiff,T., O'Driscoll,M., Rief,N., Iwabuchi,K., Lobrich,M., and Jeggo,P.A. (2004). ATM and DNA-PK function redundantly to phosphorylate H2AX after exposure to ionizing radiation. *Cancer Res.* 64, 2390-2396.
230. Stopka,T., Zakova,D., Fuchs,O., Kubrova,O., Blafkova,J., Jelinek,J., Necas,E., and Zivny,J. (2000). Chromatin remodeling gene SMARCA5 is dysregulated in primitive hematopoietic cells of acute leukemia. *Leukemia* 14, 1247-1252.
231. Stralfors,A., Walfridsson,J., Bhuiyan,H., and Ekwall,K. (2011). The FUN30 chromatin remodeler, Fft3, protects centromeric and subtelomeric domains from euchromatin formation. *PLoS. Genet.* 7, e1001334.
232. Strauss,C. and Goldberg,M. (2011). Recruitment of proteins to DNA double-strand breaks: MDC1 directly recruits RAP80. *Cell Cycle* 10, 2850-2857.
233. Stucki,M. and Jackson,S.P. (2006). gammaH2AX and MDC1: anchoring the DNA-damage-response machinery to broken chromosomes. *DNA Repair (Amst)* 5, 534-543.
234. Sumegi,J., Nishio,J., Nelson,M., Frayer,R.W., Perry,D., and Bridge,J.A. (2011). A novel t(4;22)(q31;q12) produces an EWSR1-SMARCA5 fusion in extraskeletal Ewing sarcoma/primitive neuroectodermal tumor. *Mod. Pathol.* 24, 333-342.
235. Sun,Y., Jiang,X., Chen,S., Fernandes,N., and Price,B.D. (2005). A role for the Tip60 histone acetyltransferase in the acetylation and activation of ATM. *Proc. Natl. Acad. Sci. U. S. A* 102, 13182-13187.
236. Sun,Y., Jiang,X., Xu,Y., Ayrapetov,M.K., Moreau,L.A., Whetstine,J.R., and Price,B.D. (2009). Histone H3 methylation links DNA damage detection to activation of the tumour suppressor Tip60. *Nat. Cell Biol.* 11, 1376-1382.
237. Sy,S.M., Huen,M.S., Zhu,Y., and Chen,J. (2009). PALB2 regulates recombinational repair through chromatin association and oligomerization. *J. Biol. Chem.* 284, 18302-18310.
238. Szerlong,H., Hinata,K., Viswanathan,R., Erdjument-Bromage,H., Tempst,P., and Cairns,B.R. (2008). The HSA domain binds nuclear actin-related proteins to regulate chromatin-remodeling ATPases. *Nat. Struct. Mol. Biol.* 15, 469-476.
239. Tai,H.C., Huang,H.Y., Lee,S.W., Lin,C.Y., Sheu,M.J., Chang,S.L., Wu,L.C., Shiu,Y.L., Wu,W.R., Lin,C.M., and Li,C.F. (2012). Associations of Rsf-1 overexpression with poor therapeutic response and worse survival in patients with nasopharyngeal carcinoma. *J. Clin. Pathol.* 65, 248-253.
240. Tang,J., Cho,N.W., Cui,G., Manion,E.M., Shanbhag,N.M., Botuyan,M.V., Mer,G., and Greenberg,R.A. (2013). Acetylation limits 53BP1 association with damaged chromatin to promote homologous recombination. *Nat. Struct. Mol. Biol.* 20, 317-325.
241. Tatham,M.H., Jaffray,E., Vaughan,O.A., Desterro,J.M., Botting,C.H., Naismith,J.H., and Hay,R.T. (2001). Polymeric chains of SUMO-2 and SUMO-3 are conjugated to protein substrates by SAE1/SAE2 and Ubc9. *J. Biol. Chem.* 276, 35368-35374.
242. Thorslund,T., Ripplinger,A., Hoffmann,S., Wild,T., Uckelmann,M., Villumsen,B., Narita,T., Sixma,T.K., Choudhary,C., Bekker-Jensen,S., and Mailand,N. (2015). Histone H1 couples initiation and amplification of ubiquitin signalling after DNA damage. *Nature* 527, 389-393.
243. Timinsky,G., Till,S., Hassa,P.O., Hothorn,M., Kustatscher,G., Nijmeijer,B., Colombelli,J., Altmeyer,M., Stelzer,E.H., Scheffzek,K., Hottiger,M.O., and Ladurner,A.G. (2009). A macrodomain-containing histone rearranges chromatin upon sensing PARP1 activation. *Nat. Struct. Mol. Biol.* 16, 923-929.
244. Tjeertes,J.V., Miller,K.M., and Jackson,S.P. (2009). Screen for DNA-damage-responsive histone modifications identifies H3K9Ac and H3K56Ac in human cells. *EMBO J.* 28, 1878-1889.
245. Toiber,D., Erdel,F., Bouazoune,K., Silberman,D.M., Zhong,L., Mulligan,P., Sebastian,C., Cosentino,C., Martinez-Pastor,B., Giacosa,S., D'Urso,A., Naar,A.M., Kingston,R., Rippe,K., and Mostoslavsky,R. (2013). SIRT6 recruits SNF2H to DNA break sites, preventing genomic instability through chromatin remodeling. *Mol. Cell* 51, 454-468.
246. Toto,M., D'Angelo,G., and Corona,D.F. (2014). Regulation of ISWI chromatin remodelling activity. *Chromosoma* 123, 91-102.
247. Typas,D., Luijsterburg,M.S., Wiegant,W.W., Diakou,M., Helfricht,A., Thijssen,P.E., van de Broek,B., Mullenders,L.H., and van Attikum,H. (2015). The de-ubiquitylating enzymes USP26 and USP37 regulate homologous recombination by counteracting RAP80. *Nucleic Acids Res.*
248. Ui,A., Nagaura,Y., and Yasui,A. (2015). Transcriptional Elongation Factor ENL Phosphorylated by ATM Recruits Polycomb and Switches Off Transcription for DSB Repair. *Mol. Cell* 58, 468-482.
249. van der Burg,M., IJspeert,H., Verkaik,N.S., Turul,T., Wiegant,W.W., Morotomi-Yano,K., Mari,P.O., Tezcan,I., Chen,D.J., Zdzienicka,M.Z., van Dongen,J.J., and van Gent,D.C. (2009). A DNA-PKcs mutation in a radiosensitive T-B-SCID patient inhibits Artemis activation and nonhomologous end-joining. *J. Clin. Invest* 119, 91-98.
250. Van Houdt,J.K., Nowakowska,B.A., Sousa,S.B., van Schaik,B.D., Seuntjens,E., Avonce,N., Sifrim,A., Abdul-Rahman,O.A., van den Boogaard,M.J., Bottani,A., Castori,M., Cormier-Daire,V., Deardorff,M.A., Filges,I., Fryer,A., Fryns,J.P., Gana,S., Garavelli,L., Gillissen-Kaesbach,G., Hall,B.D., Horn,D., Huylebroeck,D., Klapceki,J., Krajewska-Walasek,M., Kuechler,A., Lines,M.A., Maas,S., Macdermot,K.D., McKee,S., Magee,A., de Man,S.A., Moreau,Y., Morice-Picard,F., Obersztyn,E., Pilch,J., Rosser,E., Shannon,N., Stolte-Dijkstra,I., Van Dijck,P., Vilain,C., Vogels,A., Wakeling,E., Wiczorek,D., Wilson,L., Zuffardi,O., van Kampen,A.H., Devriendt,K., Hennekam,R., and Vermeesch,J.R. (2012). Heterozygous missense mutations in SMARCA2 cause Nicolaides-Baraitser syndrome. *Nat. Genet.* 44, 445-9, S1.
251. Vempati,R.K., Jayani,R.S., Notani,D., Sengupta,A., Galande,S., and Haldar,D. (2010). p300-mediated acetylation of histone H3 lysine 56 functions in DNA damage response in mammals. *J. Biol. Chem.* 285, 28553-28564.
252. Verhagen,M.M., Last,J.I., Hogervorst,F.B., Smeets,D.F., Roelvelde,N., Verheijen,F., Catsman-Berrevoets,C.E., Wulffraat,N.M.,

- Cobben,J.M., Hiel,J., Brunt,E.R., Peeters,E.A., Gomez Garcia,E.B., van der Knaap,M.S., Lincke,C.R., Laan,L.A., Tijssen,M.A., van Rijn,M.A., Majoor-Krakauer,D., Visser,M., van 't Veer,L.J., Kleijer,W.J., van de Warrenburg,B.P., Warris,A., de Groot,I.J., de Groot,R., Broeks,A., Preijers,F., Kremer,B.H., Weemaes,C.M., Taylor,M.A., van Deuren,M., and Willemsen,M.A. (2012). Presence of ATM protein and residual kinase activity correlates with the phenotype in ataxia-telangiectasia: a genotype-phenotype study. *Hum. Mutat.* 33, 561-571.
253. Vertegaal,A.C. (2010). SUMO chains: polymeric signals. *Biochem. Soc. Trans.* 38, 46-49.
254. Vyas,R., Kumar,R., Clermont,F., Helfricht,A., Kalev,P., Sotiropoulou,P., Hendriks,I.A., Radaelli,E., Hochepped,T., Blanpain,C., Sablina,A., van Attikum,H., Olsen,J.V., Jochemsen,A.G., Vertegaal,A.C., and Marine,J.C. (2013). RNF4 is required for DNA double-strand break repair in vivo. *Cell Death. Differ.* 20, 490-502.
255. Wang,B. and Elledge,S.J. (2007). Ubc13/Rnf8 ubiquitin ligases control foci formation of the Rap80/Abraxas/Brc1/Brc36 complex in response to DNA damage. *Proc. Natl. Acad. Sci. U. S. A* 104, 20759-20763.
256. Wang,G.G., Allis,C.D., and Chi,P. (2007). Chromatin remodeling and cancer, Part II: ATP-dependent chromatin remodeling. *Trends Mol. Med.* 13, 373-380.
257. Wang,J., Aroumougama,A., Lobrich,M., Li,Y., Chen,D., Chen,J., and Gong,Z. (2014). PTIP associates with Artemis to dictate DNA repair pathway choice. *Genes Dev.* 28, 2693-2698.
258. Wang,M., Wu,W., Wu,W., Rosidi,B., Zhang,L., Wang,H., and Iliakis,G. (2006). PARP-1 and Ku compete for repair of DNA double strand breaks by distinct NHEJ pathways. *Nucleic Acids Res.* 34, 6170-6182.
259. Wang,Y. and Dasso,M. (2009). SUMOylation and deSUMOylation at a glance. *J. Cell Sci.* 122, 4249-4252.
260. Ward,I.M. and Chen,J. (2001). Histone H2AX is phosphorylated in an ATR-dependent manner in response to replicational stress. *J. Biol. Chem.* 276, 47759-47762.
261. Weemaes,C.M., Hustinx,T.W., Scheres,J.M., van Munster,P.J., Bakkeren,J.A., and Taalman,R.D. (1981). A new chromosomal instability disorder: the Nijmegen breakage syndrome. *Acta Paediatr. Scand.* 70, 557-564.
262. Wilson,B.G. and Roberts,C.W. (2011). SWI/SNF nucleosome remodellers and cancer. *Nat. Rev. Cancer* 11, 481-492.
263. Wong,M.M., Cox,L.K., and Chrivia,J.C. (2007). The chromatin remodeling protein, SRCAP, is critical for deposition of the histone variant H2A.Z at promoters. *J. Biol. Chem.* 282, 26132-26139.
264. Wood,J.L., Singh,N., Mer,G., and Chen,J. (2007). MCPH1 functions in an H2AX-dependent but MDC1-independent pathway in response to DNA damage. *J. Biol. Chem.* 282, 35416-35423.
265. Woodbine,L., Gennery,A.R., and Jeggo,P.A. (2014). The clinical impact of deficiency in DNA non-homologous end-joining. *DNA Repair (Amst)* 16, 84-96.
266. Wu,C.Y., Kang,H.Y., Yang,W.L., Wu,J., Jeong,Y.S., Wang,J., Chan,C.H., Lee,S.W., Zhang,X., Lamothe,B., Campos,A.D., Darnay,B.G., and Lin,H.K. (2011). Critical role of monoubiquitination of histone H2AX protein in histone H2AX phosphorylation and DNA damage response. *J. Biol. Chem.* 286, 30806-30815.
267. Wu,L.C., Wang,Z.W., Tsan,J.T., Spillman,M.A., Phung,A., Xu,X.L., Yang,M.C., Hwang,L.Y., Bowcock,A.M., and Baer,R. (1996). Identification of a RING protein that can interact in vivo with the BRCA1 gene product. *Nat. Genet.* 14, 430-440.
268. Xia,B., Sheng,Q., Nakanishi,K., Ohashi,A., Wu,J., Christ,N., Liu,X., Jasin,M., Couch,F.J., and Livingston,D.M. (2006). Control of BRCA2 cellular and clinical functions by a nuclear partner, PALB2. *Mol. Cell* 22, 719-729.
269. Xiao,A., Li,H., Shechter,D., Ahn,S.H., Fabrizio,L.A., Erdjument-Bromage,H., Ishibe-Murakami,S., Wang,B., Tempst,P., Hofmann,K., Patel,D.J., Elledge,S.J., and Allis,C.D. (2009). WSTF regulates the H2A.X DNA damage response via a novel tyrosine kinase activity. *Nature* 457, 57-62.
270. Xu,Y., Ayrapetov,M.K., Xu,C., Gursoy-Yuzugullu,O., Hu,Y., and Price,B.D. (2012). Histone H2A.Z controls a critical chromatin remodeling step required for DNA double-strand break repair. *Mol. Cell* 48, 723-733.
271. Yin,Y., Seifert,A., Chua,J.S., Maure,J.F., Golebiowski,F., and Hay,R.T. (2012). SUMO-targeted ubiquitin E3 ligase RNF4 is required for the response of human cells to DNA damage. *Genes Dev.* 26, 1196-1208.
272. You,Z., Shi,L.Z., Zhu,Q., Wu,P., Zhang,Y.W., Basilio,A., Tonnu,N., Verma,I.M., Berns,M.W., and Hunter,T. (2009). CtIP links DNA double-strand break sensing to resection. *Mol. Cell* 36, 954-969.
273. Zhang,F., Fan,Q., Ren,K., and Andreassen,P.R. (2009a). PALB2 functionally connects the breast cancer susceptibility proteins BRCA1 and BRCA2. *Mol. Cancer Res.* 7, 1110-1118.
274. Zhang,F., Ma,J., Wu,J., Ye,L., Cai,H., Xia,B., and Yu,X. (2009b). PALB2 links BRCA1 and BRCA2 in the DNA-damage response. *Curr. Biol.* 19, 524-529.
275. Zimmermann,M., Lottersberger,F., Buonomo,S.B., Sfeir,A., and de,L.T. (2013). 53BP1 regulates DSB repair using Rif1 to control 5' end resection. *Science* 339, 700-704.
276. Ziv,Y., Bielopolski,D., Galanty,Y., Lukas,C., Taya,Y., Schultz,D.C., Lukas,J., Bekker-Jensen,S., Bartek,J., and Shiloh,Y. (2006). Chromatin relaxation in response to DNA double-strand breaks is modulated by a novel ATM- and KAP-1 dependent pathway. *Nat. Cell Biol.* 8, 870-876.





IDENTIFICATION OF EHMT1 AS A CHROMATIN
FACTOR THAT NEGATIVELY REGULATES 53BP1
ACCRUAL DURING THE DNA DOUBLE-
STRAND BREAK RESPONSE

2

Angela Helfricht¹, Bram Herpers², Erik H. Danen²,
Bob van de Water², Haico van Attikum¹

¹ Department of Human Genetics; Leiden University Medical Center

² Division of Toxicology; Leiden Academic Centre for Drug Research; Leiden University

ABSTRACT

DNA double-strand breaks (DSB) are the most dangerous species of DNA damage and their repair is crucial to preserve genome stability. Upon DSB induction a highly advanced signaling cascade is activated that leads to several DNA damage-associated histone modifications and the recruitment of chromatin remodelers to make the chromatin more accessible for the accrual of DNA repair proteins. However, the immense crosstalk between these dynamic chromatin modifications is so far poorly understood. To identify novel chromatin regulators that are involved in the response to DSBs, we performed a siRNA screen monitoring the early and late response to DSBs by determining the formation of ionizing radiation (IR)-induced γ H2AX and 53BP1 foci, respectively. Amongst others, we found the lysine methyltransferase EHMT1 to negatively regulate 53BP1 accrual to foci. We further show that EHMT1 itself is rapidly recruited to DSBs and promotes DSB repair via both major repair pathways, non-homologous end-joining and homologous recombination. EHMT1 targets H3K9 and other proteins for methylation and we propose that these modifications are likely important during the response to DSBs and for the preservation of genome stability. Future research will certainly demonstrate the exact role of EHMT1 in the DSB response.

INTRODUCTION

DNA double-strand breaks (DSBs) occur on a daily basis when both strands of the DNA duplex are broken. This type of lesions is highly toxic to cells and can be induced by various endogenous and exogenous sources. If not repaired accurately, DSBs can cause genome rearrangements or even cell death. Cells respond to DSBs by activating a complex signaling network that coordinates the recruitment of repair proteins, chromatin organization and cell cycle progression in order to provide time for DNA repair in a permissive chromatin environment.

Upon DSB induction, a series of chromatin modifications are initiated with the Ataxia telangiectasia mutated (ATM)-dependent phosphorylation of the histone H2A variant H2AX (termed γ H2AX) being among the first. γ H2AX in turn recruits Mediator of DNA damage checkpoint protein 1 (MDC1), which binds γ H2AX directly through its BRCT (Lukas et al., 2011; Stucki et al., 2005). MDC1 further coordinates DNA damage-induced histone modifications by providing a binding platform for different chromatin modifying enzymes. First, MDC1 recruits the multisubunit chromatin remodeling NuA4 complex including the acetyltransferase TIP60 to sites of DSBs. Upon DSB induction, Histone protein 1 (HP1) is released from the damaged chromatin, 'unmasking' the abundant H3K9me3 mark to which TIP60 binds through its chromodomain. TIP60 then activates ATM and promotes the DSB response by acetylation of histone H4 at lysine (K) 16 (Kaidi and Jackson, 2013; Sun et al., 2009).

Second, the E3 ubiquitin-protein ligase RNF8 binds through its Forkhead-associated domain to phosphorylated MDC1 and initiates an ubiquitylation signaling cascade within the damaged chromatin (Huen et al., 2007; Kolas et al., 2007; Mailand et al., 2007). RNF8 ubiquitylates histone H2A, which recruits a second E3 ubiquitin-protein ligase RNF168 that amplifies the formed ubiquitin conjugates and also induces novel monoubiquitylation on H2AK13 and 15 (Doil et al., 2009; Gatti et al., 2012; Stewart et al., 2009).

Third, MDC1 attracts the histone lysine methyltransferase MMSET to which it binds in an ATM-dependent manner. MMSET, together with the H4K20 monomethyltransferase SETD8, locally increases de novo dimethylation of H4K20 (H4K20me2) at DSB sites (Oda et al., 2010; Pei et al., 2011). These events together contribute to the accumulation of further downstream signaling factors such as Tumor suppressor p53-binding protein 1 (53BP1), which directly binds as bivalent histone modification reader to ubiquitylated H2AK15 via its ubiquitylation-dependent recruitment motif (Doil et al., 2009; Fradet-Turcotte et al., 2013; Stewart et al., 2009) and to H4K20me2 via its Tudor domain (Botuyan et al., 2006; Zgheib et al., 2009). 53BP1 binding additionally requires the activity of the histone deacetylases HDAC1/2 to counteract TIP60-induced H4K16ac, since this enables local de novo H4K20me2 formation (Hsiao and Mizzen, 2013; Miller et al., 2010; Tang et al., 2013). Furthermore, the removal of the H4K20me2-binders JMJD2A and L3MBTL1 is necessary to reveal this histone mark for 53BP1 binding (Acs et al., 2011; Lee et al., 2008; Mallette et al., 2012; Min et al., 2007). All these events are highly dynamic and scientists are only beginning to understand the immense crosstalk between these DNA damage-induced histone modifications.

Moreover, the structure and composition of chromatin can also be changed by ATP-dependent chromatin remodeling enzymes such as the ATPases Chromodomain-helicase-DNA-binding protein 4 (CHD4) and SWI/SNF-related matrix-associated actin-dependent regulator of chromatin subfamily A member 5 (SMARCA5/SNF2h). Both ATPases are recruited to DSBs and facilitate the efficient recruitment of RNF168, which leads to effective



ubiquitylation and BRCA1 accrual (Luijsterburg et al., 2012; Smeenk et al., 2013). Considering the incredible multitude of chromatin remodeling events during the DSB response, we expected novel chromatin regulating factors to participate in the signaling of DSBs and set out to identify those. To this end, we performed a high-throughput short interfering RNA (siRNA) screen for regulators of the DSB response by simultaneously monitoring the accrual of γ H2AX, happening early during the DSB response, and the accumulation of downstream factor 53BP1 into ionizing radiation (IR)-induced foci, which occurs during the later steps of the response to DSBs. Genome-wide screens with a comparable read-out have been performed before (Doil et al., 2009; Paulsen et al., 2009), however so far did not lead to the identification of chromatin modifiers. Moreover, such screens often miss hits for instance due to less strong effects on the read-out. We therefore performed this dedicated high-content microscopy siRNA screen. Amongst others, we identified the histone Euchromatic histone-lysine N-methyltransferase 1 (EHMT1), also named GLP, as a negative regulator of 53BP1 recruitment into IR-induced foci, while the formation of γ H2AX was not affected in EHMT1 knockdown cells. Interestingly, we revealed that EHMT1 is rapidly recruited and promotes DSB repair via both major pathways, non-homologous end-joining (NHEJ) and homologous recombination (HR). Our results thus suggest a role for EHMT1 within the DSB response and EHMT1 is therefore an interesting and novel candidate for maintaining genome stability.

RESULTS

siRNA screen identifies novel chromatin regulators involved in the DSB response

In order to identify novel chromatin regulators involved in the response to DSBs, we carried out a siRNA screen using the Dharmacon Epigenetics SMARTpool library complemented with a custom made SMARTpool library comprising epigenetic modifiers containing a chromo-, bromo- or SANT domain, as well as SNF2-related genes (Table S1A). U2OS cells were reversely transfected with siRNA SMARTpools spotted in 96 well plates and after three days of cultivation, the cells were exposed to 2 Gy of IR. Subsequently, one hour later the cells were fixed and co-immunostained for γ H2AX and 53BP1, which was followed by high-throughput confocal imaging. As a read-out the average number of γ H2AX and 53BP1 foci/nucleus was determined in duplicate upon knockdown of all 227 targets. To control for siRNA transfection efficiency, we included a siRNA SMARTpool directed against the essential KIF11 gene in each plate, whose knockdown induces cell killing by generating mitotic spindle catastrophes (Weil et al., 2002). Indeed, the knockdown of KIF11 resulted in a \sim 90% reduction in cell viability (Fig. S1). Further controls per plate included siRNAs directed against Luciferase (Luc, negative control) and RNF8 (positive control). The latter is essential for 53BP1 accumulation, but not for γ H2AX formation (Doil et al., 2009; Huen et al., 2007; Kolas et al., 2007; Mailand et al., 2007; Stewart et al., 2009). To provide an estimate of the variation within each 96-well plate, these control siRNAs were spotted three times on different locations on each plate. Next, the average numbers of 53BP1 foci of the negative and positive controls per location on the plate were used to calculate the Z-factor. This quality readout was performed for all plates and each time positively met the selection criteria [$0.5 < Z\text{-factor} < 1$] (data not shown). Hence, transfection variation within one 96-well plate did not vary strongly.

To exclude possible knockdown-induced cell growth defects a minimum of 100

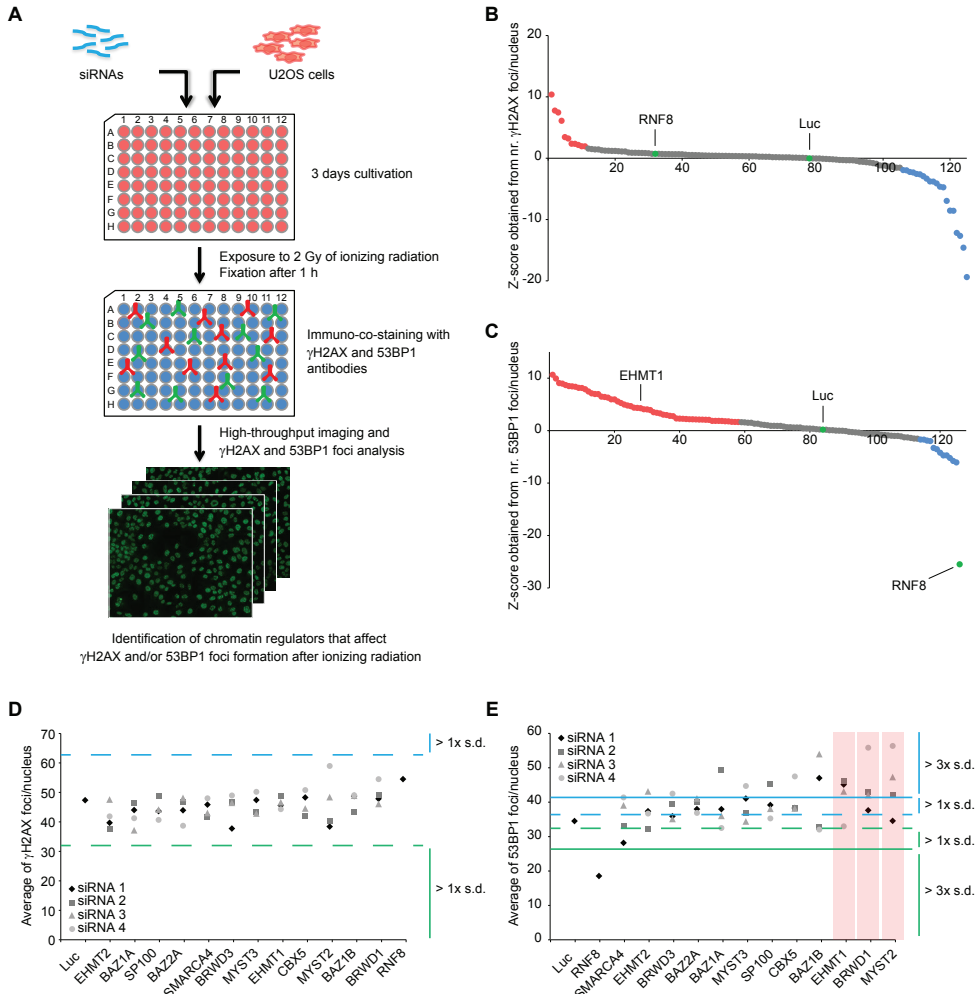


Figure 1. RNAi screen identifies EHTM1 as a regulator of 53BP1 accumulation to DSBs. (A) Schematic of siRNA screen performed to identify novel chromatin regulators involved in the DDR. (B and C) Scatter plot of 124 Z-scores derived from the siRNA screen for γ H2AX (B) and 53BP1 (C) foci formation using siRNA Smartpools. Luciferase and RNF8 are indicated as negative and positive control, respectively, for 53BP1 foci formation. The knockdown of targets depicted in red lead to an increase in foci formation, while the depletion of targets shown in blue was followed by a decrease in foci formation. (D and E) Results from secondary validation screen, where four individual siRNAs per target were used to validate the first 12 hits from the primary screen (as in B and C). Shown is the average number of γ H2AX (D) and 53BP1 (E) foci/nucleus per siRNA per target from duplicate experiments. One and three times the standard deviation (s.d.) of the Luciferase control are indicated by dashed and continuous horizontal lines, respectively, in blue for an increase and in green for a decrease in average number of foci/nucleus. Confirmed hits are indicated in red where 3 out of 4 siRNAs caused a change in the average foci number/nucleus larger than three times the s.d. of Luciferase. Data of additional 36 hits is presented in Fig. S1.

cells per well were imaged and examined in each of two independent experiments. This criteria was not met for 106 siRNA SMARTpools and led to their exclusion from the dataset (Table S1A). Next, Z-scores were calculated from the average amount of foci per nucleus for each siRNA within one 96-well plate using the siLuc and siRNF8 controls as a reference. The average Z-score from the experimental duplicates provided a measure for the change

in the amount of foci per nucleus upon siRNA treatment compared to control. As expected, depletion of RNF8 caused a dramatic drop in the number of 53BP1 IR-induced foci on each plate (Fig. 1C,E; Fig. S2B,D,F; Table S1A). The knockdown of 32 genes showed a significant effect on γ H2AX foci formation, while the depletion of 70 genes by SMARTPools changed the average amount of 53BP1 foci per nucleus considerably, all meeting the selection criteria [Z-score < -1,5 or > 1,5 and p-value < 0,05] (Fig. 1B,C, Table S1A).

To validate the obtained hit list, we performed a deconvolution screen for which 48 targets were selected, that had been identified in other screens before, but had not yet been functionally characterized (Chou et al., 2010; Hurov et al., 2010; Matic et al., 2010; Matsuoka et al., 2007; Paulsen et al., 2009). For this deconvolution screen we employed four individual siRNAs per target within the same experimental set-up as described above (Fig. 1A,D,E; Table S1B). Here, the average number of foci per nucleus was determined directly from the obtained average foci numbers per nucleus after siRNA treatment from two individual experiments. A gene was considered a hit when at least three out of four siRNAs showed a difference in foci formation larger than three times the standard deviation (s.d.) of the siLuc control. This approach provided more stringent selection criteria for the identification of hits than the thresholds applied in the initial siRNA screen, reducing the chance of obtaining false-positives. Summarizing our results, SDS3 knockdown lead to a decrease in γ H2AX foci formation upon IR with all four siRNAs (Fig. S2E; Table S1B), while EHMT1, BRWD1 or MYST2 depletion caused an increase in 53BP1 foci formation after exposure to IR with three distinct siRNAs (Fig. 1D,E; Table S1B).

EHMT1 regulates 53BP1 recruitment into foci

To define whether the siRNA screen approach indeed identified novel factors involved in the DDR, we focused on the histone-lysine N-methyltransferase 1 (EHMT1, also named GLP). EHMT1 is a closely related paralog of EHMT2 (also G9a), both being mammalian lysine methyltransferases (KMTs) that mainly facilitate H3K9 mono- and dimethylation (H3K9me1/2) in euchromatin as well as the methylation of non-histone substrates. Although EHMT1 and EHMT2 can form homomeric complexes, they predominantly exist in a heteromeric complex formed via the interaction of their SET domains (Shinkai and Tachibana, 2011; Tachibana et al., 2005). Observed phenotypes were surprisingly identical in either EHMT1- or EHMT2-deficient mice with embryonic lethality around embryonic day 9.5. Moreover, both EHMT1 and EHMT2 knockout mouse ES cells show a clear reduction in global H3K9me1/2 levels (Tachibana et al., 2002; Tachibana et al., 2005). Importantly, no additive effect was measured in double knockout ES cells, indicating a cooperative rather than a redundant function of these enzymes, and thus an equally important role in the maintenance of H3K9me1/2 throughout chromatin (Tachibana et al., 2005; Tachibana et al., 2008). Interestingly, while mouse Ehmt2 has been shown to be unstable in Ehmt1-/- cells, Ehmt2-/- cells do not show a difference in Ehmt1 protein stability (Tachibana et al., 2005). And while EHMT2 has been shown to interact with a series of DNA-binding and transcriptional repressor proteins such as the DNA methylases DNMT1, DNMT3A and DNMT3B, as well as histone protein 1 (HP1) (Epsztejn-Litman et al., 2008; Shinkai and Tachibana, 2011), a subset of EHMT1 and EHMT2 was found in a multimeric complex together with other histone KMTs such as SUV39H and SETDB1, which can facilitate di- and trimethylation of H3K9 (Fritsch et al., 2010). Upon deposition of H3K9me1/2 by the EHMT1/2 complex in euchromatin, a repressive chromatin state is induced that forms a substrate for trimethylation by SUV39H at heterochromatic regions as well as for HP1 binding (Bannister et al., 2001; Lachner et al.,

2001; Rice et al., 2003), which leads to heterochromatin formation. Furthermore, EHMT1 function has been suggested to play an important role during neuronal development since loss of function mutations in the EHMT1 gene or submicroscopic deletions of the distal long chromosome arm 9q lead to haploinsufficiency of EHMT1 causing Kleefstra syndrome (KS) (previously 9q subtelomeric deletion syndrome). KS-patients mainly display intellectual disability, childhood hypotonia and characteristic facial anomalies (Kleefstra et al., 1993; Kleefstra et al., 2012; Nillesen et al., 2011). Finally, EHMT1 as well as EHMT2 have been found to be overexpressed in various cancers (Guan et al., 2014; Huang et al., 2010). Concerning these phenotypes and the detected increase in 53BP1 foci formation upon IR exposure in our siRNA screen, we started a follow-up study addressing the role of EHMT1 during the response to DSBs. First, we used two siRNAs against EHMT1 which reduced 53BP1 focus formation in the deconvolution screen to forwardly transfect U2OS cells on 18

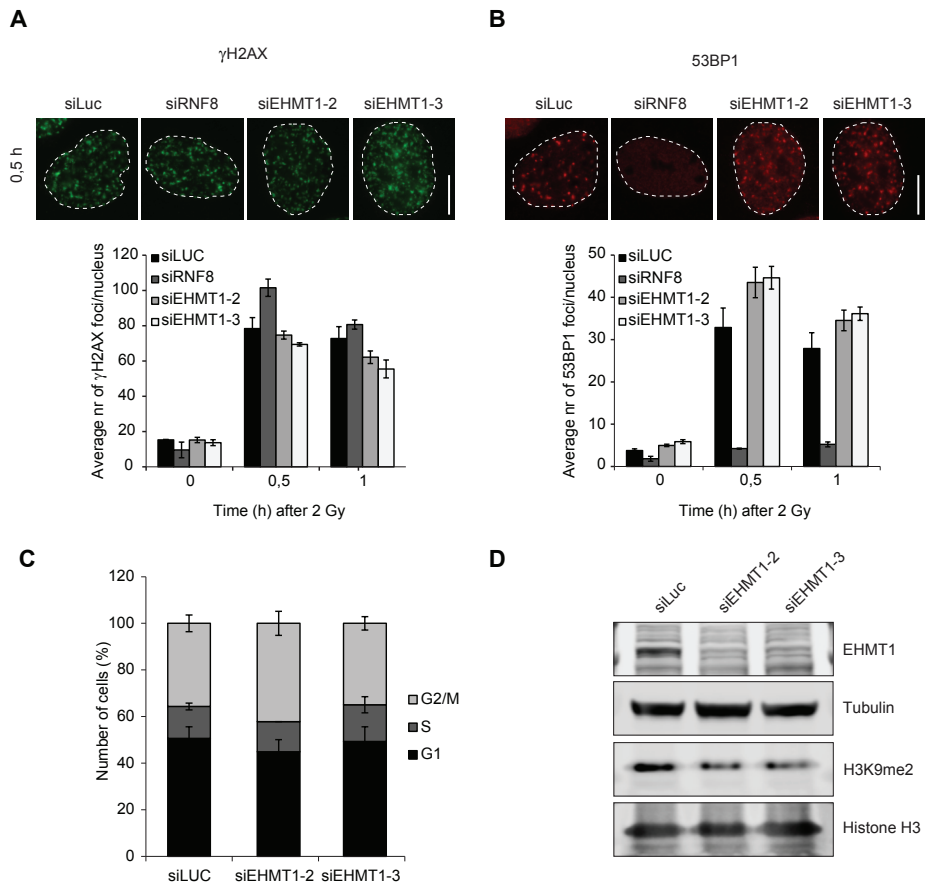


Figure 2. Depletion of EHMT1 leads to an increase in 53BP1 foci formation upon ionizing radiation (IR). (A) U2OS cells were treated with the indicated siRNAs. 48 hours later cells were either left untreated or were exposed to 2 Gy of IR. Cells were immunostained for γ H2AX 1 h later. Representative images are shown of the 0,5 h time point. Quantification is depicted using the average number (nr) of γ H2AX foci/nucleus obtained from 3 individual experiments where at least 75 cells were examined. Scale bar, 10 μ m. (B) As in (A), but immunostained for 53BP1. (C) U2OS cells were transfected with indicated siRNAs and were stained with propidium iodide 48 h later. Cells were then subjected to flow cytometry analysis. Shown is the percentage of cells in G1 (black), S (dark gray) and G2/M phase (light gray). (D) Whole cell extracts from cells in (A) and (B) were subjected to western blot analysis.

mm coverslips and 48 h later, exposed cells to 2 Gy of IR. We determined γ H2AX and 53BP1 foci formation after 0.5 and 1 h and again confirmed the increase in 53BP1 foci formation after IR, while depletion of RNF8 showed the expected decrease in 53BP1 recruitment (Fig. 2A,B) (Lukas et al., 2011). To exclude that this effect might indirectly be caused by cell cycle progression defects induced through EHMT1 depletion, we determined the percentage of U2OS cells present in G1, S and G2/M phase in control or EHMT1 knockdown cells. We did not detect a significant difference in cell cycle distribution after EHMT1 deletion, which was confirmed by western blot analysis (Fig. 2C,D). However, we did observe a partial decrease in H3K9me2 upon EHMT1 knockdown (Fig. 2D), which is in agreement with other reports (Chase and Sharma, 2013; Tachibana et al., 2005).

EHMT1 is rapidly recruited to DNA DSBs

Having identified EHMT1 as a novel factor that controls 53BP1 recruitment during the DSB response, we wondered whether EHMT1 itself is recruited to sites of DNA damage.

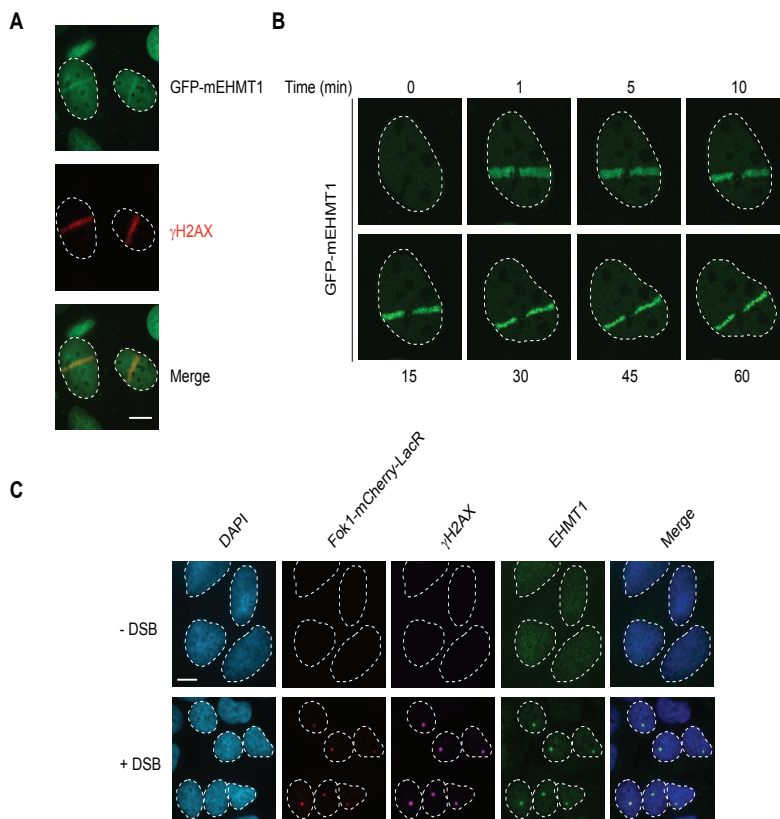


Figure 3. EHMT1 is rapidly recruited to DNA double-strand breaks decorated with γ H2AX. (A) GFP-tagged mouse EHMT1 was expressed in U2OS cells which were subsequently subjected to laser micro-irradiation. After 10 min, cells were fixed and immunostained for γ H2AX. EHMT1 co-localizes with γ H2AX at DNA damage. (B) GFP-mEHMT1 recruitment to laser-induced DNA damage in cells from (A) was monitored in time. Representative images of EHMT1 recruitment of one cell at indicated time points are shown. (C) Immunostaining for γ H2AX and EHMT1 at either no or FokI-induced DSBs, which was tagged with mCherry-LacR and re-located to a 200x integrated Lac operator genomic array in U2OS 263 ER-TA cells upon addition of Shield and 4-hydroxytamoxifen 6 h prior to fixation for translocation of FokI-fusion to the nucleus. Scale bars, 10 μ m.



Therefore, we locally introduced DNA damage with a Multi-photon (MP) laser in U2OS cells transiently expressing GFP-tagged mouse EHMT1 (Ehmt1), since mouse and human EHMT1 are highly conserved (Fig. S3). Ehmt1 rapidly localized to DSB-containing laser tracks, that were decorated with the DNA damage marker γ H2AX (Fig. 3A, B). Ehmt1 was detected already within 1 min after irradiation and remained associated with the damaged chromatin until at least 1 h after laser-mediated DNA damage induction (Fig. 3B). However, since MP laser-irradiation can induce several different types of DNA damage, we employed U2OS 2-6-3 cells to study whether EHMT1 is recruited to site-specific DSBs. Those cells contain an array of lactose operator (LacO) repeats and express instable FokI nuclease fused to the red fluorescent mCherry protein and the E. coli lactose repressor (LacR) (Fig. 3C) (Shanbhag et al., 2010). Upon translocation of the fusion protein to the nucleus mediated via 4-Hydroxytamoxifen and addition of the ligand Shield-1 for FokI-stabilization, the LacR-fusion protein got targeted to the LacO array, where FokI subsequently induced DSBs. Cells were fixed and co-immunostained for γ H2AX and EHMT1. Remarkably, endogenous EHMT1 clearly co-localized with FokI-mCherry-LacR at bona fide DSBs marked by γ H2AX. Taken together, these observations confirm the recruitment of EHMT1 to site-specific DSBs, where it somehow regulates the amount of 53BP1 assembly.

EHMT1 promotes DSB repair via Non-homologous end joining (NHEJ) and Homologous Recombination (HR)

In mammals, two major pathways have evolved to repair DSBs. The main pathway is called Non-homologous end-joining (NHEJ) and simply re-ligates the broken DNA ends back together throughout the whole cell-cycle, which can either happen in an error-free or error-prone fashion. The second repair pathway is termed homologous recombination (HR). The functioning of this pathway is restricted to S or G2-phase due to the requirement of a homologous or highly identical template, which is often provided by the sister chromatid (Chapman et al., 2012). To investigate whether EHMT1 contributes to DSB repair, we made use of two well-established reporter assays to monitor DSB repair efficiency in EHMT1-depleted Hek293T cells. The EJ5-GFP NHEJ reporter consists of a GFP gene, which is parted from its promoter due to an insertion of a Puromycine gene that is flanked by two I-SceI recognition sites. DSBs are induced upon transient expression of the rare-cutting I-SceI endonuclease and subsequent excision of the Puromycine gene. Repair of the broken DNA-ends via NHEJ fuses the promoter to the GFP gene and restores GFP expression, which can be measured by flow cytometry (Fig. 4A) (Bennardo et al., 2008). On the other hand, we employed the DR-GFP reporter to study HR, which consists of two differentially mutated GFP genes that are oriented as direct repeats. The upstream repeat carries an I-SceI restriction site, which inactivates gene function, whereas the downstream repeat is a 5' and 3' truncated version of the GFP gene. Transient expression of I-SceI leads to the induction of a DSB in the upstream GFP repeat, which can be repaired by HR using the downstream partial GFP sequence as a homologous template. This leads to the restoration of the GFP gene and consequently to GFP expression detectable by flow cytometry (Fig. 4C) (Weinstock et al., 2006). As expected, depletion of RNF8 and BRCA2 lead to a severe reduction in NHEJ and HR efficiency, respectively (Hu et al., 2014; Roy et al., 2012). Surprisingly, upon depletion of EHMT1 with three different siRNAs, the repair of DSBs via NHEJ as well as HR was considerably reduced (Fig. 4B,D). The knockdown of EHMT1 in Hek293T reporter cells (Fig. 4E) did not cause major changes in cell cycle distribution (Fig. 4F), suggesting that the observed effects were not indirect. The amount of EHMT1-depleted cells in G2/S-phase

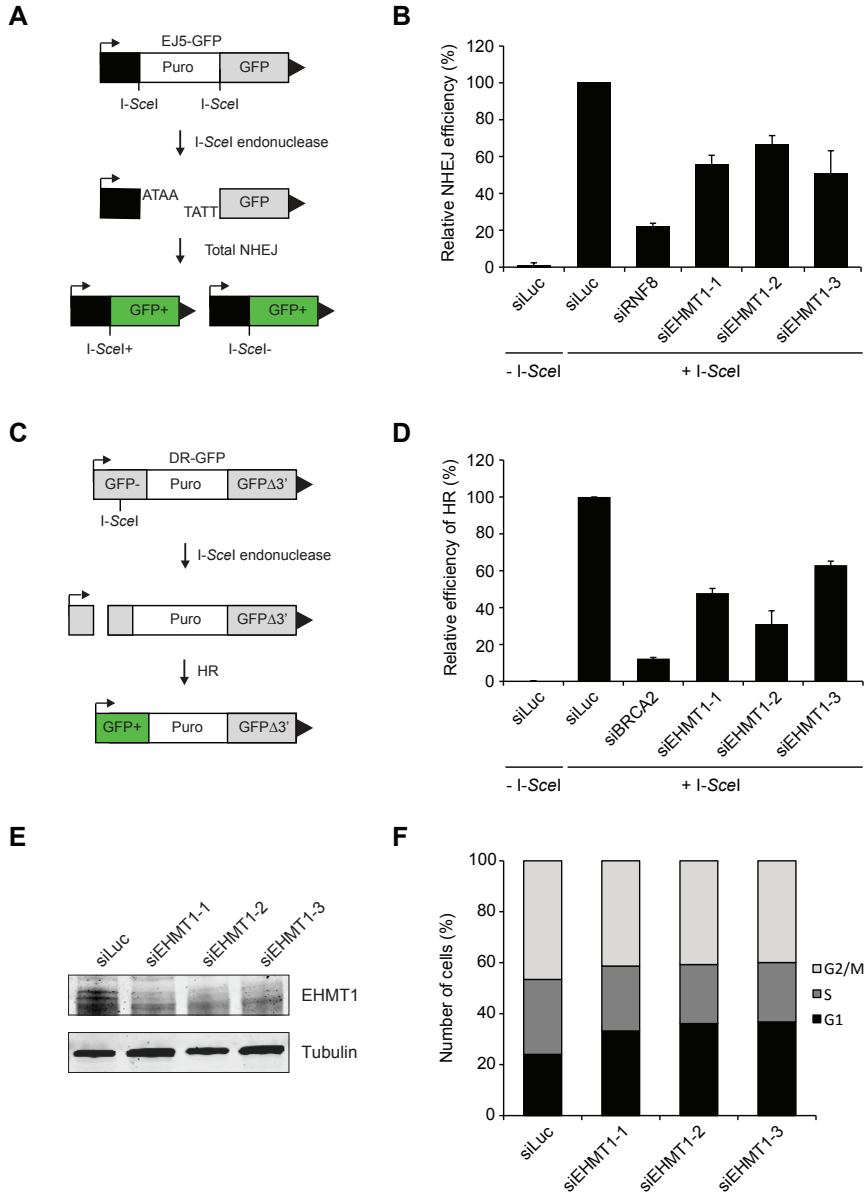


Figure 4. EHMT1 promotes the repair of DSBs via Non-homologous end joining (NHEJ) and Homologous Recombination (HR). (A) Schematic of the EJ5-GFP reporter used to monitor NHEJ efficiency in Hek293T cells (see text for details). (B) EJ5-GFP reporter cells were transfected with the indicated siRNAs. 48 hours later, cells were transfected with a control- or I-SceI expression vector (pCBA5ce). After additional 48 hours, cells were analysed for GFP expression by flow cytometry. The average of 2 experiments +/- s.e.m. is presented. (C) Schematic of the DR-GFP reporter exploited to investigate HR efficiency in Hek293T cells (see text for details). (D) DR-GFP reporter cells were treated the same way as described in (B). The average of 2 experiments +/- s.e.m. is shown. (E) Hek293T DR-GFP reporter cells were transfected with the indicated siRNAs, followed by transfection with the I-SceI expression vector 48 h later. Cells were stained with propidium iodide 24 h after that and subjected to flow cytometry analysis. The percentage of cells in G1 (black), S (dark gray) and G2/M (light gray) phase is shown. (F) Whole cell extracts from cells in (E) were subjected to western blot analysis.

might have been slightly less when compared to control cells, however it is unlikely that this small difference did cause the considerable drop in DSB repair efficiency upon EHMT1 knockdown. Therefore, these results suggest that EHMT1 promotes the effective repair of DSBs via NHEJ and HR.

DISCUSSION

Major cross-talk exists between histone modifications facilitating a permissive chromatin state in the vicinity of DSBs to promote their signaling and repair as part of the DSB response. In order to gain a better understanding of the spatio-temporal organisation of these chromatin modifications and to identify novel chromatin regulators with a role in the DSB response, we performed an siRNA-based high-throughput microscopy screen. With this approach we found the lysine methyltransferase (KTM) EHMT1 amongst several other hits to negatively regulate 53BP1 foci formation. Additionally, we showed that EHMT1 is rapidly recruited to DSBs and that it promotes DSB repair via both major repair pathways, NHEJ and HR. EHMT1 thus is a novel candidate for the maintenance of genome stability.

siRNA Screen for novel chromatin regulators

By examining γ H2AX or 53BP1 foci formation upon IR, we could monitor the early and late events during the response to DSBs. Hence, we not only gathered information about novel chromatin regulators and whether or not they have a role during the DDR, but could also define their moment of action more closely. 53BP1 thereby was a suitable read-out candidate to screen for, as several distinct chromatin modifications are required for and contribute to its accrual at DSBs.

We obtained a long list of possible chromatin regulators affecting either γ H2AX and/or 53BP1 accrual to IR-induced foci from the primary screen. Among those hits, known regulators of γ H2AX were found such as BAZ1B (WSTF), which is involved in the global phosphorylation of H2AX on Y142 (Xiao et al., 2009), a mark that needs to be removed upon damage induction for proper MDC1-binding to γ H2AX at S139 (Cook et al., 2009; Krishnan et al., 2009). Moreover, depletion of the ATP-dependent chromatin remodeler SMARCA4 (BRG1) led to a decrease in γ H2AX foci formation. This is in agreement with recent reports, which indicated that SMARCA4 is phosphorylated by ATM upon DSB induction and promotes γ H2AX formation as well as DSB repair through the binding of acetylated histone H3 in γ H2AX-containing nucleosomes (Kwon et al., 2015) (Table S1A). We further detected an increase in 53BP1 foci formation after IR in cells depleted from JMJD2A, which has been shown to mask H4K20me₂, subsequently preventing 53BP1 binding at DSBs. For 53BP1 binding to occur, JMJD2A needs to be targeted for degradation through ubiquitylation by RNF168 upon DSB induction (Lee et al., 2008; Mallette et al., 2012). Likewise, the depletion of CBX5, better known as HP1 α , was found to cause elevated levels of 53BP1 foci, which is in agreement with previously published results (Lee et al., 2013).

With a selection of 48 hits from this primary screen, a deconvolution screen was performed. We were able to confirm 4 hits, of which we selected EHMT1 for a follow-up study. Its regulatory effect on 53BP1 accrual to DSBs was successfully validated during a second IR-induced foci experiment, where another format and different siRNA transfection method was used (Fig. 2A,B). This thus shows the ability of our screening approach to identify novel factors involved in the DSB response. However, potential hits might also



have been missed out on due to knockdown efficiency issues, since we could not control siRNA transfection efficiency per individual siRNA. Nonetheless, siKIF11 transfection led to 90% cell death and a strong decrease in 53BP1 foci formation was observed upon RNF8 depletion. Hence, the controls for siRNA transfection efficiency indicated the effectiveness of the applied transfection protocol. Additionally, the reproducibility of the generated data was confirmed by the calculation of the Z-factor for each plate, that all met the threshold criteria.

Stringent selection during deconvolution screen

Due to the biased target selection of epigenetic regulators and the high number of possible hits obtained from the primary screen, we stringently applied thresholds during the analysis of the deconvolution screen. Here, 3x the standard deviation of the siLuc control was used as selection criteria, which led to the confirmation of EHMT1 as a hit, but excluded its related heterodimer-partner EHMT2 from the hit list (Table 1B) (Tachibana et al., 2005). Interestingly, EHMT2 would have been a hit under the threshold of 1x the standard deviation (Fig. 1E; Table S1A,B). This less pronounced increase in 53BP1 foci formation in EHMT2-depleted cells could have been caused by insufficient siRNA transfection efficiency. On the other hand, this could also hint towards an independent function of EHMT1 in the response to DSBs. However, the H3K9 mono- and dimethylation activities were assigned to both KMTs and loss of one or the other leads to a clear decrease in global H3K9me1/2 levels (Tachibana et al., 2005; Tachibana et al., 2008). Subsequently, further verification of the role of EHMT2 in the DSB response either dependent or independent of EHMT1 is therefore required.

EHMT1 recruitment to DSBs

Although EHMT1 was identified as a negative regulator of 53BP1 accrual into IR-induced foci, we found that γ H2AX formation remained unaffected in EHMT1-depleted cells (Fig. 1D,E; Table S1A,B). This suggests that the activity of EHMT1 is important for the more downstream steps of the DSB response. However, EHMT1 is recruited rather rapidly to DSBs (Fig. 3), which might hint towards a role in a process taking place immediately after DNA damage induction, yet one that controls 53BP1 recruitment. To further categorize EHMT1 into the numerous events of the DDR, the recruitment of other important DSB response factors such as MDC1, RNF8 or RNF168 to IR-induced foci or laser-induced DNA damage should be monitored in the absence of EHMT1. Moreover, the recruitment of several DSB response factors is highly dependent on the phosphorylation activity of ATM on serine (S) target sites. Both, EHMT1 and EHMT2, have shown to contain ATM-/ATR-target sites on Ser466 and Ser569, respectively (Matsuoka et al., 2007). It is therefore likely, that EHMT1 and EHMT2 are recruited in an ATM-dependent fashion, but this still requires experimental confirmation. Another way to rapidly recruit EHMT1 could be facilitated through the action of poly(ADP-ribose) polymerase 1 (PARP1), which attaches poly(ADP-ribose) chains onto itself and other target proteins upon DSB induction (Bekker-Jensen and Mailand, 2010; Smeenk et al., 2013). Since the recruitment of the histone tri-methylase SUV39H was found to be PARP-dependent (Ayrapetov et al., 2014), it would be interesting to investigate the contribution of PARP to EHMT1 recruitment in cells depleted from PARP or treated with a PARP inhibitor.

Possible role of EHMT1 at DSBs

Once EHMT1 is recruited to DSBs, it exerts a yet unknown function. However, it has been

generally described to mono- and dimethylate H3K9 within euchromatin, together with EHMT2 (Tachibana et al., 2005). Since di- and trimethylation of H3K9 was shown to locally increase upon DSB induction (Ayrappetov et al., 2014; Khurana et al., 2014), the question arises whether EHMT1/2 contribute to establish H3K9me2 at DSBs. For the binding of oligomerized 53BP1 at DSBs, RNF168-ubiquitylated H2AK15 (Fradet-Turcotte et al., 2013) and H4K20me2, established through the combined action of MMSET and SETD8, are required (Panier et al., 2012). But how could the H3K9 methyltransferase activity of EHMT1 affect 53BP1 accumulation? We hypothesize that it might perform the first two methylation steps on H3K9 upon DSB induction providing the substrate for SUV39H H3K9 trimethylation, which is an important mark for the recruitment and activation of TIP60 to DSBs (Sun et al., 2009). TIP60 binds H3K9me3 and acetylates H4K16 (Hsiao and Mizzen, 2013; Tang et al., 2013), which prevents de novo H4K20 mono- and dimethylation by SETD8 and MMSET (Huen et al., 2008; Pei et al., 2011). However, upon DSB induction the histone deacetylases HDAC1/2 are recruited and facilitate the deacetylation of H4K16 (Miller et al., 2010), paving the way for SETD8 and MMSET and promoting 53BP1 accrual. Other proteins bound to H4K20me2 such as L3MBTL1 and JMJD2A are then removed from chromatin in the vicinity to the DSB by eviction or proteasomal degradation (Acs et al., 2011; Mallette et al., 2012; Meerang et al., 2011). Hypothetically, when translating these events to the case of EHMT1-depletion, H3K9me3 would not be established for TIP60 binding, highly stimulating H4K20 methylation followed by an increase of 53BP1 assembly at DSBs, which describes the exact phenotype obtained during the siRNA screen and validation experiments (Fig. 1E,2B).

To investigate this hypothesis experimentally, one could use ChIP to examine whether a local decrease in H3K9 methylation levels at DSBs can be detected in EHMT1-depleted or -inhibitor treated cells compared to untreated cells. Additionally in a similar set-up, H4K16ac levels could be examined at DSBs looking for a decrease in H4K16ac in cells with no functional EHMT1 like it has been done for SUV39H-depleted cells showing a loss in H4K16-acetylation (Ayrappetov et al., 2014). This would indicate that EHMT1/2-mediated H3K9 methylation is required for TIP60 binding and activity. And since a portion of EHMT1 and EHMT2 was found to form a multimeric complex with SUV39H and the histone di-/trimethyltransferase SETDB1 (Fritsch et al., 2010), the combined action of these histone mono-/di- and trimethylases seems plausible in order to facilitate DSB-dependent local H3K9me3 regulating 53BP1 accrual.

EHMT1 also would not be the first H3K9 dimethyltransferase implicated in the DSB response, since the PR domain zinc finger protein 2 (PRDM2), together with the repressive macrohistone variant macroH2A1, has been shown to promote the formation of condensed chromatin in a manner dependent on ATM and dimethylation of H3K9. These events ultimately facilitate DSB end resection, BRCA1 recruitment and DSB repair via HR (Khurana et al., 2014). Conversely, H3K9me3 has been suggested to only transiently increase following the rapid accumulation of the KAP1/HP1/SUV39H complex to DSBs. Once TIP60 is activated through the binding of the established H3K9me3 mark, it acetylates ATM and H4. This is immediately followed by ATM-dependent KAP1 phosphorylation, which leads to the release of the KAP1/HP1/SUV39H complex from chromatin (Ayrappetov et al., 2014). The authors reasoned that ATM activation functions as negative feedback loop through the removal of repressive SUV39H from DSBs, possibly limiting DSB repair. However, whether KAP1/HP1/SUV39H only induces transient H3K9me3 is questionable, since SET just recently has been shown to be recruited to DSBs, where it interacts with KAP1 and induces the retention of KAP1 and HP1 at DSBs. When overexpressed, a compact chromatin state is established that

limits uncontrolled DSB signaling and inhibits DNA end resection as well as repair via HR during S/G2 phase of the cell cycle (Kalouosi et al., 2015). Thus, that H3K9 methylation is strictly regulated during the DSB response to induce repressive chromatin formation either transiently or in general becomes increasingly clear. However, future research is required to define the persistence of H3K9me3 and the role of EHMT1/2 in H3K9me3 establishment at DSBs.

Potential consequences of EHMT1 overexpression

Where the depletion of EHMT1 leads to an increase in 53BP1 recruitment to DSBs, its overexpression might actively abrogate the response to DSBs by promoting H3K9 methylation and simultaneous HP1- or TIP60-binding that subsequently leads to H4K16-acetylation. This would result in a restrained availability of binding sites for 53BP1 at DSBs. When testing this hypothesis experimentally, we observed that transiently overexpressed Ehmt1 is rapidly recruited to DSB-containing laser tracks, where Ehmt1 remained present for at least 1 h at the site of DNA damage (Fig. 3A). Interestingly, upon a more closely investigation of those laser tracks, we could detect a decrease in the spreading of GFP-tagged Ehmt1 within the damaged chromatin compartment over time, which would support the hypothesis that Ehmt1 overexpression negatively regulates the DSB response. However, to map the consequences of EHMT1 overexpression, the track width, which is a measure reflecting the extent to which factors spread into the damaged chromatin compartment, should be determined in time after DNA damage induction by laser micro-irradiation for EHMT1 and 53BP1. If this theory holds, 53BP1 accrual would be clearly decreased and less expanded upon excessive EHMT1 expression. Additional research however needs to point out whether that is the case.

EHMT1 also methylates non-histone targets

EHMT1/2 can methylate itself, H3K9 and, several non-histone proteins. Methylation of the Widely-interspaced zinc finger-containing protein (WIZ) stabilizes EHMT1/EHMT2 complex formation through the binding of its sixth zinc-finger motif to the SET-domains of EHMT1/EHMT2. WIZ thereby acts as an adaptor molecule that stabilizes EHMT2 and might drive the dominant heteromeric complex formation of EHMT1/2 in vivo (Tachibana et al., 2005; Ueda et al., 2006). Hence, WIZ might indirectly be involved in the regulation of 53BP1 levels during the DSB response via the action of the EHMT1/2-WIZ complex. Another established target of EHMT1/2 methylation is the tumor suppressor p53 which is primarily dimethylated on K737. This process in turn is regulated by the E3 ubiquitin ligase MDM2 (Chen et al., 2010; Huang et al., 2010). Upon DSB induction, MDM2 and p53 are phosphorylated by ATM leading to a de- or increase in their protein stability, respectively (Khosravi et al., 1999). However under these conditions, K737me2 levels of p53 remained the same, which indicates that this mark correlates with inactive p53. This is supported by the fact that upon EHMT1/EHMT2-depletion the levels of apoptotic cells increase due to p53 release from K373me2-mediated repression (Huang et al., 2010), something we did observe visually but did not measure in the performed cell-cycle experiments of EHMT1-depleted cells (Fig. 2C,4F). Whether and if so, how the methylation of these and possible unknown targets is related to the role of EHMT1 in regulating 53BP1 levels during the DSB response remains unclear and requires further investigation.

Additionally, EHMT1/EHMT2 targets have been identified by immunoprecipitating methylation target proteins with the GST-tagged methyl-binding domain of L3MBTL1 from

cells treated without or with an inhibitor for EHMT1/EHMT2 (UNC0638). Interestingly, amongst others the DNA repair factors DNA ligase 1 (LIG1), DNA-dependent protein kinase catalytic subunit (DNA-PKcs) and the chromatin remodeler SMARCA5 have been identified as methylation-candidate targets of EHMT1/EHMT2 (Moore et al., 2013). Future studies need to reveal the role of EHMT1/EHMT2-dependent methylation of these factors during the response to DSBs. However, there is also a possibility that EHMT1 might exert a yet unknown function, which is not connected to its described lysine methylation activity. In that case, recruitment studies of DSB response factors would provide insights on the spatio-temporal activity of EHMT1 during the DSB response and would lead to appropriate follow up studies.

EHMT1 is involved in the efficient repair of DSBs via NHEJ and HR

The well-established EJ5-GFP and DR-GFP reporters used to monitor DSB repair efficiency of NHEJ or HR, respectively, clearly suggest a role for EHMT1 during the repair of DSBs (Fig. 4A-D). As previously discussed, EHMT1 seems to regulate 53BP1 accrual, which has been identified as an important factor driving NHEJ by preventing resection at DSBs and the subsequent assembly of HR factors (Panier et al., 2012). However, EHMT1 depletion promotes both repair pathways in the employed reporter assays. To gain a better understanding of how EHMT1 can promote NHEJ as well as HR, a possible additive effect on DSB repair efficiency could be monitored by additional depletion of 53BP1 from siEHMT1 treated DR-GFP reporter cells. Moreover, besides the recruitment of 53BP1 and BRCA1 in siEHMT1 treated cells, the accumulation of DSB signalling factors like RNF8 and RNF168, DNA end resection factors like CtIP and RPA or DSB repair factors like XRCC4 and RAD51 could be monitored to locally laser micro-irradiated regions or IR-induced foci. This would more precisely define EHMT1's mode of action during DSB signalling and repair. Finally, there is also a possibility that EHMT1 exerts diverse, yet unknown functions within the two different repair pathways. In any case, revealing the function of EHMT1 will instantly lead to a better understanding of how it can contribute to the repair of DSBs via both repair pathways.

EHMT1 involved in intellectual disability syndrome and cancer

Loss of function mutations in EHMT1 are one cause of the intellectual disability disorder Kleefstra syndrome in humans (Kleefstra et al., 1993; Kleefstra et al., 2012; Nillesen et al., 2011). This phenotype is also conserved in *Drosophila* where EHMT-deficiency apparently leads to defects in learning and memory (Kramer et al., 2011). Moreover, EHMT1 and EHMT2 knockout mice are embryonic lethal and global H3K9me1/2 levels are highly reduced in knockout ES cells (Tachibana et al., 2002; Tachibana et al., 2005), indicating an important role for EHMT1/2 activity in mammalian development. Furthermore, EHMT1 and EHMT2 have been reported to be overexpressed in various cancers (Guan et al., 2014; Huang et al., 2010), which suggests a role as putative oncogenes. Consequently, they may form promising anti-cancer drug targets for the development of chemical inhibitors. Encouragingly for such a purpose, EHMT2 knockdown appeared to inhibit tumor cell growth in vitro and induced extensive chromosome instability (Kondo et al., 2008). Consequently, EHMT1- and EHMT2-dependent maintenance of H3K9 methylation in euchromatin and/or methylation of other target proteins such as p53 and mentioned DNA repair factors seems highly important for the preservation of genome stability.

MATERIAL AND METHODS

Cell culture

U2OS cells, U2OS 263 cells containing a 200x integrated Lac operator genomic array and HEK293T cells were grown in DMEM (Gibco) containing 10% FCS (Bodinco BV) and 1% penicillin/streptomycin unless stated otherwise. U2OS 263 cells were a gift from Susan Janicki (Shanbhag et al., 2010) and were grown in the presence of G418 [400 µg/ml].

siRNA screen

siRNAs, from Dharmacon siGENOME® SMARTpool® Epigenetics siRNA library supplemented with 80 custom siGENOME® SMARTpool® siRNAs for the first screen and from a customized library containing sets of four single siRNA per target for the validation screen, were spotted into 96-well glass bottom plates. Additionally, the negative control Luciferase (Luc) and positive controls RNF8 and KIF11 were spotted 3 times at different locations per 96-well screening plate. Reverse siRNA transfection was performed by adding first HiPerFect transfection reagent (QIAGEN) to each well according to manufacturer instructions and secondly U2OS cells in DMEM (Gibco) containing 10% FCS (Bodinco BV). Cells were cultivated at 37°C and after 24 h, media was refreshed with DMEM containing 10% FCS and 1% penicillin/streptomycin. 48 hours later, cells were exposed to 2 Gy of ionizing radiation (IR) and fixed after 1 h at 37°C with 4% formaldehyde for 10 min. Cells were treated with 0.1% Triton X-100 in PBS for 5 min and rinsed with PBS, followed by equilibration of cells in PBS containing 5 g BSA/L and 1.5 g glycine/L prior to immunostaining for γH2AX (1:2000, #07-164, Millipore) and 53BP1 (1:1000, #NB100-304, Novus Biologicals). Detection of primary antibodies was accomplished using goat anti-mouse or goat anti-rabbit IgG coupled to Alexa 488 or 555 (Invitrogen Molecular probes). Cells were incubated with DAPI [0.1 µg/ml] and after several PBS washes kept in PBS at 4°C. High-throughput imaging was performed on a BD pathway equipped with a Nipkow spinning disc for confocal imaging and a 40x objective. Each screen was executed in duplicate and BD Image Data Explorer software version 2.3.1 was used from BD Biosciences for automated analysis to determine the average number of foci/nucleus. Z-scores were calculated from the duplicates per 96-well plate with following formula:

$$Z\text{-score} = (x - \mu) / \sigma$$

x – raw score,
 μ – mean of Luc per plate,
 σ – std dev of Luc per plate (Doil et al., 2009).

Z-scores with a cut-off of 1.5 below or above the reference and a p-value lower than 0,05 were categorized as hit in the first screen using SMARTpool® siRNAs. During the validation screen the average amount of foci/nucleus was determined from duplicates employing the set of four single siRNAs per target of which at least three needed to cause a difference of more than 3 times the standard deviation from Luciferase to be assigned as hit.

Transfections and RNAi interference

siRNA and plasmid transfections were performed using Lipofectamine RNAiMAX (Invitrogen) or Lipofectamine 2000 (Invitrogen), respectively, according to the manufacturer's instructions. During the follow-up study, the following siRNA sequences were used:

5'- CGUACGCGGAAUACUUCGA -3' (Luciferase, Dharmacon),
5'- GAGGGCCAAUGGACAAUUA -3' (RNF8, Dharmacon),
5'- CAAACAGCGUGGUCAAGUA -3' (EHMT1-1, Dharmacon),
5'- CAAGAAAGGCCACUACGAA -3' (EHMT1-2, Dharmacon),
5'- GGAAUUCUGUCUUCACAAG -3' (EHMT1-3, Dharmacon),
5'- AUAUGUUGGUGAACUGAGA -3' (XRCC4, Dharmacon),
5'- GAAGAAUGCAGGUUUAUA - 3' (BRCA2, Dharmacon).

Cells were transfected twice with siRNAs [40 nM] within 24 h and examined further 48 h after the second transfection unless stated otherwise.

Generation of DSBs

IR was delivered by a YXlon X-ray generator (YXlon International, 200 KV, 4 mA, dose rate 1.1 Gy/min). In U2OS 263 cells, DSBs were induced throughout the addition of Shield [1 μ M] (Clontech) and 4-Hydroxytamoxifen [300 nM] to the growth media (Guan et al., 2014; Shanbhag et al., 2010) to induce nuclear expression of the mCherry-LacR-FokI fusion that localizes to the LacO array, where FokI induces DSBs (Shanbhag et al., 2010). Cells were subsequently fixed with 4% formaldehyde after 6 h followed by immunostaining.

Plasmid

GFP-mEHMT1 expression vectors were obtained from Yoichi Shinkai (Tachibana et al., 2005).

Laser micro-irradiation

Multiphoton laser micro-irradiation was carried out on a Leica SP5 confocal microscope equipped with an environmental chamber set to 37°C (Helfricht et al., 2013). Briefly, U2OS cells were grown on 18 mm glass coverslips and media was replaced with CO₂-independent Leibovitz L15 medium, both supplemented with 10% FCS and 1% penicillin/streptomycin. Cells were placed in a Chamlide TC-A live-cell imaging chamber before imaging and were kept at 37°C. DSB-containing tracks (1.5 μ m width) were generated with a Mira modelocked Ti:Sapphire laser (λ = 800 nm, pulse length = 200 fs, repetition rate = 76 MHz, output power = 80 mW). Typically, cells were micro-irradiated with 1 iteration per pixel using LAS-AF software, incubated for the indicated time-points at 37°C and subsequently fixed with 4% formaldehyde before immunostaining. For live cell imaging, confocal images were recorded before and after laser irradiation at different time intervals.

Immunofluorescent labelling

Immunofluorescent labeling of γ H2AX and EHMT1 was performed as described previously (Helfricht et al., 2013). Briefly, cells were grown on glass coverslips and treated as indicated in the figure legends. Subsequently, cells were washed with PBS, fixed with 4% formaldehyde for 10 min and treated with 0.1% Triton X-100 in PBS for 5 min. Cells were rinsed with PBS and equilibrated in PBS containing BSA [5 g/l] and glycine [1.5 g/l] prior to immunostaining. Detection was done using goat anti-mouse or goat anti-rabbit IgG coupled to Alexa 488, 555 or 647 (Invitrogen Molecular probes). Samples were incubated with DAPI [0.1 μ g/ml] and mounted in Polymount.

Microscopy analysis

Images of fixed samples were acquired on a Zeiss AxioImager M2 widefield fluorescence



microscope equipped with 40×, 63×, and 100× PLAN APO (1.4 NA) oil-immersion objectives (Zeiss) and an HXP 120 metal-halide lamp used for excitation, as well as ZEN software (2012). Fluorescent probes were detected using the following filters: DAPI (excitation filter: 350/50 nm, dichroic mirror: 400 nm, emission filter: 460/50 nm), GFP/Alexa 488 (excitation filter: 470/40 nm, dichroic mirror: 495 nm, emission filter: 525/50 nm), mCherry (excitation filter: 560/40 nm, dichroic mirror: 585 nm, emission filter: 630/75 nm), Alexa 555 (excitation filter: 545/25 nm, dichroic mirror: 565 nm, emission filter: 605/70 nm), Alexa 647 (excitation filter: 640/30 nm, dichroic mirror: 660 nm, emission filter: 690/50 nm). The average number of IR-induced foci per nucleus was determined using ImageJ and the IRIF analysis 3.2 Macro as previously described (Typas et al., 2015).

Cell cycle profiling

For cell cycle analysis cells were fixed in 70% ethanol, followed by DNA staining with 50 µg/ml propidium iodide in the presence of RNase A (0.1 mg/ml). Cell sorting was performed on a BD LSRII flow cytometer (BD Bioscience) using FACSDiva software version 5.0.3. Obtained data was quantified with Flowing software 2.5.1 (by Perttu Terho in collaboration with Turku Bioimaging).

Western blot analysis

Protein extracts were generated by direct lysis of cells in 2x Laemmli buffer and boiled for 10 min at 95°C. Proteins were size separated using Novex 4-12% Bis-Tris mini gels (Invitrogen) in 1x MOPS buffer (Invitrogen) and transferred to PVDF membranes, which were blocked in 4% milk for at least 30 minutes and incubated with the indicated antibodies overnight. Several wash steps before and after 1 h incubation with secondary antibodies rabbit-anti-700 and mouse-anti-800 (Sigma) were executed. Protein bands were visualized using the Odyssey infrared imaging system (Licor) according to manufacturer's instructions.

Antibodies

Immunofluorescence and western blot analysis were performed using antibodies against γ H2AX (1:1000-2000, #07-164, Millipore), 53BP1 (1:1000, #NB100-304, Novus Biologicals), EHMT1 (1:500, #B0422, R&D Systems), α -Tubulin (1:1000, #T6199 clone DM1A, Sigma), Histone H3K9me2 (1:500, #1220, Abcam) and Histone H3 (1:1000, #1791, Abcam).

Homologous recombination and Non-homologous end-joining repair assay

HEK293 cell lines containing a stably integrated copy of the DR-GFP or EJ5-GFP reporter, respectively, were used to measure the repair of I-SceI-induced DSBs via NHEJ or HR (Bennardo et al., 2008; Pierce and Jasin, 2014; Weinstock et al., 2006). Briefly, 48 h after siRNA transfection, cells were transfected with the I-SceI expression vector pCBASce and a mCherry expression vector (Pierce et al., 1999). 48 h later the fraction of GFP-positive cells among the mCherry-positive cells was determined by FACS on a BD LSRII flow cytometer (BD Bioscience) using FACSDiva software version 5.0.3. Quantifications were performed using Flowing software 2.5.1 (by Perttu Terho in collaboration with Turku Bioimaging).

ACKNOWLEDGEMENTS

We thank Louise von Stechow, Jordi Carreras Puigvert and Ram Sidappa for sharing experimental knowledge and assistance with spotting siRNAs.

REFERENCES

1. Acs,K., Luijsterburg,M.S., Ackermann,L., Salomons,F.A., Hoppe,T., and Dantuma,N.P. (2011). The AAA-ATPase VCP/p97 promotes 53BP1 recruitment by removing L3MBTL1 from DNA double-strand breaks. *Nat. Struct. Mol. Biol.* 18, 1345-1350.
2. Ayrapetov,M.K., Gursoy-Yuzugullu,O., Xu,C., Xu,Y., and Price,B.D. (2014). DNA double-strand breaks promote methylation of histone H3 on lysine 9 and transient formation of repressive chromatin. *Proc. Natl. Acad. Sci. U. S. A* 111, 9169-9174.
3. Bannister,A.J., Zegerman,P., Partridge,J.F., Miska,E.A., Thomas,J.O., Allshire,R.C., and Kouzarides,T. (2001). Selective recognition of methylated lysine 9 on histone H3 by the HP1 chromo domain. *Nature* 410, 120-124.
4. Bekker-Jensen,S. and Mailand,N. (2010). Assembly and function of DNA double-strand break repair foci in mammalian cells. *DNA Repair (Amst)* 9, 1219-1228.
5. Bennardo,N., Cheng,A., Huang,N., and Stark,J.M. (2008). Alternative-NHEJ is a mechanistically distinct pathway of mammalian chromosome break repair. *PLoS. Genet.* 4, e1000110.
6. Botuyan,M.V., Lee,J., Ward,I.M., Kim,J.E., Thompson,J.R., Chen,J., and Mer,G. (2006). Structural basis for the methylation state-specific recognition of histone H4-K20 by 53BP1 and Crb2 in DNA repair. *Cell* 127, 1361-1373.
7. Chapman,J.R., Taylor,M.R., and Boulton,S.J. (2012). Playing the end game: DNA double-strand break repair pathway choice. *Mol. Cell* 47, 497-510.
8. Chase,K.A. and Sharma,R.P. (2013). Nicotine induces chromatin remodelling through decreases in the methyltransferases GLP, G9a, Setdb1 and levels of H3K9me2. *Int. J. Neuropsychopharmacol.* 16, 1129-1138.
9. Chen,L., Li,Z., Zwolinska,A.K., Smith,M.A., Cross,B., Koomen,J., Yuan,Z.M., Jenuwein,T., Marine,J.C., Wright,K.L., and Chen,J. (2010). MDM2 recruitment of lysine methyltransferases regulates p53 transcriptional output. *EMBO J.* 29, 2538-2552.
10. Chou,D.M., Adamson,B., Dephoure,N.E., Tan,X., Nottke,A.C., Hurov,K.E., Gygi,S.P., Colaiacovo,M.P., and Elledge,S.J. (2010). A chromatin localization screen reveals poly (ADP ribose)-regulated recruitment of the repressive polycomb and NuRD complexes to sites of DNA damage. *Proc. Natl. Acad. Sci. U. S. A* 107, 18475-18480.
11. Cook,P.J., Ju,B.G., Telese,F., Wang,X., Glass,C.K., and Rosenfeld,M.G. (2009). Tyrosine dephosphorylation of H2AX modulates apoptosis and survival decisions. *Nature* 458, 591-596.
12. Doil,C., Mailand,N., Bekker-Jensen,S., Menard,P., Larsen,D.H., Pepperkok,R., Ellenberg,J., Panier,S., Durocher,D., Bartek,J., Lukas,J., and Lukas,C. (2009). RNF168 binds and amplifies ubiquitin conjugates on damaged chromosomes to allow accumulation of repair proteins. *Cell* 136, 435-446.
13. Epsztejn-Litman,S., Feldman,N., Abu-Remaileh,M., Shufaro,Y., Gerson,A., Ueda,J., Deplus,R., Fuks,F., Shinkai,Y., Cedar,H., and Bergman,Y. (2008). De novo DNA methylation promoted by G9a prevents reprogramming of embryonically silenced genes. *Nat. Struct. Mol. Biol.* 15, 1176-1183.
14. Fradet-Turcotte,A., Canny,M.D., Escibano-Diaz,C., Orthwein,A., Leung,C.C., Huang,H., Landry,M.C., Kitevski-LeBlanc,J., Noordermeer,S.M., Sicheiri,F., and Durocher,D. (2013). 53BP1 is a reader of the DNA-damage-induced H2A Lys 15 ubiquitin mark. *Nature* 499, 50-54.
15. Fritsch,L., Robin,P., Mathieu,J.R., Souidi,M., Hinaux,H., Rougeulle,C., Harel-Bellan,A., Ameyar-Zazoua,M., and Ait-Si-Ali,S. (2010). A subset of the histone H3 lysine 9 methyltransferases Suv39h1, G9a, GLP, and SETDB1 participate in a multimeric complex. *Mol. Cell* 37, 46-56.
16. Gatti,M., Pinato,S., Maspero,E., Soffientini,P., Polo,S., and Penengo,L. (2012). A novel ubiquitin mark at the N-terminal tail of histone H2As targeted by RNF168 ubiquitin ligase. *Cell Cycle* 11, 2538-2544.
17. Guan,X., Zhong,X., Men,W., Gong,S., Zhang,L., and Han,Y. (2014). Analysis of EHMT1 expression and its correlations with clinical significance in esophageal squamous cell cancer. *Mol. Clin. Oncol.* 2, 76-80.
18. Helfricht,A., Wiegant,W.W., Thijssen,P.E., Vertegaal,A.C., Luijsterburg,M.S., and van Attikum,H. (2013). Remodeling and spacing factor 1 (RSF1) deposits centromere proteins at DNA double-strand breaks to promote non-homologous end-joining. *Cell Cycle* 12, 3070-3082.
19. Hsiao,K.Y. and Mizzen,C.A. (2013). Histone H4 deacetylation facilitates 53BP1 DNA damage signaling and double-strand break repair. *J. Mol. Cell Biol.* 5, 157-165.
20. Hu,Y., Wang,C., Huang,K., Xia,F., Parvin,J.D., and Mondal,N. (2014). Regulation of 53BP1 protein stability by RNF8 and RNF168 is important for efficient DNA double-strand break repair. *PLoS. One.* 9, e110522.
21. Huang,J., Dorsey,J., Chuiikov,S., Perez-Burgos,L., Zhang,X., Jenuwein,T., Reinberg,D., and Berger,S.L. (2010). G9a and Glp methylate lysine 373 in the tumor suppressor p53. *J. Biol. Chem.* 285, 9636-9641.
22. Huen,M.S., Grant,R., Manke,I., Minn,K., Yu,X., Yaffe,M.B., and Chen,J. (2007). RNF8 transduces the DNA-damage signal via histone ubiquitylation and checkpoint protein assembly. *Cell* 131, 901-914.
23. Huen,M.S., Sy,S.M., van Deursen,J.M., and Chen,J. (2008). Direct interaction between SET8 and proliferating cell nuclear antigen couples H4-K20 methylation with DNA replication. *J. Biol. Chem.* 283, 11073-11077.
24. Hurov,K.E., Cotta-Ramusino,C., and Elledge,S.J. (2010). A genetic screen identifies the Triple T complex required for DNA damage signaling and ATM and ATR stability. *Genes Dev.* 24, 1939-1950.

25. Kaidi,A. and Jackson,S.P. (2013). KAT5 tyrosine phosphorylation couples chromatin sensing to ATM signalling. *Nature* 498, 70-74.
26. Kalousi,A., Hoffbeck,A.S., Selemenakis,P.N., Pinder,J., Savage,K.I., Khanna,K.K., Brino,L., Dellaire,G., Gorgoulis,V.G., and Soutoglou,E. (2015). The Nuclear Oncogene SET Controls DNA Repair by KAP1 and HP1 Retention to Chromatin. *Cell Rep.* 11, 149-163.
27. Khosravi,R., Maya,R., Gottlieb,T., Oren,M., Shiloh,Y., and Shkedy,D. (1999). Rapid ATM-dependent phosphorylation of MDM2 precedes p53 accumulation in response to DNA damage. *Proc. Natl. Acad. Sci. U. S. A* 96, 14973-14977.
28. Khurana,S., Kruhlak,M.J., Kim,J., Tran,A.D., Liu,J., Nyswaner,K., Shi,L., Jailwala,P., Sung,M.H., Hakim,O., and Oberdoerffer,P. (2014). A macrohistone variant links dynamic chromatin compaction to BRCA1-dependent genome maintenance. *Cell Rep.* 8, 1049-1062.
29. Kleefstra,T., Kramer,J.M., Neveling,K., Willemsen,M.H., Koemans,T.S., Vissers,L.E., Wissink-Lindhout,W., Fencikova,M., van den Akker,W.M., Kasri,N.N., Nillesen,W.M., Prescott,T., Clark,R.D., Devriendt,K., van,R.J., de Brouwer,A.P., Gilissen,C., Zhou,H., Brunner,H.G., Veltman,J.A., Schenck,A., and van,B.H. (2012). Disruption of an EHMT1-associated chromatin-modification module causes intellectual disability. *Am. J. Hum. Genet.* 91, 73-82.
30. Kleefstra,T., Nillesen,W.M., and Yntema,H.G. (1993). Kleefstra Syndrome.
31. Kolas,N.K., Chapman,J.R., Nakada,S., Ylanko,J., Chahwan,R., Sweeney,F.D., Panier,S., Mendez,M., Wildenhain,J., Thomson,T.M., Pelletier,L., Jackson,S.P., and Durocher,D. (2007). Orchestration of the DNA-damage response by the RNF8 ubiquitin ligase. *Science* 318, 1637-1640.
32. Kondo,Y., Shen,L., Ahmed,S., Boumber,Y., Sekido,Y., Haddad,B.R., and Issa,J.P. (2008). Downregulation of histone H3 lysine 9 methyltransferase G9a induces centrosome disruption and chromosome instability in cancer cells. *PLoS. One.* 3, e2037.
33. Kramer,J.M., Kochinke,K., Oortveld,M.A., Marks,H., Kramer,D., de Jong,E.K., Asztalos,Z., Westwood,J.T., Stunnenberg,H.G., Sokolowski,M.B., Keleman,K., Zhou,H., van,B.H., and Schenck,A. (2011). Epigenetic regulation of learning and memory by *Drosophila* EHMT/G9a. *PLoS. Biol.* 9, e1000569.
34. Krishnan,N., Jeong,D.G., Jung,S.K., Ryu,S.E., Xiao,A., Allis,C.D., Kim,S.J., and Tonks,N.K. (2009). Dephosphorylation of the C-terminal tyrosyl residue of the DNA damage-related histone H2A.X is mediated by the protein phosphatase eyes absent. *J. Biol. Chem.* 284, 16066-16070.
35. Kwon,S.J., Park,J.H., Park,E.J., Lee,S.A., Lee,H.S., Kang,S.W., and Kwon,J. (2015). ATM-mediated phosphorylation of the chromatin remodeling enzyme BRG1 modulates DNA double-strand break repair. *Oncogene* 34, 303-313.
36. Lachner,M., O'Carroll,D., Rea,S., Mechtler,K., and Jenuwein,T. (2001). Methylation of histone H3 lysine 9 creates a binding site for HP1 proteins. *Nature* 410, 116-120.
37. Lee,J., Thompson,J.R., Botuyan,M.V., and Mer,G. (2008). Distinct binding modes specify the recognition of methylated histones H3K4 and H4K20 by JMJD2A-tudor. *Nat. Struct. Mol. Biol.* 15, 109-111.
38. Lee,Y.H., Kuo,C.Y., Stark,J.M., Shih,H.M., and Ann,D.K. (2013). HP1 promotes tumor suppressor BRCA1 functions during the DNA damage response. *Nucleic Acids Res.* 41, 5784-5798.
39. Luijsterburg,M.S., Acs,K., Ackermann,L., Wiegant,W.W., Bekker-Jensen,S., Larsen,D.H., Khanna,K.K., van Attikum,H., Mailand,N., and Dantuma,N.P. (2012). A new non-catalytic role for ubiquitin ligase RNF8 in unfolding higher-order chromatin structure. *EMBO J.* 31, 2511-2527.
40. Lukas,J., Lukas,C., and Bartek,J. (2011). More than just a focus: The chromatin response to DNA damage and its role in genome integrity maintenance. *Nat. Cell Biol.* 13, 1161-1169.
41. Mailand,N., Bekker-Jensen,S., Fastrup,H., Melander,F., Bartek,J., Lukas,C., and Lukas,J. (2007). RNF8 ubiquitylates histones at DNA double-strand breaks and promotes assembly of repair proteins. *Cell* 131, 887-900.
42. Mallette,F.A., Mattioli,F., Cui,G., Young,L.C., Hendzel,M.J., Mer,G., Sixma,T.K., and Richard,S. (2012). RNF8- and RNF168-dependent degradation of KDM4A/JMJD2A triggers 53BP1 recruitment to DNA damage sites. *EMBO J.* 31, 1865-1878.
43. Matic,I., Schimmel,J., Hendriks,I.A., van Santen,M.A., van de Rijke,F., van,D.H., Gnad,F., Mann,M., and Vertegaal,A.C. (2010). Site-specific identification of SUMO-2 targets in cells reveals an inverted SUMOylation motif and a hydrophobic cluster SUMOylation motif. *Mol. Cell* 39, 641-652.
44. Matsuoka,S., Ballif,B.A., Smogorzewska,A., McDonald,E.R., III, Hurov,K.E., Luo,J., Bakalarski,C.E., Zhao,Z., Solimini,N., Lerenthal,Y., Shiloh,Y., Gygi,S.P., and Elledge,S.J. (2007). ATM and ATR substrate analysis reveals extensive protein networks responsive to DNA damage. *Science* 316, 1160-1166.
45. Meerang,M., Ritz,D., Paliwal,S., Garajova,Z., Bosshard,M., Mailand,N., Janscak,P., Hubscher,U., Meyer,H., and Ramadan,K. (2011). The ubiquitin-selective segregase VCP/p97 orchestrates the response to DNA double-strand breaks. *Nat. Cell Biol.* 13, 1376-1382.
46. Miller,K.M., Tjeertes,J.V., Coates,J., Legube,G., Polo,S.E., Britton,S., and Jackson,S.P. (2010). Human HDAC1 and HDAC2 function in the DNA-damage response to promote DNA nonhomologous end-joining. *Nat. Struct. Mol. Biol.* 17, 1144-1151.
47. Min,J., Allali-Hassani,A., Nady,N., Qi,C., Ouyang,H., Liu,Y., MacKenzie,F., Vedadi,M., and Arrowsmith,C.H. (2007). L3MBTL1 recognition of mono- and dimethylated histones. *Nat. Struct. Mol. Biol.* 14, 1229-1230.
48. Moore,K.E., Carlson,S.M., Camp,N.D., Cheung,P., James,R.G., Chua,K.F., Wolf-Yadlin,A., and Gozani,O. (2013). A general

- molecular affinity strategy for global detection and proteomic analysis of lysine methylation. *Mol. Cell* 50, 444-456.
49. Nillesen,W.M., Yntema,H.G., Moscarda,M., Verbeek,N.E., Wilson,L.C., Cowan,F., Schepens,M., Raas-Rothschild,A., Gafni-Weinstein,O., Zollino,M., Vijzelaar,R., Neri,G., Nelen,M., Bokhoven,H., Giltay,J., and Kleefstra,T. (2011). Characterization of a novel transcript of the EHMT1 gene reveals important diagnostic implications for Kleefstra syndrome. *Hum. Mutat.* 32, 853-859.
 50. Oda,H., Hubner,M.R., Beck,D.B., Vermeulen,M., Hurwitz,J., Spector,D.L., and Reinberg,D. (2010). Regulation of the histone H4 monomethylase PR-Set7 by CRL4(Cdt2)-mediated PCNA-dependent degradation during DNA damage. *Mol. Cell* 40, 364-376.
 51. Panier,S., Ichijima,Y., Fradet-Turcotte,A., Leung,C.C., Kaustov,L., Arrowsmith,C.H., and Durocher,D. (2012). Tandem protein interaction modules organize the ubiquitin-dependent response to DNA double-strand breaks. *Mol. Cell* 47, 383-395.
 52. Paulsen,R.D., Soni,D.V., Wollman,R., Hahn,A.T., Yee,M.C., Guan,A., Hesley,J.A., Miller,S.C., Cromwell,E.F., Solow-Cordero,D.E., Meyer,T., and Cimprich,K.A. (2009). A genome-wide siRNA screen reveals diverse cellular processes and pathways that mediate genome stability. *Mol. Cell* 35, 228-239.
 53. Pei,H., Zhang,L., Luo,K., Qin,Y., Chesi,M., Fei,F., Bergsagel,P.L., Wang,L., You,Z., and Lou,Z. (2011). MMSET regulates histone H4K20 methylation and 53BP1 accumulation at DNA damage sites. *Nature* 470, 124-128.
 54. Pierce,A.J. and Jasin,M. (2014). Measuring recombination proficiency in mouse embryonic stem cells. *Methods Mol. Biol.* 1105, 481-495.
 55. Pierce,A.J., Johnson,R.D., Thompson,L.H., and Jasin,M. (1999). XRCC3 promotes homology-directed repair of DNA damage in mammalian cells. *Genes Dev.* 13, 2633-2638.
 56. Rice,J.C., Briggs,S.D., Ueberheide,B., Barber,C.M., Shabanowitz,J., Hunt,D.F., Shinkai,Y., and Allis,C.D. (2003). Histone methyltransferases direct different degrees of methylation to define distinct chromatin domains. *Mol. Cell* 12, 1591-1598.
 57. Roy,R., Chun,J., and Powell,S.N. (2012). BRCA1 and BRCA2: different roles in a common pathway of genome protection. *Nat. Rev. Cancer* 12, 68-78.
 58. Shanbhag,N.M., Rafalska-Metcalf,I.U., Balane-Bolivar,C., Janicki,S.M., and Greenberg,R.A. (2010). ATM-dependent chromatin changes silence transcription in cis to DNA double-strand breaks. *Cell* 141, 970-981.
 59. Shinkai,Y. and Tachibana,M. (2011). H3K9 methyltransferase G9a and the related molecule GLP. *Genes Dev.* 25, 781-788.
 60. Smeenk,G., Wiegant,W.W., Marteiijn,J.A., Luijsterburg,M.S., Sroczynski,N., Costelloe,T., Romeijn,R.J., Pastink,A., Mailand,N., Vermeulen,W., and van,A.H. (2013). Poly(ADP-ribosylation) links the chromatin remodeler SMARCA5/SNF2H to RNF168-dependent DNA damage signaling. *J. Cell Sci.* 126, 889-903.
 61. Stewart,G.S., Panier,S., Townsend,K., Al-Hakim,A.K., Kolas,N.K., Miller,E.S., Nakada,S., Ylanko,J., Olivarius,S., Mendez,M., Oldreive,C., Wildenhain,J., Tagliaferro,A., Pelletier,L., Taubenheim,N., Durandy,A., Byrd,P.J., Stankovic,T., Taylor,A.M., and Durocher,D. (2009). The RIDDLE syndrome protein mediates a ubiquitin-dependent signaling cascade at sites of DNA damage. *Cell* 136, 420-434.
 62. Stucki,M., Clapperton,J.A., Mohammad,D., Yaffe,M.B., Smerdon,S.J., and Jackson,S.P. (2005). MDC1 directly binds phosphorylated histone H2AX to regulate cellular responses to DNA double-strand breaks. *Cell* 123, 1213-1226.
 63. Sun,Y., Jiang,X., Xu,Y., Ayrapetov,M.K., Moreau,L.A., Whetstone,J.R., and Price,B.D. (2009). Histone H3 methylation links DNA damage detection to activation of the tumour suppressor Tip60. *Nat. Cell Biol.* 11, 1376-1382.
 64. Tachibana,M., Matsumura,Y., Fukuda,M., Kimura,H., and Shinkai,Y. (2008). G9a/GLP complexes independently mediate H3K9 and DNA methylation to silence transcription. *EMBO J.* 27, 2681-2690.
 65. Tachibana,M., Sugimoto,K., Nozaki,M., Ueda,J., Ohta,T., Ohki,M., Fukuda,M., Takeda,N., Niida,H., Kato,H., and Shinkai,Y. (2002). G9a histone methyltransferase plays a dominant role in euchromatic histone H3 lysine 9 methylation and is essential for early embryogenesis. *Genes Dev.* 16, 1779-1791.
 66. Tachibana,M., Ueda,J., Fukuda,M., Takeda,N., Ohta,T., Iwanari,H., Sakihama,T., Kodama,T., Hamakubo,T., and Shinkai,Y. (2005). Histone methyltransferases G9a and GLP form heteromeric complexes and are both crucial for methylation of euchromatin at H3-K9. *Genes Dev.* 19, 815-826.
 67. Tang,J., Cho,N.W., Cui,G., Manion,E.M., Shanbhag,N.M., Botuyan,M.V., Mer,G., and Greenberg,R.A. (2013). Acetylation limits 53BP1 association with damaged chromatin to promote homologous recombination. *Nat. Struct. Mol. Biol.* 20, 317-325.
 68. Typas,D., Luijsterburg,M.S., Wiegant,W.W., Diakatou,M., Helfricht,A., Thijssen,P.E., van de Broek,B., Mullenders,L.H., and van,A.H. (2015). The de-ubiquitylating enzymes USP26 and USP37 regulate homologous recombination by counteracting RAP80. *Nucleic Acids Res.*
 69. Ueda,J., Tachibana,M., Ikura,T., and Shinkai,Y. (2006). Zinc finger protein Wiz links G9a/GLP histone methyltransferases to the co-repressor molecule CtBP. *J. Biol. Chem.* 281, 20120-20128.
 70. Weil,D., Garcon,L., Harper,M., Dumenil,D., Dautry,F., and Kress,M. (2002). Targeting the kinesin Eg5 to monitor siRNA transfection in mammalian cells. *Biotechniques* 33, 1244-1248.
 71. Weinstock,D.M., Nakanishi,K., Helgadottir,H.R., and Jasin,M. (2006). Assaying double-strand break repair pathway choice in mammalian cells using a targeted endonuclease or the RAG recombinase. *Methods Enzymol.* 409, 524-540.
 72. Xiao,A., Li,H., Shechter,D., Ahn,S.H., Fabrizio,L.A., Erdjument-Bromage,H., Ishibe-Murakami,S., Wang,B., Tempst,P., Hofmann,K., Patel,D.J., Elledge,S.J., and Allis,C.D. (2009). WSTF regulates the H2A.X DNA damage response via a novel tyrosine



kinase activity. *Nature* 457, 57-62.

72. Zgheib, O., Pataky, K., Brugger, J., and Halazonetis, T.D. (2009). An oligomerized 53BP1 tudor domain suffices for recognition of DNA double-strand breaks. *Mol. Cell Biol.* 29, 1050-1058.

SUPPLEMENTAL INFORMATION

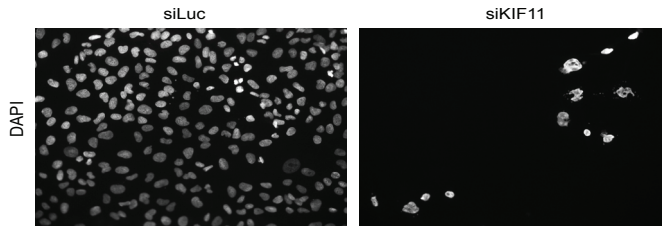


Figure S1. Knockdown efficiency confirmed with KIF11 knockdown. U2OS cells were reversely transfected with the indicated siRNAs and fixed after 3 days of cultivation. DNA was stained with DAPI to indicate cell nuclei, images were taken and the percentage of surviving cells in control and siKIF11 treated cells was estimated to 10%.

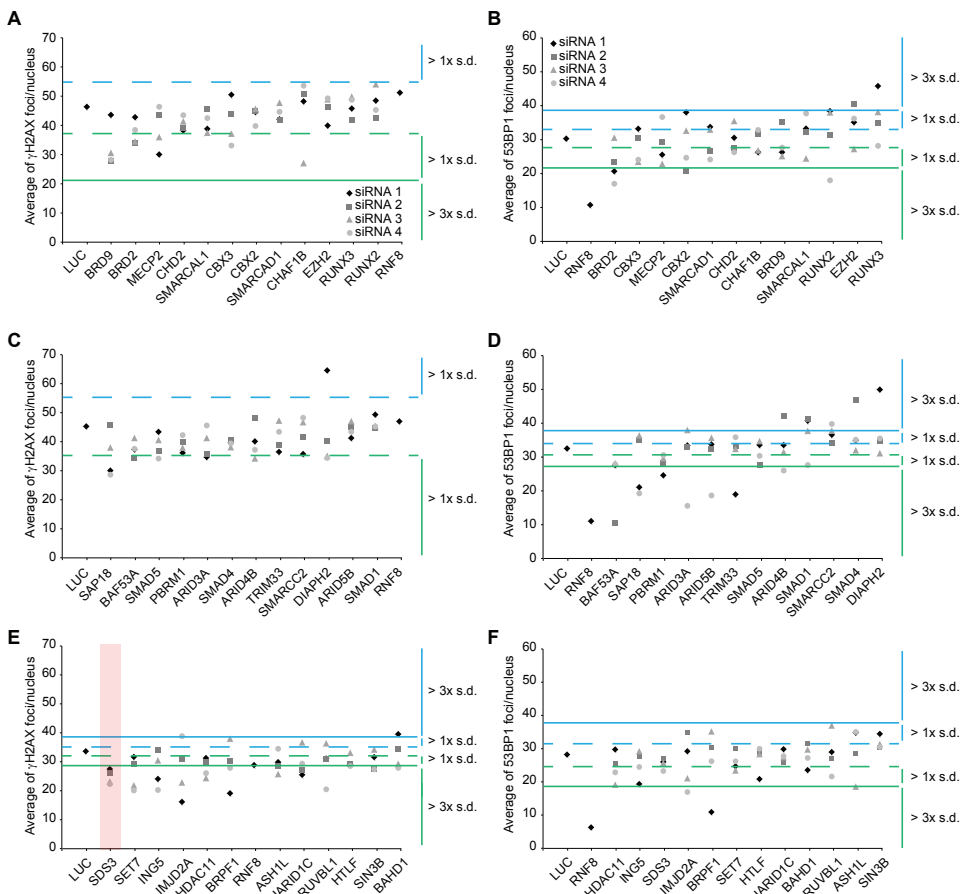


Figure S2. RNAi validation screen for novel regulators of γ H2AX and 53BP1. Presented are the results from secondary validation screen, where four individual siRNAs per target were used to validate another 36 hits from primary screen (see first 12 hits in Fig. 1. D and E). Shown is the average number of γ H2AX (A,C and E) and 53BP1 (B,D and F) foci/nucleus per siRNA per target from duplicate experiments. One and three times the standard deviation (s.d.) of the Luciferase control are indicated by dashed and continuous horizontal lines, respectively, in blue for an increase and in green for a decrease in average foci number/nucleus. Confirmed hits are indicated in red where at least 3 out of 4 siRNAs caused a change in average foci number/nucleus larger than three times the s.d. of Luciferase.


```

EHMT1_human YERIPIPCVAVDSEPCPSNYKYVSQNCVTSPMNIDRNITHLQYCVCLDDCSSSNCMCGQ 1077
Ehmt1_mouse YERIPIPCVAVDSELCPNTNYKYVSQNCVTSPMNIDRNITHLQYCVVDDCSSSTCMCGQ 1075
***** **;*****;*****.*****

EHMT1_human LSMRCWYDKDGRLLPEFNMAEPPLIFECNHACSCWRNCRNRVVQNGLRARLQLYRTRDMG 1137
Ehmt1_mouse LSMRCWYDKDGRLLPEFNMAEPPLIFECNHACSCWRNCRNRVVQNGLRARLQLYRTQDMG 1135
*****;***

EHMT1_human WGVRSLQDIPPGTFVCEYVGELISDSEADVREEDSYLFDLDNKGDEVYCIDARFYGNVSR 1197
Ehmt1_mouse WGVRSLQDIPPLGTFVCEYVGELISDSEADVREEDSYLFDLDNKGDEVYCIDARFYGNVSR 1195
*****

EHMT1_human FINHHCEPNLVPVRVFMHQDLRFPPRIAFFSTRLEAGEQLGFDYGERFWDIKGKLFSCR 1257
Ehmt1_mouse FINHHCEPNLVPVRVFMHQDLRFPPRIAFFSTRLIQAGEQLGFDYGERFWDVKGKLFSCR 1255
*****;*****;*****;*****

EHMT1_human CGSPKCRHSSAALAQRQASAAQEAQEDGLPDTSSAAAADPL 1298
Ehmt1_mouse CGSSKCRHSSAALAQRQASAAQEPQENGLPDTSSAAAADPL 1296
*** ***** **;*****

```

Figure S3. EHMT1 protein sequence is quiet conserved between mouse and human.
 Entries Q9H9B1 for human EHMT1 and Q5DW34 for mouse Ehmt1 were aligned using the Uniprot alignment tool available at www.uniprot.org. The conserved amino acids are indicated by a green asterisk.



Table S1. List of siRNA screen gene targets and results. (A) List of 227 gene targets and positive (siLUC) and negative (siRNF8) controls. Indicated are gene symbols, Gene IDs, Accession numbers and the obtained Z-scores calculated from the average amount of γ H2AX or 53BP1 foci determined during the first siRNA screen. Blue indicates an increase and green a decrease in the average foci number/nucleus. Gray specifies the validation selected targets. (B) List of 48 target genes against which four single siRNAs were employed during the deconvolution screen. Depicted are gene symbols and the average number of foci/ nucleus for γ H2AX and 53BP1. Hit results are indicated in red, when minimal 3 out of 4 siRNAs caused an increase (blue) or decrease (green) larger than three times the standard deviation of the control Luciferase.

A		Gene ID	Accession Number	Z-score γ H2AX foci	Z-score 53BP1 foci
1	AOF2	23028	NM_015013	-0,052	-0,616
2	ARID1A	8289	NM_006015	-0,307	1,159
3	ARID1B	57495	NM_0137519	-	-
4	ARID2	196528	NM_152641	-	-
5	ARID3A	1820	NM_005224	2,348	4,968
6	ARID3B	10620	NM_006445	0,860	3,039
7	ARID4A	8841	NM_003883	-	-
8	ARID4B	51742	NM_016374	-12,181	-0,234
9	ARID5A	10862	NM_012481	0,649	0,171
10	ARID5B	84190	NM_032100	-0,291	-3,124
11	ASH1L	55870	NM_018489	-2,329	6,283
12	ATAD2	29028	NM_014109	0,135	0,910
13	ATRX	546	NM_000889	0,517	0,647
14	BAHCC1	57597	NM_371084	-	-
15	BAF33A	86	NM_004301	0,638	-6,061
16	BAHD1	22891	NM_014952	-1,196	4,796
17	BAZ1A	11177	NM_013448	-0,145	-
18	BAZ1B	9031	NM_032408	-1,548	8,691
19	BAZZA	11176	NM_013449	-0,425	9,938
20	BAZZB	29998	NM_013550	0,356	0,221
21	BM11	648	NM_005180	-	-
22	BPF1	2186	NM_182641	-	-
23	BRD1	23774	NM_014577	-	-
24	BRD2	6046	NM_01113182	2,160	-4,732
25	BRD3	8019	NM_007271	-0,041	6,962
26	BRD4	23476	NM_014299	-	-
27	BRD7	29117	NM_013263	-0,293	-
28	BRD8	10902	NM_006096	-4,647	-5,215
29	BRD9	66980	NM_023924	0,517	7,887
30	BRD9	676	NM_007189	-	-
31	BRPF1	7862	NM_00103694	0,712	5,263
32	BRPF1	27154	NM_015695	0,139	-4,728
33	BRWD1	54014	NM_138656	0,309	8,359
34	BRWD3	254065	NM_153952	0,327	8,958
35	BTG1	694	NM_001713	-	-
36	BTG2	7832	NM_006763	0,315	-1,104
37	BTG3	10950	NM_01130914	-1,307	-
38	BTG4	54766	NM_172959	0,064	-1,299
39	CARM1	10498	NM_159141	0,681	1,614
40	CBX1	10951	NM_006807	-	-
41	CBX2	84733	NM_032647	-0,329	3,398
42	CBX3	11335	NM_007276	0,883	3,916
43	CBX4	8535	NM_003655	-	-
44	CBX5	23466	NM_01127221	7,777	2,163
45	CBX6	23466	NM_014292	0,407	6,409
46	CBX7	23492	NM_175709	1,191	9,059
47	CBX8	57323	NM_020649	-	-
48	CECR2	27443	NM_031413	1,233	2,287
49	CHC1	1104	NM_001269	-	-
50	CHAF1B	8208	NM_005441	1,492	2,167
51	CHD1	1105	NM_001270	0,085	8,161
52	CHD1L	9557	NM_004284	-	-
53	CHD2	1106	NM_001271	-0,232	7,103
54	CHD3	1107	NM_00105273	0,164	4,038
55	CHD5	26038	NM_015557	-	-
56	CHD6	84181	NM_032221	-	-
57	CHD7	55638	NM_008762	-	-
58	CHD8	57680	NM_020920	0,340	5,954
59	CHD9	80205	NM_025134	1,430	10,656
60	CHREBP	1387	NM_01079846	-	-
61	DIAPH1	17291	NM_001078612	-	-
62	DIAPH2	1730	NM_006729	-23,710	-1,904
63	DNAI1	64215	NM_022365	-	-
64	DNAI2	27000	NM_01129887	-1,546	-1,509
65	DNMT1	1786	NM_001379	-0,036	-
66	DNMT2	1787	NM_004412	1,938	-1,001
67	DNMT3B	1788	NM_006892	-2,630	0,894
68	DNMT3L	29947	NM_013369	-	-
69	DNMAP1	55929	NM_019100	-	-
70	DOT1L	84444	NM_032482	-3,333	2,056
71	EHMT1	79811	NM_024757	-0,352	4,076
72	EHMT2	10919	NM_006709	0,580	3,274
73	EID1	23741	NM_014335	-	-
74	EID2	163236	NM_153232	-0,710	0,280
75	EID2B	126272	NM_152361	-	-
76	EID3	49386	NM_001008394	-	-
77	EP300	2031	NM_001429	-	-
78	EP400	57638	NM_015409	-1,165	-1,402
79	FPC1	80314	NM_025209	0,499	1,839
80	FPC2	20122	NM_015630	-	-
81	FRC5	2074	NM_000124	-	-
82	IRCC6L	54821	NM_017669	0,243	0,914
83	IRCC6L2	375748	NM_00110895	0,847	1,765
84	EZH1	2146	NM_003951	-	-
85	EZH2	2146	NM_004456	0,378	2,211
86	GAS1	8089	NM_006530	-3,792	-1,971
87	H2AF2	3015	NM_002106	0,145	-0,589
88	HDAC1	3061	NM_049664	-	-
89	HDAC2	3066	NM_001527	-	-
90	HDAC3	8847	NM_003883	-0,913	0,360
91	HDAC4	9757	NM_006037	0,657	8,444
92	HDAC5	10014	NM_001015053	-	-
93	HDAC6	10013	NM_006044	0,390	4,666
94	HDAC7	51564	NM_001098416	-	-
95	HDAC8	55869	NM_018486	-	-
96	HDAC9	9734	NM_014707	-	-
97	HDAC10	83931	NM_032019	-	-
98	HDAC11	79881	NM_01116041	0,416	5,562
99	HHELLS	3070	NM_018063	0,669	1,859
100	HLTF	6596	NM_003071	0,812	2,104
101	HTATP	10524	NM_006388	0,026	6,983
102	ING1	3621	NM_152817	0,664	0,888
103	ING2	3622	NM_015164	-	-
104	ING3	54556	NM_139071	-	-
105	ING5	84280	NM_033229	0,238	2,097
106	JARID1A	5927	NM_001242603	-	-
107	JARID1B	10765	NM_006618	0,099	1,086
108	JARID1C	8244	NM_004187	1,144	6,477
109	JARID1D	8284	NM_004653	-	-
110	JARID2	3720	NM_040973	-	-
111	JMJD1A	55818	NM_018433	-0,656	-1,538
112	JMJD1B	51780	NM_016604	-	-

B		single siRNAs	Average nr. of γ H2AX foci	Average nr. of 53BP1 foci
1	ARID3A-1	34,709	33,431	
1	ARID3A-2	35,872	32,983	
1	ARID3A-3	41,208	38,000	
1	ARID3A-4	45,607	15,583	
2	ARID4B-1	40,113	33,527	
2	ARID4B-2	48,028	45,218	
2	ARID4B-3	34,288	31,498	
2	ARID4B-4	37,187	26,017	
3	ARID5B-1	41,248	33,742	
3	ARID5B-2	41,691	32,407	
3	ARID5B-3	47,079	35,690	
3	ARID5B-4	43,398	18,635	
4	ASH1L-1	28,857	34,707	
4	ASH1L-2	28,510	28,637	
4	ASH1L-3	25,773	18,578	
4	ASH1L-4	34,499	35,024	
5	BAF33A-1	37,137	27,653	
5	BAF33A-2	34,337	10,598	
5	BAF33A-3	41,310	28,172	
5	BAF33A-4	37,566	27,898	
6	BAHD1-1	39,551	23,547	
6	BAHD1-2	34,254	31,420	
6	BAHD1-3	29,322	29,740	
6	BAHD1-4	27,907	27,183	
7	BAZ1A-1	44,008	37,954	
7	BAZ1A-2	46,402	49,154	
7	BAZ1A-3	37,175	39,327	
7	BAZ1A-4	41,249	32,503	
8	BAZ1B-1	48,752	46,985	
8	BAZ1B-2	42,338	39,317	
8	BAZ1B-3	48,881	53,982	
8	BAZ1B-4	49,071	32,026	
9	BAZZA-1	43,911	37,987	
9	BAZZA-2	49,865	39,916	
9	BAZZA-3	48,140	41,062	
9	BAZZA-4	38,701	36,868	
10	BRD2-1	42,756	39,602	
10	BRD2-2	34,069	23,351	
10	BRD2-3	34,466	30,597	
10	BRD2-4	38,466	17,000	
11	BRD9-1	43,541	38,397	
11	BRD9-2	27,618	35,081	
11	BRD9-3	30,567	25,157	
11	BRD9-4	29,127	27,609	
12	BRPF1-1	19,121	10,885	
12	BRPF1-2	30,179	30,455	
12	BRPF1-3	37,980	30,500	
12	BRPF1-4	27,873	26,217	
13	BRWD1-1	47,821	37,626	
13	BRWD1-2	45,041	39,327	
13	BRWD1-3	46,082	44,951	
13	BRWD1-4	54,512	38,418	
14	BRWD3-1	37,748	35,885	
14	BRWD3-2	46,648	39,327	
14	BRWD3-3	46,486	35,114	
14	BRWD3-4	48,968	42,493	
15	CBX2-1	44,519	38,029	
15	CBX2-2	44,928	20,631	
15	CBX2-3	45,643	32,665	
15	CBX2-4	39,741	24,657	
16	CBX3-1	40,434	39,813	
16	CBX3-2	43,752	30,588	
16	CBX3-3	37,122	23,478	
16	CBX3-4	34,044	24,984	
17	CBX5-1	48,271	38,292	
17	CBX5-2	41,808	38,217	
17	CBX5-3	46,553	38,700	
17	CBX5-4	50,795	47,493	
18	CHAF1B-1	48,149	33,236	
18	CHAF1B-2	50,627	31,618	
18	CHAF1B-3	27,068	26,824	
18	CHAF1B-4	53,529	32,853	
19	CHD2-1	38,172	30,544	
19	CHD2-2	39,159	27,515	
19	CHD2-3	41,335	35,504	
19	CHD2-4	43,432	26,287	
20	DIAPH2-1	64,573	49,938	
20	DIAPH2-2	40,284	34,614	
20	DIAPH2-3	35,143	31,135	
20	DIAPH2-4	34,391	35,518	
21	EHMT1-1	45,574	46,011	
21	EHMT1-2	48,704	46,011	
21	EHMT1-3	46,625	46,011	
21	EHMT1-4	44,215	33,989	
22	EHMT2-1	39,674	37,355	
22	EHMT2-2	37,511	32,100	
22	EHMT2-3	47,576	43,159	
22	EHMT2-4	41,884	36,700	
23	EZH2-1	39,880	29,526	
23	EZH2-2	46,136	40,425	
23	EZH2-3	48,924	27,246	
23	EZH2-4	49,208	36,206	
24	JMJD1C-1	31,271	29,743	
24	JMJD1C-2	29,741	25,594	
24	JMJD1C-3	24,397	19,157	
24	JMJD1C-4	26,088	22,879	
25	HLTF-1	28,887	20,826	
25	HLTF-2	29,363	29,701	
25	HLTF-3	33,097	28,346	
25	HLTF-4	28,550	29,955	
26	ING5-1	35,073	35,811	
26	ING5-2	30,486	29,216	
26	ING5-3	20,220	24,502	
26	ING5-4	29,492	29,813	
27	JARID1C-1	27,112	25,785	
27	JARID1C-2	36,700	27,412	
27	JARID1C-3	29,350	21,097	
27	JARID1C-4	16,118	29,191	
28	JMJD2A-1	31,051	34,878	
28</				

113	JMJD1C	221037	NM_004241	-	-	-
114	JMJD2A	9602	NM_014663	0,053	2,317	-
115	JMJD2B	23030	NM_015015	-	-	-
116	JMJD2C	23081	NM_015061	-	-	-
117	JMJD2D	55693	NM_018039	-	-	-
118	JMJD3	23135	NM_001080424	0,144	-0,616	-
119	JMJD4	65094	NM_023007	-	-	-
120	JMJD5	79831	NM_024773	-	-	-
121	KATZA	26448	NM_021078	-	-	-
122	KATZB	8850	NM_003884	-	-	-
123	LIRCH4	4034	NM_002319	0,369	1,860	-
124	Luciferase	-	-	-0,024	0,188	-
125	LOC33012	-	-	-	-	-
126	MBD1	4152	NM_002384	-	-	-
127	MBD2	8932	NM_003927	-8,576	-1,711	-
128	MBD3	53615	NM_003926	-	-	-
129	MBD4	8930	NM_003925	-	-	-
130	MBD5	55777	NM_018328	-	-	-
131	MBD6	114785	NM_052897	-14,592	0,392	-
132	MEAF6	64769	NM_022756	-0,084	-0,593	-
133	MCEP2	4204	NM_001110792	6,108	0,646	-
134	METTL5	29085	NM_014168	-0,181	-0,030	-
135	MLL	4297	NM_005933	-	-	-
136	MLL2	8085	NM_003482	-	-	-
137	MLL3	58508	NM_170606	-	-	-
138	MLL4	9757	NM_014727	-	-	-
139	MLL5	55904	NM_018682	-	-	-
140	MORF4	10933	NM_006791	-1,942	-0,272	-
141	MORF4L1	10934	NM_006792	-12,662	2,971	-
142	MSL3	10943	NM_006800	-	-	-
143	MYBL2	4605	NM_002466	-	-	-
144	MYM1	114803	NM_001085487	-	-	-
145	MYT1	84148	NM_002388	-	-	-
146	MYST2	11143	NM_007067	7,448	2,752	-
147	MYST3	7994	NM_006766	10,388	2,813	-
148	MYST4	23522	NM_012330	-	-	-
149	NCOR1	9611	NM_005911	0,357	0,593	-
150	NCOR2	9612	NM_006312	-	-	-
151	OR1LH2	79334	NM_001197287	2,360	0,601	-
152	PBRM1	55193	NM_018165	0,661	-5,779	-
153	PCGF1	84759	NM_032673	-0,116	-0,822	-
154	PCGF2	7703	NM_007444	-	-	-
155	PCGF3	10336	NM_006115	-	-	-
156	PCGF5	84333	NM_032373	0,228	-0,011	-
157	PCGF6	84108	NM_001011663	-	-	-
158	PHF19	26147	NM_001009926	-	-	-
159	PTDSR	23210	NM_015167	-	-	-
160	RAD21	5885	NM_006265	0,721	0,601	-
161	RAD54B	25788	NM_012415	1,199	1,645	-
162	RAD54L	8438	NM_003379	0,885	1,652	-
163	RCOR1	23186	NM_015156	-	-	-
164	RCOR2	283248	NM_173587	-1,438	0,010	-
165	RCOR3	57159	NM_012524	0,429	1,678	-
166	REER	473	NM_001042681	-	-	-
167	RNF8	9025	NM_003958	0,720	-25,492	-
168	RNF2	6045	NM_007212	-	-	-
169	RUNX2	860	NM_001015051	-2,247	-0,661	-
170	RUNX3	864	NM_001031680	-0,328	2,131	-
171	RUVBL1	8607	NM_003707	-4,117	-1,698	-
172	RUVBL2	10856	NM_006666	-	-	-
173	SAP18	10284	NM_005870	-19,393	-0,976	-
174	SAP90	8819	NM_003864	0,298	0,421	-
175	SCHL2	10289	NM_006089	-1,983	0,777	-
176	SDS3	64426	NM_022491	-3,815	-0,325	-
177	SET7	80854	NM_030648	-	-	-
178	SETD1A	9739	NM_004712	0,491	0,437	-
179	SETD1B	23067	NM_015048	-1,258	-0,511	-
180	SETD2	29072	NM_014159	-0,812	-0,383	-
181	SETD4	54093	NM_017438	0,456	-1,289	-
182	SETD7	80854	NM_030648	-	-	-
183	SETD8	387893	NM_020382	-	-	-
184	SHPRH	257218	NM_173082	0,377	-0,089	-
185	SIN3A	25942	NM_001477	-	-	-
186	SIN3B	23309	NM_015260	3,442	4,329	-
187	SMAD1	4086	NM_001001688	1,946	4,277	-
188	SMAD2	4087	NM_001001652	-	-	-
189	SMAD3	4088	NM_005902	1,213	2,091	-
190	SMAD4	4089	NM_005359	0,926	2,254	-
191	SMAD5	4090	NM_001001419	-4,744	-3,551	-
192	SMAD6	4091	NM_005585	-	-	-
193	SMAD7	4092	NM_005904	-	-	-
194	SMAD9	4093	NM_001127217	-	-	-
195	SMARCA1	6594	NM_003069	-	-	-
196	SMARCA2	6595	NM_003070	-	-	-
197	SMARCA4	6597	NM_001128844	-2,566	-1,001	-
198	SMARCA5	8467	NM_006601	-6,965	-0,911	-
199	SMARCA11	50516	NM_020159	1,213	2,091	-
200	SMARCA11	50485	NM_001127207	3,211	0,074	-
201	SMARCC1	6599	NM_006074	-	-	-
202	SMARCC2	6601	NM_001130420	-0,559	3,506	-
203	SMC1A	8243	NM_006306	-	-	-
204	SMURF1	57154	NM_020429	-	-	-
205	SMURF2	64750	NM_022739	-	-	-
206	SMYD1	150572	NM_198274	-	-	-
207	SMYD2	56950	NM_020197	-8,556	-0,848	-
208	SMYD3	64754	NM_022743	-	-	-
209	SMYD4	114826	NM_052928	-	-	-
210	SMYD5	10322	NM_006062	-	-	-
211	SP100	6672	NM_001313	-0,587	4,373	-
212	SP110	3431	NM_080424	-	-	-
213	SP140L	93349	NM_138402	-1,378	0,070	-
214	SUPF7L	9913	NM_014860	-	-	-
215	SUV39H1	6839	NM_003173	-	-	-
216	SUV39H2	79723	NM_024670	-	-	-
217	TADA2A	6871	NM_001488	1,094	1,783	-
218	TADA2B	93624	NM_152293	-	-	-
219	TAF1	6872	NM_006406	1,425	5,945	-
220	TAF3	83860	NM_031923	-	-	-
221	TAF8	129685	NM_138572	1,287	8,499	-
222	TEN1	7013	NM_017489	0,168	1,330	-
223	TEN2	7014	NM_005652	0,831	1,565	-
224	TRIM28	10155	NM_005762	-	-	-
225	TRIM33	51592	NM_015906	0,437	7,458	-
226	TRIM6	9866	NM_086529	-	-	-
227	TRRAP	8295	NM_003496	-2,941	1,017	-
228	VPS72	6944	NM_005997	1,563	1,852	-
229	ZZZ3	26009	NM_015534	-	-	-

29	MCEP2-1	29,996	25,534
	MCEP2-2	43,504	29,213
	MCEP2-3	35,965	22,877
	MCEP2-4	46,336	36,654
30	MYST2-1	38,398	34,566
	MYST2-2	40,413	40,383
	MYST2-3	48,390	47,111
	MYST2-4	58,962	47,111
31	MYST3-1	47,404	41,053
	MYST3-2	43,238	36,808
	MYST3-3	42,828	34,410
	MYST3-4	54,035	48,705
32	PBRM1-1	36,131	24,594
	PBRM1-2	39,934	28,288
	PBRM1-3	37,933	29,673
	PBRM1-4	42,264	30,588
33	RUNX2-1	48,417	45,783
	RUNX2-2	42,341	31,484
	RUNX2-3	54,035	38,037
	RUNX2-4	45,251	18,002
34	RUNX3-1	45,730	32,427
	RUNX3-2	41,724	34,769
	RUNX3-3	49,802	38,163
	RUNX3-4	48,719	28,175
35	RUVBL1-1	31,084	28,982
	RUVBL1-2	20,497	21,613
	RUVBL1-3	36,389	36,962
	RUVBL1-4	20,497	21,613
36	SAP18-1	38,001	31,051
	SAP18-2	45,632	35,004
	SAP18-3	38,001	36,388
	SAP18-4	28,637	19,251
37	SDS3-1	26,337	25,971
	SDS3-2	26,337	26,337
	SDS3-3	23,345	25,753
	SDS3-4	23,345	25,753
38	SET7-1	31,671	24,693
	SET7-2	29,397	30,115
	SET7-3	21,868	23,444
	SET7-4	20,993	26,192
39	SIN3B-1	31,613	34,431
	SIN3B-2	27,615	30,182
	SIN3B-3	34,242	31,382
	SIN3B-4	27,409	30,489
40	SMAD1-1	49,333	40,716
	SMAD1-2	44,636	41,325
	SMAD1-3	45,448	37,746
	SMAD1-4	45,260	27,640
41	SMAD4-1	39,672	34,932
	SMAD4-2	40,632	46,858
	SMAD4-3	38,128	32,007
	SMAD4-4	39,416	35,117
42	SMAD5-1	43,368	33,552
	SMAD5-2	36,655	27,726
	SMAD5-3	40,625	34,702
	SMAD5-4	34,178	30,364
43	SMARCA4-1	45,851	28,184
	SMARCA4-2	41,750	33,136
	SMARCA4-3	43,027	39,069
	SMARCA4-4	48,007	41,378
44	SMARCA11-1	42,035	33,727
	SMARCA11-2	41,820	26,656
	SMARCA11-3	47,700	32,860
	SMARCA11-4	44,607	24,154
45	SMARCAL1-1	38,758	35,131
	SMARCAL1-2	45,404	32,068
	SMARCAL1-3	37,424	24,474
	SMARCAL1-4	42,449	37,733
46	SMARCC2-1	35,750	36,590
	SMARCC2-2	41,507	34,078
	SMARCC2-3	46,748	37,802
	SMARCC2-4	48,262	39,778
47	SP100-1	43,653	39,158
	SP100-2	48,938	45,393
	SP100-3	44,175	38,094
	SP100-4	40,979	35,287
48	TRIM33-1	36,470	18,963
	TRIM33-2	38,833	33,239
	TRIM33-3	47,287	32,415
	TRIM33-4	43,421	35,873

Increase in average number of foci/nucleus

Decrease in average number of foci/nucleus

Hits selected for validation screen

Hit

* faulty selection



REMODELING AND SPACING FACTOR 1 (RSF1)
DEPOSITS CENTROMERE PROTEINS AT DNA
DOUBLE-STRAND BREAKS TO PROMOTE
NON-HOMOLOGOUS END-JOINING

3

Angela Helfricht¹, Wouter W. Wiegant¹, Peter E. Thijssen^{1,2},
Alfred C. Vertegaal³, Martijn S. Luijsterburg¹ and Haico van Attikum¹

¹Department of Toxicogenetics; Leiden University Medical Center

²Department of Human Genetics; Leiden University Medical Center

³Department of Molecular Cell Biology; Leiden University Medical Center

An adapted version of this manuscript has been
published in Cell Cycle 2013 vol 12 (18)

ABSTRACT

The cellular response to ionizing radiation (IR)-induced DNA double-strand breaks (DSBs) in native chromatin requires a tight coordination between the activities of DNA repair machineries and factors that modulate chromatin structure. SMARCA5 is an ATPase of the SNF2 family of chromatin remodeling factors that has recently been implicated in the DSB response. It forms distinct chromatin-remodeling complexes with several non-canonical subunits, including the remodeling and spacing factor 1 (RSF1) protein. Despite the fact that RSF1 is often overexpressed in tumors and linked to tumorigenesis and genome instability, its role in the DSB response remains largely unclear. Here we show that RSF1 accumulates at DSB sites and protects human cells against IR-induced DSBs by promoting repair of these lesions through homologous recombination (HR) and non-homologous end-joining (NHEJ). Although SMARCA5 regulates the RNF168-dependent ubiquitin response that targets BRCA1 to DSBs, we found RSF1 to be dispensable for this process. Conversely, we found that RSF1 facilitates the assembly of centromere proteins CENP-S and CENP-X at sites of DNA damage, while SMARCA5 was not required for these events. Mechanistically, we uncovered that CENP-S and CENP-X, upon their incorporation by RSF1, promote assembly of the NHEJ factor XRCC4 at damaged chromatin. In contrast, CENP-S and CENP-X were dispensable for HR, suggesting that RSF1 regulates HR independently of these centromere proteins. Our findings reveal distinct functions of RSF1 in the two major pathways of DSB repair and explain how RSF1, through the loading of centromere proteins and XRCC4 at DSBs, promotes repair by non-homologous end-joining.

INTRODUCTION

Chromosomal DNA double-strand breaks (DSBs), which can arise after exposure of cells to ionizing radiation (IR) or as a consequence of DNA replication stress, form a major threat to genome stability. Their inefficient or inaccurate repair can result in chromosome rearrangements and translocations, which may result in cancer development or cell death (Jackson and Bartek, 2009). To circumvent the deleterious effects of DSBs, cells activate the DNA damage response (DDR), which comprises events that lead to detection and repair of these lesions, as well as a delay in cell cycle progression (Ciccia and Elledge, 2010; Jackson and Bartek, 2009). DSB repair involves two dedicated pathways known as non-homologous end-joining (NHEJ) and homologous recombination (HR) (Chapman et al., 2012). While NHEJ re-joins the ends of a DSB in an error-free or error-prone manner and is active throughout the cell cycle, HR mediates the error-free repair of DSBs in S or G2 phase by using the sequence information obtained from a homologous template, usually a sister chromatid. DSBs occur in DNA that is tightly packaged into higher-order chromatin fibers. Emerging evidence suggests that DSB repair is closely coordinated with chromatin structure and function. Several proteins involved in modulating chromatin structure, including histone-modifying enzymes and ATP-dependent chromatin remodeling complexes are critically important for DSB repair (Luijsterburg and van, 2011; Smeenk and van, 2013). A key modification that occurs throughout DSB-associated chromatin is the ATM kinase-dependent phosphorylation of histone H2A variant H2AX (γ H2AX). This γ H2AX histone mark then leads to the recruitment of two distinct ubiquitin E3 ligases, RNF8 and RNF168, which are responsible for the ubiquitylation of damaged chromatin and the subsequent accumulation of BRCA1 through its ubiquitin-binding partner RAP80 (Doil et al., 2009; Huen et al., 2007; Mailand et al., 2007; Stewart et al., 2009; Wang and Elledge, 2007). Interestingly, these histone marks have recently been shown to co-operate with distinct ATP-dependent remodeling factors in orchestrating the DSB response. Specifically, we found that the chromatin remodelers CHD4 and SMARCA5 are recruited to DSBs where they interact with the RNF8 and RNF168 ubiquitin ligases and affect the ubiquitin-dependent signaling of DSBs at the level of RNF8 and RNF168, respectively (Larsen et al., 2010; Luijsterburg et al., 2012a; Smeenk et al., 2010; Smeenk et al., 2013). Consequently, loss of CHD4 or SMARCA5 abrogates BRCA1 accumulation and leads to defects in DSB repair (Lan et al., 2010; Larsen et al., 2010; Luijsterburg et al., 2012a; Nakamura et al., 2011; Polo et al., 2010; Smeenk et al., 2010; Smeenk et al., 2013). Thus, there is significant crosstalk between different histone marks and distinct chromatin remodeling enzymes in coordinating signaling and repair activities within damaged chromatin compartments.

Interestingly, while CHD4 is unique to the NuRD chromatin remodeling complex, SMARCA5 resides in a variety of different complexes, including ACF (consisting of SMARCA5 and ACF1), CHRAC (SMARCA5, ACF1, CHRAC15, and CHRAC17), and RSF (SMARCA5 and RSF1) (Wang et al., 2007). The catalytic subunit SMARCA5 (Lan et al., 2010; Nakamura et al., 2011; Sanchez-Molina et al., 2011; Smeenk et al., 2013), as well as the non-catalytic accessory proteins ACF1, CHRAC15, and CHRAC17 have been implicated in DSB repair (Lan et al., 2010; Sanchez-Molina et al., 2011). Remarkably, the role of the accessory factor RSF1 in the DSB response has not been investigated, although tumors harboring RSF1 amplification display chromosomal instability likely through an altered DDR (Sheu et al., 2010).

Here we uncover RSF1 as a novel factor that is recruited to sites of DSBs and protects human cells against the toxic consequences of IR-induced DSBs. While RSF1 is dispensable for RNF8/

RNF168-dependent ubiquitin signaling of DSBs, it promotes the repair of DSBs by NHEJ and HR. Mechanistically, we show that RSF1 promotes the deposition of the centromere proteins CENP-S and CENP-X at DSBs, which, in turn, promote the assembly of the NHEJ protein XRCC4. Thus, RSF1 is a novel chromatin accessory factor that regulates DSB repair independently of the SMARCA5 ATPase to prevent chromosome aberrations and maintain genome stability.

RESULTS

RSF1 protects cells against DNA damage

The ATPase SMARCA5 forms distinct chromatin remodeling complexes with the chromatin assembly factor ACF1, the histone-fold proteins CHRAC15/CHRCA17 and the remodeling and spacing factor RSF1 (Wang et al., 2007). We and others have recently implicated SMARCA5 in the signaling and repair of DSBs (Lan et al., 2010; Nakamura et al., 2011; Smeenk et al., 2013). However, while the available data suggest that ACF1 and CHRAC15/CHRCA17 assist in modulating SMARCA5 activity, the role of RSF1 in the DNA damage response (DDR) remains unclear. Here we set out to study the role of this protein in the DDR by first addressing whether RSF1 protects human cells against the toxic consequences of ionizing radiation (IR)-induced DSBs. To this end, we transfected human VH10-SV40 cells with siRNAs against either RSF1, the repair factor XRCC4 (positive control), or luciferase (negative control). Cells were subsequently exposed to different doses of IR after which we determined their clonogenic survival capacity. Strikingly, cells depleted for RSF1 were more sensitive to IR than control cells and were nearly as sensitive as XRCC4-depleted cells (Fig. 1A and B), suggesting that RSF1 protects cells against the DSB-inducing effects of ionizing radiation.

RSF1 is recruited to DNA double-strand breaks

Based on this result we reasoned that RSF1 like SMARCA5 and ACF1 may act directly in the DSB response by operating at sites of DNA damage (Lan et al., 2010; Nakamura et al., 2011; Smeenk et al., 2013). To test this we used laser micro-irradiation to examine whether RSF1 directly assembles at sites of DNA damage. DNA damage was induced in a sub-nuclear volume in U2OS cells by multi-photon laser irradiation followed by immunostaining for RSF1 and the DDR factor MDC1, which binds to the DNA damage marker γ H2AX. We found that endogenous RSF1 accumulates at sites of laser-induced DNA damage that are marked by MDC1 (Fig. 1C). In addition, we also observed recruitment of GFP-RSF1 to γ H2AX-decorated sites following multiphoton-induced laser irradiation in cells stably expressing GFP-RSF1 at near physiological levels (Fig. 1D and E). However, while these results suggest that RSF1 accumulates at DNA lesions we cannot exclude that RSF1 accumulates at lesions other than DSBs given that laser-based approaches have been shown to induce DSBs as well as a variety of other lesions such as single-strand breaks and base damages (Dinant et al., 2007). In order to examine whether RSF1 localizes to bona fide DSBs, we co-expressed GFP-RSF1 and the Fok1 nuclease domain fused to the E. coli lactose repressor (LacR) and the red fluorescent mCherry protein (Fok1-mCherry-LacR) in U2OS cells containing an array of lactose operator (LacO) repeats (Shanbhag et al., 2010). Targeting of Fok1-Cherry-LacR, but not Fok1-Cherry-LacRD450A encoding a nuclease-dead isoform of Fok1, led to DSB induction at the array as visualized by the appearance of γ H2AX (Fig. 1F). Importantly, GFP-RSF1 localized to the

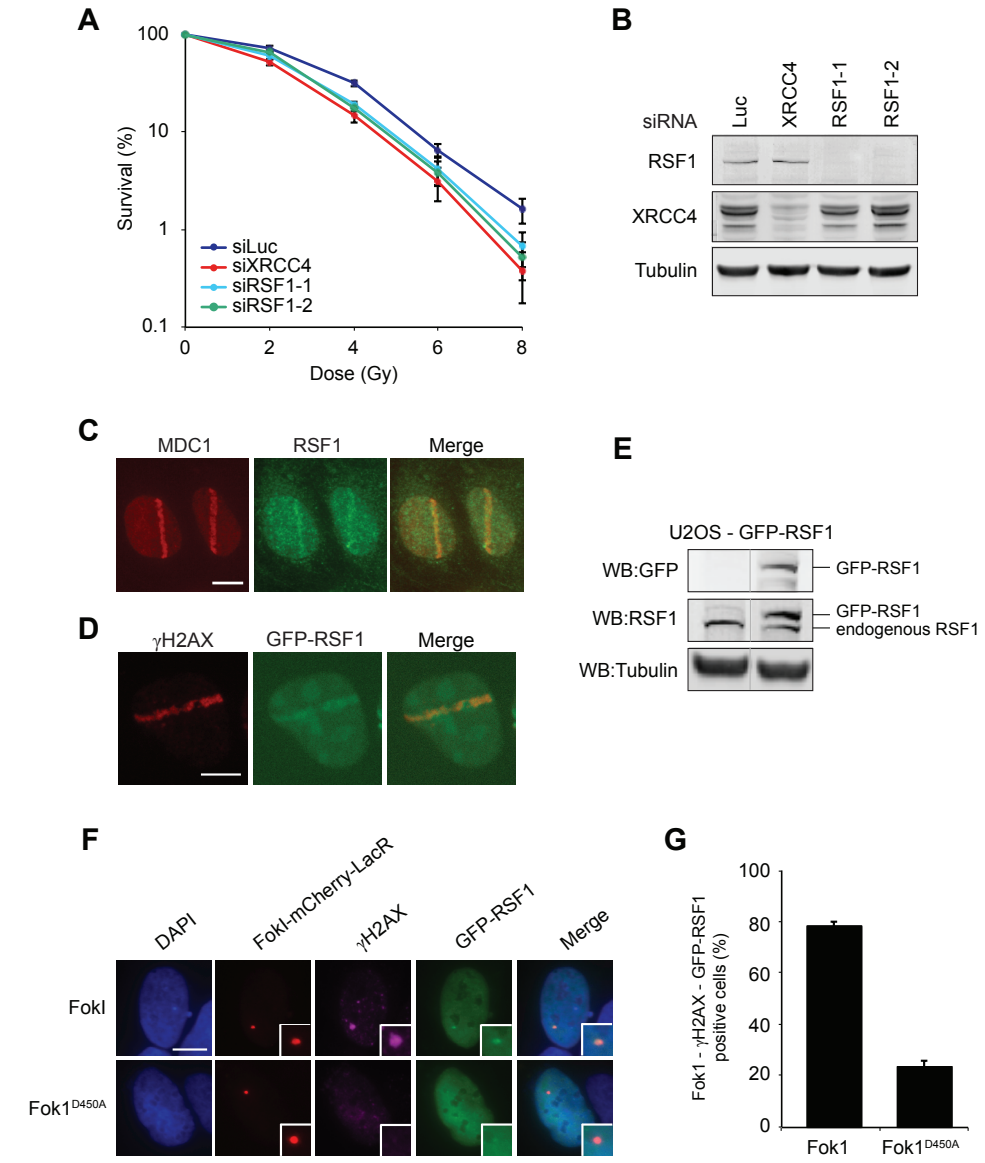


Figure 1. RSF1 protects cells against IR and is recruited to DNA double-strand breaks. (A) VH10-SV40 cells were transfected with the indicated siRNAs, exposed to IR and scored for clonogenic survival. Graphs represent the mean \pm s.e.m. of 3 independent experiments. (B) RSF1 and XRCC4 levels were monitored by western blot analysis using whole cell extracts (WCE) of cells in A. Tubulin is a loading control. (C) U2OS cells were subjected to multiphoton laser irradiation. After 10 min cells were immunostained for endogenous RSF1 and MDC1. Scale bar, 10 μ m. (D) As in (C), except that cells stably expressing GFP-RSF1 were used and stained for γ H2AX. (E) RSF1 and GFP-RSF1 levels were monitored by western blot analysis using whole cell extracts (WCE) of cells in (D). Tubulin is a loading control. (F) Immunofluorescence staining of γ H2AX and visualization of GFP-RSF1 at DSBs induced by FokI-mCherry-LacR at a tandemly integrated 256 \times Lac operator genomic array in U2OS cells. Nuclease-deficient FokI^{D450A}-mCherry-LacR was used as a control. (G) Quantification of co-localization of γ H2AX and GFP-RSF1 at FokI-induced DSBs in cells from (F). Graphs represent the mean \pm s.e.m. of 2 independent experiments. At least 100 individual cells were analyzed. Scale bar, 10 μ m.

array upon targeting Fok1, but not upon targeting nuclease dead-Fok1, suggesting that it assembles at Fok1-induced DSBs (Fig. 1F and G). Together, our results show that RSF1 is a novel DDR factor that assembles at DSBs in human cells.

SMARCA5, but not RSF1, regulates the ubiquitin-dependent accumulation of BRCA1 at DSBs

Next, we sought to unravel how RSF1 regulates the DSB response. We recently reported that SMARCA5 regulates the ubiquitin-dependent accumulation of BRCA1 at DSBs (Smeenk et al., 2013). This process is triggered by the MDC1-dependent recruitment of the RNF8 and RNF168 E3 ubiquitin ligases to DSBs, followed by the ubiquitylation of DSB-flanking chromatin and the subsequent recruitment of the RAP80-BRCA1 complex (Doil et al., 2009; Huen et al., 2007; Mailand et al., 2007; Stewart et al., 2009; Wang and Elledge, 2007). We

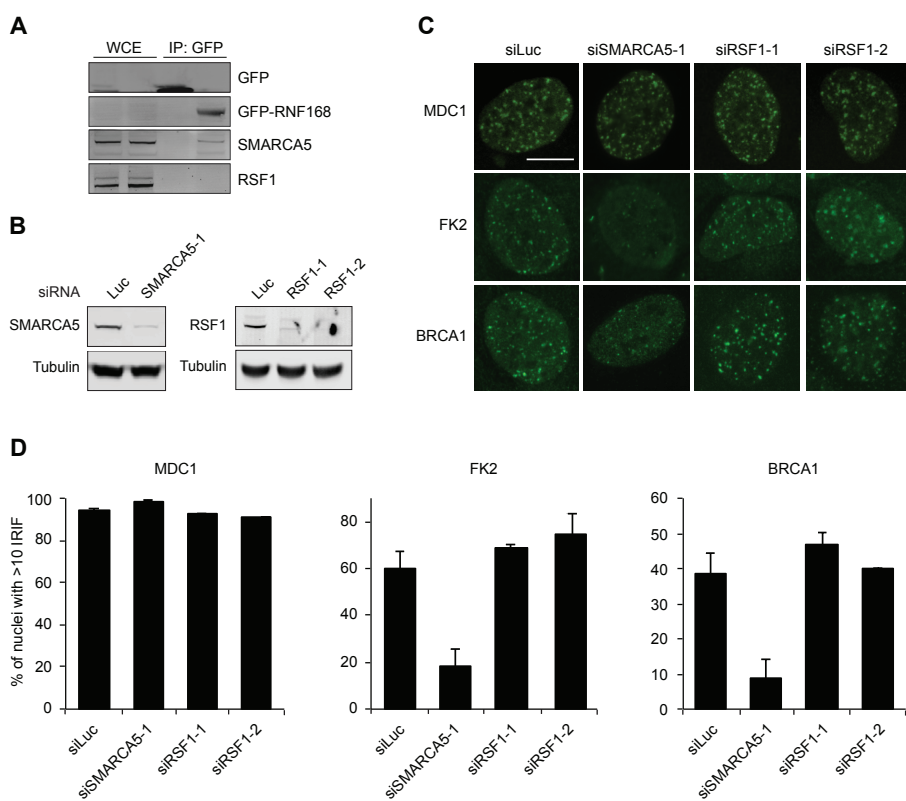


Figure 2. SMARCA5, but not RSF1, associates with RNF168 to regulate the ubiquitin-dependent accumulation of BRCA1 at DSBs. (A) Whole cell extracts (WCE) of U2OS cells expressing either GFP (lane 1 and 3) or GFP-RNF168 (lane 2 and 4) were subjected to GFP immunoprecipitation (IP) followed by western blot analysis of the indicated proteins. GFP-RNF168 expression was too low to be detectable in WCE. (B) U2OS cells were transfected with the indicated siRNAs and subjected to western blot analysis to monitor the efficiency of SMARCA5 and RSF1 knockdown. Tubulin is a loading control. (C) Cells from (B) were exposed to 2 Gy IR or left untreated, and 1 h later immunostained for MDC1, conjugated ubiquitin (FK2) or BRCA1 to visualize ionizing radiation-induced foci (IRIF). Images of untreated cells are presented in Fig. S1A. Scale bar, 10 μ m. (D) Quantitative representation of IRIF formation in C. The average percentage of cells with more than 10 IRIF \pm s.e.m. is presented. More than 120 nuclei were scored per sample in 2–3 independent experiments. Quantification of foci in untreated cells is presented in Fig. S1B.

found that SMARCA5 physically associates with RNF168 and affects the BRCA1 response by promoting RNF168-dependent chromatin ubiquitylation (Smeenk et al., 2013). Since RSF1 interacts with SMARCA5 (Perpelescu et al., 2009), we reasoned that it may be part of the RNF168-SMARCA5 complex and as such contribute to this response at the level of RNF168. To test this, we examined whether RSF1, like SMARCA5, associates with the RNF168 E3 ligase. However, although immunoprecipitation of GFP-tagged RNF168 from U2OS cells followed by western blot analysis revealed an interaction with SMARCA5, which is in agreement with our previous observations (Smeenk et al., 2013), we noticed that RNF168 did not interact with RSF1 (Fig. 2A). This suggests that RSF1 is not a constituent of the RNF168-SMARCA5 complex. Supporting the physiological relevance of the observed interactions, we found that depletion of SMARCA5, but not of RSF1, impaired the accumulation of conjugated ubiquitin and BRCA1 into IR-induced foci, whereas MDC1 IRIF formation remained unaffected by the loss of SMARCA5 or RSF1 (Fig. 2B–D; Fig. S1). These results, together with our previous work (Smeenk et al., 2013), suggest that RSF1, in contrast to SMARCA5, does not interact with RNF168 and is dispensable for the ubiquitin-dependent accumulation of BRCA1 at DSBs.

RSF1 regulates DSB repair by homologous recombination and non-homologous end-joining

Given that RSF1 does not affect the RNF168-dependent signaling of DSBs we reasoned that it could be involved in the repair of DSBs. We used two established reporter assays to monitor the role of RSF1 in HR and NHEJ, which are the two major pathways that have evolved to repair DSBs. The DR-GFP reporter for HR is composed of two differentially mutated GFP genes oriented as direct repeats. While the upstream repeat carries a recognition site for the rare-cutting I-SceI endonuclease, the downstream repeat consists of a 5' and 3' truncated GFP gene. Transient expression of I-SceI leads to the induction of a DSB in the upstream GFP gene, which can be repaired by HR using the downstream GFP fragment as a homologous template. Repair by HR following I-SceI cleavage thus results in the restoration of a functional GFP gene and subsequent GFP expression, which can be quantified by flow cytometry (Fig. 3A and C; compare siLuc $-/+$ I-SceI samples in C) (Weinstock et al., 2006). On the other hand, the EJ5-GFP reporter for NHEJ consists of a GFP gene that is separated from its promoter by the insertion of a Puromycine gene that is flanked by I-SceI recognition sites. Transient expression of I-SceI leads to the induction of DSBs and excision of the Puromycine gene. NHEJ-mediated repair of the broken ends fuses the promoter to the GFP gene, rendering the cells positive for GFP (Fig. 3B) (Bennardo et al., 2008). As expected, depletion of BRCA2, a key factor involved in HR, dramatically reduced the fraction of GFP-positive DR-GFP cells, but not EJ5-GFP cells, whereas depletion of the NHEJ factor XRCC4 reduced the fraction of GFP-positive EJ5-GFP cells (Fig. 3C and D). Importantly, when we depleted RSF1 we observed a significant reduction in the fraction of both GFP-positive DR-GFP and EJ5-GFP cells (Fig. 3C–E). As cell cycle profiles remained unchanged after knockdown of RSF1, we can rule out that cell cycle changes affected the HR and NHEJ efficiencies (Fig. S3). Therefore, our results demonstrate that RSF1 promotes efficient DSB repair by both HR and NHEJ.

RSF1 promotes the assembly of CENP-X and CENP-S at damaged chromatin

The RSF complex is required for the incorporation of centromere protein A (CENP-A), a histone H3 variant, into centromeric chromatin (Perpelescu et al., 2009). Interestingly, Zeitlin and colleagues showed that CENP-A accumulates at laser- and nuclease-induced DSBs and proposed a role for CENP-A in DSB repair (Zeitlin et al., 2009). These observations prompted

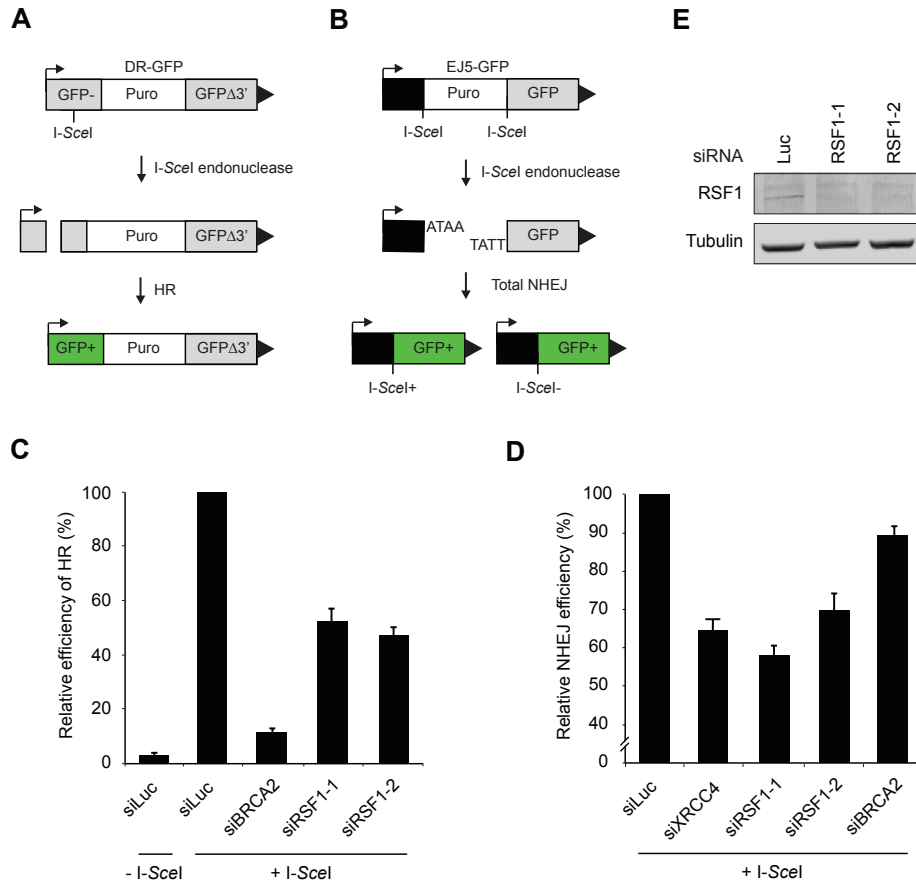


Figure 3. RSF1 regulates DSB repair by homologous recombination and non-homologous end-joining. (A) Schematic of the DR-GFP reporter used to monitor HR in HEK293T cells (see text for details). (B) Schematic of the EJ5-GFP reporter used to monitor NHEJ in HEK293T cells (see text for details). (C) DR-GFP reporter cells were transfected with the indicated siRNAs and 48 h later transfected with an I-SceI expression vector (pCBA5ce). 48 h later cells were analyzed for GFP expression by flow cytometry. The mean \pm s.e.m. of 4 experiments is shown. (D) As in (C), except that cells containing the NHEJ reporter EJ5-GFP were used. The mean \pm s.e.m. of 3 experiments is shown. (E) Western blot analysis showing the knockdown efficiency for the indicated siRNAs in HEK293T cells used in (C) and (D).

us to investigate whether RSF1, by targeting CENP-A to DNA breaks, could affect DSB repair. However, we failed to detect the accumulation of endogenous CENP-A at sites of DNA damage induced by our multiphoton laser when using irradiation conditions similar to those used to detect RSF1 assembly (Fig. S4A). When using U2OS cells stably expressing GFP-CENP-A, we observed weak GFP-CENP-A accumulation in laser tracks, but only in a very limited number of cells when high laser power was applied (Fig. S4B). In addition, we also found laser tracks in which GFP-CENP-A was excluded (Fig. S4B). Due to the difficulties to detect CENP-A recruitment to DSBs using our multiphoton laser set-up, we concluded that it would be very difficult to experimentally link RSF1 to the targeting of CENP-A to DSBs. Instead, we focused on the possibility that RSF1 may load other centromere proteins onto damaged chromatin. Recently, the centromere proteins CENP-S and CENP-X (also called MHF1 and MHF2) were isolated in a complex with the Fanconi anemia (FA) protein M (FANCM) (Singh et al., 2010;

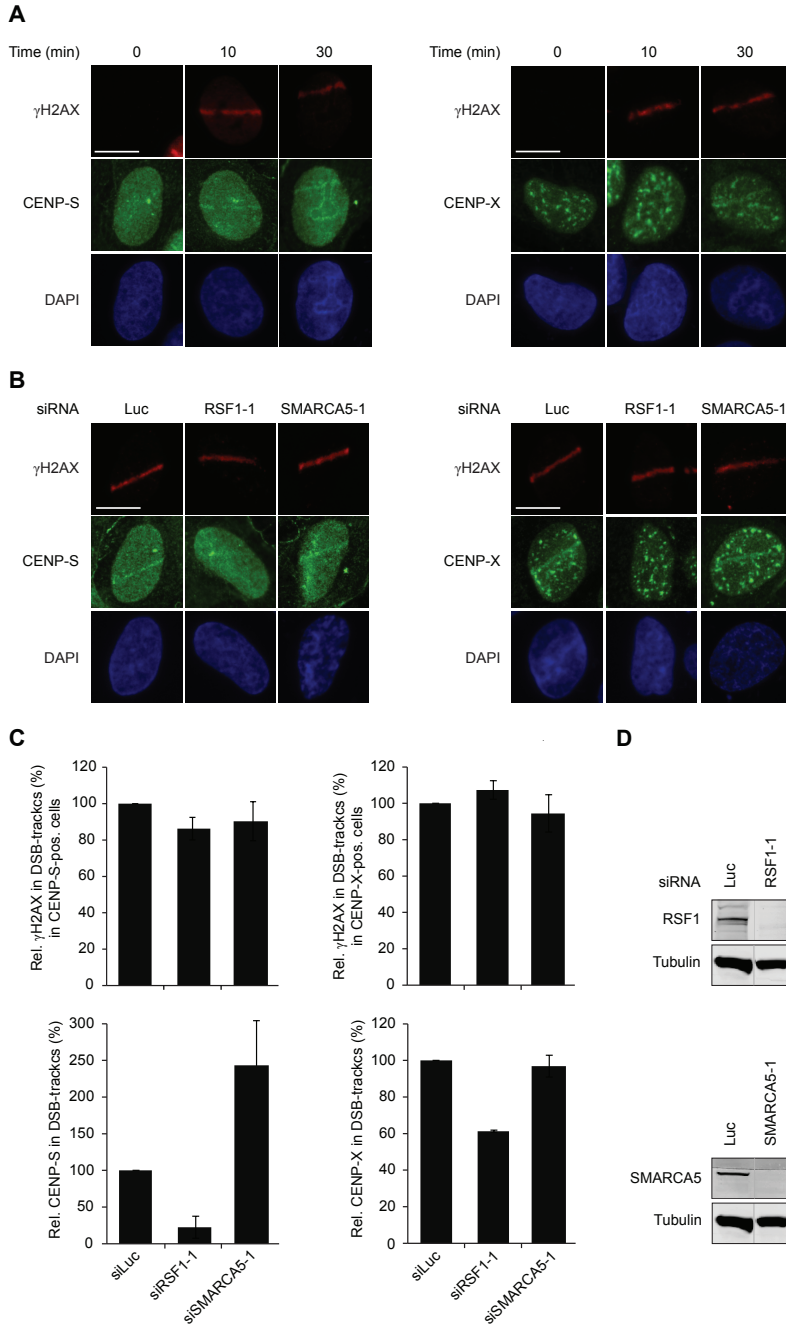


Figure 4. RSF1 promotes the assembly of CENP-S and CENP-X at damaged chromatin. (A) U2OS cells were subjected to multiphoton laser irradiation and immunostained for γ H2AX and endogenous CENP-S (left panel) or CENP-X (right panel) at the indicated time-points. Scale bar, 10 μ m. (B) As in (A), except that cells were treated with the indicated siRNAs and immunostained at 30 min after laser irradiation. (C) Quantification of the relative levels of γ H2AX and CENP-S or CENP-X in laser tracks after transfection with the indicated siRNAs. The levels in siLuc-treated cells (control) were set to 100%. Graphs represent the mean \pm s.e.m. of 40–130 individual cells from 2 independent experiments. (D) Western blot analysis showing the knockdown efficiency for the indicated siRNAs.

Yan et al., 2010). FANCM is a member of the Fanconi core complex that consists of at least seven other components and is required to protect cells against the cytotoxic effects of agents that induce DNA inter-strand crosslinks (ICLs) (Kottemann and Smogorzewska, 2013). Interestingly, CENP-S and CENP-X are required for the loading of FANCM at ICLs, suggesting that these factors play a role in ICL repair (Singh et al., 2010; Yan et al., 2010). However, whether these centromere proteins act in other DNA repair pathways remains unclear. Therefore, we first addressed whether these CENP proteins are recruited to laser-induced DNA damage. Strikingly, we found that following multiphoton laser micro-irradiation both endogenous CENP-S and CENP-X assembled at DSB-containing laser tracks that were marked by γ H2AX (Fig. 4A). To verify these results we generated GFP-tagged fusions of both CENP proteins and observed recruitment of GFP-tagged CENP-S and CENP-X to such damaged areas (Fig. S5). Having established that CENP-S and CENP-X accumulate at sites of DNA damage we then asked whether this event requires RSF1. Indeed, we found that RSF1 depletion by two independent siRNAs reduced the accumulation of endogenous CENP-S and CENP-X (Fig. 4B–D). Notably, the stronger centromeric localization of CENP-X compared with CENP-S detected by our antibodies may have obscured its accumulation in laser tracks and therefore complicated quantification. This is likely why the impact of RSF1 depletion on CENP-X appears milder in comparison to the striking reduction of CENP-S accumulation (Fig. 4B–D). Remarkably, however, knockdown of SMARCA5 did not impair the assembly of these centromere proteins at sites of DNA damage, suggesting that RSF1 can act independently of SMARCA5 during the DSB response (Fig. 4B–D). In support of such a scenario, we found that RSF1 and SMARCA5, although recruited to sites of DNA damage with similar kinetics (Fig. S6A and B), assembled independently from each other at DSBs (Fig. S6C–G). Finally, the effect of RSF1 on CENP-S and CENP-X loading was not indirect through transcriptional regulation, as the expression levels of both CENP proteins remained unchanged after RSF1 or SMARCA5 knockdown (Fig. S7A). Together, these results suggest that CENP-S and CENP-X assemble at damaged chromatin in an RSF1-dependent manner, while SMARCA5 is not involved in the loading of these proteins. We infer that CENP-S and CENP-X may be involved in regulating RSF1-dependent DSB repair events.

CENP-S and CENP-X promote NHEJ, but not HR

We next addressed whether we could functionally link the role of RSF1 in promoting DSB repair to its effect on CENP-S and CENP-X loading at DNA lesions. To deplete cells of the centromere proteins CENP-S and CENP-X we used either a single siRNA or a smartpool of siRNAs in the DR-GFP and EJ5-GFP reporter cells. As we could not detect CENP-S and CENP-X on western blots using any of the available antibodies, we established that the siRNAs not only dramatically reduced CENP-S and CENP-X mRNA levels, but also severely reduced the expression of exogenously expressed GFP-tagged CENP-S and CENP-X, demonstrating the functionality and specificity of our siRNAs (Fig. 5A; Fig. S2B). Surprisingly, while we found that depletion of RSF1, similar to that of BRCA2, significantly reduced the levels of GFP-positive DR-GFP cells (Figs. 3C and 5B), we did not observe this phenotype after CENP-S or CENP-X depletion (Fig. 5B). This suggests that RSF1 does not drive DSB repair by HR through loading of CENP-S or CENP-X at DSBs. In contrast, knockdown of CENP-S or CENP-X, similar to that of RSF1 or XRCC4 (Figs. 3D and 5C), significantly reduced the levels of GFP-positive EJ5-GFP cells (Fig. 5C), which suggests that RSF1 may promote DSB repair by NHEJ through regulating the assembly of CENP-S and CENP-X at DSBs.

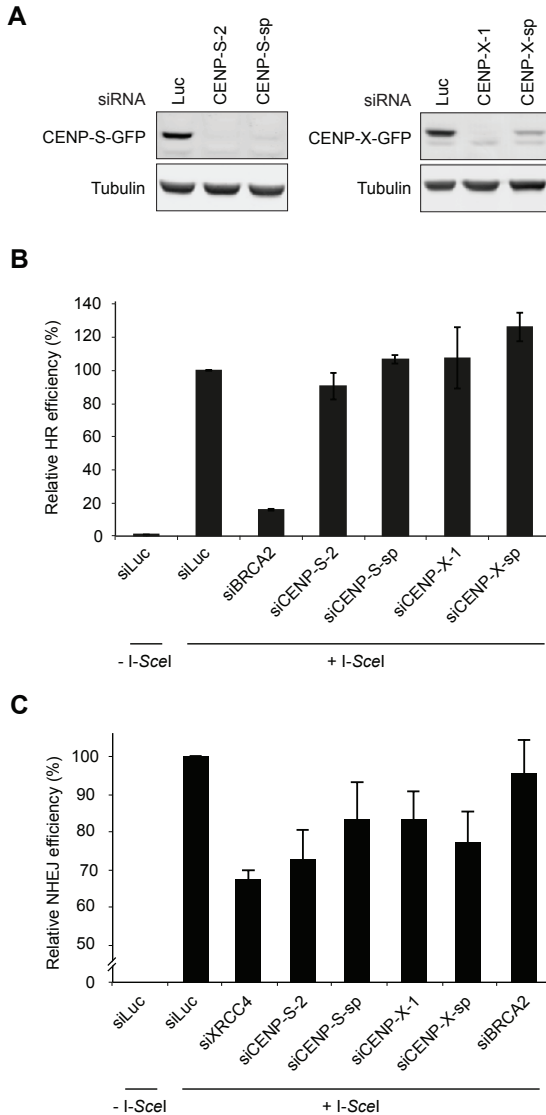
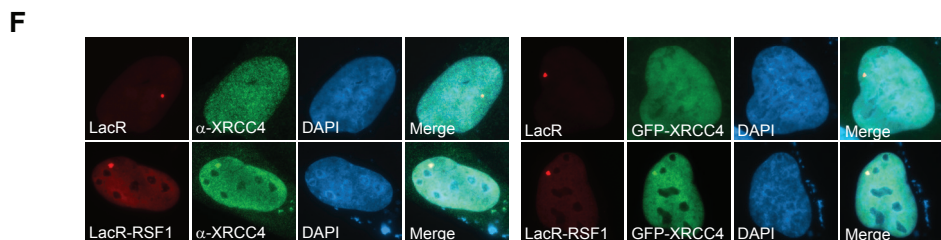
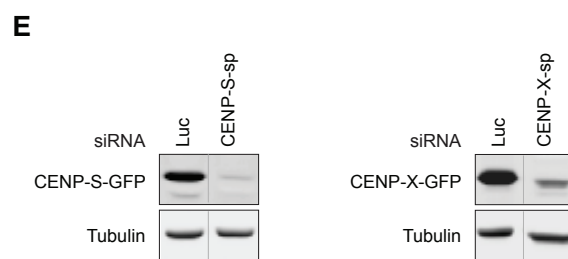
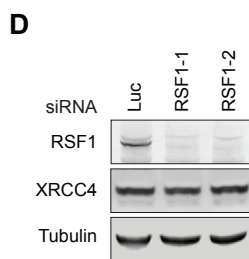
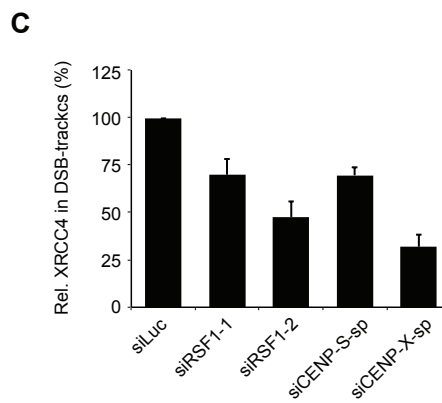
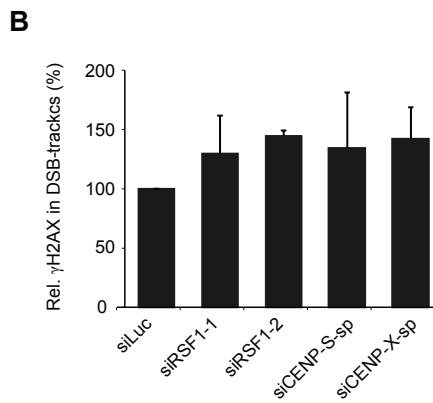
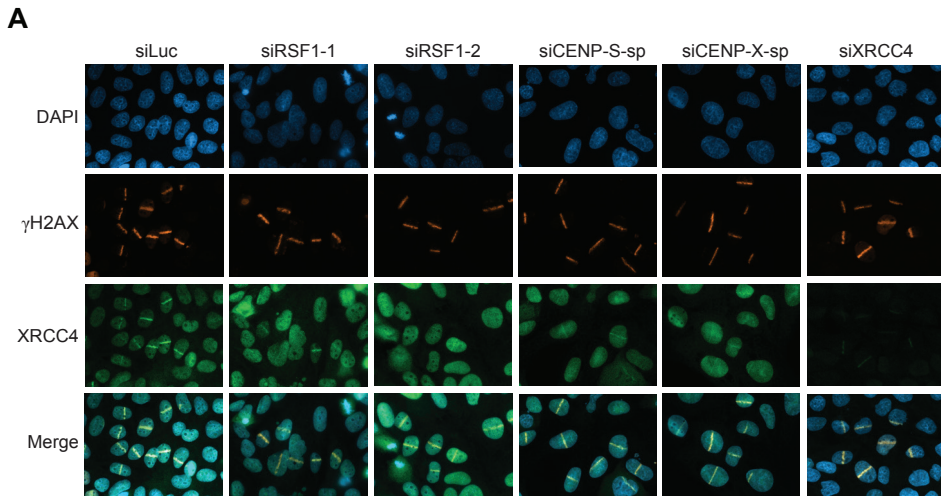


Figure 5. CENP-S and CENP-X promote NHEJ, but not HR. (A) HEK293T cells were treated with the indicated siRNAs and 48 h later transfected with either a GFP-CENP-S or GFP-CENP-X expression vector. Twenty-four h later cells were subjected to western blot analysis to show the knockdown efficiency for the indicated siRNAs. (B) HEK293T cells containing the HR reporter DR-GFP were transfected with the indicated siRNAs and 48 h later transfected with an I-SceI expression vector (pCBASce). Forty-eight h later cells were analyzed for GFP expression by flow cytometry. The mean \pm s.e.m. of 3 experiments is shown. (C) As in (B), except that cells containing the NHEJ reporter EJ5-GFP were used.

RSF1, CENP-S and CENP-X promote the assembly of the NHEJ factor XRCC4

One of the key factors involved in NHEJ is the XRCC4 protein, which forms a stable heterodimer with DNA ligase IV, a protein required for rejoining the broken ends during NHEJ.³ Indeed, we found that endogenous XRCC4 accumulates in DSB-containing laser tracks following UV-A laser micro-irradiation (Fig. 6A; see siLuc control samples). We then asked whether RSF1 and CENP-S and CENP-X would function together to recruit XRCC4 to damaged chromatin. Indeed, we found that depletion of either RSF1, CENP-S, or CENP-X resulted in a significant reduction in DSB-associated XRCC4, while the level of DNA damage induction as monitored by γ H2AX formation was comparable in the different knockdown cells (Fig. 6). The effect of RSF1 and the CENP proteins on XRCC4 loading was not indirect through transcriptional regulation as the XRCC4 expression levels remained unchanged in the knockdown cell lines



<

Figure 6. RSF1, CENP-S and CENP-X load XRCC4 onto damaged chromatin. (A) U2OS cells were treated with the indicated siRNAs, then subjected to UV-A laser irradiation and 30 min later immunostained for γ H2AX and endogenous XRCC4. Scale bar, 10 μ m. (B) Quantitative representation of results in (A). The relative levels of γ H2AX in laser tracks were plotted. The level of γ H2AX in siLuc-treated cells (control) was set to 100%. Graphs represent the mean \pm s.e.m. of at least 60 individual cells from 2 independent experiments. (C) As in (B), except for XRCC4. (D) Western blot analysis showing the knockdown efficiency for the indicated siRNAs in cells from (B) and (C). (E) U2OS cells were treated with the indicated siRNAs and 48 h later transfected with either a CENP-S-GFP or CENP-X-GFP expression vector. Twenty-four h later cells were subjected to western blot analysis to show the knockdown efficiency for the indicated siRNAs in (B and C). (F) U2OS 2–6–3 cells harboring a LacO array were transfected with mCherry-LacR or mCherry-LacR-RSF1 and (left panel) immunostained for endogenous XRCC4 or (right panel) co-transfected with GFP-XRCC4.

(Fig. S7B). Given that RSF1 is required for CENP-S and CENP-X assembly onto damaged chromatin, this suggests that the RSF1, CENP-S and CENP-X proteins collaborate to promote NHEJ by regulating chromatin-bound XRCC4 levels at DSB sites. To provide further evidence for the RSF1-mediated loading of XRCC4, we generated a mCherry-LacR-tagged version of RSF1, which was targeted to a LacO-containing genomic locus in U2OS cells (Luijsterburg et al., 2012a; Luijsterburg et al., 2012b; Soutoglou and Misteli, 2008). Strikingly, endogenous as well as GFP-tagged XRCC4 clearly accumulated at the LacO array upon targeting of LacR-RSF1 to chromatin in virtually all cells examined, while targeting of LacR alone failed to recruit XRCC4 (Fig. 6F). These findings show that prolonged binding of RSF1 to chromatin triggers the recruitment of XRCC4 even in the absence of DSBs. Together, these results suggest that the RSF1-dependent loading of CENP-S and CENP-X at DSB sites promotes the assembly of the XRCC4-DNA ligase IV complex, thereby promoting efficient NHEJ.

DISCUSSION

Here we uncover novel functions for the spacing and remodeling factor 1 (RSF1) protein in the repair of DSBs. RSF1 regulates the two major DSB repair pathways, NHEJ and HR, through distinct mechanisms. At centromeres, RSF1 was shown to deposit the centromere protein CENP-A (Perpelescu et al., 2009). Reminiscent of such a mechanism, we uncovered that in response to genomic insult RSF1 loads the centromere proteins CENP-S and CENP-X onto damaged chromatin. These two factors, in turn, facilitate the efficient assembly of the NHEJ factor XRCC4 to promote repair through NHEJ. Remarkably, CENP-S and CENP-X were dispensable for the function of RSF1 in HR, suggesting an alternative pathway for RSF1-dependent regulation of HR, which remains to be elucidated but may involve the reported functional interaction between RSF1 and cyclin proteins involved in DSB repair (Jirawatnotai et al., 2011). Thus, RSF1 is a critical factor involved in the efficient execution of the two major pathways of DSB repair.

SMARCA5, but not RSF1 is linked to RNF168-dependent signaling of DSBs

While it is evident from our studies that RSF1 regulates DSB repair, we did not uncover a role for this protein in the ubiquitin-dependent BRCA1 response pathway. This result is surprising given that we have previously shown that the RSF1-associated ATPase SMARCA5 directly interacts with ubiquitin ligase RNF168 and is essential for the DNA damage-induced conjugation of ubiquitin and subsequent BRCA1 accumulation at DSBs (Smeenk et al., 2013). However, SMARCA5 resides in different multi-protein complexes and it may be that complexes other than the RSF complex (e.g., ACF or CHRAC) regulate the RNF168-

3

driven response at DSBs. On the other hand, it is interesting to note that several SMARCA5-associated non-canonical subunits appear to have distinct SMARCA5-independent functions in the DDR. For instance, ACF1 was previously shown to regulate the recruitment of the NHEJ factors KU70/80 to DSBs, while this event did not require SMARCA5 (Lan et al., 2010). In this study, we report that RSF1 is recruited independently from SMARCA5 to DSBs and regulates the assembly of centromere proteins CENP-S and CENP-X in a manner that did not require SMARCA5.

CENP-S and CENP-X: Novel factors involved in DSB repair

We found that RSF1 promotes DSB repair by both NHEJ and HR. Our data suggest that RSF1 regulates NHEJ by recruiting CENP-S and CENP-X to DSB-associated chromatin, which in turn promotes assembly of the XRCC4-LigIV complex. It is currently not clear whether RSF1 promotes CENP-S/CENP-X assembly through recruiting CENP-A, or whether RSF1 directly loads CENP-S/CENP-X onto damaged chromatin. In addition, how CENP-S and CENP-X assembly contributes to XRCC4 binding at DSB sites remains to be elucidated. Previous studies demonstrated that CENP-S and CENP-X form a compact tetramer that can bind DNA and resembles H3-H4 tetramers found in histone octamers (Nishino et al., 2012; Tao et al., 2012). CENP-S and CENP-X localize to centromeres where they promote the assembly of kinetochore proteins (Amano et al., 2009; Foltz et al., 2006). Consequently, loss of either CENP-S or CENP-X leads to mitotic abnormalities and genome instability (Amano et al., 2009). However, CENP-S and CENP-X function does not seem to be restricted to centromeres. Recently, the FANCM protein was found to associate with the CENP-S – CENP-X tetramer. Moreover, CENP-S and CENP-X appeared to be important for the accumulation of FANCM at psoralen-induced ICL, indicating that CENP-S and CENP-X may function at genomic sites other than centromeres (Singh et al., 2010; Yan et al., 2010). Here we extend the repertoire of genomic locations at which CENP-S and CENP-X could execute their function by showing that these factors assemble at DSB-containing laser tracks.

CENP proteins, chromatin structure and DSB repair

Analogous to their function at ICLs, it is possible that these CENP proteins may also target FANCM to DSBs sites, although it is currently unclear whether FANCM is involved in the IR-induced DSB response. On the other hand, our results suggest that the CENP-S/CENP-X complex may functionally interact with factors other than FANCM, such as the NHEJ factor XRCC4. To this end, it would be interesting to investigate whether XRCC4, either directly or indirectly, is able to associate with the CENP-S – CENP-X tetramer and whether this physical connection is important for its relocation to DSB sites. However, we can also not exclude the possibility that CENP-S and CENP-X by modulating chromatin structure affect the retention of XRCC4 at DSB sites. The available data suggest that CENP-S and CENP-X are not incorporated into nucleosomes. Rather, the CENP-S – CENP-X tetramer itself may bind to DNA nucleosome-free regions (Nishino et al., 2012; Tao et al., 2012), including those that are in close proximity to DSBs. The binding of CENP proteins to DNA may enhance the binding of DNA repair factors such as XRCC4, which possess DNA-binding properties, possibly through cooperative interactions on the DNA. Finally, CENP-S and CENP-X also form a stable complex with two other centromere proteins known as CENP-T and CENP-W. The CENP-T-W-X-S complex can bind DNA and form nucleosome-like structures (Nishino et al., 2012). Given that CENP-T, like CENP-S and CENP-X, is recruited to sites of DNA damage (Zeitlin et al., 2009), we cannot rule out the possibility that this complex associates with

damaged chromatin to modulate its structure and facilitates binding of repair factors such as XRCC4. Biochemical studies will be required to further study the importance of the CENP-T-W-X-S complex in modulating chromatin structure at sites of DNA damage.

RSF1, CENP-S and CENP-X in ICL repair and cancer

CENP-S and CENP-X have been suggested to play a role in the FANCM-dependent repair of ICLs by recruiting this FA protein to such lesions. However, how the assembly of CENP-S and CENP-X at ILCs is regulated remains unclear. Here we identify RSF1 as a novel factor that loads CENP-S and CENP-X at sites of DNA damage. Future studies may uncover whether RSF1 is also responsible for CENP-S and CENP-X loading at sites of ICLs and plays a role in the repair of ICLs along with FA proteins such as FANCM. Overexpression of RSF1 is found in many types of cancer and is correlated with poor prognosis (Sheu et al., 2010; Shih et al., 2005). It would be of interest to study if higher levels of RSF1 in such tumors affect the equilibrium between the different SMARCA5 complexes. An increased abundance of SMARCA5-RSF1 complexes at the expense of other SMARCA5-containing complexes (e.g., ACF or CHRAC) may impact DNA damage-induced ubiquitin signaling. Moreover, given that lower levels of RSF1 clearly impact repair through NHEJ and HR, it is feasible that increased RSF1 levels may affect DSB repair pathway choice and even lead to DSB repair defects in tumors overexpressing RSF1. Given the known synthetic lethality between HR defects and chemical inhibitors of poly(ADP-ribose)polymerase (PARP), this could make RSF1 a potential candidate for PARP inhibitor-based cancer treatment (Helleday, 2011). In summary, our results identify RSF1 as a novel factor that regulates DSB repair and outline a molecular mechanism for the RSF1-mediated assembly of centromere proteins at DSBs to promote non-homologous end-joining.

3

MATERIAL AND METHODS

Cell culture

U2OS, HEK293 and VH10-SV40-immortalized fibroblast cells were grown in DMEM (Gibco) containing 10% FCS (Bodinco BV) unless stated otherwise. U2OS cells stably expressing GFP-RNF168 and U2OS 2–6–3 cells containing 200 copies of a LacO-containing cassette (~4 Mbp) were gifts from Jiri Lukas and Susan Janicki (Doil et al., 2009; Shanbhag et al., 2010). U2OS cells stably expressing GFP-RSF1 were generated by selection on G418 (100 µg/ml).

Plasmids

Fok1-mCherry-LacR, Fok1-mCherry-LacRD450A and GFP-CENP-A expression vectors were obtained from Roger Greenberg and Don Cleveland (Shanbhag et al., 2010; Zeitlin et al., 2009). GFP-XRCC4 was obtained from Penny Jeggo (Girard et al., 2004). The cDNA for human RSF1 (Open Biosystems, pENTR223.1) was cloned into pDEST-EGFP-C1-STOP, a kind gift of Dr Jason Swedlow, using the GATEWAY® system. The cDNA for human RSF1 was also cloned into mCherry-LacR-C1 (Coppotelli et al., 2013). CENP-S and CENP-X cDNAs were amplified from plasmids that were kindly provided by Iain Cheeseman (Amano et al., 2009), and cloned into pEGFP-C1 and pEGFP-N1 (Addgene).

Transfections and RNAi interference

siRNA and plasmid transfections were performed using HiPerfect (Qiagen), Lipofectamine

RNAiMAX (Invitrogen), Lipofectamine 2000 (Invitrogen), and JetPEI (Polyplus Transfection), respectively, according to the manufacturer's instructions. The following siRNA sequences were used:

5'-CGUACGCGGAAUACUUCGA-3' (Luciferase),
 5'-GGAAAGACAUCUCUACUUAU-3' (RSF1-1, Dharmacon),
 5'-UAAAUGAUCUGGACAGUGA-3' (RSF1-2, Dharmacon),
 5'-AGACAAAGGAAGAGAGCTA-3' (RSF1-3, Dharmacon),
 5'-GGAUUAAACUGGCUCAUUU-3' (SMARCA5-1, Dharmacon),
 5'-GAGGAGAUGUAAUACCUUA-3' (SMARCA5-2, Dharmacon),
 5'-GGAAUGGUUACUCGGAUA-3' (SMARCA5-3, Dharmacon),
 5'-GGGCAAAUAGAUUCGAGUA-3' (SMARCA5-6, Dharmacon),
 5'-AUAUGUUGGUGAACUGAGA-3' (XRCC4, (Sartori et al., 2007)),
 5'-GAAGAAUGCAGGUUUAUA-3' (BRCA2, MWG),
 5'-AGAUUAACCUAGAACGAAA-3' (CENP-S-2, Dharmacon),
 5'-GGAAGGAGCUGGUGAGCAG-3' (CENP-X-1, Dharmacon).

In addition, SMARTpools of siRNAs against CENP-S or CENP-X were used (Dharmacon). Cells were transfected twice with siRNAs (40 or 80 nM) within 24 h and examined further 48 h after the second transfection unless stated otherwise.

Generation of DSBs

IR was delivered by a YXlon X-ray generator (YXlon International, 200 KV, 4 mA, dose rate 1.1 Gy/min).

Cell survival assay

VH10-SV40 cells were transfected with siRNAs, trypsinized, seeded at low density, and exposed to IR. Seven days later cells were washed with 0.9% NaCl and stained with methylene blue. Colonies of more than 10 cells were scored.

Fok1 assays

RSF1 localization at FokI-induced DSBs was examined essentially as described (Costelloe et al., 2012; Shanbhag et al., 2010). Briefly, U2OS 2-6-3 cells were co-transfected with GFP-RSF1 and either Fok1-mCherry-LacR, or Fok1-mCherry-LacRD450A. Twenty-four hours later cells were fixed, immunostained for γ H2AX and examined microscopically for co-localization of γ H2AX, GFP-RSF1, and mCherry-LacR fused to either Fok1 or Fok1D450A using Zeiss AxioImager M2 and D2 widefield fluorescence microscopes.

Laser micro-irradiation

Multiphoton laser micro-irradiation was performed on a Leica SP5 confocal microscope equipped with an environmental chamber set to 37 °C and 5% CO₂ as described (Smeenck et al., 2010; Smeenck et al., 2013; Vyas et al., 2013). Briefly, U2OS cells were grown on MatTek glass bottom dishes. Media was replaced with colorless DMEM supplemented with 10% FCS and penicillin/streptomycin before imaging. DSB-containing tracks (1.5 μ m width) were generated with a Mira modelocked Ti:Sapphire laser (λ = 800 nm, pulselength = 200 fs, repetition rate = 76 MHz, output power = 80 mW). Typically, an average of 75 cells was micro-irradiated (1 iteration per pixel) within 10 min using LAS-AF software. For live cell

imaging, confocal images were recorded before and after laser irradiation at different time intervals. For UV-A laser micro-irradiation U2OS cells were grown on 18 mm coverslips and sensitized with 10 μ M 5-bromo-2-deoxyuridine (BrdU) for 24 h, as described (Acs et al., 2011; Luijsterburg et al., 2012a). For micro-irradiation, the cells were placed in a ChamSlide TC-A live-cell imaging chamber that was mounted on the stage of a Leica DM IRBE widefield microscope stand (Leica) integrated with a pulsed nitrogen laser (Micropoint Ablation Laser System; Photonic Instruments, Inc). The pulsed nitrogen laser (16 Hz, 364 nm) was directly coupled to the epifluorescence path of the microscope and focused through a Leica 40 \times HCX PLAN APO 1.25–0.75 oil-immersion objective. The growth medium was replaced by CO₂-independent Leibovitz L15 medium supplemented with 10% FCS and pen/strep and cells were kept at 37 °C. The laser output power was set to 78 to generate strictly localized sub-nuclear DNA damage. Following micro-irradiation, cells were incubated for the indicated time-points at 37 °C in Leibovitz L15 and subsequently fixed with 4% formaldehyde before immunostaining. Typically, an average of 50 cells was micro-irradiated (2 iterations per pixel) within 10–15 min using Andor IQ software.

Microscopy analysis

Images of fixed samples were acquired on a Zeiss Axiolmager M2 or D2 widefield fluorescence microscope equipped with 40 \times , 63 \times , and 100 \times PLAN APO (1.4 NA) oil-immersion objectives (Zeiss) and an HXP 120 metal-halide lamp used for excitation. Fluorescent probes were detected using the following filters: DAPI (excitation filter: 350/50 nm, dichroic mirror: 400 nm, emission filter: 460/50 nm), GFP/Alexa 488 (excitation filter: 470/40 nm, dichroic mirror: 495 nm, emission filter: 525/50 nm), mCherry (excitation filter: 560/40 nm, dichroic mirror: 585 nm, emission filter: 630/75 nm), Alexa 555 (excitation filter: 545/25 nm, dichroic mirror: 565 nm, emission filter: 605/70 nm), Alexa 647 (excitation filter: 640/30 nm, dichroic mirror: 660 nm, emission filter: 690/50 nm). Images were recorded using ZEN 2012 software and IRIF were scored by eye or by using home-made Stacks software as described (Smeenk et al., 2010; Smeenk et al., 2013). Images recorded after multi-photon- and UV-laser micro-irradiation and immunofluorescence stainings were analyzed using ImageJ. The average pixel intensity of laser tracks induced by either the multi-photon- or the UV-A laser system was measured within the locally irradiated area (I_{damage}), in the nucleoplasm outside the locally irradiated area ($I_{\text{nucleoplasm}}$) and in a region not containing cells in the same field of view ($I_{\text{background}}$) using ImageJ. The relative level of accumulation expressed relative to the protein level in the nucleoplasm was calculated as follows: $((I_{\text{damage}} - I_{\text{background}}) / (I_{\text{nucleoplasm}} - I_{\text{background}}) - 1)$. The accumulation in the control cells transfected with siLuc within each experiment was normalized to 100%. Images obtained from live cell imaging after multi-photon micro-irradiation were analyzed using LAS-AF software. Fluorescence intensities were subtracted by the pre-bleach values and normalized to the first data point, which was set to 0, to obtain relative fluorescence units (RFU). The average reflects the quantification of between 50–150 cells from 2–3 independent experiments.

Antibodies

Immunofluorescence and western blot analysis were performed using antibodies against γ H2AX, α -Tubulin (Sigma), GFP (Roche), ubiquitin (FK2, Enzo Life Sciences), BRCA1 (Calbiochem and Santa Cruz), MDC1 (Abcam), and SMARCA5/SNF2h (Abcam). The antibodies against RSF1 (Perpelescu et al., 2009), CENP-S and CENP-X (Yan et al., 2010), and XRCC4 were gifts from Kinya Joda, Weidong Wang, Roland Kanaar and Mauro Modesti.

Immunofluorescent labeling

Immunofluorescent labeling of γ H2AX, RSF1, MDC1, FK2, BRCA1, CENP-S, CENP-X, and XRCC4 was performed as described previously (Luijsterburg et al., 2012a; Luijsterburg et al., 2012b; Smeenk et al., 2010; Smeenk et al., 2013). Briefly, cells were grown on glass coverslips and treated as indicated in the figure legends. Subsequently, cells were either washed with PBS (for immunostaining of γ H2AX, RSF1, MDC1, FK2, BRCA1, XRCC4) or pre-extracted with 0.25% Triton X-100 in cytoskeletal (CSK) buffer (10 mM Hepes-KOH, 300 mM Sucrose, 100 mM NaCl, 3 mM MgCl₂, pH 7.4) on ice for 5 min (for immunostaining of CENP-S and -X), fixed with 4% formaldehyde for 10 min and 0.25% Triton X-100 or NP-40 in PBS for 5 min. Cells were rinsed with phosphate-buffered saline (PBS) and equilibrated in WB (PBS containing 5 g BSA/L, 1.5 g glycine/L) prior to immunostaining, except for immunostaining of XRCC4, cells were equilibrated in a different WB (PBS containing 0.5% BSA and 0.05% Tween 20) and then treated with 100 mM glycine in PBS for 10 min to block unreacted aldehyde groups. Detection was done using goat anti-mouse or goat anti-rabbit IgG coupled to Alexa 488, 555 or 647 (Invitrogen Molecular probes). Samples were incubated with 0.1 μ g/ml DAPI and mounted in Polymount.

Protein interaction studies

To study RNF168 interactions, cells were lysed in EBC buffer (50 mM Tris, pH 7.5, 150 mM NaCl, 0.5% NP-40, 1 mM EDTA) supplemented with protease and phosphatase inhibitor cocktails. Cleared lysates were subjected to immunoprecipitation with GFP Trap beads (Chromotek) for 1.5 h. Beads were washed 4 times with EBC buffer and boiled in sample buffer. Bound proteins were resolved by SDS-PAGE and processed for immunoblotting.

Homologous recombination and non-homologous end-joining assays

HEK293 cell lines containing either a stably integrated copy of the DR-GFP or EJ5-GFP reporter were used to measure the repair of I-SceI-induced DSBs by HR or NHEJ, respectively (Bennardo et al., 2008; Pierce et al., 1999). Briefly, 48 h after siRNA transfection, cells were transfected with the I-SceI expression vector pCBASce and a RFP expression vector (Pierce et al., 1999). 48 h later the fraction of GFP-positive cells among the RFP-positive cells was determined by FACS on a BD LSRII flow cytometer (BD Bioscience) using FACSDiva software version 5.0.3. Quantifications were performed using WinMDI 2.9 software.

Cell cycle profiling

For cell cycle analysis cells were fixed in 70% ethanol, followed by DNA staining with 50 μ g/ml propidium iodide in the presence of RNase A (0.1 mg/ml). Cell sorting was performed on a flow cytometer (LSRII; BD) using FACSDiva software (version 5.0.3; BD). Quantifications were performed using WinMDI software (version 2.9; J. Trotter).

RNA isolation, cDNA synthesis, and quantitative PCR

RNA was isolated using the miRNeasy minikit (Qiagen). cDNA was generated with the RevertAid first strand cDNA synthesis kit (Thermo scientific) using polydT primers and 1 μ g of total RNA as input. After cDNA synthesis, all samples were treated with 1 u RNase H (Life Technologies) for 20 min at 37 °C and diluted 1:10 in water. Realtime qPCR was performed in duplicate on the CFX96/384 system using SYBR green mastermix (Bio-Rad). Cycling conditions: initial melting at 95 °C for 3 min, 40 cycles of 95 °C for 10 s, and 60 °C for 30 s, followed by melting curve analysis (65 °C to 95 °C, stepwise increment of 0.5 °C) to control product specificity. Each reaction contained 4 μ l of diluted cDNA and 0.75 pM of each primer

in a total volume of 10 μ l. All primer pairs were designed using Primer3Plus software (<http://primer3plus.com>), tested for efficiency and are listed in Table S1. Relative expression levels were obtained with the CFX manager (vs 3.0), correcting for primer efficiencies and using GAPDH and GUSB as reference genes, unless indicated otherwise.

ACKNOWLEDGMENTS

We would like to thank Noel Lowndes for sharing unpublished data and Jiri Lukas, Susan Janicki, Roger Greenberg, Kinya Joda, Weidong Wang, Roland Kanaar, Mauro Modesti, Penny Jeggo, Jason Swedlow, Jeremy Stark, and Maria Jasin for generously providing valuable reagents. We acknowledge Willem Sloos, Annelies van der Laan, and Hans Tanke for assistance with the laser micro-irradiation experiments. This work was funded by an LUMC Epigenetics grant to ACO and HvA, a VIDI grant from the Netherlands Organization for Scientific Research (NWO) and a CDA grant from HFSP to HvA, and a VENI grant from NWO to MSL.



REFERENCES

1. Acs,K., Luijsterburg,M.S., Ackermann,L., Salomons,F.A., Hoppe,T., and Dantuma,N.P. (2011). The AAA-ATPase VCP/p97 promotes 53BP1 recruitment by removing L3MBTL1 from DNA double-strand breaks. *Nat. Struct. Mol. Biol.* 18, 1345-1350.
2. Amano,M., Suzuki,A., Hori,T., Backer,C., Okawa,K., Cheeseman,I.M., and Fukagawa,T. (2009). The CENP-S complex is essential for the stable assembly of outer kinetochore structure. *J. Cell Biol.* 186, 173-182.
3. Bennardo,N., Cheng,A., Huang,N., and Stark,J.M. (2008). Alternative-NHEJ is a mechanistically distinct pathway of mammalian chromosome break repair. *PLoS. Genet.* 4, e1000110.
4. Chapman,J.R., Taylor,M.R., and Boulton,S.J. (2012). Playing the end game: DNA double-strand break repair pathway choice. *Mol. Cell* 47, 497-510.
5. Ciccia,A. and Elledge,S.J. (2010). The DNA damage response: making it safe to play with knives. *Mol. Cell* 40, 179-204.
6. Coppotelli,G., Mughal,N., Callegari,S., Sompallae,R., Caja,L., Luijsterburg,M.S., Dantuma,N.P., Moustakas,A., and Masucci,M.G. (2013). The Epstein-Barr virus nuclear antigen-1 reprograms transcription by mimicry of high mobility group A proteins. *Nucleic Acids Res.* 41, 2950-2962.
7. Costelloe,T., Louge,R., Tomimatsu,N., Mukherjee,B., Martini,E., Khadaroo,B., Dubois,K., Wiegant,W.W., Thierry,A., Burma,S., van,A.H., and Llorente,B. (2012). The yeast Fun30 and human SMARCAD1 chromatin remodellers promote DNA end resection. *Nature* 489, 581-584.
8. Dinant,C., de,J.M., Essers,J., van Cappellen,W.A., Kanaar,R., Houtsmuller,A.B., and Vermeulen,W. (2007). Activation of multiple DNA repair pathways by sub-nuclear damage induction methods. *J. Cell Sci.* 120, 2731-2740.
9. Doil,C., Mailand,N., Bekker-Jensen,S., Menard,P., Larsen,D.H., Pepperkok,R., Ellenberg,J., Panier,S., Durocher,D., Bartek,J., Lukas,J., and Lukas,C. (2009). RNF168 binds and amplifies ubiquitin conjugates on damaged chromosomes to allow accumulation of repair proteins. *Cell* 136, 435-446.
10. Foltz,D.R., Jansen,L.E., Black,B.E., Bailey,A.O., Yates,J.R., III, and Cleveland,D.W. (2006). The human CENP-A centromeric nucleosome-associated complex. *Nat. Cell Biol.* 8, 458-469.
11. Girard,P.M., Kyselova,B., Harer,C.J., Doherty,A.J., and Jeggo,P.A. (2004). Analysis of DNA ligase IV mutations found in LIG4 syndrome patients: the impact of two linked polymorphisms. *Hum. Mol. Genet.* 13, 2369-2376.
12. Helleday,T. (2011). The underlying mechanism for the PARP and BRCA synthetic lethality: clearing up the misunderstandings. *Mol. Oncol.* 5, 387-393.
13. Huen,M.S., Grant,R., Manke,I., Minn,K., Yu,X., Yaffe,M.B., and Chen,J. (2007). RNF8 transduces the DNA-damage signal via histone ubiquitylation and checkpoint protein assembly. *Cell* 131, 901-914.
14. Jackson,S.P. and Bartek,J. (2009). The DNA-damage response in human biology and disease. *Nature* 461, 1071-1078.
15. Jirawatnotai,S., Hu,Y., Michowski,W., Elias,J.E., Becks,L., Bienvenu,F., Zagodzina,A., Goswami,T., Wang,Y.E., Clark,A.B., Kunkel,T.A., van,H.T., Xia,B., Correll,M., Quackenbush,J., Livingston,D.M., Gygi,S.P., and Sicinski,P. (2011). A function for cyclin D1 in DNA repair uncovered by protein interactome analyses in human cancers. *Nature* 474, 230-234.
16. Kottmann,M.C. and Smogorzewska,A. (2013). Fanconi anaemia and the repair of Watson and Crick DNA crosslinks. *Nature* 493, 356-363.
17. Lan,L., Ui,A., Nakajima,S., Hatakeyama,K., Hoshi,M., Watanabe,R., Janicki,S.M., Ogiwara,H., Kohno,T., Kanno,S., and Yasui,A. (2010). The ACF1 complex is required for DNA double-strand break repair in human cells. *Mol. Cell* 40, 976-987.
18. Larsen,D.H., Poinssignon,C., Gudjonsson,T., Dinant,C., Payne,M.R., Hari,F.J., Rendtew Danielsen,J.M., Menard,P., Sand,J.C., Stucki,M., Lukas,C., Bartek,J., Andersen,J.S., and Lukas,J. (2010). The chromatin-remodeling factor CHD4 coordinates signaling and repair after DNA damage. *J. Cell Biol.* 190, 731-740.
19. Luijsterburg,M.S., Acs,K., Ackermann,L., Wiegant,W.W., Bekker-Jensen,S., Larsen,D.H., Khanna,K.K., van Attikum,H., Mailand,N., and Dantuma,N.P. (2012a). A new non-catalytic role for ubiquitin ligase RNF8 in unfolding higher-order chromatin structure. *EMBO J.* 31, 2511-2527.
20. Luijsterburg,M.S., Lindh,M., Acs,K., Vrouwe,M.G., Pines,A., van Attikum,H., Mullenders,L.H., and Dantuma,N.P. (2012b). DDB2 promotes chromatin decondensation at UV-induced DNA damage. *J. Cell Biol.* 197, 267-281.
21. Luijsterburg,M.S. and van Attikum,H. (2011). Chromatin and the DNA damage response: the cancer connection. *Mol. Oncol.* 5, 349-367.
22. Mailand,N., Bekker-Jensen,S., Fastrup,H., Melander,F., Bartek,J., Lukas,C., and Lukas,J. (2007). RNF8 ubiquitylates histones at DNA double-strand breaks and promotes assembly of repair proteins. *Cell* 131, 887-900.
23. Nakamura,K., Kato,A., Kobayashi,J., Yanagihara,H., Sakamoto,S., Oliveira,D.V., Shimada,M., Tauchi,H., Suzuki,H., Tashiro,S., Zou,L., and Komatsu,K. (2011). Regulation of homologous recombination by RNF20-dependent H2B ubiquitination. *Mol. Cell* 41, 515-528.
24. Nishino,T., Takeuchi,K., Gascoigne,K.E., Suzuki,A., Hori,T., Oyama,T., Morikawa,K., Cheeseman,I.M., and Fukagawa,T. (2012). CENP-T-W-S-X forms a unique centromeric chromatin structure with a histone-like fold. *Cell* 148, 487-501.
25. Perpelescu,M., Nozaki,N., Obuse,C., Yang,H., and Yoda,K. (2009). Active establishment of centromeric CENP-A chromatin by

- RSF complex. *J. Cell Biol.* 185, 397-407.
26. Pierce,A.J., Johnson,R.D., Thompson,L.H., and Jasin,M. (1999). XRCC3 promotes homology-directed repair of DNA damage in mammalian cells. *Genes Dev.* 13, 2633-2638.
 27. Polo,S.E., Kaidi,A., Baskcomb,L., Galanty,Y., and Jackson,S.P. (2010). Regulation of DNA-damage responses and cell-cycle progression by the chromatin remodelling factor CHD4. *EMBO J.* 29, 3130-3139.
 28. Sanchez-Molina,S., Mortusewicz,O., Bieber,B., Auer,S., Eckey,M., Leonhardt,H., Friedl,A.A., and Becker,P.B. (2011). Role for hACF1 in the G2/M damage checkpoint. *Nucleic Acids Res.* 39, 8445-8456.
 29. Sartori,A.A., Lukas,C., Coates,J., Mistrik,M., Fu,S., Bartek,J., Baer,R., Lukas,J., and Jackson,S.P. (2007). Human CtIP promotes DNA end resection. *Nature* 450, 509-514.
 30. Shanbhag,N.M., Rafalska-Metcalf,I.U., Balane-Bolivar,C., Janicki,S.M., and Greenberg,R.A. (2010). ATM-dependent chromatin changes silence transcription in cis to DNA double-strand breaks. *Cell* 141, 970-981.
 31. Sheu,J.J., Guan,B., Choi,J.H., Lin,A., Lee,C.H., Hsiao,Y.T., Wang,T.L., Tsai,F.J., and Shih,I. (2010). Rsf-1, a chromatin remodeling protein, induces DNA damage and promotes genomic instability. *J. Biol. Chem.* 285, 38260-38269.
 32. Shih,I., Sheu,J.J., Santillan,A., Nakayama,K., Yen,M.J., Bristow,R.E., Vang,R., Parmigiani,G., Kurman,R.J., Trope,C.G., Davidson,B., and Wang,T.L. (2005). Amplification of a chromatin remodeling gene, Rsf-1/HBXAP, in ovarian carcinoma. *Proc. Natl. Acad. Sci. U. S. A* 102, 14004-14009.
 33. Singh,T.R., Saro,D., Ali,A.M., Zheng,X.F., Du,C.H., Killen,M.W., Sachpatzidis,A., Wahengbam,K., Pierce,A.J., Xiong,Y., Sung,P., and Meetei,A.R. (2010). MHF1-MHF2, a histone-fold-containing protein complex, participates in the Fanconi anemia pathway via FANCM. *Mol. Cell* 37, 879-886.
 34. Smeenk,G. and van Attikum,H. (2013). The chromatin response to DNA breaks: leaving a mark on genome integrity. *Annu. Rev. Biochem.* 82, 55-80.
 35. Smeenk,G., Wiegant,W.W., Marteiijn,J.A., Luijsterburg,M.S., Sroczynski,N., Costelloe,T., Romeijn,R.J., Pastink,A., Mailand,N., Vermeulen,W., and van Attikum,H. (2013). Poly(ADP-ribosyl)ation links the chromatin remodeler SMARCA5/SNF2H to RNF168-dependent DNA damage signaling. *J. Cell Sci.* 126, 889-903.
 36. Smeenk,G., Wiegant,W.W., Vrolijk,H., Solari,A.P., Pastink,A., and van Attikum,H. (2010). The NuRD chromatin-remodeling complex regulates signaling and repair of DNA damage. *J. Cell Biol.* 190, 741-749.
 37. Soutoglou,E. and Misteli,T. (2008). Activation of the cellular DNA damage response in the absence of DNA lesions. *Science* 320, 1507-1510.
 38. Stewart,G.S., Panier,S., Townsend,K., Al-Hakim,A.K., Kolas,N.K., Miller,E.S., Nakada,S., Ylanko,J., Olivarius,S., Mendez,M., Oldreive,C., Wildenhain,J., Tagliaferro,A., Pelletier,L., Taubenheim,N., Durandy,A., Byrd,P.J., Stankovic,T., Taylor,A.M., and Durocher,D. (2009). The RIDDLE syndrome protein mediates a ubiquitin-dependent signaling cascade at sites of DNA damage. *Cell* 136, 420-434.
 39. Tao,Y., Jin,C., Li,X., Qi,S., Chu,L., Niu,L., Yao,X., and Teng,M. (2012). The structure of the FANCM-MHF complex reveals physical features for functional assembly. *Nat. Commun.* 3, 782.
 40. Vyas,R., Kumar,R., Clermont,F., Helfricht,A., Kalev,P., Sotiropoulou,P., Hendriks,I.A., Radaelli,E., Hochepped,T., Blanpain,C., Sablina,A., van,A.H., Olsen,J.V., Jochemsen,A.G., Vertegaal,A.C., and Marine,J.C. (2013). RNF4 is required for DNA double-strand break repair in vivo. *Cell Death. Differ.* 20, 490-502.
 41. Wang,B. and Elledge,S.J. (2007). Ubc13/Rnf8 ubiquitin ligases control foci formation of the Rap80/Abraxas/Brc1/Brcc36 complex in response to DNA damage. *Proc. Natl. Acad. Sci. U. S. A* 104, 20759-20763.
 42. Wang,G.G., Allis,C.D., and Chi,P. (2007). Chromatin remodeling and cancer, Part II: ATP-dependent chromatin remodeling. *Trends Mol. Med.* 13, 373-380.
 43. Weinstock,D.M., Nakanishi,K., Helgadottir,H.R., and Jasin,M. (2006). Assaying double-strand break repair pathway choice in mammalian cells using a targeted endonuclease or the RAG recombinase. *Methods Enzymol.* 409, 524-540.
 44. Yan,Z., Delannoy,M., Ling,C., Daeë,D., Osman,F., Muniandy,P.A., Shen,X., Oostra,A.B., Du,H., Steltenpool,J., Lin,T., Schuster,B., Decaillet,C., Stasiak,A., Stasiak,A.Z., Stone,S., Hoatlin,M.E., Schindler,D., Woodcock,C.L., Joenje,H., Sen,R., de Winter,J.P., Li,L., Seidman,M.M., Whitby,M.C., Myung,K., Constantinou,A., and Wang,W. (2010). A histone-fold complex and FANCM form a conserved DNA-remodeling complex to maintain genome stability. *Mol. Cell* 37, 865-878.
 45. Zeitlin,S.G., Baker,N.M., Chapados,B.R., Soutoglou,E., Wang,J.Y., Berns,M.W., and Cleveland,D.W. (2009). Double-strand DNA breaks recruit the centromeric histone CENP-A. *Proc. Natl. Acad. Sci. U. S. A* 106, 15762-15767.

SUPPLEMENTAL INFORMATION

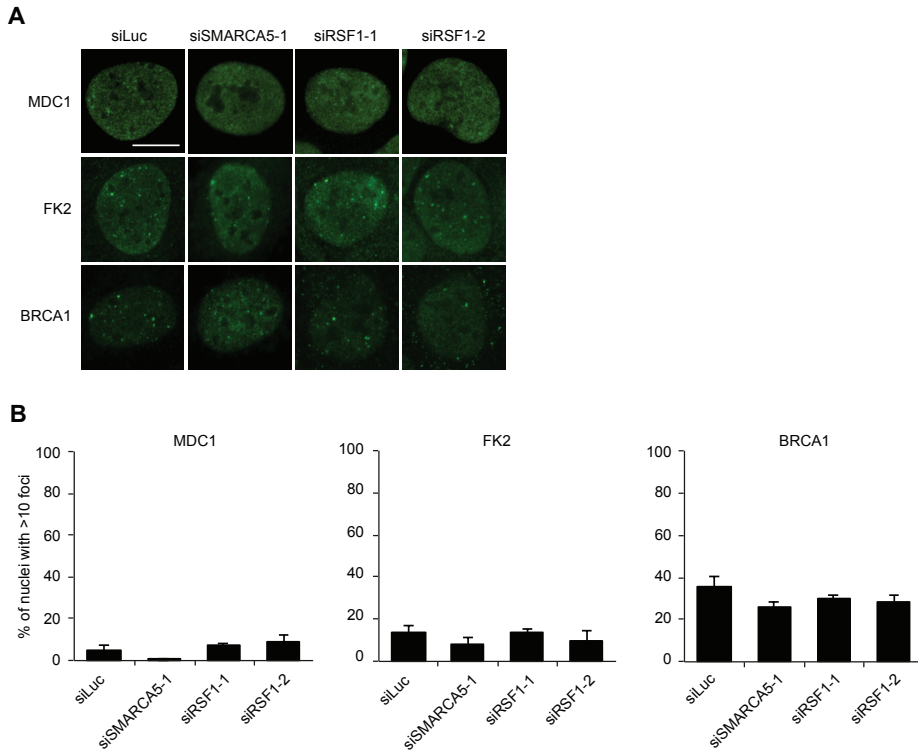


Figure S1. Analysis of spontaneous MDC1, conjugated ubiquitin and BRCA1 in unchallenged SMARCA5 and RSF1 knockdown cells. (A) U2OS cells were transfected with the indicated siRNAs. After 48 h cells were exposed to 2Gy IR or left untreated, and 1 h later immunostained for MDC1, conjugated ubiquitin (FK2) or BRCA1. Representative images of untreated cells showing spontaneously formed foci are presented. Those of IR-exposed cells are presented in Fig. 2 (Fig. 2, c). Scale bar, 10 μ m. (B) Quantitative representation of foci formation in A. The average of the percentage of cells with more than 10 foci \pm s.e.m. is presented. More than 120 nuclei were scored per sample in 2-3 independent experiments.

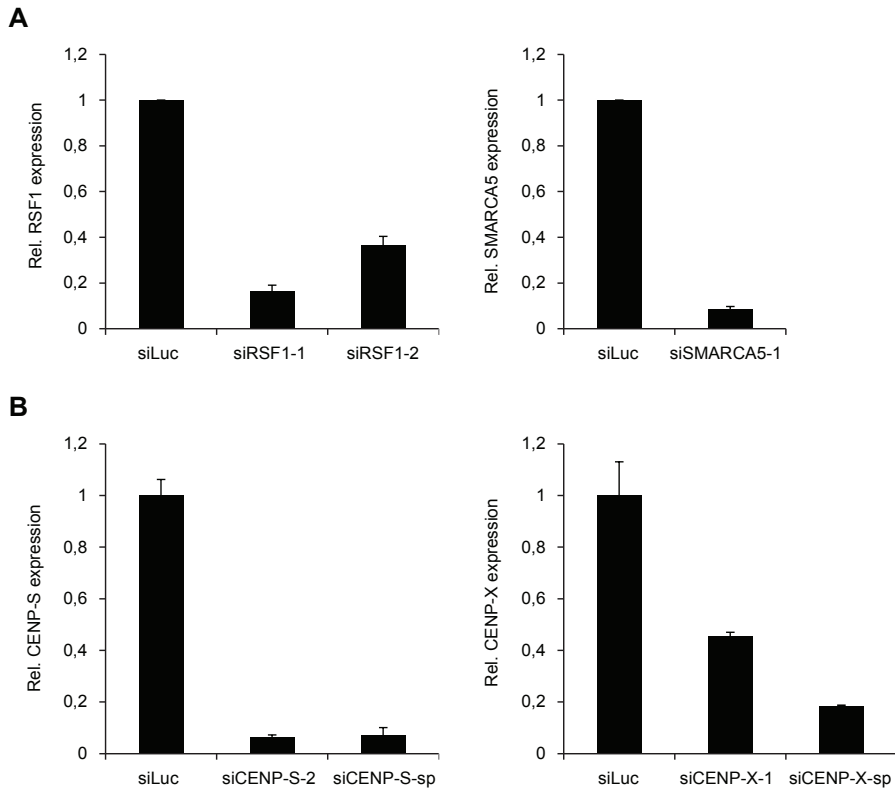


Figure S2. Expression analysis of RSF1, SMARCA5, CENP-S and CENP-X in different knockdown cell lines. U2OS cells were transfected with the indicated siRNAs and 48 h later subjected to RNA extraction. cDNA was synthesized from total RNA samples followed by qPCR to determine the expression levels of RSF1 and SMARCA5 (A), or CENP-S and CENP-X (B) relative to the GAPDH and GUSB reference genes.

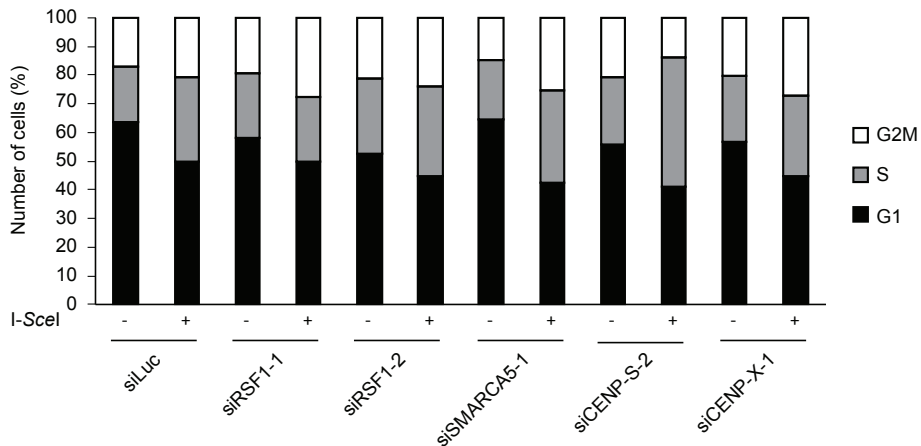


Figure S3. Knockdown of RSF1, SMARCA5, CENP-S or CENP-X does not affect cell cycle progression. HEK293T cells containing the DR-GFP reporter system were transfected with the indicated siRNAs. After 48 h cells were transfected with an I-SceI expression vector (pCBASce). 24 h later cells were stained with propidium iodide and subjected to flow cytometry analysis. The percentage of cells in G1 (black bar), S (grey bar) and G2/M (white bar) phase is represented.

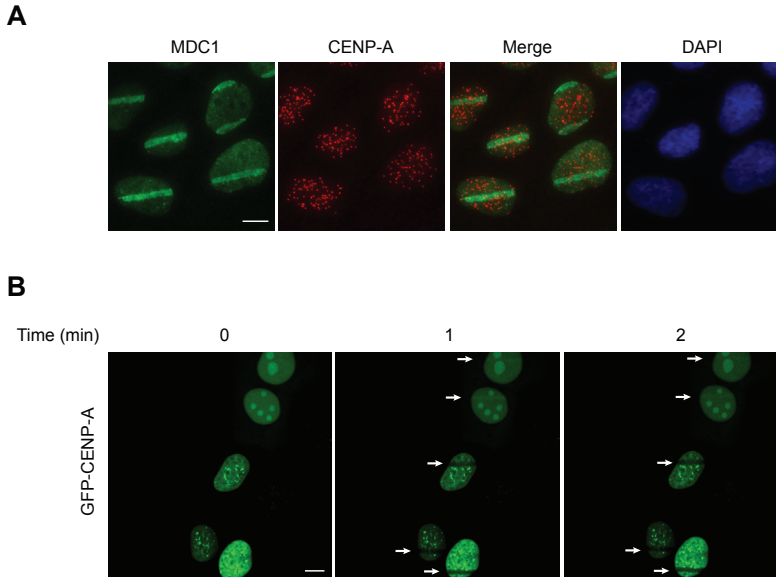


Figure S4. Analysis of CENP-A and GFP-CENP-A recruitment to sites of DNA damage. (A) U2OS cells were subjected to multiphoton laser irradiation and immunostained for MDC1 and endogenous CENP-A at 10 min after irradiation. Scale bar, 10 μ m. (B) As in A, except that U2OS cells stably expressing GFP-CENP-A were used. Representative images are shown for the indicated time-points. Arrows indicate micro-irradiated areas.

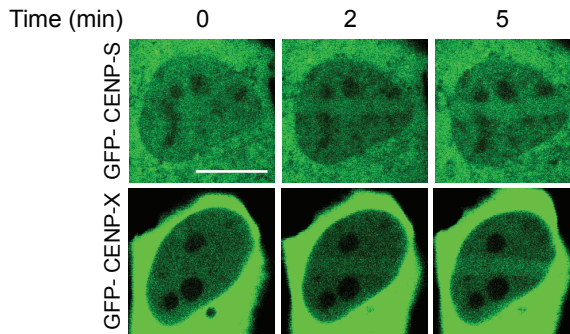
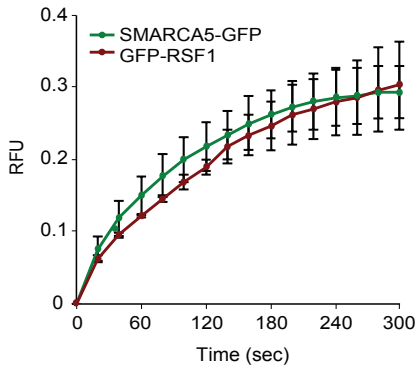
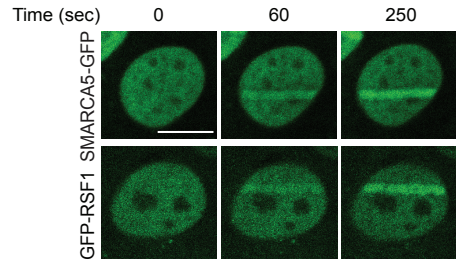
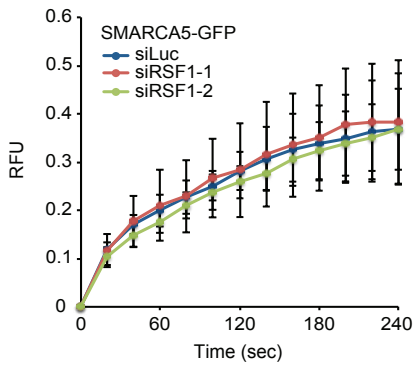
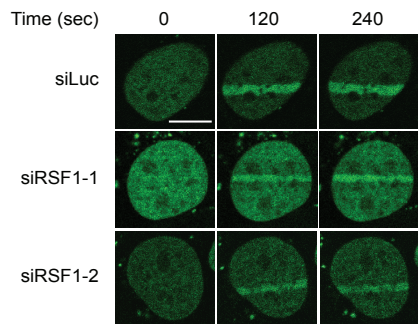
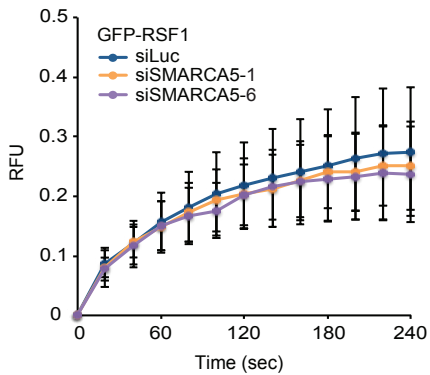
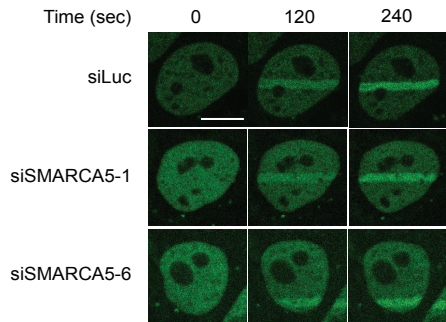
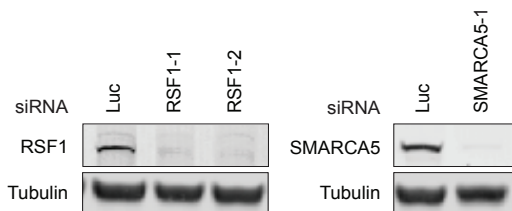


Figure S5. GFP-CENP-S and CENP-X accumulate at damaged chromatin. (A) U2OS cells transiently expressing GFP-CENP-S or GFP-CENP-X were irradiated using a multiphoton laser and subjected to real-time recording of protein assembly at the damaged area. Images show recruitment of GFP-CENP-S and GFP-CENP-X at the indicated time-points. Scale bar, 10 μ m.

Figure S6. Recruitment of SMARCA5 and RSF1 to sites of DNA damage is mutually independent. (A) U2OS cells stably expressing SMARCA5-GFP or GFPRSF1 were laser-irradiated and subjected to real-time recording of protein assembly at the damaged area. Scale bars, 10 μ m. (B) Quantitative representation of results in A. Relative Fluorescence Units (RFU) are plotted on a time scale. Graphs represent the mean \pm s.e.m. of at least 25 individual cells from 2 independent experiments. (C) As in A, except that U2OS cells stably expressing SMARCA5-GFP were used and transfected with siRNAs against RSF1. (D) As in B, except that cells from C were analyzed. (E) As in A, except that U2OS cells stably expressing GFP-RSF1 were used and transfected with siRNAs against SMARCA5. (F) As in B, except that cells from E were analyzed. (G) RSF1 and SMARCA5 levels were monitored by western blot analysis using whole cell extracts of cells in C and F. Tubulin is a loading control.

A**B****C****D****E****F****G**

3

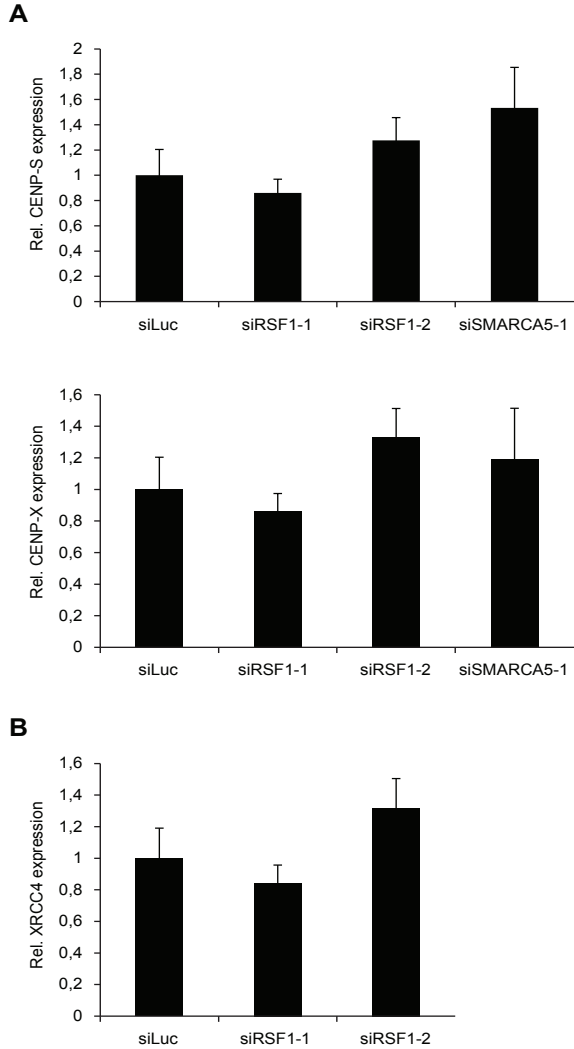


Figure S7. Expression analysis of CENP-S, CENP-X and XRCC4 in RSF1 and SMARCA5 knockdown cells. U2OS cells were transfected with the indicated siRNAs and 48 h later subjected to RNA extraction. cDNA was synthesized from total RNA samples followed by qPCR to determine the expression levels of CENP-S and CENP-X (A), or XRCC4 (B) relative to the GAPDH and GUSB reference genes.

Tabel S1: Primers used for RT-qPCR-based gene expression analysis

Gene	Forward primer (5'>3')	Reverse primer (5'>3')
GAPDH	GAGTCAACGGATTTGGTCGT	TTGATTTTGGAGGGATCTCG
GUSB	CTCATTGGGAATTTTGCCGATT	CCGAGTGAAGATCCCCTTTTA
RSF1	GCGAAGACTTTCCAGCTCAG	CGAACTGACCGCTTTGATTC
SMARCA5	AAACGAGGACCAAAGCCTTC	TTTTTCTCCTCGACCATCAG
CENP-S	CTGAAGATGTGAAGCTCTTAGCC	GGCTGCCTTGAATTTTGC
CENP-X	TGGACTTCTAGGGATCTCAGC	CAAATCCTTCAGGTCCTTCC
XRCC4	AGGAGACAGCGAATGCAAAG	TGTTTTCAGCTGAGATGTGCTC



INVESTIGATING DNA DAMAGE-
INDUCED RSF1 SUMOYLATION

4

Angela Helfricht¹, Karolin Eifler-Olivi²,
Haico van Attikum¹ and Alfred C. Vertegaal²

¹ Department of Human Genetics, Leiden University Medical Center

² Department of Molecular Cell Biology, Leiden University Medical Center

ABSTRACT

The small ubiquitin-like modifier (SUMO) has been described to regulate the activity, stability and /or interactions of numerous proteins within the DNA damage response (DDR) including the Remodeling and Spacing Factor 1 (RSF1). RSF1 is extensively SUMOylated, as evidenced by the identification of 21 SUMO-acceptor lysines, and has been implicated in facilitating repair of DNA double-strand breaks (DSBs) by promoting the incorporation of centromere proteins CENP-S and CENP-X into the damaged chromatin. Here, we show the DNA damage-regulated SUMOylation of endogenous RSF1 in time after exposure of human cells to ionizing radiation (IR). A SUMO-deficient RSF1 mutant, containing 21 lysine to arginine (21KR) point mutations, appeared to be incapable of recruiting the key DSB repair factor XRCC4 of the non-homologous end joining pathway (NHEJ) to chromatin, although this RSF1 mutant was still recruited to DSB-containing laser tracks. Consequently, this suggests that the DNA damage-dependent SUMOylation of RSF1 is dispensable for the accumulation of RSF1, but it is likely required for XRCC4 accrual to DSBs.

4

INTRODUCTION

The Remodeling and Spacing Factor 1 (RSF1) is a histone chaperone that has been described to form the RSF complex together with the chromatin remodelling ATPase SWI/SNF-related matrix-associated actin-dependent regulator of chromatin subfamily A member 5 (SMARCA5/SNF2h) of the ISWI family. SMARCA5 has been shown to physically associate with the E3 ubiquitin-protein ligase RNF168 upon DNA damage-induction and to promote the formation of RNF168-dependent ubiquitin conjugates, which facilitate the recruitment of downstream DNA double-strand break (DSB) response factors such as the Breast cancer type 1 susceptibility protein (BRCA1). Moreover, SMARCA5 is required for the proper execution of the two major DSB repair pathways i.e. nonhomologous end-joining (NHEJ) and homologous recombination (HR) (Lan et al., 2010; Smeenk et al., 2013).

More recently, we and others have shown a role for RSF1 in the cellular response to DNA damage. RSF1 is recruited to DSBs in an Ataxia telangiectasia mutated (ATM)-dependent fashion, but unexpectedly, its recruitment did not require its binding partner SMARCA5 (Helfricht et al., 2013; Min et al., 2014; Pessina and Lowndes, 2014). At DSBs, RSF1 deposits the centromere proteins CENP-S and CENP-X and thereby promotes the recruitment of the important DSB-repair factor X-ray repair cross-complementing protein 4 (XRCC4) of the NHEJ pathway (Helfricht et al., 2013). Interestingly, RSF1 also promotes the mono-ubiquitylation of the Fanconi Anemia proteins FANCD2 and FANCI upon DNA damage induction (Pessina and Lowndes, 2014). Thus, RSF1 contributes to a permissive chromatin state to allow efficient DNA repair by at least two mechanisms.

Proteins in the DNA damage response (DDR) are extensively regulated by post-translational modifications, including ubiquitin and small ubiquitin-like modifier (SUMO) (Jackson and Durocher, 2013). Similar to ubiquitin, SUMO is present in an inactive precursor state in cells and needs to be processed by specific proteases to become the mature protein. Conjugation of SUMO to a target protein is an ATP-dependent reaction and is catalysed by an enzymatic cascade. In humans the first step is mediated by the heterodimeric SUMO-activating enzyme (SAE1/SAE2), often indicated as the SUMO E1 enzyme. Once activated, SUMO is transferred to the SUMO-conjugating or E2 enzyme Ubiquitin carrier protein 9 (UBC9), which selects and binds directly to a SUMOylation consensus site in any of the target proteins (Flotho and Melchior, 2013). The common SUMOylation consensus motif starts with a large hydrophobic residue followed by the SUMO acceptor lysine and contains a glutamic acid two positions downstream of the SUMOylated lysine (Hendriks et al., 2014; Matic et al., 2010). Other SUMOylation motifs include the inverted consensus motif [(ED)xKx(≠ED)] (E: glutamic acid; D: aspartic acid, K: lysine) and a hydrophobic cluster motif (Matic et al., 2010).

The most efficient way for assuring substrate specificity is achieved by an E3 enzyme or SUMO ligase, which can transfer SUMO from the E2 onto a specific substrate (Flotho and Melchior, 2013). The SUMO E3 ligases PIAS1 and PIAS4 have been shown to be recruited to DSBs and to promote the accrual of SUMO at the site of DNA damage thereby facilitating the recruitment of 53BP1 and BRCA1 (Galanty et al., 2009).

In human cells, 3 different modifiers are distinguished, SUMO-1, -2 and -3. SUMO-2 and SUMO-3 are virtually identical and are also the most abundant SUMO family members (Saitoh and Hinchev, 2000). Furthermore, SUMO-2 and SUMO-3 contain an internal SUMOylation site, enabling SUMO-chain formation. In contrast, SUMO-1 is missing this internal SUMOylation motif and therefore can function as a chain-terminator when being included in SUMO polymers.



Since SUMO is attached covalently to lysine residues in substrates, it potentially competes with other lysine-directed posttranslational modifications like poly(ADP-ribosyl)ation (PARylation), methylation, acetylation or ubiquitylation (Hendriks et al., 2014). Moreover, SUMOylation has distinct roles; it can promote protein-protein interactions, or interfere with protein-protein interactions due to steric hindrance (Flotho and Melchior, 2013; Jentsch and Psakhye, 2013). In addition proteins containing one or more SUMO-interacting motifs (SIMs) formed by a stretch of hydrophobic amino acids or a specific ZZ zinc finger, are able to bind to SUMO (Danielsen et al., 2012; Song et al., 2004).

SUMOylation is involved in numerous cellular processes including the DDR, but mechanistic understanding of its mode of action is hampered by the lack of detailed knowledge of its substrates. PIAS4-mediated SUMOylation plays a crucial role during the ubiquitylation-dependent signalling of DSBs. Notably, the SUMOylation of HERC2 facilitates the interaction of HERC2 with RNF8, and the assembly of UBC13 with RNF8 thereby promoting DNA damage-induced formation of Lys 63-linked ubiquitin chains, while the SUMOylation of RNF168 actually promotes its own recruitment to DSBs (Bekker-Jensen et al., 2010; Danielsen et al., 2012). Moreover, the DNA damage-induced SUMOylation of the early DSB response factor MDC1 might provide potential binding sites for RAP80 and thereby stimulate the subsequent BRCA1 assembly (Hu et al., 2012; Luo et al., 2012; Strauss and Goldberg, 2011; Strauss et al., 2011). On the contrary, MDC1-SUMOylation on lysine 1840 by PIAS4 is required for its removal from DNA lesions through the SUMO-dependent recruitment of the SUMO-targeted ubiquitin ligase (STUbL) RNF4, which targets MDC1 for degradation (Luo et al., 2012). In addition, the ubiquitin E3 ligase activity of BRCA1 is increased upon SUMOylation (Hu et al., 2012; Morris et al., 2009).

Novel SUMOylation acceptor lysines identified recently (Hendriks et al., 2014; Matic et al., 2010) disclosed RSF1 as a SUMOylation target (Hendriks et al., 2014; Hendriks et al., 2015; Matic et al., 2010). In this study we used straight-forward immunoprecipitation methods to show the SUMOylation of RSF1 upon exposure to ionizing radiation (IR) and investigated the functional relevance of RSF1 SUMOylation, by generation of a SUMO-deficient mutant (K21R). This RSF1 K21R mutant was less capable to target XRCC4 to a LacO-array enriched with RSF1 21KR in a DNA damage-independent assay compared to wild-type RSF1. We thus speculate that RSF1 SUMOylation may be critical to promote XRCC4 loading at DSBs during NHEJ.

RESULTS

RSF1 is SUMOylated upon DNA-damage induction

We recently showed that RSF1 regulates NHEJ by promoting the recruitment of the core DNA repair factor XRCC4 through the deposition of the centromeric proteins CENP-S and CENP-X (Helfricht et al., 2013). At the same time, proteomic studies identified RSF1 as a potential SUMO-2 target protein (Hendriks et al., 2014; Matic et al., 2010) raising the question whether RSF1's role in DNA repair is regulated by SUMOylation. To this end, we monitored ionizing radiation (IR)-induced SUMOylation of RSF1 in U2OS cells at different time points after DNA damage induction. In these experiments we used U2OS cells stably expressing FLAG-SUMO-2 and anti-FLAG immunoprecipitation (IP) to enrich for SUMO-2 conjugates as well as parental U2OS cells (Schimmel et al., 2014), to investigate the SUMOylation levels of endogenous RSF1 upon exposure of cells to IR. SUMOylated forms of RSF1 were detected by

western blot running slightly higher than endogenous RSF1. A clear increase in SUMOylated RSF1 was detected already 0.5 h after exposure of cells to IR (Fig. 1A). The SUMOylation increase was even more pronounced after 2 hours, while the IP of SUMO-2 conjugates was equally efficient (Fig. 1A). In this particular experiment, the levels of endogenous RSF1 in the input samples decreased over time upon irradiation, but additional experiments revealed that the detected decrease in RSF1 expression was not observed reproducibly (Fig. S1A) and ruled out that RSF1 was degraded by the proteasome (data not shown).

Furthermore, we tried to detect SUMOylation of overexpressed GFP-RSF1, since GFP-RSF1 wt could serve as control in experiments employing an RSF1 SUMO mutant. We therefore transfected parental HeLa cells or HeLa cells stably expressing His6-SUMO-2 with either a control plasmid or a plasmid encoding GFP-RSF1 and performed a His-pulldown (PD) to enrich for SUMO conjugates. Consistent with our previous results, we could detect a strong SUMOylation signal for GFP-RSF1, but not in control PD samples (Fig. 1B). SUMOylated full-length GFP-RSF1 appeared in a typical SUMO ladder-type of signal above the marked GFP-RSF1 band (*). However additional lower molecular weight SUMOylation bands were detected on the immunoblot before and after His-PD, which suggest that ectopically expressed GFP-RSF1 got partially degraded in the absence of DNA damage (Fig. 1B).

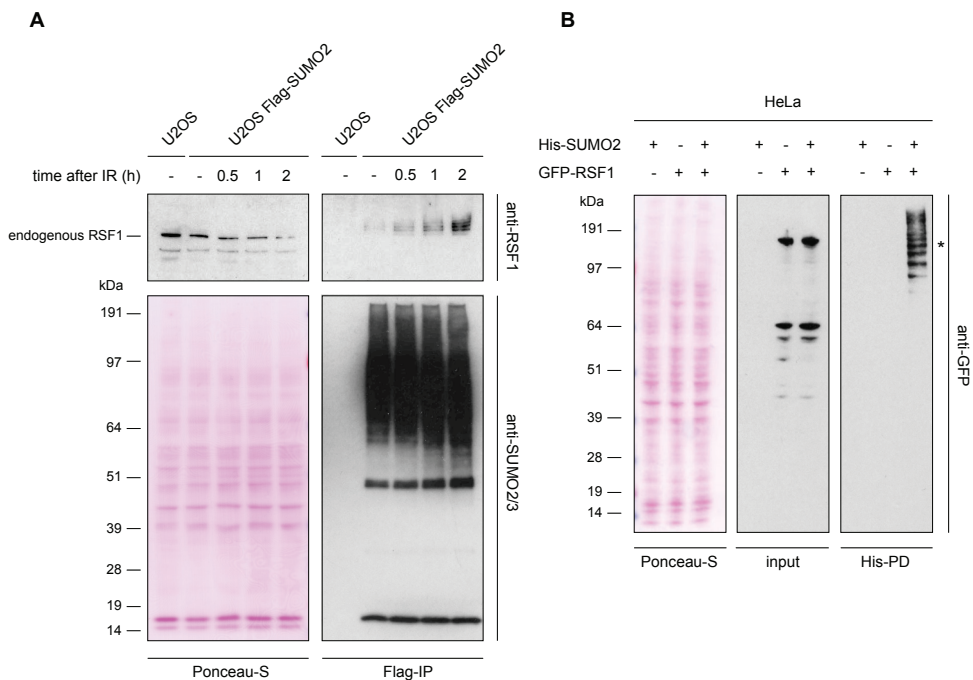


Figure 1. RSF1 is SUMOylated upon DSB induction. (A) Immunoblot analysis of total lysates and Flag-IP samples from U2OS cells stably expressing Flag-SUMO-2 or parental control cells, which were mock treated or exposed to 4 Gy of IR and lysed after the indicated time points. The SUMOylation of endogenous RSF1 is shown, while Ponceau-S stain serves as a loading control and SUMO-2/3-levels show IP-efficiency. (B) HeLa cells stably expressing His-tagged SUMO-2 or parental control cells, were transfected with a control or the indicated plasmid 24 h prior to cell lysis. Total lysates were subjected to His-PD procedure enriching SUMO-2 conjugates. Precipitates were visualized using anti-GFP antibody during immunoblot analysis. Ponceau-S staining is included as loading control. * marks full-length GFP-RSF1.

SUMOylation of the RSF1 21KR mutant is abrogated

RSF1 is a protein with two functional domains, a DNA binding homeobox and Different Transcription factors (DDT) domain at the N-terminus facilitating DNA binding, and a Phd-type Zinc-finger towards the C-terminus of the protein (Fig. 2A). A significant number of lysines in the RSF1 amino acid (aa) sequence have been identified as SUMO acceptor lysines, making it one of the most extensively SUMOylated proteins described so far (Hendriks et al., 2014; Matic et al., 2010). Through site-directed mutagenesis we introduced point mutations to replace 21 lysines (K) for arginines (R). Arginine has been selected as a replacement for lysine, since both amino acids contain positively charged side chains and only one mutation per codon was necessary to mediate the amino acid change. The position of all 21 aa conversions of the RSF1 21KR mutant are distributed over a region between the more N-terminally located K243 and the K768 of the 1441 aa counting RSF1 sequence and are not positioned within one of the described functional domains (Fig. 2A, Table S1). Plasmids encoding GFP fusions of RSF1 wt or the 21KR mutant, or encoding GFP only as a negative control, were transiently expressed in U2OS cells stably expressing His-SUMO-2. Cell lysates were subjected to the His-PD procedure to enrich for SUMO conjugates. While the PD was equally efficient, only GFP-RSF1 wt was SUMOylated, but the GFP-RSF1 21KR mutant was not (Fig. 2B and Fig. S1B). This indicates that point mutations of the RSF1 21KR mutant led to its loss of SUMOylation. Interestingly, previous mass spectrometry studies had identified six SUMO acceptor sites in RSF1 and revealed K294 as the most abundant one (Matic et al., 2010). We therefore created a K294R mutant and a 6KR RSF1 mutant at first, however these mutants were still SUMOylated similar to wild-type RSF1 (data not shown).

The RSF1 21KR mutant is recruited to laser tracks

RSF1 was shown to be recruited to DSBs in a manner dependent on ATM (Helfricht et al., 2013; Min et al., 2014; Pessina and Lowndes, 2014). To investigate whether SUMOylation of RSF1 plays a role in its recruitment to DSBs, we inflicted DNA damage by laser micro-irradiation in U2OS cells transiently expressing either GFP-RSF1 wt or the 21KR mutant. Interestingly both, RSF1 wt and 21KR were rapidly recruited to DSB-containing laser tracks with similar kinetics (Fig. 2C,D). This indicates that the SUMOylation of RSF1 is not important for its recruitment to DSBs and that the laser dependent recruitment of RSF1 was compromised by the replacement of 21 lysines to arginines.

XRCC4 accumulation is hampered in the RSF1 21KR mutant

Since we have shown that RSF1 promotes NHEJ repair by loading of XRCC4 onto DSB-containing chromatin (Helfricht et al., 2013), it is an obvious question whether the RSF1 21KR mutant is still capable to promote XRCC4 loading onto chromatin. We therefore generated mCherry-LacR-RSF1 wt and mCherry-LacR-21KR fusions, which upon expression in U2OS cells containing a LacO array (U2OS 2-6-3) were targeted through the binding of LacR to the array (Luijsterburg et al., 2012; Soutoglou and Misteli, 2008). To suppress endogenous RSF1 expression, U2OS 2-6-3 cells were treated with a siRNA against RSF1 prior to co-expression of siRNA-resistant mCherry-LacR-RSF1 and GFP-XRCC4. By means of mCherry fused to LacR, we could visualize the targeting of mCherry-LacR-NLS (neg. control) as well as mCherry-LacR-RSF1 wt and mCherry-LacR-21KR to the array and subsequently monitored GFP-XRCC4 accumulation (Fig. 3A). XRCC4 did not accumulate at the LacO array in the absence of RSF1, as has been shown in chapter 3 Fig. 6. But XRCC4 clearly assembled at RSF1 wt covered arrays, while in comparison the amount of XRCC4 detected at targeted RSF1 21KR was

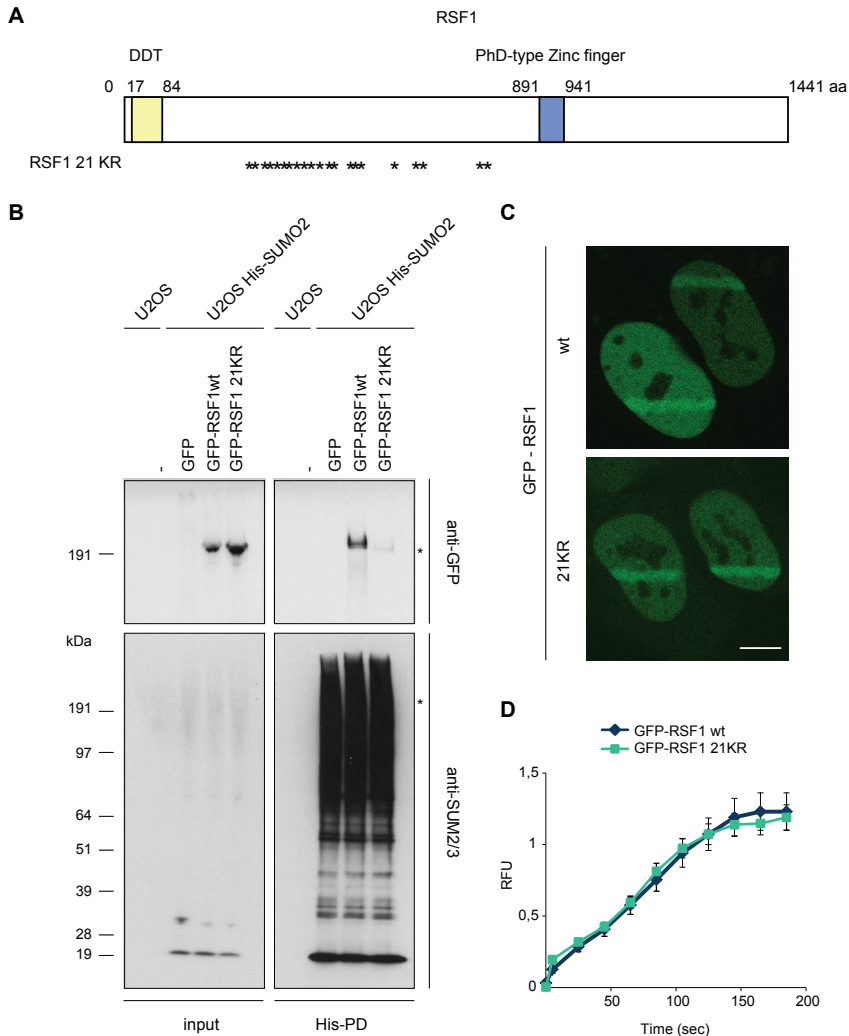


Figure 2. The RSF1 21KR mutant does not get SUMOylated. (A) Overview of full-length human RSF1 amino acid (aa) sequence. 21 K to R mutation positions are indicated by asterisks. (B) U2OS cells stably expressing His-SUMO-2 or parental control cells were either mock treated or transfected with the indicated plasmids. 24 h after transfection, lysates were prepared and analysed by immunoblotting using anti GFP antibody and anti SUMO-2/3 antibody. SUMO-2/3 levels show equal PD efficiency and equal loading. GFP signals indicate GFP-tagged RSF1 wt or 21KR. The asterisks shows the location of full-length GFP-RSF1 on the blot. (C) Live cell microscopy experiment: U2OS cells were transiently transfected with GFP-RSF1 wt or 21KR. Cells were subjected to local laser micro-irradiation and monitored in time. Representative images are shown for the 180 sec time point. The scale bar indicates 10 μ m. (D) Quantification of GFP-RSF1 recruitment to DNA-damage containing laser tracks from cells in (C) presented in Relative Fluorescent Units (RFU) over time.

decreased by approximately 75% (Fig. 3B). This suggests a role for SUMOylation of RSF1 in the recruitment of XRCC4 to chromatin.

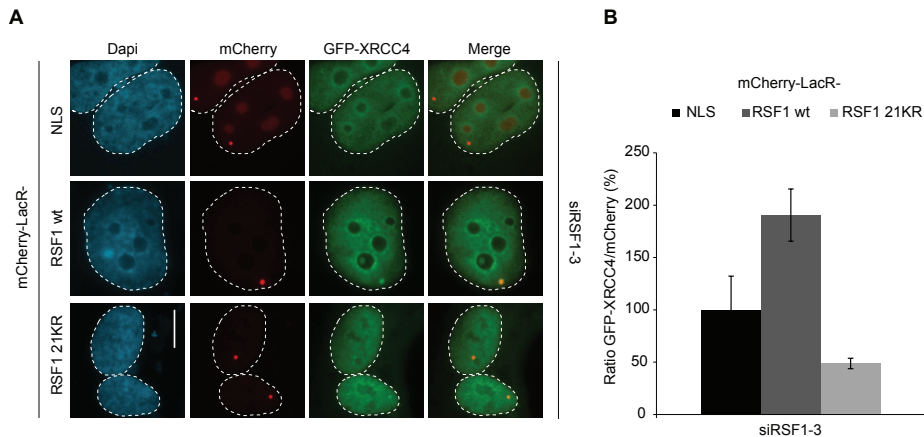


Figure 3. XRCC4 targeting is strongly decreased upon expression of RSF1 21KR mutant. (A) U2OS 2-6-3 cells containing 256 copies of a LacO repeat were treated with siRSF1-3. 48 h later, cells were co-transfected with the indicated mCherry-LacR-fusion plasmids and GFP-XRCC4. After additional 24 h, cells were fixed and stained with Dapi. Representative images are shown for mCherry-fusion constructs targeted to the LacO array and subsequent GFP-XRCC4 recruitment. The scale bar indicates 10 μ m. (B) Quantification of the signal intensity of DNA-damage independent recruitment of GFP-XRCC4 to mCherry-LacR-fusions located at the LacO array from cells in (A). The ratio of GFP-XRCC4 over the mCherry-LacR-fusions from two independent experiments with more than 60 cells analysed per condition is presented. Error bars indicate the standard error of the mean (s.e.m).

DISCUSSION

SUMOylation is a post-translational modification (PTM) that can change the stability of a protein, its localization or interactions when it is attached to a substrate. Since RSF1 was identified as a SUMO target protein (Hendriks et al., 2015; Matic et al., 2010) and implicated in the DNA damage response (Helfricht et al., 2013; Min et al., 2014; Pessina and Lowndes, 2014), we initiated an investigation to determine the role of RSF1 SUMOylation during DSB repair. Here we demonstrate for the first time the DNA damage-dependent SUMOylation of endogenous RSF1 (Fig. 1A). In order to assess the impact of SUMOylation on RSF1 function, we generated the RSF1 21KR SUMO mutant, which comprised 21 lysine to arginine point mutations and was deficient in RSF1 SUMOylation. While this mutant was still recruited to laser-induced DNA damage (Fig. 2C,D) with similar kinetics as RSF1 wt, its ability to load XRCC4 was highly decreased (Fig. 3A,B).

The RSF1 21KR mutant

Recently, several SUMO acceptor lysines had been found in RSF1 (Hendriks et al., 2014; Hendriks et al., 2015; Matic et al., 2010), hence we generated several RSF1 SUMO mutants. In contrast to the 21KR mutant, the RSF1 K294K and 6KR mutants did not show reduced SUMOylation levels (data not shown) and for that reason were excluded from further experimental testing. Importantly, when introducing lysine to arginine mutations, not only SUMO acceptor sites might be disrupted, but also acceptor lysines for other PTMs might be lost, which could influence one or more functions of RSF1. It is therefore of interest to investigate whether the RSF1 21KR is exclusively deficient for SUMOylation. An alternative way for the disruption of SUMOylation sites that leaves the PTM-acceptor lysines intact,

is to mutate glutamate (E) to alanine (A) within the SUMO consensus sites [ExK;KxE]. Unfortunately only 17 sites out of the 21 mutated lysines within the RSF1 21KR sequence belong to a consensus motif containing a glutamate (Tabel S1).

Another important point is that two mutated lysines, K468 and K565 fit the Phosphorylation-Dependent SUMOylation Motif (PDSM) [KxExx(pS)P] (Table S1), with S473 and S570, being the phosphorylation-acceptor serine (S) in these motifs, respectively (Table S2). Whether the loss of SUMOylation at these phosphorylation-dependent sites influences a particular function of RSF1, is currently unknown. Interestingly, also other PTMs can have a stimulatory or repressive effect on the SUMOylation of target proteins. Phosphorylation frequently acts in a stimulating way through PDSMs, even at the single serine residue level (Flotho and Melchior, 2013). However, the role of crosstalk between SUMOylation and other PTMs on the function of RSF1 has not been investigated so far.

Recruitment of the RSF1 21KR mutant to DSBs

The RSF1 21KR mutant was recruited to laser-induced DSBs with the same kinetics as wild-type RSF1, suggesting that the recruitment of RSF1 to DNA damage is not dependent on its SUMOylation. Previous studies have shown that the recruitment of RSF1 mainly depends on ATM-mediated phosphorylation on S524, S1226 and S1325 (Matsuoka et al., 2007; Min et al., 2014; Pessina and Lowndes, 2014). These results also implicate that ATM-dependent phosphorylation of RSF1 upon DSB induction is not disturbed by the K to R mutations within the RSF1 21KR mutant, although this is not experimentally tested. Conversely, SUMOylation could also simply occur after RSF1 recruitment, and recruitment would therefore not be affected.

The RSF1 21KR mutant might be unable to recruit XRCC4

We observed a clear decrease in XRCC4 accumulation to the targeted RSF1 21KR mutant compared to RSF1 wt in LacO array-containing U2OS 2-6-3 cells (Fig. 3). As this recruitment was in the absence of DSBs, we can only speculate on the role of RSF1 SUMOylation in the process of DSB repair via NHEJ and the recruitment of XRCC4 to damaged chromatin. Nonetheless, a clear co-localization of XRCC4 and RSF1 wt was detected (Helfricht et al., 2013), which was abrogated within the RSF1 21KR SUMO mutant expressing cells (Fig. 3). Since SUMOylation was suggested to have a glue-like character promoting protein-protein interactions within diverse pathways (Jentsch and Psakhye, 2013), we wondered whether XRCC4 might bind to SUMOylated RSF1 during NHEJ. Surprisingly, using the GPS-SUMO tool that predicts SUMOylation sites and SIMs based on a proteins sequence, no SIM was predicted for XRCC4. Also the sequences of the centromere proteins CENP-S and CENP-X, which are deposited at DSBs by RSF1 to promote XRCC4 recruitment (Helfricht et al., 2013), appear to lack SIM domains. Hence, the binding of DSB-repair proteins to SUMOylated RSF1 upon DSB induction does not seem likely.

Importantly, we cannot exclude the possibility that the 21 K to R point mutations might lead to differences in protein folding, which possibly could interrupt direct or indirect interactions of RSF1 with other proteins and might affect XRCC4 loading. Thus, observations made with this artificial targeting approach need to be confirmed using a different experimental approach, showing that RSF1 SUMOylation is indeed involved in XRCC4 recruitment upon DSB induction.

It is furthermore noteworthy that SUMOylation-deficient mutant proteins frequently lack severe phenotypes (Sacher et al., 2006; Silver et al., 2011). Accordingly, Psakhye et al. found that a wave of SUMOylation events is triggered upon DNA damage

induction (Psakhye and Jentsch, 2012). Instead of individual proteins, several repair proteins within the HR pathway had been SUMOylated, often at multiple sites. Together, this supports a model where strictly controlled SUMOylation acts in a glue-like manner on closely located substrates to stabilize protein complexes by facilitating physical interactions (Psakhye and Jentsch, 2012). Which phenotypes are associated with SUMOylation deficient RSF1 and whether RSF1 contributes to the stability of protein interactions during DSB repair however remain to be investigated.

Identification of a SUMO E3 ligase for RSF1

Another unaddressed point is the identity of a SUMO E3 ligase responsible for RSF1 SUMOylation upon DNA-damage induction. PIAS1 and PIAS4 are likely candidates to facilitate RSF1 SUMOylation, due to the fact that they have been implicated in the DSB response (Galanty et al., 2009). Unfortunately, no investigation towards the identification of the SUMO ligase of RSF1 has been initiated yet. But to monitor the SUMOylation levels of RSF1 and the subsequent recruitment of XRCC4 to DSBs in cells depleted from PIAS1 and/or PIAS4, would provide useful information on the requirement of one or both of these SUMO ligases for RSF1 SUMOylation.

Potential strategies for future functional studies

Efforts to generate experimental data to elucidate a possible function of RSF1 SUMOylation in the DDR were inconclusive. Expression of a siRNA-resistant version of RSF1 wt did not complement the knockdown-induced reduction of XRCC4 recruitment to DSB-containing laser tracks (Fig. S2). This could have had several reasons, one being inappropriate expression levels of RSF1. Not only does the depletion of RSF1 leads to defects in the response to DNA damage, the overexpression of RSF1 actually induces DNA damage (i.e. γ H2AX), thereby initiating cell growth arrest and apoptosis (Sheu et al., 2010). For such complementation approaches, near-endogenous expression levels of RSF1 wt and 21KR mutant are therefore vital and further investigations are required to proof the functionality of tagged RSF1 and the importance of RSF1 SUMOylation when compared to RSF1 21KR mutant during complementation experiments.

An alternative approach to search for DNA damage-dependent interactors of RSF1 wt and 21KR would be either employing Co-IPs or mass spectrometry (MS) analysis. Possible SUMOylation-dependent interactors could be identified in this manner and the question, whether RSF1 recruits XRCC4 directly or indirectly via a NHEJ protein, could be addressed. Besides promoting NHEJ upon DSB induction, RSF1 has also been suggested to be required for efficient HR (Helfricht et al., 2013; Min et al., 2014). This study so far however only focused on the possible involvement of RSF1 SUMOylation during NHEJ, which was based on former results (Helfricht et al., 2013). But RSF1 has also been suggested to promote the recruitment of the HR factors RPA and RAD51 to laser-induced DSBs (Min et al., 2014). Whether SUMOylation of RSF1 plays a role in the HR pathway however requires further investigation. Thus additional efforts have to be made in order to dissect the role of RSF1 SUMOylation during the DSB response via NHEJ as well as HR. Additionally, it would be interesting to research whether SUMOylation of RSF1 is specific for DSBs or occurs more globally in response to various types of DNA damage.

MATERIAL AND METHODS

Cell culture

U2OS cells and U2OS 2-6-3 cells containing a 200x integrated Lac operator genomic array were grown in DMEM (Gibco) containing 10% FCS (Bodinco BV) and 1% penicillin/streptomycin unless stated otherwise. U2OS 2-6-3 cells were a gift from Susan Janicki (Shanbhag et al., 2010) and were grown in DMEM supplemented with G418 [400 µg/ml].

Plasmids

The cDNA for human RSF1 in the vector pENTR223.1 was obtained from Open Biosystems and cloned into pDEST-EGFP-C1-STOP, a generous gift from Jason Swedlow, using the GATEWAY® system as described before (Helfricht et al., 2013). The mCherry-LacR encoding sequence from the mCherry-LacR-C1 vector (Coppotelli et al., 2013) and pDEST-EGFP-RSF1wt were digested by AgeI/XhoI and fused to generate the pDEST-mCherry-LacR-RSF1wt vector. Both constructs were made siRNA resistant to siRSF1-3 using site-directed mutagenesis to introduce 8 silent mutations.

The siRSF1-3-resistant RSF1 21KR sequence, flanked by suitable restriction sites, was synthesized by Genscript. This 21KR encoding sequence was swapped with the wt sequence by XhoI and PmlI digestion, purification and re-ligation into pDEST-GFP-RSF1. The RSF1 21KR insert of construct pDEST-EGFP-RSF1 21KR was cloned into the vector pDEST-mCherry-LacR using the restriction enzymes AgeI/XhoI generating the plasmid pDEST-mCherry-LacR-RSF1 21KR.

The NLS-sequence was cloned into GFP in a pEGFP-C1 vector and GFP-XRCC4 was kindly provided by Penny Jeggo (Girard et al., 2004).

Transfections and RNAi interference

siRNA and plasmid transfections were performed using Lipofectamine RNAiMAX (Invitrogen) or Lipofectamine 2000 (Invitrogen), respectively, according to the manufacturer's instructions. During the follow-up study, the following siRNA sequences were used:

5'- CGUACGCGAAUACUUCGA -3' (Luciferase, Dharmacon),
5'- AGACAAAGGAAGAGAGCTA -3' (RSF1-3, Dharmacon).

Cells were transfected twice with siRNAs [40 nM] within 24 h and examined further 48 h after the second transfection, unless stated otherwise.

Immunoprecipitation

Flag-IPs were performed as previously described (Schimmel et al., 2014), lysing U2OS cells in four pellet volumes of lysis buffer (1% SDS, 0.5% NP-40 in PBS, including phosphatase and protease inhibitors). 70 mM Chloroacetamide was added freshly to Flag-IP lysates. After sonication, samples were incubated for 30 minutes at room temperature, followed by sample equalization using BCA Protein Assay Reagent (Thermo Scientific). 30 µl of each lysate was taken and stored as input sample. An equal volume of dilution buffer (2% Triton X-100, 0.5% sodium deoxycholate, 1% BSA, freshly added 70 mM chloroacetamide, 5 mM sodium fluoride, 1 mM sodium orthovanadate, 5 mM β-glycerol phosphate, 5 mM sodium pyrophosphate, 0.5 mM EGTA, 5 mM 1,10-phenanthroline, protease inhibitor including EDTA (Roche; 1 tablet per 10 ml buffer) was added to the lysates. Subsequently, samples



were centrifuged for 45 minutes at 13.2 krpm at 4°C. The supernatant was transferred to a clean tube and mixed with prewashed Flag-M2 beads (Sigma; 30 µl beads per 1 ml of diluted sample). Tubes were left rolling during incubation at 4°C for 90 minutes. Next, the beads were washed 5x with wash buffer (50 mM Tris, 150 mM NaCl, 70 mM chloroacetamide, 0.5% NP-40, 5 mM sodium fluoride, 1 mM sodium orthovanadate, 5 mM β-glycerolphosphate, 5 mM sodium pyrophosphate, 0.5 mM EGTA, 5 mM 1,10-phenanthroline protease inhibitor including EDTA (Roche; 1 tablet per 10 ml buffer)), including 3 tube changes. The Flag-SUMO-2 conjugates were eventually eluted with one bead volume of 5% SDS and 1 mM Flag M2 epitope peptide in wash buffer.

Purification of His-SUMO conjugates

U2OS cells stably expressing His-SUMO-2 were rinsed with and collected in icecold PBS. To prepare input samples, small aliquots of cells were lysed in 1x LDS sample buffer. For cell lysis, Guanidinium lysis buffer (6 M guanidinium-HCl, 0.1 M Na₂HPO₄/NaH₂PO₄, 0.01 M Tris/HCl, pH 8.0 and competing imidazole) was added to the cell pellet, followed by sonication to reduce the viscosity. The protein concentration of these lysates was subsequently determined using the BCA kit to equalize the samples. The His-SUMO-2 conjugates were enriched on nickel-nitrilotriacetic acid-agarose beads (Qiagen), which were subjected to washing using buffers A to D. Wash buffer A: 6 M guanidinium-HCl, 0.1 M Na₂HPO₄/NaH₂PO₄, 0.01 M Tris/HCl, pH 8.0, 10 mM β-mercaptoethanol, 0.3% Triton X-100. Wash buffer B: 8 M urea, 0.1 M Na₂HPO₄/NaH₂PO₄, 0.01 M Tris/HCl, pH 8.0, 10 mM β-mercaptoethanol, 0.3% Triton X-100. Wash buffer C: 8 M urea, 0.1 M Na₂HPO₄/NaH₂PO₄, 0.01 M Tris/HCl, pH 6.3, 10 mM β-mercaptoethanol, 0.3% Triton X-100. Wash buffer D: 8 M urea, 0.1 M Na₂HPO₄/NaH₂PO₄, 0.01 M Tris/HCl, pH 6.3, 10 mM β-mercaptoethanol, 0.1% Triton X-100. Eventually, samples were eluted in 7 M urea, 0.1 M Na₂HPO₄/NaH₂PO₄, 0.01 M Tris/HCl, pH 7.0, 500 mM imidazole.

GFP-IP

U2OS cells transiently expressing GFP, GFP-RSF1 wt or the 21KR mutant were either mock treated or exposed to 4 Gy of IR and incubated at 37°C for 1 h. Cells were trypsinized and washed in ice-cold PBS, followed by lysis in EBC buffer (50 mM Tris (pH 7.5), 150 mM NaCl, 0.5% NP-40, 1 mM EDTA, 5 mM 1,10-phenanthroline protease inhibitor including EDTA (Roche; 1 tablet per 10 ml buffer)) with 500 Units/ml Benzonase. Cell lysates were centrifuged for 10 min at full speed and cleared lysates were transferred to new tubes. For input sample preparation, 50 µl samples were transferred to new tubes and boiled in 2x Laemmli buffer at 95°C. Equal amounts of GFP Trap beads (Chromotek) were added to cleared lysates for immunoprecipitation and incubated on a rotator for 1,5 h. Beads were subjected to 5 washing steps with EBC buffer [300mM NaCl] and eventually boiled in 2x Laemmli buffer at 95°C.

Antibodies

Western blot analysis was performed using antibodies against RSF1 (1:10, #m38B5, provided by Marinela Perpelescu and Kinya Yoda (Perpelescu et al., 2009)), SUMO-2/3 (1:1000, as previously described produced by A.C. Vertegaal in collaboration with Eurogentec (Vertegaal et al., 2004)), GFP (1:5000, #290, Abcam). Immunofluorescence analysis was performed using antibodies against γH2AX (1:1000-2000, #07-164, Millipore) and XRCC4 (1:500, provided by Mauro Modesti and Dik van Gent (Mari et al., 2006; Modesti et al., 1999)).

Laser micro-irradiation

For multiphoton or UV-A laser micro-irradiation, the media of U2OS cells grown on 18 mm glass coverslips was replaced with CO₂-independent Leibovitz L15 medium complemented with 10% FCS and 1% penicillin/streptomycin. Next, cells were placed in a Chamlide TC-A live-cell imaging chamber and were kept at 37°C during imaging. The multiphoton laser was implemented on a Leica SP5 confocal microscope to which an environmental chamber set to 37°C was fitted as had been described before (Helfricht et al., 2013). Briefly, DSB-containing tracks (1.5 μm width) were generated with a Mira modelocked Ti:Sapphire laser ($\lambda = 800$ nm, pulselength = 200 fs, repetition rate = 76 MHz, output power = 80 mW). Using LAS-AF software, cells were micro-irradiated with 1 iteration per pixel and images were recorded before and after laser irradiation until 180 sec. UV-A laser micro-irradiation was performed after sensitization of cells with 10 μM 5'-bromo-2-deoxyuridine (BrdU) for 24 h, as described (ref). A Leica DM IRBE widefield microscope stand (Leica) with an integrated pulsed nitrogen laser (Micropoint Ablation Laser System; Photonic Instruments, Inc) was used for DNA-damage induction. The pulsed nitrogen laser (16 Hz, 364 nm) was thereby directly coupled to the epifluorescence path of the microscope and focused through a Leica 40× HCX PLAN APO 1.25–0.75 oil-immersion objective. To strictly induce localized sub-nuclear DNA damage, the laser output power was set to 78 and 2 iterations per pixel were applied with the Andor software. Cells were incubated for 10 minutes at 37 °C and subsequently fixed with 4% formaldehyde before immunostaining.

Immunofluorescent labeling

Immunostaining of cells for γ H2AX and XRCC4 was performed as described previously (Helfricht et al., 2013). Briefly, cells were grown on glass coverslips and treated as indicated in the figure legends. Consequently, cells were washed with PBS, fixed with 4% formaldehyde for 10 min and treated with 0.1% Triton X-100 in PBS for 5 min. Cells were rinsed with PBS and equilibrated in PBS containing BSA [5 g/l] and glycine [1.5 g/l] prior to immunostaining. Detection was made possible through the use of goat anti-mouse or goat anti-rabbit IgG coupled to Alexa 555 or 647 (Invitrogen Molecular probes). Samples were incubated with DAPI [0.1 μg/ml] and mounted using Polymount (Polysciences, Inc.).

Microscopy analysis

A Zeiss AxioImager M2 widefield fluorescence microscope was used for image acquisition of fixed samples. The microscope was equipped with 40×, 63×, and 100× PLAN APO (1.4 NA) oil-immersion objectives (Zeiss) and an HXP 120 metal-halide lamp used for excitation, as well as ZEN software (2012). The fluorescent probes could be detected using the following filters: DAPI (excitation filter: 350/50 nm, dichroic mirror: 400 nm, emission filter: 460/50 nm), GFP/Alexa 488 (excitation filter: 470/40 nm, dichroic mirror: 495 nm, emission filter: 525/50 nm), mCherry (excitation filter: 560/40 nm, dichroic mirror: 585 nm, emission filter: 630/75 nm), Alexa 555 (excitation filter: 545/25 nm, dichroic mirror: 565 nm, emission filter: 605/70 nm), Alexa 647 (excitation filter: 640/30 nm, dichroic mirror: 660 nm, emission filter: 690/50 nm).

REFERENCES

1. Bekker-Jensen,S, Rendtew,D.J., Fugger,K., Gromova,I., Nerstedt,A., Lukas,C., Bartek,J., Lukas,J., and Mailand,N. (2010). HERC2 coordinates ubiquitin-dependent assembly of DNA repair factors on damaged chromosomes. *Nat. Cell Biol.* 12, 80-86.
2. Choudhary,C., Kumar,C., Gnad,F., Nielsen,M.L., Rehman,M., Walther,T.C., Olsen,J.V., and Mann,M. (2009). Lysine acetylation targets protein complexes and co-regulates major cellular functions. *Science* 325, 834-840.
3. Coppotelli,G., Mughal,N., Callegari,S., Sompallae,R., Caja,L., Luijsterburg,M.S., Dantuma,N.P., Moustakas,A., and Masucci,M.G. (2013). The Epstein-Barr virus nuclear antigen-1 reprograms transcription by mimicry of high mobility group A proteins. *Nucleic Acids Res.* 41, 2950-2962.
4. Danielsen,J.R., Povlsen,L.K., Villumsen,B.H., Streicher,W., Nilsson,J., Wikstrom,M., Bekker-Jensen,S., and Mailand,N. (2012). DNA damage-inducible SUMOylation of HERC2 promotes RNF8 binding via a novel SUMO-binding Zinc finger. *J. Cell Biol.* 197, 179-187.
5. Flotho,A. and Melchior,F. (2013). Sumoylation: a regulatory protein modification in health and disease. *Annu. Rev. Biochem.* 82, 357-385.
6. Galanty,Y., Belotserkovskaya,R., Coates,J., Polo,S., Miller,K.M., and Jackson,S.P. (2009). Mammalian SUMO E3-ligases PIAS1 and PIAS4 promote responses to DNA double-strand breaks. *Nature* 462, 935-939.
7. Girard,P.M., Kysela,B., Harer,C.J., Doherty,A.J., and Jeggo,P.A. (2004). Analysis of DNA ligase IV mutations found in LIG4 syndrome patients: the impact of two linked polymorphisms. *Hum. Mol. Genet.* 13, 2369-2376.
8. Helfricht,A., Wiegant,W.W., Thijssen,P.E., Versteeg,A.C., Luijsterburg,M.S., and van Attikum,H. (2013). Remodeling and spacing factor 1 (RSF1) deposits centromere proteins at DNA double-strand breaks to promote non-homologous end-joining. *Cell Cycle* 12, 3070-3082.
9. Hendriks,I.A., D'Souza,R.C., Yang,B., Verlaan-de,V.M., Mann,M., and Versteeg,A.C. (2014). Uncovering global SUMOylation signaling networks in a site-specific manner. *Nat. Struct. Mol. Biol.* 21, 927-936.
10. Hendriks,I.A., Treffers,L.W., Verlaan-de,V.M., Olsen,J.V., and Versteeg,A.C. (2015). SUMO-2 Orchestrates Chromatin Modifiers in Response to DNA Damage. *Cell Rep.*
11. Hu,X., Paul,A., and Wang,B. (2012). Rap80 protein recruitment to DNA double-strand breaks requires binding to both small ubiquitin-like modifier (SUMO) and ubiquitin conjugates. *J. Biol. Chem.* 287, 25510-25519.
12. Jackson,S.P. and Durocher,D. (2013). Regulation of DNA damage responses by ubiquitin and SUMO. *Mol. Cell* 49, 795-807.
13. Jentsch,S. and Psakhye,I. (2013). Control of nuclear activities by substrate-selective and protein-group SUMOylation. *Annu. Rev. Genet.* 47, 167-186.
14. Lan,L., Ui,A., Nakajima,S., Hatakeyama,K., Hoshi,M., Watanabe,R., Janicki,S.M., Ogiwara,H., Kohno,T., Kanno,S., and Yasui,A. (2010). The ACF1 complex is required for DNA double-strand break repair in human cells. *Mol. Cell* 40, 976-987.
15. Luijsterburg,M.S., Acs,K., Ackermann,L., Wiegant,W.W., Bekker-Jensen,S., Larsen,D.H., Khanna,K.K., van Attikum,H., Mailand,N., and Dantuma,N.P. (2012). A new non-catalytic role for ubiquitin ligase RNF8 in unfolding higher-order chromatin structure. *EMBO J.* 31, 2511-2527.
16. Luo,K., Zhang,H., Wang,L., Yuan,J., and Lou,Z. (2012). Sumoylation of MDC1 is important for proper DNA damage response. *EMBO J.* 31, 3008-3019.
17. Mari,P.O., Florea,B.I., Persengiev,S.P., Verkaik,N.S., Bruggenwirth,H.T., Modesti,M., Giglia-Mari,G., Bezstarosti,K., Demmers,J.A., Luider,T.M., Houtsmuller,A.B., and van Gent,D.C. (2006). Dynamic assembly of end-joining complexes requires interaction between Ku70/80 and XRCC4. *Proc. Natl. Acad. Sci. U. S. A.* 103, 18597-18602.
18. Matic,I., Schimmel,J., Hendriks,I.A., van Santen,M.A., van de Rijke,F., van,D.H., Gnad,F., Mann,M., and Versteeg,A.C. (2010). Site-specific identification of SUMO-2 targets in cells reveals an inverted SUMOylation motif and a hydrophobic cluster SUMOylation motif. *Mol. Cell* 39, 641-652.
19. Matsuoka,S., Ballif,B.A., Smogorzewska,A., McDonald,E.R., Hurov,K.E., Luo,J., Bakalarski,C.E., Zhao,Z., Solimini,N., Lerenthal,Y., Shiloh,Y., Gygi,S.P., and Elledge,S.J. (2007). ATM and ATR substrate analysis reveals extensive protein networks responsive to DNA damage. *Science* 316, 1160-1166.
20. Min,S., Jo,S., Lee,H.S., Chae,S., Lee,J.S., Ji,J.H., and Cho,H. (2014). ATM-dependent chromatin remodeler Rsf-1 facilitates DNA damage checkpoints and homologous recombination repair. *Cell Cycle* 13, 666-677.
21. Modesti,M., Hesse,J.E., and Gellert,M. (1999). DNA binding of Xrcc4 protein is associated with V(D)J recombination but not with stimulation of DNA ligase IV activity. *EMBO J.* 18, 2008-2018.
22. Morris,J.R., Boutell,C., Keppler,M., Densham,R., Weekes,D., Alamshah,A., Butler,L., Galanty,Y., Pangon,L., Kiuchi,T., Ng,T., and Solomon,E. (2009). The SUMO modification pathway is involved in the BRCA1 response to genotoxic stress. *Nature* 462, 886-890.
23. Perpelescu,M., Nozaki,N., Obuse,C., Yang,H., and Yoda,K. (2009). Active establishment of centromeric CENP-A chromatin by RSF complex. *J. Cell Biol.* 185, 397-407.
24. Pessina,F. and Lowndes,N.F. (2014). The RSF1 histone-remodelling factor facilitates DNA double-strand break repair by

- recruiting centromeric and Fanconi Anaemia proteins. *PLoS. Biol.* 12, e1001856.
25. Psakhye,I. and Jentsch,S. (2012). Protein group modification and synergy in the SUMO pathway as exemplified in DNA repair. *Cell* 151, 807-820.
 26. Sacher,M., Pfander,B., Hoege,C., and Jentsch,S. (2006). Control of Rad52 recombination activity by double-strand break-induced SUMO modification. *Nat. Cell Biol.* 8, 1284-1290.
 27. Saitoh,H. and Hinchev,J. (2000). Functional heterogeneity of small ubiquitin-related protein modifiers SUMO-1 versus SUMO-2/3. *J. Biol. Chem.* 275, 6252-6258.
 28. Schimmel,J., Eifler,K., Sigurethsson,J.O., Cuijpers,S.A., Hendriks,I.A., Verlaan-de,V.M., Kelstrup,C.D., Francavilla,C., Medema,R.H., Olsen,J.V., and Vertegaal,A.C. (2014). Uncovering SUMOylation dynamics during cell-cycle progression reveals FoxM1 as a key mitotic SUMO target protein. *Mol. Cell* 53, 1053-1066.
 29. Shanbhag,N.M., Rafalska-Metcalf,I.U., Balane-Bolivar,C., Janicki,S.M., and Greenberg,R.A. (2010). ATM-dependent chromatin changes silence transcription in cis to DNA double-strand breaks. *Cell* 141, 970-981.
 30. Sheu,J.J., Guan,B., Choi,J.H., Lin,A., Lee,C.H., Hsiao,Y.T., Wang,T.L., Tsai,F.J., and Shih,I. (2010). Rsf-1, a chromatin remodeling protein, induces DNA damage and promotes genomic instability. *J. Biol. Chem.* 285, 38260-38269.
 31. Silver,H.R., Nissley,J.A., Reed,S.H., Hou,Y.M., and Johnson,E.S. (2011). A role for SUMO in nucleotide excision repair. *DNA Repair (Amst)* 10, 1243-1251.
 32. Smeenk,G., Wiegant,W.W., Marteiijn,J.A., Luijsterburg,M.S., Sroczynski,N., Costelloe,T., Romeijn,R.J., Pastink,A., Mailand,N., Vermeulen,W., and van Attikum,H. (2013). Poly(ADP-ribosyl)ation links the chromatin remodeler SMARCA5/SNF2H to RNF168-dependent DNA damage signaling. *J. Cell Sci.* 126, 889-903.
 33. Song,J., Durrin,L.K., Wilkinson,T.A., Krontiris,T.G., and Chen,Y. (2004). Identification of a SUMO-binding motif that recognizes SUMO-modified proteins. *Proc. Natl. Acad. Sci. U. S. A* 101, 14373-14378.
 34. Soutoglou,E. and Misteli,T. (2008). Activation of the cellular DNA damage response in the absence of DNA lesions. *Science* 320, 1507-1510.
 35. Strauss,C. and Goldberg,M. (2011). Recruitment of proteins to DNA double-strand breaks: MDC1 directly recruits RAP80. *Cell Cycle* 10, 2850-2857.
 36. Strauss,C., Halevy,T., Macarov,M., Argaman,L., and Goldberg,M. (2011). MDC1 is ubiquitylated on its tandem BRCT domain and directly binds RAP80 in a UBC13-dependent manner. *DNA Repair (Amst)* 10, 806-814.
 37. Vertegaal,A.C., Ogg,S.C., Jaffray,E., Rodriguez,M.S., Hay,R.T., Andersen,J.S., Mann,M., and Lamond,A.I. (2004). A proteomic study of SUMO-2 target proteins. *J. Biol. Chem.* 279, 33791-33798.



SUPPLEMENTAL INFORMATION

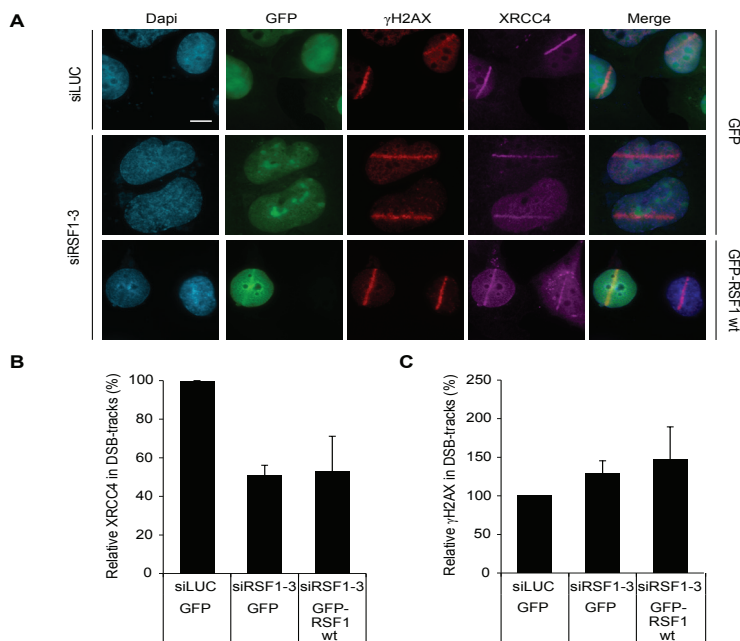
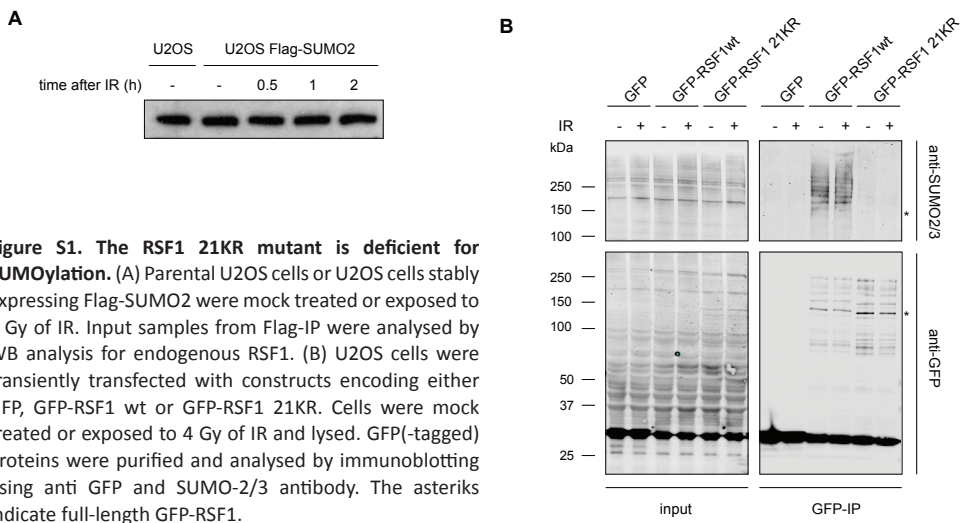


Table S1. List of SUMO target sites mutated in RSF1 21KR. (A) Listed are identified SUMO target sites and additional inverted motifs, (¹Hendriks et al., 2014). Blue: Lysine fitting the Phosphorylation-dependent SUMOylation motif (PDSM) [KxE_x(pS)P], Red: SUMO acceptor lysine not belonging to glutamate (E)-containing SUMO consensus motifs. (B) Listed are SIMs in the amino acid (aa) sequence of RSF1 predicted by the GPS-SUMO tool.

Nr.	SUMO sites ¹	
	Lysine position	aa sequence
1	K243	EETPKQEEQ
2	K254	SEKMKSEEQ
3	K277	ETTVKKEKE
4	K280	VKKEKEDEK
5	K294	PVICKLEKP
6	K306	NEEKIIKE
7	K309	KKIIKEESD
8	K323	VKPIKVEVK
9	K337	PKDTKSSM
10	K358	GGNIKSSHE
11	K390	KREIKLSDD
12	K415	KEFLKDEIK
13	K419	KDEIKQEEE
14	K456	APNFKTEPI
15	K463	PIETKFYET
16	K468	FYETKEESY
17	K565	SCTMKGEEK
18	K670	LETLKEDSE
19	K677	SEFTKVEMD
20	K758	EPENKQEK
21	K768	KEEKTNVG

PDSM ≠ ExK or KxE

Table S2. List of described phosphorylation and acetylation target sites found in RSF1.

www.phosphosite.org.

Yellow: ATM-/ATR phosphorylation target sites (¹Matsuoka et al., 2007, ²Choudhary et al., 2009).

Nr.	Phosphorylation sites ¹	Acetylation sites ²
	erine/Threonine position	Lysine position
1	S392	K1050
2	S397	K1339
3	T408	
4	S473	
5	S524	
6	S570	
7	S604	
8	S622	
9	S629	
10	S748	
11	S1221	
12	S1223	
13	S1226	
14	S1245	
15	S1277	
16	T1278	
17	Y1281	
18	S1282	
19	T1305	
20	S1310	
21	S1325	
22	S1345	
23	S1359	
24	S1375	

ATM-/ATR-target sites





LOSS OF ZBTB24, A NOVEL NON-
HOMOLOGOUS END-JOINING PROTEIN,
IMPAIRS CLASS-SWITCH RECOMBINATION IN
ICF SYNDROME

IN PREPARATION FOR PUBLICATION

5

Angela Helfricht^{1,#}, Peter E. Thijssen^{1,#}, Hanna IJspeert², Rashmi G. Shah³, Chantal Stoeperker¹, Monique M. van Ostaijen-ten Dam⁴, Martijn S. Luijsterburg¹, Anton de Groot¹, Rianca Jak¹, Gwendolynn Grootaers¹, Jun Wang^{1,‡}, Pooja Rao⁵, Alfred C.O. Vertegaal⁶, Maarten J.D. van Tol⁴, Qiang Pan-Hammarström⁷, Girish M. Shah³, Mirjam van der Burg², Silvère M. van der Maarel¹ and Haico van Attikum¹

¹ Department of Human Genetics, Leiden University Medical Center

² Department of Immunology, Erasmus Medical Center Rotterdam

³ CHU de Québec Research Centre (site CHUL), and Université Laval, Laboratory for Skin Cancer Research and Axe Neuroscience, Québec (QC), Canada

⁴ Laboratory for Immunology, Department of Pediatrics, Leiden University Medical Center

⁵ ServiceXS B.V., Leiden

⁶ Department of Molecular Cell Biology, Leiden University Medical Center

⁷ Department of Laboratory Medicine, Karolinska Institute, Sweden

Equally contributing authors

ABSTRACT

The autosomal recessive immunodeficiency, centromeric instability and facial anomalies (ICF) syndrome is a genetically heterogeneous disorder. Despite recent successes in the identification of the underlying gene defects, it is currently unclear how mutations in any of the four known ICF genes cause a primary immunodeficiency. Here we demonstrate that loss of ZBTB24 in B cells from ICF2 patients impairs non-homologous end-joining (NHEJ) during immunoglobulin class-switch recombination and consequently impairs immunoglobulin production and subtype balance. Mechanistically, we found that ZBTB24 associates with poly(ADP-ribose) polymerase 1 (PARP1) and stimulates auto-poly(ADP-ribosylation) of this enzyme. The zinc finger in ZBTB24 binds PARP1-associated poly(ADP-ribose) chains and mediates the PARP1-dependent recruitment of ZBTB24 to DNA breaks. Moreover, by binding to poly(ADP-ribose) chains ZBTB24 protects these moieties from degradation by poly(ADP-ribose) glycohydrolase (PARG). This enhances the poly(ADP-ribose)-dependent interaction between PARP1 and the LIG4/XRCC4 NHEJ complex and promotes NHEJ by facilitating the assembly of this repair complex at DNA breaks. Thus, we uncover ZBTB24 as a regulator of PARP1-dependent NHEJ and class-switch recombination, providing a molecular basis for the immunodeficiency in ICF syndrome.

INTRODUCTION

Immunodeficiency with centromeric instability and facial anomalies (ICF) syndrome (OMIM 242860; 614069) is a rare autosomal recessive disorder characterized by a triad of phenotypes (Hagleitner et al. 2008; Weemaes et al. 2013). Patients suffer from a variable immunodeficiency, mainly characterized by hypo- or agammaglobulinemia in the presence of B cells, resulting in recurrent and often fatal respiratory and gastrointestinal infections. Furthermore, patients often present with a distinct set of facial anomalies, including a flat nasal bridge, hypertelorism and epicanthal folds. The cytogenetic hallmark of the disease is centromeric instability, specifically at chromosomes 1, 9 and 16, which is associated with CpG hypomethylation of the pericentromeric satellite II and III repeats.

ICF syndrome is genetically heterogeneous and can be subdivided into five different groups (ICF1-4 and ICFX) based on the genetic defect underlying the phenotype (Weemaes et al. 2013; Thijssen et al. 2015). ICF1 patients, comprising approximately 50% of the total patient population, carry mutations in the de novo DNA methyltransferase 3B gene (DNMT3B, ICF1) (Hansen et al. 1999; Xu et al. 1999). Around 30% of the cases carry mutations in the Zinc finger and BTB (bric-a-bric, tramtrack, broad complex) containing 24 gene (ZBTB24, ICF2) (de Greef et al. 2011; Chouery et al. 2012; Nitta et al. 2013). Recently, mutations in the cell division cycle-associated protein 7 (CDCA7, ICF3) or helicase, lymphoid-specific (HELLS, ICF4) were reported in ten patients (~20% of the total patient population), leaving only few cases genetically unaccounted for (ICFX) (Thijssen et al. 2015). Remarkably, however, while the genetic defects underlying ICF syndrome have been largely elucidated, it remains largely unclear how these defects lead to ICF syndrome, in particular the associated life-threatening immunodeficiency.

Interestingly, the number of circulating B-lymphocytes in ICF patients is normal, but a lack of switched memory B cells and an increased proportion of immature B cells have been reported (Blanco-Betancourt et al. 2004), suggesting a defect in the final stages of B-cell differentiation. A key step in B-cell maturation is isotype switching of immunoglobulins (Ig) through class-switch recombination (CSR). Effective CSR heavily relies on the controlled formation and correct repair of DNA double-strand breaks (DSB) induced by Activation-Induced (Cytidine) Deaminase (AID) at conserved motifs within the switch (S) regions, which are upstream from gene segments that encode distinct constant regions of antibody heavy chains (Alt et al. 2013). Upon break formation, two switch regions are rejoined by non-homologous end-joining (NHEJ), the main cellular pathway to repair DSBs (Alt et al. 2013). This leads to loss of the intervening DNA between the S regions, removal of μ and δ heavy chain constant regions, substitution by a γ , α or ϵ constant region, and consequently a change in the class of immunoglobulins that is expressed by a B cell.

NHEJ is carried out by the concerted action of the DNA-dependent protein-kinase complex (DNA-PK), comprised of the KU70/KU80 heterodimer and the DNA-PK catalytic subunit (DNA-PKcs), and the downstream effector proteins X-ray repair cross-complementing protein 4 (XRCC4), DNA ligase 4 (LIG4) and non-homologous end-joining factor 1 (NHEJ1) (Alt et al. 2013). In the absence of this classical (c-)NHEJ mechanism, effective CSR is significantly impaired but not absent, as DSB repair is carried out by alternative NHEJ (a-NHEJ). a-NHEJ is a poorly characterized process dependent on poly(ADP-ribose) polymerase 1 (PARP1), X-ray repair cross-complementing protein 1 (XRCC1) and DNA ligase 1 and 3 (LIG1 and LIG3) (Audebert et al. 2004; Paul et al. 2013; Lu et al. 2016).

Mutations in NHEJ genes (e.g. DNA-PKcs and LIG4) are increasingly recognized as the

primary cause of immunodeficiency in patients (Woodbine et al. 2014). Considering the similarities between the immunodeficiency in ICF patients and individuals with defective NHEJ, this raises the question as to whether loss of NHEJ might explain the compromised immune system in ICF patients. Here we demonstrate that ICF2 patient-derived B cells are defective in NHEJ during CSR. Mechanistically, we uncover a regulatory function for ZBTB24 in NHEJ by cooperating with PARP1 and XRCC4/LIG4 during this repair process. This provides a molecular basis for the humoral immunodeficiency in ICF2 patients.

RESULTS

ICF2 patients display features of defective CSR

The immunodeficiency in ICF2 syndrome is characterized by a reduction or even an absence of immunoglobulins (Igs) (hypo- or agammaglobulinemia) and decreased numbers of switched memory B cells, while normal levels of total B cells are observed (de Greef et al. 2011; Weemaes et al. 2013). We corroborated these findings by showing hypogammaglobulinemia in sera of three independent ICF2 patients, but normal serum levels in age-matched controls (Table S1). Moreover, we characterized peripheral blood lymphocytes by immunophenotyping and found a decrease in the number of switched memory B cells, while numbers of total B cells, naive B cells and unswitched memory B cells were unaffected (Fig. 1A). Of note, total numbers of CD4+ T cells, as well as naive, central memory and CD27+CD28+ early antigen experienced CD4+ T cells were increased when compared to age-matched controls, while those for CD8+ T cells were normal (Fig. S1).

These findings could suggest a defect in V(D)J recombination or class-switch recombination (CSR), which are processes that are critical for B-cell development and ultimately define antibody production and diversification. We therefore first examined the combinatorial diversity of VDJ usage and composition of the junctional region during V(D)J recombination by sequencing immunoglobulin heavy chain gene rearrangements in B cells derived from peripheral blood mono-nuclear cells (PBMCs) of the three ICF2 patients. However, the usage of V, D and J gene segments, as well as the composition of the junctional regions, meaning the number of nucleotide deletions and insertions of non-templated nucleotides by terminal deoxynucleotidyl transferase (TdT) (N-nucleotides), in these patients resembled that of controls (Fig. S2). This suggests that ICF2 patients do not suffer from major defects in V(D)J recombination.

To examine CSR defects in these ICF2 patients, we tested whether patient-derived B cells can undergo CSR *in vitro*, by stimulating PBMCs in cell culture and measuring the production of total IgA and IgG. For all patients analyzed, the capacity to produce IgA and IgG *in vitro* was significantly impaired compared to healthy controls (Fig. 1B). We then analyzed the relative abundance of IgG subclasses through RNA sequence analysis of IgH transcripts in the patient-derived PBMCs (Fig. 1C). When comparing relative abundance of IgG1-4 to age-matched controls, we observed a decrease in the relative expression of IgG1, accompanied by an increase in relative IgG3 expression in ICF2 patients (Fig. 1D). Together, these data show that the absence or reduction of Igs in combination with changes in the relative abundance of Ig subclasses in ICF2 patients is most likely caused by impaired CSR.

Loss of ZBTB24 resembles NHEJ-deficiency in CSR

CSR heavily relies on the c-NHEJ-mediated repair of AID-induced DSBs upstream of the

constant regions of the IgH locus (Alt et al. 2013). To study the functional consequences of ZBTB24 mutations in the repair of DSBs during CSR, a PCR-based assay for amplification of $\Sigma\mu$ - $\Sigma\alpha$ junctions (located upstream of the Cm and Ca regions of the IgH locus, respectively; Fig. 1C) was performed on the ICF2-patient cells. Twelve $\Sigma\mu$ - $\Sigma\alpha$ junctions from the patients were then compared to our previously published 183 $\Sigma\mu$ - $\Sigma\alpha$ junctions from healthy children controls (Du et al. 2008; Enervald et al. 2013). The junctions from the ICF2-deficient patients showed an altered repair pattern with an increased usage of long (7-9bp) microhomologies (33% vs. 10% in controls, χ^2 test, $p=0.035$, Table 1), suggesting a shift to the use of an alternative end-joining pathway in the cells from the patients. A similar shift is also apparent in NHEJ-deficient cells from patients with mutations in Artemis or LIG4 (Table 1), suggesting that the shift to alternative repair may be due to a defect in NHEJ. Furthermore, 11 $\Sigma\mu$ - $\Sigma\gamma$ junctions (located upstream of the Cm and Cg regions of the IgH locus, respectively; Fig. 1C) were isolated from the ICF2-deficient cells and compared to our previously published 58 $\Sigma\mu$ - $\Sigma\gamma$ junctions from healthy children controls (Du et al. 2008). Although the repair pattern at the $\Sigma\mu$ - $\Sigma\gamma$ junctions were largely normal (Table 1), one $\Sigma\mu$ - $\Sigma\gamma$ junction showed a “footprint”

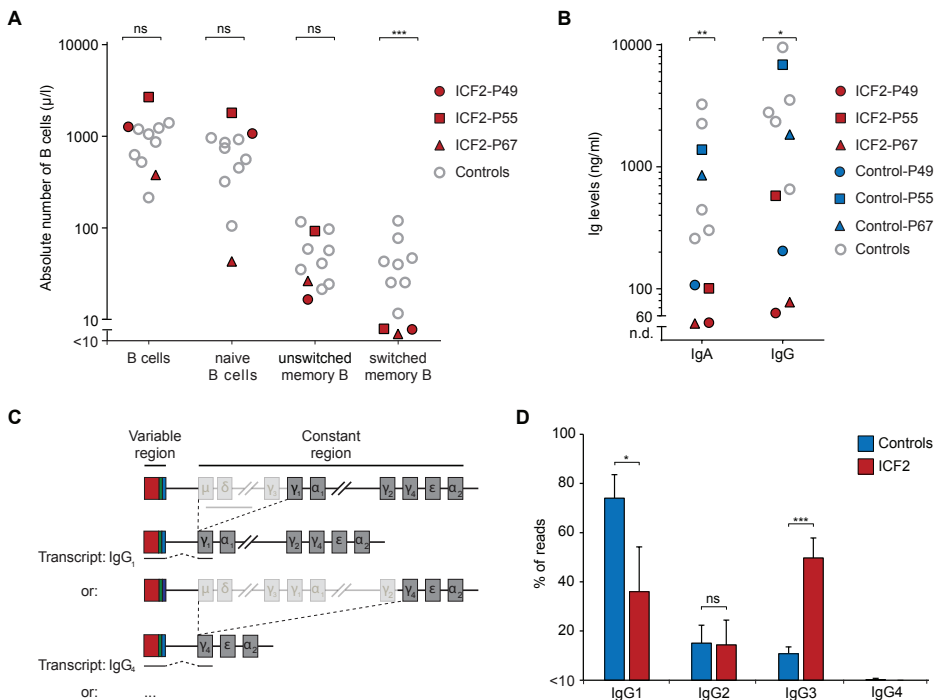


Figure 1. Defective CSR in ICF2 patients due to loss of ZBTB24-dependent NHEJ. (A) Number of cells within the indicated differentiation stages of the total peripheral blood CD19+/CD20+ B-cell population was measured by flow cytometry. Naive B cells: IgMdull, IgD++, CD27-; unswitched memory B cells: IgM+, IgDdull, CD27+; switched memory B cells: IgM-, IgD-, CD27+. Closed red symbols are the ICF2 patients P49, P55 and P67. Open grey circles represent 8 healthy age-matched controls (age range 0.8 to 4.3 years). (B) PBMC were stimulated with aCD40L, algM, CpG and IL-21. After 7 days IgG and IgA concentrations were determined by ELISA assays. Respective controls for the ICF patients P49, P55 and P67 (red symbols) are a healthy brother, a father and a mother (blue symbols). Open grey circles represent 5 unrelated adult controls. PBMC of patients at the age of 0.9, 0.8 and 3.6 years were used. n.d.: not detectable. (C) Schematic representation of the IgH locus with a rearranged VDJ exon (variable domain) and the constant regions. Switching to IgG1 and IgG4 is depicted. (D) Frequency of IgG subclass usage with unique switched IGG transcripts in ICF2 patients and controls.

Table 1: Characterization of CSR junctions^a

Study subjects	Perfectly matched short homology						No. of junctions
	0 bp		1-3 bp	4-6 bp	7-9 bp	≥ 10 bp	
	Direct end-joining	Small insertions					
<i>Sμ-Sα</i>							
ICF2-deficient	1 (8%)	0 (0%)	3 (25%)	3 (25%)	5 (42%)**↑	0 (0%)	12
Lig4-deficient ^b	1 (3%)	0 (0%)**↓	7 (23%)	4 (13%)	4 (13%)	14 (47%)***↑	30
Artemis-deficient ^c	0 (0%)	6 (11%)	10 (19%)	8 (15%)	9 (17%)	21 (39%)***↑	54
Controls (1-13 years) ^d	31 (17%)	42 (23%)	36 (20%)	29 (16%)	19 (10%)	26 (14%)	183
<i>Sμ-Sγ</i>							
ICF2-deficient	4 (36%)	0 (0%)	7 (64%)	0 (0%)	0 (0%)	0 (0%)	11
Lig4-deficient ^b	4 (12%)	11 (32%)	15 (44%)	4 (12%)	0 (0%)	0 (0%)	34
Artemis-deficient ^c	5 (21%)	4 (17%)	14 (58%)	1 (4%)	0 (0%)	0 (0%)	24
Controls (1-6 years) ^e	13 (22%)	9 (16%)	26 (45%)	10 (17%)	0 (0%)	0 (0%)	58

- a. Statistical analysis was performed by χ^2 test and significant changes are indicated in bold. * $p < 0.05$, ** $p < 0.01$, *** $p < 0.001$
- b. Previously published CSR junctions from Lig4-deficient patients (Pan-Hammarström et al., 2005)
- c. Previously published CSR junctions from Artemis-deficient patients (Du et al., 2008)
- d. Previously published *Sμ-Sα* junctions from children controls (Du et al., 2008; Enervald et al., 2013)
- e. Previously published *Sμ-Sγ* junctions from children controls (Du et al., 2008)

of sequential switching (Sm-Sg3-Sg2; 9%), which is rarely observed in controls (2%), but frequently seen in NHEJ-defective cells such as Artemis- or DNA-PKcs-deficient cells (Du et al. 2008; Bjorkman et al. 2015). Thus, the altered CSR patterns in ICF2 patient cells and their resemblance to those observed in several known NHEJ-deficient patients suggest that ZBTB24 might be a novel NHEJ factor involved in CSR.

ZBTB24 promotes DSB repair via classical NHEJ

To assess whether ZBTB24 is involved in NHEJ, which is the dominant pathway for the repair of DSBs in mammalian cells, we made use of the well-established HEK293T EJ5-GFP reporter cell line. This reporter contains a GFP expression cassette in which the promoter is separated from the GFP gene by a puromycin-resistance gene that is flanked by I-SceI recognition sequences. Following expression of I-SceI endonuclease, repair of the ensuing DSBs will occur through NHEJ and restore GFP expression, which can be used as a measure of NHEJ efficiency (Fig. 2A) (Bennardo et al. 2008). Strikingly, depletion of ZBTB24 by different siRNAs resulted in a marked decrease in NHEJ, which was comparable to the impact of depleting XRCC4 (Fig. 2B-C). Cell cycle profiles remained unaffected in these cells, ruling out effects of cell cycle misregulation (Fig. S3A). siRNAs against ZBTB24 not only reduced expression of ZBTB24 mRNA (Fig. 2C), but also that of exogenously expressed GFP-ZBTB24 (Fig. S3B).

The two major known pathways for the end-joining-dependent repair of DSBs in

mammalian cells are c-NHEJ and a-NHEJ (Alt et al. 2013). Although the EJ5 reporter cannot differentiate between these pathways (Bennardo et al. 2008), we observed a remarkably similar phenotype following loss of ZBTB24 or the c-NHEJ factor XRCC4. Moreover, ICF2

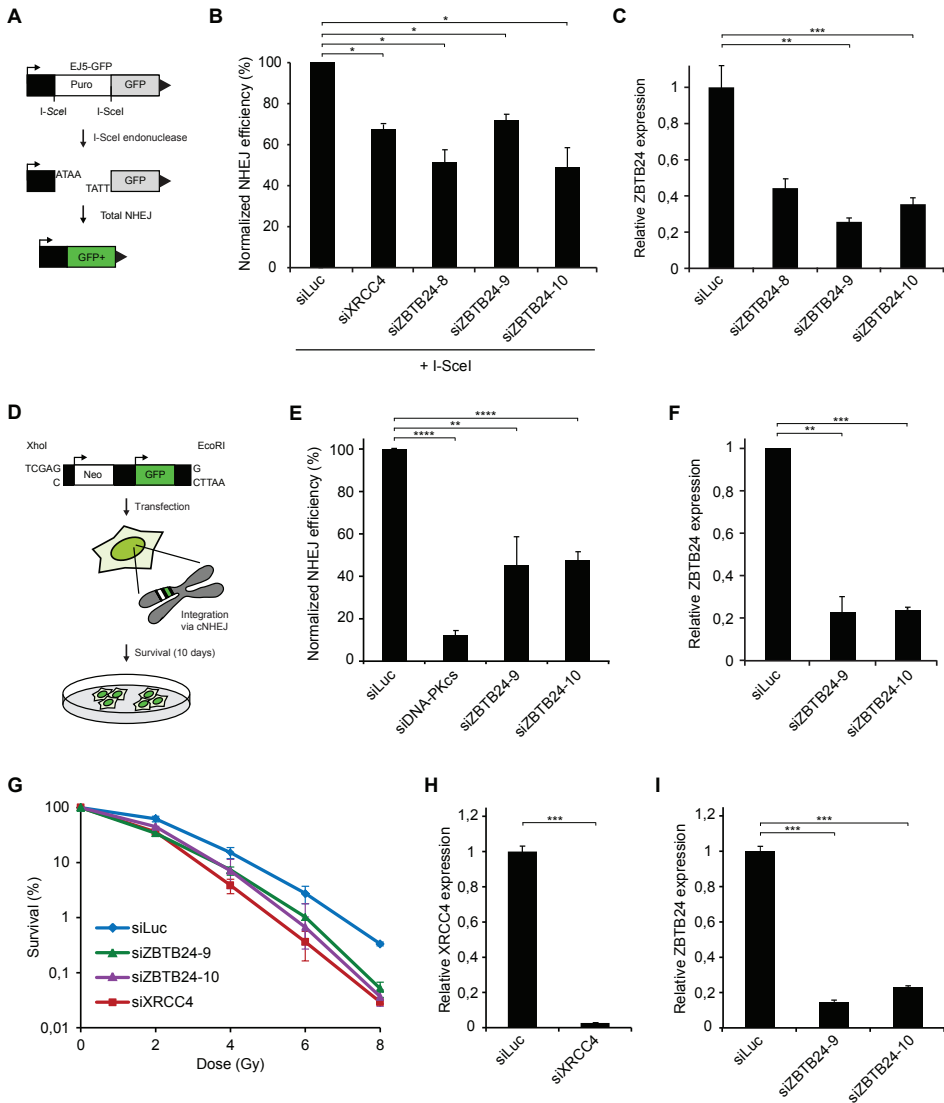


Figure 2. ZBTB24 promotes DSB repair via c-NHEJ. (A) Schematic representation of the EJ5-GFP reporter for NHEJ. (B) HEK293T EJ5-GFP cells were treated with the indicated siRNAs and 48h later co-transfected with I-SceI (pCBASe) and mCherry expression vectors. The ratio of GFP/mCherry expressing cells was counted by flow cytometry 48h later. (C) Cells from B were subjected to RNA extraction. cDNA was synthesized from total RNA samples followed by qPCR to determine the expression levels of ZBTB24. (D) Schematic of the plasmid integration assay. pEGFP-C1 plasmid containing Neo and GFP markers is linearized with the indicated restriction enzymes and transfected into U2OS cells. Stable integrants are selected on medium containing G418. GFP was used as a control for transfection efficiency. (E) Plasmid integration assays in U2OS cells transfected with indicated siRNAs. (F) As in C, except that cells from E were used. (G) Vh10-SV40 cells were treated with the indicated siRNAs for 48h, exposed to different doses of IR and scored for clonogenic survival. (H) As in C, except that cells from G were used to monitor XRCC4 expression. (I) As in C, except that cells from G were used.

patient cells showed altered CSR patterns that resembled those observed in patient cells deficient for the c-NHEJ factor LIG4 (Table 1), suggesting a role for ZBTB24 in c-NHEJ. To provide further support for this, we used a plasmid integration assay to specifically study the role of ZBTB24 in c-NHEJ. In this assay, a linearized plasmid encoding GFP and a Neomycin-selection marker is transfected into U2OS cells. Survival of G418-resistant colonies relies on the genomic integration of the linear plasmid via c-NHEJ (Fig. 2D). Depletion of DNA-PKcs (catalytic subunit of DNA-PK complex) resulted in an 80-90% decrease in cell survival, indicating the assay provides a read-out for c-NHEJ (Fig. 2E and S3C). Moreover, knockdown of ZBTB24 caused a ~50% reduction in c-NHEJ efficiency when compared to control cells (Fig. 2E-F and S3D).

To rule out that ZBTB24 regulates NHEJ indirectly through transcriptional regulation of DSB repair factors, we depleted ZBTB24 and performed whole transcriptome analysis using RNA sequencing in HEK293T cells. In total we found 158 differentially expressed genes (FDR < 0.05), of which 90 are upregulated and 68 are downregulated (Table S2). We compared the list of deregulated genes with 66 unique genes in GO-term 0006302 (DSB repair), but did not find any overlapping genes (Fig. S4). This strongly suggests that ZBTB24 does not affect NHEJ through transcription regulation of DSB repair genes.

To assess the functional relevance of ZBTB24 in NHEJ, we investigated its ability to protect cells against DNA breaks induced by ionizing radiation (IR). To this end, clonogenic survival of VH10-SV40 cells depleted for ZBTB24 or XRCC4 was determined after exposure to IR. This showed a similar dose-dependent decrease in the survival capacity of ZBTB24-depleted and XRCC4-depleted cells when compared to control cells (siLuc; Fig. 2G-I). Collectively, these results underpin the functional importance of ZBTB24 in the protection of cells against DNA breaks and implicate a role for ZBTB24 in DSB repair by NHEJ.

ZBTB24 interacts with PARP1 in a PARylation-dependent manner

To assess how ZBTB24 affects NHEJ, we aimed to identify its interaction partners using an unbiased, quantitative proteomics approach. We expressed GFP-ZBTB24 or GFP (control) in U2OS cells and performed GFP-trap-based immunoprecipitation (IP) followed by mass spectrometry (MS) after stable isotope labelling of amino acids in culture (SILAC) (Fig. 3A). Our screen identified 110 proteins that were at least four-fold enriched over control cells (Table S3). Interestingly, besides all core histones, poly(ADP-ribose) polymerase 1 (PARP1), an enzyme implicated in DNA repair, was among the potential interactors of ZBTB24 (Fig. 3A and Table S3). To explore this further, we performed the reciprocal experiment using cells expressing GFP-PARP1. This screen identified 21 proteins that were at least two-fold enriched over control cells (Table S4). Remarkably, not only did we find several known PARP1-interactors such as XRCC1, LIG3 and DNA polymerase beta (POLB) (Pines et al. 2013), also ZBTB24 was among the top hits of this screen (Fig. 3B and Table S4). To confirm the ZBTB24-PARP1 interactions, we performed co-immunoprecipitation (co-IP) experiments followed by western blot analysis. PARP1, as well as histone H3, were detected in the IP fraction of GFP-ZBTB24, whereas in the reciprocal co-IP GFP-PARP1 efficiently precipitated Myc-ZBTB24 (Fig. 3C and S5A). Control co-IP experiments using GFP-NLS expressing cells did not reveal interactions between GFP and either PARP1, H3 or Myc-ZBTB24 (Fig. 3C and S5A). We were unable to demonstrate an interaction between PARP1 and endogenous ZBTB24, because all available antibodies failed to detect ZBTB24 on western blots (data not shown). PARP1 can attach negatively charged ADP-ribose units to itself or other target proteins, forming poly(ADP)-ribose (PAR) chains through a process known as PARylation (Pines et al.

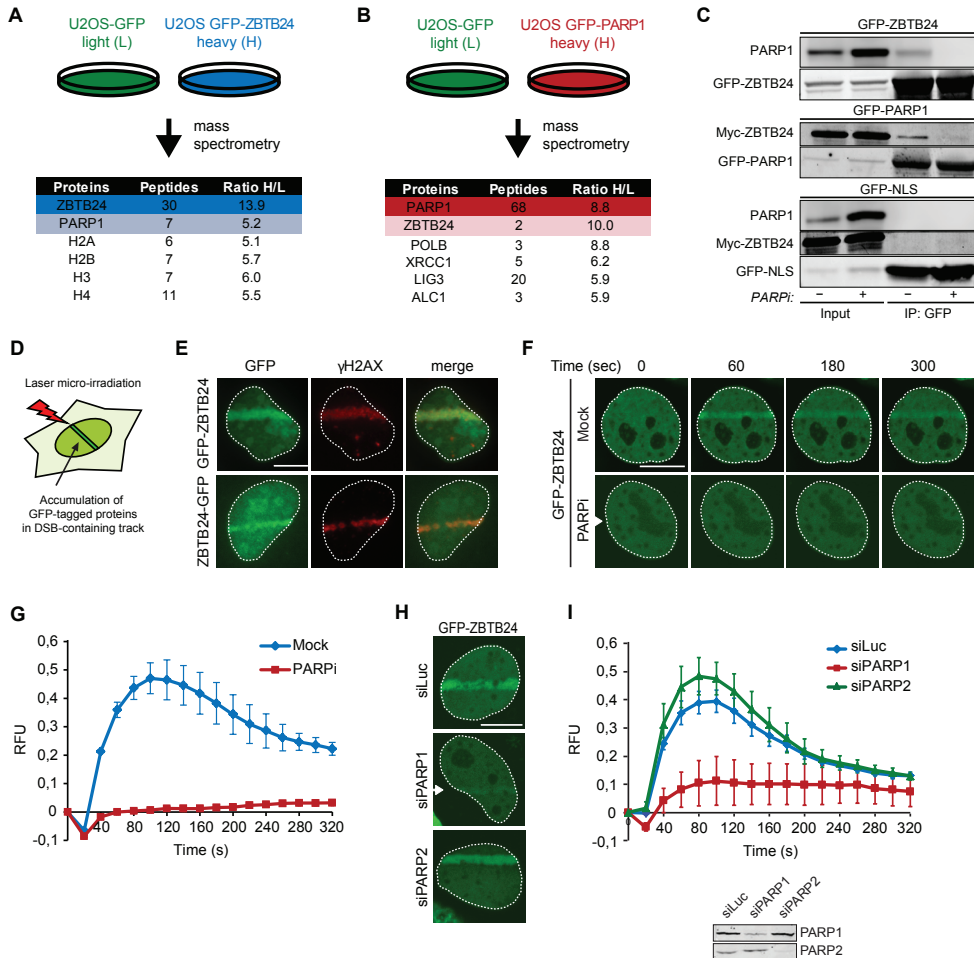


Figure 3. PARP1 interacts with ZBTB24 in a PARYlation-dependent manner and recruits ZBTB24 to sites of DNA damage. (A) Schematic representation of SILAC-based mass spectrometry (MS) approach. GFP- or GFP-ZBTB24 expressing U2OS cells were labelled with Lys0 and Arg0 (L) or Lys8 and Arg10 (H), respectively. Lysates were subjected to GFP-Immunoprecipitation (IP) and equal amounts of both IP fractions were mixed. Proteins in the IP fractions were digested by trypsin and subjected to MS analysis. A list of ZBTB24-interacting proteins, including the number of peptides and the interaction ratio from heavy (H)- over light (L)-labelled cell extracts as revealed by MS, is shown. (B) As in A, but with GFP- and GFP-PARP1 expressing U2OS cells. (C) Cells expressing GFP-ZBTB24, GFP-PARP1 and Myc-ZBTB24, or GFP-NLS and Myc-ZBTB24 were either treated with DMSO (Mock) or with PARP inhibitor (PARPi). Whole cell extracts (WCEs) were subjected to GFP-IP followed by western blot analysis of the indicated proteins. (D) Schematic representation of the laser micro-irradiation approach. (E) GFP-ZBTB24 or ZBTB24-GFP accumulate at γ H2AX-decorated DNA damage tracks following transient expression and laser micro-irradiation in U2OS cells. (F) As in E, except that transiently expressing GFP-ZBTB24 cells were either treated with DMSO (Mock) or PARPi before GFP-ZBTB24 accumulation was monitored at the indicated time points after laser micro-irradiation. (G) Quantification of the results from F. RFU is Relative Fluorescent Units. (H) As in F, expect that cells were co-transfected with GFP-ZBTB24 and the indicated siRNAs. (I) Quantification of the results from H (upper panel). Western blot showing the knockdown efficiency of PARP1 and PARP2 (bottom). Scale bar 10 μ m.

2013). Upon addition of PARP inhibitor (PARPi), PARYlation was efficiently inhibited and the interaction between ZBTB24 and PARP1 was lost (Fig. 3C and S5B). Together, these results suggest that ZBTB24 and PARP1 interact in a PARYlation-dependent manner.

PARP1 recruits ZBTB24 to sites of DNA damage

PARP1 binds to both single- and double-strand breaks, where it promotes the assembly of chromatin remodelers and DNA repair proteins (Pines et al. 2013). Given the interaction between ZBTB24 and PARP1, we tested whether ZBTB24 is recruited to sites of DNA damage. We found that both N- and C-terminally tagged ZBTB24 localize at laser micro-irradiation-induced tracks containing γ H2AX, a known marker of DNA damage (Fig. 3D-E). Importantly, ZBTB24 recruitment to such DNA damage tracks was completely abrogated upon treatment with PARPi (Fig. 3F-G), demonstrating its dependency on PARylation. Furthermore, the accumulation of ZBTB24 at DNA damage tracks was rapid but transient, reaching maximum levels at \sim 100 seconds after DNA damage induction (Fig. 3G) and resembling much the reported dynamics of PARP1 accrual and PARylation at sites of DNA damage (Mortusewicz et al. 2007). Importantly, siRNA-mediated depletion of PARP1, but not PARP2, abrogated ZBTB24 accumulation in laser tracks (Fig. 3H-I). These results show that ZBTB24 is rapidly recruited to sites of DNA damage in a PARP1- and PARylation dependent manner.

PAR chains are rapidly hydrolysed by the activity of poly(ADP-ribose) glycohydrolase (PARG), which explains the rapid turn-over of PAR chains at sites of DNA damage (Pines et al., 2013). To prevent this rapid turnover, we increased the steady-state levels of PAR chains by siRNA-mediated depletion of PARG (Fig. S6A). Under these conditions, we observed enhanced and more persistent accumulation of ZBTB24 at sites of damage (Fig. S6B-C). In contrast, overexpression of mCherry-tagged PARG resulted in a dramatic decrease in the total level of PARylation and abrogated recruitment of ZBTB24 to sites of damage (Fig. S6D-F), phenocopying the effect observed after loss of PARP1 activity (Fig. 3F-G). Thus, the PARP1- and PARG-dependent turnover of PAR chains at DNA lesions is a critical determinant of the rapid and transient accumulation of ZBTB24.

The ZNF of ZBTB24 binds PAR to promote PARP1-dependent ZBTB24 recruitment

Three conserved domains can be identified in ZBTB24: an N-terminal BTB domain (amino acids 9-132), a small AT-hook DNA-binding domain (amino acids 159-171) and 8 tandem C2H2 zinc-finger (ZNF) motifs (amino acids 294-512) (Fig. 4A). To dissect the relevance of these domains for ZBTB24's interaction with PARP1 and localization to DNA damage, we generated and expressed GFP-fusion constructs of the different domains (Fig. 4B-E). Interestingly, GFP-BTB, GFP-BTB-AT or GFP- Δ ZNF did not accumulate at sites of laser-induced DNA damage, whereas GFP-BTB-AT-ZNF (GFP-BAZ) and GFP-ZNF were recruited with similar kinetics as GFP-ZBTB24 (Fig. 4C and S7). Moreover, similar to GFP-ZBTB24 (Fig. 3F-G), GFP-BAZ and GFP-ZNF accumulation was abolished upon PARP inhibition (Fig. S7). This suggests that the ZNF domain is essential for the PARP1 activity-dependent accumulation of ZBTB24 at sites of DNA damage.

PARP1 is responsible for \sim 85% of the synthesized PAR chains and attaches these moieties to itself and other proteins (Shieh et al. 1998; Mortusewicz et al. 2007). The PAR-dependent accumulation of ZBTB24 could be a consequence of the PARylation of ZBTB24 by PARP1 or could be due to the capacity of ZBTB24 to bind PARP1-associated PAR chains. To examine whether ZBTB24 itself is PARylated, we exposed cells to IR or the DNA-alkylating agent N-methyl-N'-nitro-N-nitrosoguanidine (MNNG) and compared the PARylation status of ZBTB24 to that of PARP1. We observed a significant increase in PARylated proteins after MNNG treatment, and a modest increase shortly after exposure to IR (Fig. S8A), indicating that these treatments result in activation of PARP enzymes. We subsequently immunoprecipitated GFP-ZBTB24 or GFP-PARP1 from these cells using stringent, high-salt wash conditions to disrupt all non-

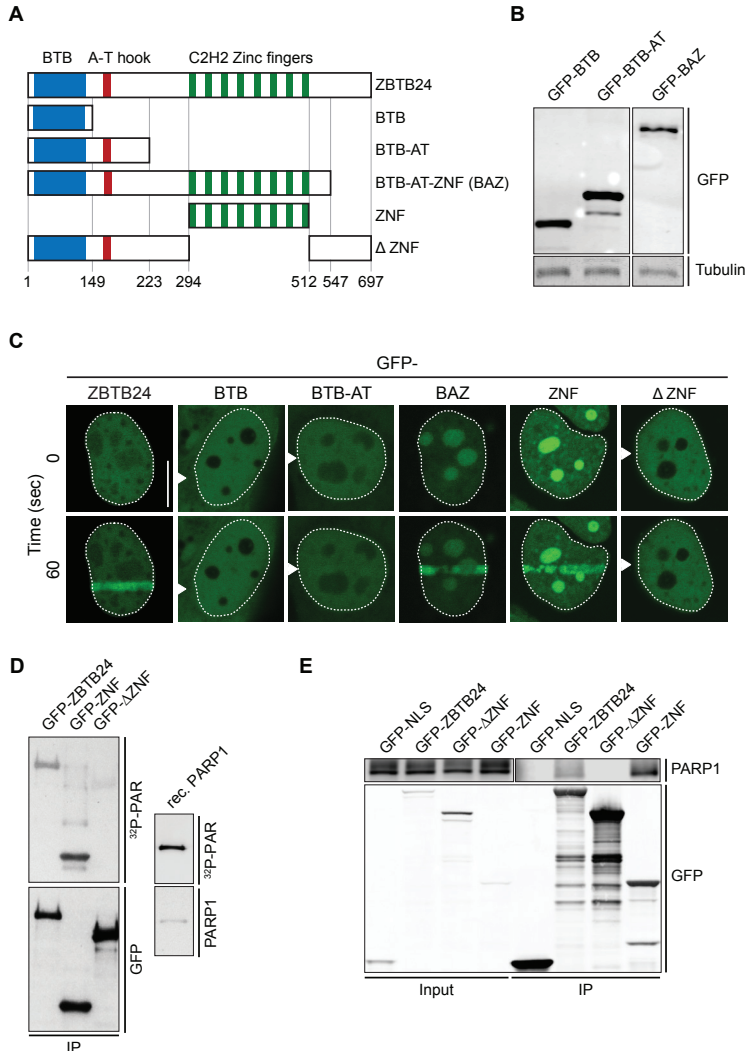


Figure 4. The ZNF domain in ZBTB24 interacts with PAR and mediates its recruitment to sites of DNA damage. (A) Schematic representation of isoform 1 of ZBTB24 and its BTB-, DNA-binding AT hook- and 8 x C2H2 zinc finger domain. Protein domains were separated as indicated and fused to GFP for functional analysis. (B) Western blot analysis of WCEs from U2OS cells expressing the indicated GFP-tagged ZBTB24 domains. (C) Accumulation of the indicated GFP-tagged ZBTB24 domain in laser micro-irradiated U2OS cells. Representative images of unirradiated and irradiated cells (taken at the indicated time point after irradiation) are shown. Scale bar 10 μ m. (D) HEK293T cells expressing the indicated GFP-tagged ZBTB24 domains were subjected to GFP-IP followed by western blot analysis and membrane-exposure to radioactive PAR (32P-PAR). Recombinant (rec.) PARP1 is a positive control. (E) Lysates from U2OS cells transiently expressing either GFP-NLS or the indicated GFP-tagged ZBTB24 domains were subjected to GFP-IP and western blot analysis for the indicated proteins.

covalent protein-protein interactions, and examined their PARYlation status by western blot analysis. As expected, PARP1 was strongly PARYlated under all conditions (Fig. S8B), showing that our approach can detect the attachment of PAR chains to proteins. However, we failed to detect PARYlation of ZBTB24 under these conditions, suggesting that ZBTB24 is not a preferred target for PARYlation by PARP1 (Fig. S8B).

Next, we examined if ZBTB24 could physically associate with PAR chains *in vitro* by using southwestern blotting. GFP-ZBTB24 was immunoprecipitated, transferred to a membrane and exposed to *in vitro* generated ³²P-labelled PAR chains. Indeed, GFP-ZBTB24, similar to recombinant PARP1, was able to bind PAR chains efficiently (Fig. 4D). Since the ZNF domain in ZBTB24 is a key determinant of the PARP1 activity-dependent recruitment of ZBTB24 to sites of DNA damage, we examined if this domain would mediate the interaction with PAR polymers. We observed that GFP-ZNF, but not GFP- Δ ZNF (full-length ZBTB24 lacking the ZNF domain), could bind to PAR chains (Fig. 4D). In concordance, co-IP experiments revealed an interaction between PARP1 and GFP-ZNF, but not GFP- Δ ZNF (Fig. 4E). Together these results suggest that the ZNF of ZBTB24 is a novel PAR-binding domain that mediates ZBTB24 recruitment to DNA damage through interactions with PARylated PARP1.

ZBTB24 promotes PAR synthesis and protects PAR chains

Considering that ZBTB24 efficiently associates with PARP1-generated PAR chains, we wondered whether ZBTB24 could be involved in regulating the steady-state levels of such chains in response to DNA damage. To examine this possibility, we monitored global PAR levels by western blot analysis in cells exposed to IR. While hardly any PARylation could be observed in mock-treated cells, exposure to IR triggered robust DNA damage-induced PARylation (Fig. 5A-B), which was largely suppressed (~60-70%) by knockdown of PARP1 (Fig. 5A-B). Strikingly, knockdown of ZBTB24 also caused a significant reduction (~50%) in PARylation in IR-exposed cells (Fig. 5A-B), suggesting that ZBTB24 is required to boost the DNA damage-induced PARylation response.

It is feasible that ZBTB24 regulates steady-state PAR levels by either stimulating the synthesis of such chains, or by preventing their degradation. To examine a potential stimulatory role for ZBTB24 in PAR synthesis, we reconstituted PARP1-dependent synthesis of PAR in an *in vitro* system in the absence or presence of recombinant ZBTB24 (Fig. 5C). In the presence of NAD⁺ and a damaged DNA template, we found that the capacity of recombinant PARP1 to synthesize PAR chains was enhanced in a dose-dependent manner by the presence of recombinant ZBTB24 (Fig. 5D-E), suggesting that ZBTB24 stimulates PARP1-dependent PAR synthesis.

Another non-mutually exclusive possibility is that ZBTB24 binding to PAR chains protects such chains from efficient hydrolysis by the PARP1 antagonist PARG (Fig. 5D). To explore this possibility, we allowed PARP1-dependent synthesis of PAR in our *in vitro* system and, following the inactivation of PARP1 by PARPi, added recombinant PARG hydrolase with increasing amounts of recombinant ZBTB24 (Fig. 5F). We could detect efficient hydrolysis of nearly all PAR chains in the absence of ZBTB24 (lane 1 versus 2; Fig. 5G). Interestingly, ZBTB24 inhibited in a dose-dependent manner the break-down of PAR products in the hydrolysis reaction (Fig. 5G-H), suggesting that ZBTB24 can protect PAR chains from PARG-dependent degradation. In conclusion, we found that ZBTB24 promotes the steady-state levels of DNA damage-induced PAR chains by simultaneously stimulating the PARP1-dependent synthesis and inhibiting the PARG-dependent hydrolysis of such chains.

ZBTB24 and PARP1 promote c-NHEJ by regulating XRCC4/LIG4 assembly

We then sought to address how ZBTB24's role in PAR synthesis and protection is linked to its involvement in c-NHEJ (Fig. 2). It is known that c-NHEJ involves the binding of KU70/KU80 to the broken ends, followed by the accrual of DNA-PKcs and ligation of the break by the XRCC4/DNA ligase 4 (LIG4) complex (Alt et al. 2013). Interestingly, recent *in vitro* studies

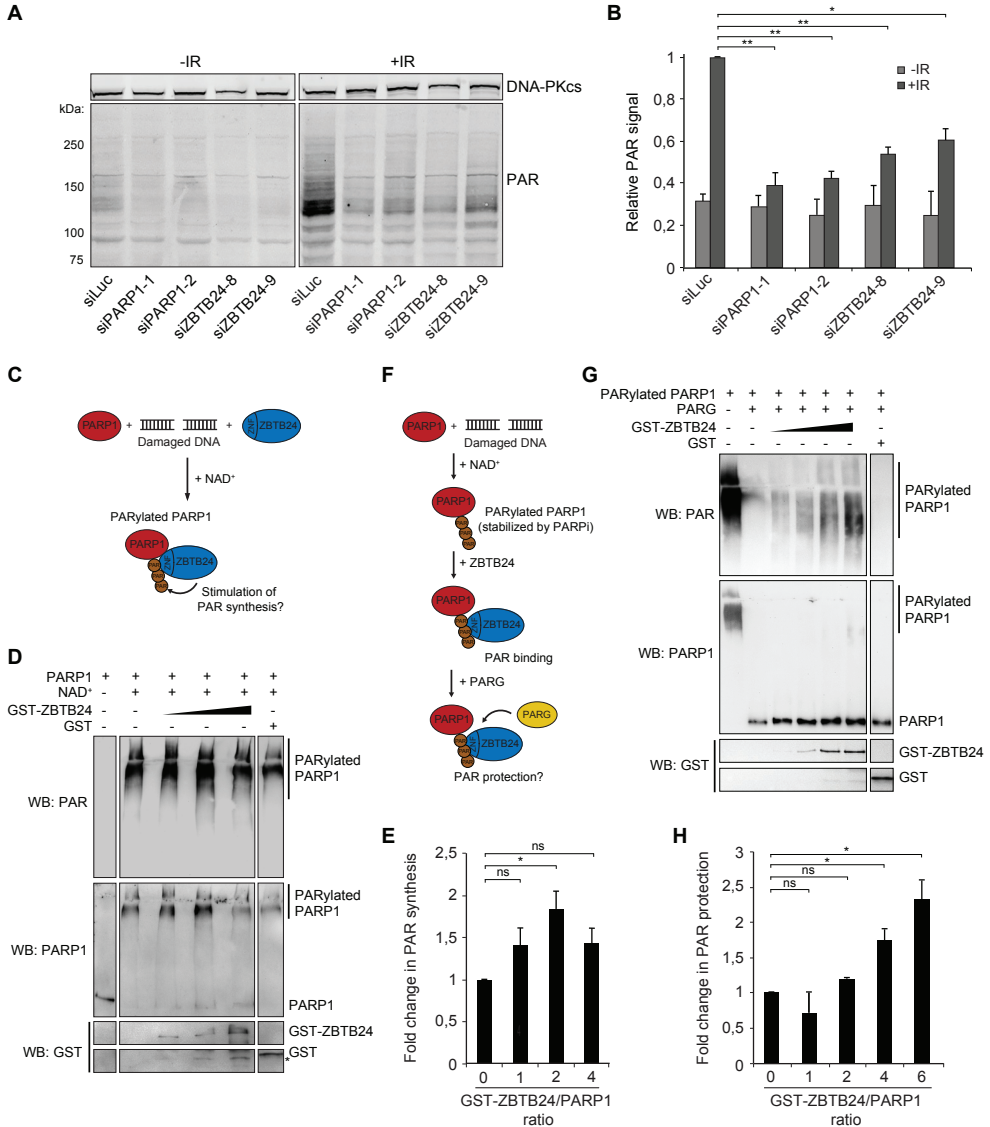


Figure 5. ZBTB24 stimulates PARP1-dependent PAR synthesis and protects PAR chain stability. (A) U2OS cells transfected with the indicated siRNAs were left untreated or exposed to IR. Five minutes later WCE were prepared and subjected to western blot analysis for DNA-PKcs and PAR. DNA-PKcs is a loading control. (B) Quantification of the results from A and a second independent experiment. The ratio of PAR/loading control signals per sample was normalized to that of the IR-exposed siLuc sample, which was set to 1. (C) Schematic of the PAR synthesis assay. (D) Recombinant PARP1 was incubated with a damaged DNA template and activated by NAD⁺ in the presence of increasing concentrations of GST-ZBTB24 or GST only. The presence of 10H-PAR chains and recombinant proteins was monitored by western blot analysis. (E) Quantification of ZBTB24-dependent stimulation of PAR synthesis from D and two other independent experiments. The signal of 10H-PAR for each sample containing GST-ZBTB24 was normalized to that without GST-ZBTB24, which was set to 1. (F) Schematic of the PAR protection assay. (G) Recombinant PARP1 was incubated with a damaged DNA template and activated by NAD⁺ to generate PARylated PARP1. Increasing concentrations of GST-ZBTB24 or GST alone were added, followed by incubation with PARG. The presence of 10H-PAR chains and recombinant proteins was monitored by western blot analysis. (H) As in E, except that PAR protection was measured from G and another independent experiment.

demonstrated that the c-NHEJ ligase LIG4 interacts with PAR chains through its C-terminal BRCT domain (Li et al. 2013), providing a possible link between ZBTB24's involvement in PAR stability and NHEJ. To study this further, we first applied laser micro-irradiation to monitor the recruitment of GFP-XRCC4 to damaged DNA in U2OS cells that were either treated with PARP inhibitor or depleted for PARP1. Strikingly, the loss of both PARP activity and PARP1 protein markedly impaired the recruitment of GFP-XRCC4 (Fig. 6A-D), suggesting that PARP1-dependent PARylation regulates the assembly of XRCC4/LIG4 complexes at sites of DNA damage to promote c-NHEJ. To investigate this, we used the plasmid integration assay to specifically examine PARP1's contribution to c-NHEJ. In agreement with our recruitment data, we found that PARP1 depletion resulted in a ~40% reduction in c-NHEJ efficiency (Fig. 6E and S3C), suggesting that PARP1, similar to ZBTB24 (Fig. 2E), plays a role in c-NHEJ. Given ZBTB24's role in NHEJ, its interaction with PARP1 and its stimulatory effect on PARylation, we addressed whether it affects the PARP1-dependent assembly of XRCC4/LIG4 at DSBs. Depletion of ZBTB24, similar to that of PARP1, resulted in a strong reduction in GFP-XRCC4 recruitment at sites of laser-induced DNA damage (Fig. 6F-G). Moreover, ZBTB24 depletion also reduced the accumulation of endogenous XRCC4, while DNA damage levels measured by γ H2AX formation were comparable to that of control cells (Fig. S9). Importantly, the accumulation of GFP-XRCC4 at a stably integrated Lactose operator (LacO) array upon tethering of a Lactose repressor (LacR)-tagged FokI nuclease in U2OS cells was also strongly reduced in cells depleted for ZBTB24 (Fig. 6H-K). This indicates that ZBTB24 acts at bona fide DSBs to facilitate the accumulation of functional XRCC4/LIG4 complexes. Together our results show that ZBTB24, by ensuring robust steady-state levels of DNA damage-induced PARylation, acts as a scaffold for the PARP1 - LIG4 interaction to promote XRCC4/LIG4-dependent c-NHEJ (Fig. 6L).

DISCUSSION

Mutations in at least four different genes cause the primary immunodeficiency ICF. About 30% of the ICF patients carry causal mutations in the uncharacterized ZBTB24 gene (ICF2) (Weemaes et al. 2013; Thijssen et al. 2015). Here, we functionally characterized the role of ZBTB24 by biochemical, cell biological and patient-based approaches. In ICF2 patients, we report a severe reduction in immunoglobulin production and diversification capacity, and a shift towards a-NHEJ events during CSR, which is reminiscent of the phenotype observed in c-NHEJ-deficient patients (Pan-Hammarstrom et al. 2005; Du et al. 2008). These findings provide a plausible molecular explanation for the currently unexplained immunodeficiency in ICF2 and suggest a role for ZBTB24 in c-NHEJ. Indeed, we reveal that ZBTB24 is recruited to sites of DNA damage in a PARP1-dependent manner by associating with PARP1-generated PAR-chains through its ZNF domain. Our biochemical and cellular analyses show that ZBTB24 promotes PARP1-mediated PAR synthesis and acts as a scaffold protein that protects PAR chains from degradation, thereby enhancing the PARP1-dependent recruitment of the LIG4-XRCC4 complex to facilitate efficient DSB repair by c-NHEJ (see model; Fig. 6L).

ZBTB24 is required for CSR, a process defective in ICF2 patients

Mutations in ZBTB24 lead to defective CSR in ICF2 patients, while V(D)J recombination remains unaffected. This may be unexpected considering that both processes heavily rely on c-NHEJ. However, mutations in several other DNA damage response (DDR) genes, such

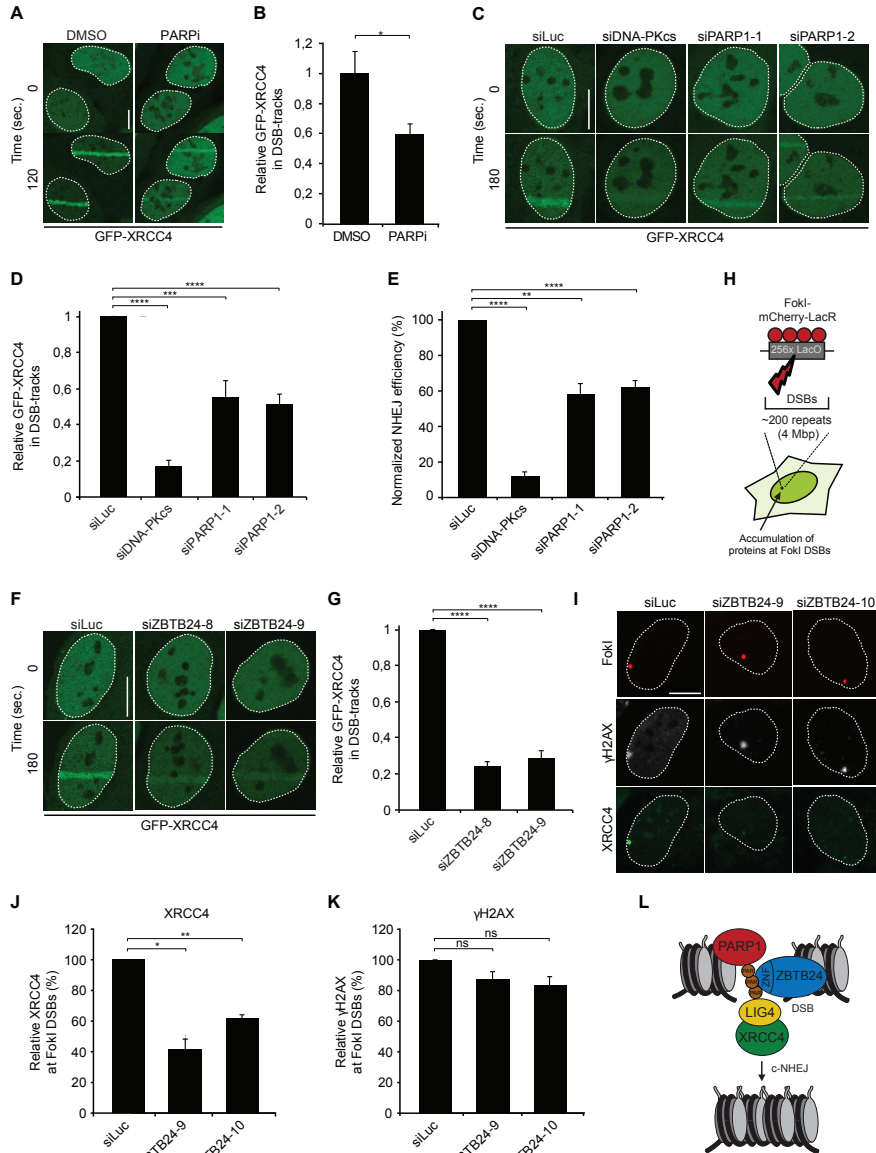


Figure 6. ZBTB24 and PARP1 promote XRCC4/LIG4 assembly at DNA damage sites. (A) U2OS stably expressing GFP-XRCC4 were treated with DMSO (Mock) or PARPi and subjected to laser micro-irradiation. Representative images of unirradiated and irradiated cells (taken at the indicated time point after irradiation) are shown. Arrowheads indicate laser-irradiated regions. Scale bar 10 μ m. (B) Quantification of A. (C) As in A, except that cells were transfected with the indicated siRNAs. (D) Quantification of C. (E) Plasmid integration assays in U2OS cells transfected with indicated siRNAs. (F) As in C. (G) Quantification of F. (H) Schematic of the system in U2OS 2-6-3 cells used to locally induce multiple DSBs upon tethering of the FokI endonuclease. (I) Accumulation of XRCC4 (green) to γ H2AX-marked (white) DSBs induced by FokI-mCherry-LacR at a LacO array (red) in cells transfected with the indicated siRNAs. Scale bar 10 μ m. (J) Quantification of XRCC4 accumulation in F. (K) As in J, except for γ H2AX. (L) Model for the role of ZBTB24 in DSB repair by NHEJ. ZBTB24 accumulates at DSBs, where it functions as a scaffold to protect PARP1-associated PAR-chains, which serve as a docking site for the LIG4-XRCC4 complex, facilitating efficient DSB repair via c-NHEJ.

as H2AX, NIPBL and ATM in both mice and humans, cause a remarkably similar defect in CSR without affecting V(D)J recombination (Pan et al. 2002; Reina-San-Martin et al. 2003; Manis et al. 2004; Envervald et al. 2013). It has been suggested that the ends of RAG1/2-induced DSB are held together by these enzymes during V(D)J recombination. In contrast, AID-initiated DSBs during CSR are likely held together by factors involved in the signalling of DSB, such as the core chromatin component H2AX and 53BP1 (Petersen et al. 2001; Manis et al. 2004). The role of ZBTB24 may resemble that of the latter DDR components, explaining its specific impact on CSR. Alternatively, RAG1/2 induce DSBs that are characterized by the production of a hairpin structure at the broken ends. PARP1 swiftly binds to single- and double-strand breaks (Eustermann et al. 2011; Langelier et al. 2012), as well as to hairpin structures in vitro (Lonskaya et al. 2005). However, whether it also displays affinity for RAG1/2-induced hairpin structures at DSBs in vivo remains to be determined. It is conceivable that these structures are not bound by PARP1 due to their processing by the structure-specific endonuclease Artemis (Alt et al. 2013), which could rule out a function for PARP1 and most likely ZBTB24 in V(D)J recombination and would be in agreement with our observations. However, PARP1 seems to have affinity for AID-induced breaks in mice, where it promotes CSR through a-NHEJ (Robert et al. 2009). Whether it also modulates CSR in humans remains elusive, mainly because patients with loss-of-function mutations in PARP1 have not been reported yet.

ZBTB24 and PARP1 in NHEJ

The current models for NHEJ distinguish a dominant c-NHEJ pathway that is fully dependent on KU70/KU80 from a PARP1-dependent a-NHEJ pathway that only becomes active in the absence of KU70/KU80 (Wang et al. 2006). However, while PARP1 is required for a-NHEJ, this does not exclude a stimulatory role for PARP1 in c-NHEJ. Indeed, several studies reported that the loss of PARP1 activity modulates the c-NHEJ-dependent re-joining of DSBs in hamster, mouse and human cells (Veuger et al. 2003; Mitchell et al. 2009). Our results corroborate and extend these observations and further support a role for PARP1 in DSB repair through c-NHEJ.

Our work identifies ZBTB24 as an effector of PARP1-dependent c-NHEJ. However, the c-NHEJ-specific phenotypes, such as impaired random plasmid integration or XRCC4 recruitment to laser/nuclease-induced DSBs, which we observed after knockdown of ZBTB24 or PARP1, were not as strong as seen after depletion of core NHEJ factors, such as DNA-PKcs. This suggests that the PARP1-ZBTB24 axis is not essential for c-NHEJ, but greatly stimulates this process in human cells.

Loss of ZBTB24 also reduces NHEJ in the EJ5-GFP reporter. Since this reporter cannot discriminate between c-NHEJ and a-NHEJ, we cannot rule out the possibility that ZBTB24 might promote both c-NHEJ and a-NHEJ. An involvement in the latter repair pathway would not be surprising given its interaction with PARP1, which is required for a-NHEJ (Pines et al. 2013).

The C2H2 ZNF of ZBTB24 binds PAR chains

Four structurally distinct protein motifs have been characterized to mediate interactions with PAR chains: 1) a consensus of eighth interspersed basic and hydrophobic amino acid residues, 2) macro domains containing a conserved ligand-binding pocket, 3) the WWE domain that recognizes iso-ADP-ribose, which is the smallest internal structural unit of PAR, and 4) the PAR-binding zinc (PBZ) finger (Kalisch et al. 2012). Here we expand the latter

category by showing that the C2H2 ZNF, as present in ZBTB24, is a new type of motif that mediates PAR binding. While this motif has been suggested to predominantly bind to DNA (Najafabadi et al. 2015), we demonstrate that the eight C2H2 ZNFs within ZBTB24 associate with PAR chains *in vitro* and mediate the interaction with PARP1 *in vivo*. Interestingly, a recent screen for DDR factors identified more than 100 new proteins, many of which were ZNF-containing transcription factors that, similar to ZBTB24, were recruited to sites of laser-induced DNA damage in a PARP/PARYlation-dependent manner (Izhar et al. 2015). Further studies on these DNA damage-associated ZNF-containing proteins may reveal, whether they have evolved as general PAR-binding proteins with specialized functions in the PARP-dependent DDRs.

ZBTB24 stimulates PAR synthesis and protects PAR chains

Based on its functional domains ZBTB24 seems to lack enzymatic activity. Indeed, our work suggests that ZBTB24 has at least two non-catalytic roles: it can enhance PAR synthesis by PARP1 and can bind and protect PAR chains from hydrolysis by PARG. How does ZBTB24 stimulate PAR synthesis by PARP1? Two models exist for the activation of human PARP1: the *cis* and *trans* model. In the *cis* model a single PARP1 protein binds a DNA end, which triggers intramolecular interactions and conformational changes that enhance the flexibility of the catalytic domain to induce auto-PARYlation (Langelier et al. 2012). One possibility is that ZBTB24 by binding to PARP1 stimulates these intramolecular interactions and conformational changes, resulting in enhanced PARP1 activation. Alternatively, in the *trans* model, two PARP1 proteins dimerize at a DSB, subsequently enabling one of these PARP1 molecules to modify the catalytic domain of its interaction partner (Ali et al. 2012). BTB domains, such as those found in ZBTB24, are known to mediate dimerization between proteins (Bardwell and Treisman 1994). It is therefore possible that ZBTB24's interaction with PARP1 and its ability to dimerize could stimulate PARP1 dimerization and its subsequent activation. Additional biochemical work will be required to reveal whether ZBTB24 promotes *in cis* and/or *in trans* activation of PARP1.

In contrast to ZBTB24's role in PARP1 activation, its contribution to PAR protection may be easier to explain. We demonstrated that ZBTB24 through its ZNF domain directly associates with PARP1-associated PAR chains. This may sterically hinder PARG from attacking PAR chains. However, some PAR chains are digested despite the presence of excess ZBTB24 (Fig. 5G-H), which could be due to the highly versatile endo- and exoglycosidic activities of PARG towards PAR (Brochu et al. 1994). It may be that additional PAR-binding factors are required to provide full protection against PARG hydrolysis. These factors may for instance include one or more ZNF-containing transcription factors or DDR proteins with intrinsically disordered domains that are recruited to sites of DNA damage in a PAR-dependent manner (Altmeyer et al. 2015; Izhar et al. 2015).

We observed that at concentrations up to two times that of PARP1, ZBTB24 can only activate PARP1, while at more than two times the concentration of PARP1 it protects PAR chains rather than that it helps to activate PARP1 (Fig. 5D-E and 5G-H). This suggests that ZBTB24 may switch function dependent on its concentration relative to PARP1. Based on this, at sites of DNA damage we envision a scenario in which ZBTB24, following its initial recruitment, helps with the activation of PARP1 and subsequently protects the synthesized PARP1-associated PAR chains. As such it could facilitate the PARYlation-dependent interaction between the c-NHEJ ligase LIG4 and PARP1 (Li et al. 2013), and promote DSB repair by c-NHEJ (Fig. 6L).

MATERIALS AND METHODS

Patients

Sera and PBMC were obtained after informed consent from two ICF2 patients that have been described previously (patients 49 and 55;(Weemaes et al. 2013)) and one novel ICF2 patient (p67) carrying the same recessive mutation as patient 49.

Lymphocyte phenotyping and Ig production analysis

PBMC from patients and healthy individuals were stained with fluorochrome-labelled antibodies against cell surface antigens. Stimulated PBMC were analyzed for IgG and IgA production by sandwich ELISA (see Supplemental Material).

IgH repertoire analysis and switch recombination junctions sequencing

IGH rearrangements and C α and C γ transcripts were amplified from PBMC by multiplex PCR (Ijspeert et al. 2014). Purified PCR products were sequenced on 454 GS junior instrument (Roche) according to the manufacturer's recommendations and data analysis was performed using the IGGalaxy tool (Moorhouse et al. 2014). S μ -S α and S μ -S γ fragments were amplified, cloned and sequenced as described (Pan-Hammarstrom et al. 2005). Repair pattern analysis of CSR junctions was done according to guidelines (Stavnezer et al. 2010).

Cell lines, chemicals, plasmids and transfections

Human cells (see Supplemental Material) were cultured in DMEM, supplemented with antibiotics and 10% fetal calf serum. PARP inhibitor (KU-0058948) was used at a concentration of 10 μ M. All indicated ZBTB24 constructs were generated by PCR and general cloning procedures. Plasmid DNA or siRNAs were transfected using JetPEI (Polyplus Transfection), Lipofectamine 2000 or RNAiMAX (Invitrogen) according to the manufacturer's instructions.

DSB repair assays

EJ5-GFP reporter assays were carried out as described previously (Helfricht et al. 2013). Gel-purified XhoI-EcoRI-linearized pEGFP-C1 plasmid was transfected into siRNA-depleted cells to measure random plasmid integration events (see Supplemental Material).

Immunoprecipitation for mass spectrometry and PAR-binding assay

GFP-tagged ZBTB24 and PARP1 were immunoprecipitated, trypsinized, desalted and analyzed on a Q-Exactive Orbitrap mass spectrometer (Thermo Scientific, Germany) coupled to an EASY-nanoLC 1000 system (Proxeon, Odense, Denmark). GFP-ZBTB24 and derivatives were immunoprecipitated, separated by SDS-PAGE and incubated with radioactive PAR. Radioactivity was detected by a phosphor-imager screen.

PARP1 activation and PAR protection

PARP1 activation and PAR protection assays were done as described (Shah et al. 2011), using purified GST or GST-ZBTB24 proteins (see Supplemental Material).

Laser micro-irradiation and FokI assays

Laser micro-irradiation was performed by UV-A micro-irradiation of BrdU-sensitized cells or by multi-photon (MP) irradiation using a titanium-sapphire laser were done as described (Helfricht et al., 2013). U2OS 2-6-3 cells expressing inducible FokI-mCherry-LacR were

treated with 300 nM 4-OHT and 1 μ M Shield-I for 5 hrs (Shah et al. 2011). Subsequently, cells were fixed with formaldehyde and immunostained as described (Luijsterburg et al. 2012; Helfricht et al. 2013). 20 – 200 cells from two or more independent experiments were analyzed. Antibodies are listed in Supplemental Material.

Statistical analysis

Statistical significance was assessed by a χ^2 -test (Fig. 1D), a two-tailed Mann-Whitney test (Fig. S2C) or a two-tailed, unpaired t-test (all other figures), and is indicated as **** = $p < 0.0001$, *** = $p < 0.001$, ** = $p < 0.01$, * = $p < 0.05$ and ns = not significant. Average values of two to four independent experiments \pm SEM are shown.

ACKNOWLEDGEMENTS

The authors would like to thank Nisha Verweij, Jer-gung Chang, Anton de Groot, Andrea Björkman and Steve Jackson for help with cloning experiments, MS sample analysis, MS data analysis, CSR junction analysis and plasmid integration assays, respectively. GFP-XRCC4 was a kind gift from Penny Jeggo. This work was financially supported by grants from the Dutch Scientific Organisation (NWO-VENI; M.S.L. and NWO-VIDI; H.IJ and M.v.d.B.), People Programme - Marie Curie Actions (P.R.), Natural Sciences and Engineering Research Council of Canada (G.M.S.), Dutch Cancer Society (S.M.v.d.M and H.v.A.) and European Research Council (Starting grant; A.C.O.V and Q.P-H., Consolidator; H.v.A.).



REFERENCES

1. Ali AA, Timinszky G, Arribas-Bosacoma R, Kozlowski M, Hassa PO, Hassler M, Ladurner AG, Pearl LH, Oliver AW. 2012. The zinc-finger domains of PARP1 cooperate to recognize DNA strand breaks. *Nat Struct Mol Biol* 19: 685-692.
2. Alt FW, Zhang Y, Meng FL, Guo C, Schwer B. 2013. Mechanisms of programmed DNA lesions and genomic instability in the immune system. *Cell* 152: 417-429.
3. Altmeyer M, Neelsen KJ, Teloni F, Pozdnyakova I, Pellegrino S, Grofte M, Rask MB, Streicher W, Jungmichel S, Nielsen ML et al. 2015. Liquid demixing of intrinsically disordered proteins is seeded by poly(ADP-ribose). *Nat Commun* 6: 8088.
4. Audebert M, Salles B, Calsou P. 2004. Involvement of poly(ADP-ribose) polymerase-1 and XRCC1/DNA ligase III in an alternative route for DNA double-strand breaks rejoining. *JBiolChem* 279: 55117-55126.
5. Bardwell VJ, Treisman R. 1994. The POZ domain: a conserved protein-protein interaction motif. *Genes Dev* 8: 1664-1677.
6. Bennardo N, Cheng A, Huang N, Stark JM. 2008. Alternative-NHEJ is a mechanistically distinct pathway of mammalian chromosome break repair. *PLoSGenet* 4: e1000110.
7. Bjorkman A, Qvist P, Du L, Bartish M, Zaravinos A, Georgiou K, Borglum AD, Gatti RA, Torngren T, Pan-Hammarstrom Q. 2015. Aberrant recombination and repair during immunoglobulin class switching in BRCA1-deficient human B cells. *ProcNatAcadSciUSA* 112: 2157-2162.
8. Blanco-Betancourt CE, Moncla A, Milili M, Jiang YL, Viegas-Pequignot EM, Roquelaure B, Thuret I, Schiff C. 2004. Defective B-cell-negative selection and terminal differentiation in the ICF syndrome. *Blood* 103: 2683-2690.
9. Brochu G, Duchaine C, Thibeault L, Lagueux J, Shah GM, Poirier GG. 1994. Mode of action of poly(ADP-ribose) glycohydrolase. *Biochim Biophys Acta* 1219: 342-350.
10. Chouery E, Abou-Ghoch J, Corbani S, El AN, Korban R, Salem N, Castro K, Klayme S, Azoury-Abou RM, Khoury-Matar R et al. 2012. A novel deletion in ZBTB24 in a Lebanese family with immunodeficiency, centromeric instability, and facial anomalies syndrome type 2. *ClinGenet* 82: 489-493.
11. de Greef JC, Wang J, Balog J, den Dunnen JT, Frants RR, Straasheijm KR, Aytekin C, van der Burg M, Duprez L, Ferster A et al. 2011. Mutations in ZBTB24 are associated with immunodeficiency, centromeric instability, and facial anomalies syndrome type 2. *AmJHumGenet* 88: 796-804.
12. Du L, van der Burg M, Popov SW, Kotnis A, van Dongen JJ, Gennery AR, Pan-Hammarstrom Q. 2008. Involvement of Artemis in nonhomologous end-joining during immunoglobulin class switch recombination. *JExpMed* 205: 3031-3040.
13. Enervald E, Du L, Visnes T, Bjorkman A, Lindgren E, Wincent J, Borck G, Colleaux L, Cormier-Daire V, van Gent DC et al. 2013. A regulatory role for the cohesin loader NIPBL in nonhomologous end joining during immunoglobulin class switch recombination. *JExpMed* 210: 2503-2513.
14. Eustermann S, Videler H, Yang JC, Cole PT, Gruszka D, Veprintsev D, Neuhaus D. 2011. The DNA-binding domain of human PARP-1 interacts with DNA single-strand breaks as a monomer through its second zinc finger. *JMolBiol* 407: 149-170.
15. Hagleitner MM, Lankester A, Maraschio P, Hulten M, Fryns JP, Schuetz C, Gimelli G, Davies EG, Gennery A, Belohradsky BH et al. 2008. Clinical spectrum of immunodeficiency, centromeric instability and facial dysmorphism (ICF syndrome). *JMedGenet* 45: 93-99.
16. Hansen RS, Wijmenga C, Luo P, Stanek AM, Canfield TK, Weemaes CM, Gartler SM. 1999. The DNMT3B DNA methyltransferase gene is mutated in the ICF immunodeficiency syndrome. *ProcNatAcadSciUSA* 96: 14412-14417.
17. Helfricht A, Wiegant WW, Thijssen PE, Vertegaal AC, Luijsterburg MS, van Attikum H. 2013. Remodeling and spacing factor 1 (RSF1) deposits centromere proteins at DNA double-strand breaks to promote non-homologous end-joining. *Cell Cycle* 12: 3070-3082.
18. Ijspeert H, Driessen GJ, Moorhouse MJ, Hartwig NG, Wolska-Kusnierz B, Kalwak K, Pituch-Noworolska A, Kondratenko I, van Montfrans JM, Mejstrikova E et al. 2014. Similar recombination-activating gene (RAG) mutations result in similar immunobiological effects but in different clinical phenotypes. *JAllergy ClinImmunol* 133: 1124-1133.
19. Izhar L, Adamson B, Ciccia A, Lewis J, Pontano-Vaites L, Leng Y, Liang AC, Westbrook TF, Harper JW, Elledge SJ. 2015. A Systematic Analysis of Factors Localized to Damaged Chromatin Reveals PARP-Dependent Recruitment of Transcription Factors. *Cell Rep* 11: 1486-1500.
20. Kalisch T, Ame JC, Dantzer F, Schreiber V. 2012. New readers and interpretations of poly(ADP-ribose)ylation. *Trends BiochemSci* 37: 381-390.
21. Langelier MF, Planck JL, Roy S, Pascal JM. 2012. Structural basis for DNA damage-dependent poly(ADP-ribose)ylation by human PARP-1. *Science* 336: 728-732.
22. Li M, Lu LY, Yang CY, Wang S, Yu X. 2013. The FHA and BRCT domains recognize ADP-riboseylation during DNA damage response. *Genes Dev* 27: 1752-1768.
23. Lonskaya I, Potaman VN, Shlyakhtenko LS, Oussatcheva EA, Lyubchenko YL, Soldatenkov VA. 2005. Regulation of poly(ADP-ribose) polymerase-1 by DNA structure-specific binding. *J Biol Chem* 280: 17076-17083.
24. Lu G, Duan J, Shu S, Wang X, Gao L, Guo J, Zhang Y. 2016. Ligase I and ligase III mediate the DNA double-strand break ligation

- in alternative end-joining. *Proc Natl Acad Sci U S A* 113: 1256-1260.
25. Luijsterburg MS, Acs K, Ackermann L, Wiegant WW, Bekker-Jensen S, Larsen DH, Khanna KK, van Attikum H, Mailand N, Dantuma NP. 2012. A new non-catalytic role for ubiquitin ligase RNF8 in unfolding higher-order chromatin structure. *EMBO J* 31: 2511-2527.
 26. Manis JP, Morales JC, Xia Z, Kutok JL, Alt FW, Carpenter PB. 2004. 53BP1 links DNA damage-response pathways to immunoglobulin heavy chain class-switch recombination. *Nat Immunol* 5: 481-487.
 27. Mitchell J, Smith GC, Curtin NJ. 2009. Poly(ADP-Ribose) polymerase-1 and DNA-dependent protein kinase have equivalent roles in double strand break repair following ionizing radiation. *IntJRadiatOncolBiolPhys* 75: 1520-1527.
 28. Moorhouse MJ, van ZD, Ijspeert H, Hiltemann S, Horsman S, van der Spek PJ, van der Burg M, Stubbs AP. 2014. ImmunoGlobulin galaxy (IGGalaxy) for simple determination and quantitation of immunoglobulin heavy chain rearrangements from NGS. *BMC Immunol* 15: 59.
 29. Mortusewicz O, Ame JC, Schreiber V, Leonhardt H. 2007. Feedback-regulated poly(ADP-ribosyl)ation by PARP-1 is required for rapid response to DNA damage in living cells. *Nucleic Acids Res* 35: 7665-7675.
 30. Najafabadi HS, Mnaimneh S, Schmitges FW, Garton M, Lam KN, Yang A, Albu M, Weirauch MT, Radovani E, Kim PM et al. 2015. C2H2 zinc finger proteins greatly expand the human regulatory lexicon. *Nat Biotechnol* 33: 555-562.
 31. Nitta H, Unoki M, Ichiyonagi K, Kosho T, Shigemura T, Takahashi H, Velasco G, Francastel C, Picard C, Kubota T et al. 2013. Three novel ZBTB24 mutations identified in Japanese and Cape Verdean type 2 ICF syndrome patients. *JHumGenet* 58: 455-460.
 32. Pan Q, Petit-Frere C, Lahdesmaki A, Gregorek H, Chrzanowska KH, Hammarstrom L. 2002. Alternative end joining during switch recombination in patients with ataxia-telangiectasia. *EurJImmunol* 32: 1300-1308.
 33. Pan-Hammarstrom Q, Jones AM, Lahdesmaki A, Zhou W, Gatti RA, Hammarstrom L, Gennery AR, Ehrenstein MR. 2005. Impact of DNA ligase IV on nonhomologous end joining pathways during class switch recombination in human cells. *JExpMed* 201: 189-194.
 34. Paul K, Wang M, Mladenov E, Bencsik-Theilen A, Bednar T, Wu W, Arakawa H, Iliakis G. 2013. DNA ligases I and III cooperate in alternative non-homologous end-joining in vertebrates. *PLoS One* 8: e59505.
 35. Petersen S, Casellas R, Reina-San-Martin B, Chen HT, Difilippantonio MJ, Wilson PC, Hanitsch L, Celeste A, Muramatsu M, Pilch DR et al. 2001. AID is required to initiate Nbs1/gamma-H2AX focus formation and mutations at sites of class switching. *Nature* 414: 660-665.
 36. Pines A, Mullenders LH, van Attikum H, Luijsterburg MS. 2013. Touching base with PARPs: moonlighting in the repair of UV lesions and double-strand breaks. *Trends BiochemSci* 38: 321-330.
 37. Reina-San-Martin B, Difilippantonio S, Hanitsch L, Masilamani RF, Nussenzweig A, Nussenzweig MC. 2003. H2AX is required for recombination between immunoglobulin switch regions but not for intra-switch region recombination or somatic hypermutation. *JExpMed* 197: 1767-1778.
 38. Robert I, Dantzer F, Reina-San-Martin B. 2009. Parp1 facilitates alternative NHEJ, whereas Parp2 suppresses IgH/c-myc translocations during immunoglobulin class switch recombination. *JExpMed* 206: 1047-1056.
 39. Shah GM, Kandan-Kulangara F, Montoni A, Shah RG, Brind'Amour J, Vodenicharov MD, Affar eB. 2011. Approaches to detect PARP-1 activation in vivo, in situ, and in vitro. *Methods MolBiol* 780: 3-34.
 40. Shieh WM, Ame JC, Wilson MV, Wang ZQ, Koh DW, Jacobson MK, Jacobson EL. 1998. Poly(ADP-ribose) polymerase null mouse cells synthesize ADP-ribose polymers. *JBiolChem* 273: 30069-30072.
 41. Stavnezer J, Bjorkman A, Du L, Cagigi A, Pan-Hammarstrom Q. 2010. Mapping of switch recombination junctions, a tool for studying DNA repair pathways during immunoglobulin class switching. *AdvImmunol* 108: 45-109.
 42. Thijssen PE, Ito Y, Grillo G, Wang J, Velasco G, Nitta H, Unoki M, Yoshihara M, Suyama M, Sun Y et al. 2015. Mutations in CDCA7 and HELLS cause immunodeficiency-centromeric instability-facial anomalies syndrome. *Nat Commun* 6: 7870.
 43. Veuger SJ, Curtin NJ, Richardson CJ, Smith GC, Durkacz BW. 2003. Radiosensitization and DNA repair inhibition by the combined use of novel inhibitors of DNA-dependent protein kinase and poly(ADP-ribose) polymerase-1. *Cancer Res* 63: 6008-6015.
 44. Wang M, Wu W, Wu W, Rosidi B, Zhang L, Wang H, Iliakis G. 2006. PARP-1 and Ku compete for repair of DNA double strand breaks by distinct NHEJ pathways. *Nucleic Acids Res* 34: 6170-6182.
 45. Weemaes CM, van Tol MJ, Wang J, van Ostaijen-ten Dam MM, van Eggermond MC, Thijssen PE, Aytekin C, Brunetti-Pierri N, van der Burg M, Graham DE et al. 2013. Heterogeneous clinical presentation in ICF syndrome: correlation with underlying gene defects. *EurJHumGenet* 21: 1219-1225.
 46. Woodbine L, Gennery AR, Jeggo PA. 2014. The clinical impact of deficiency in DNA non-homologous end-joining. *DNA Repair (Amst)* 16: 84-96.
 47. Xu GL, Bestor TH, Bourc'his D, Hsieh CL, Tommerup N, Bugge M, Hulten M, Qu X, Russo JJ, Viegas-Pequignot E. 1999. Chromosome instability and immunodeficiency syndrome caused by mutations in a DNA methyltransferase gene. *Nature* 402: 187-191.

SUPPLEMENTAL MATERIALS AND METHODS

Patients

Sera and PBMCs were obtained after informed consent from two ICF2 patients that have been described previously (patients 49 and 55; (Weemaes et al. 2013) and one novel ICF2 patient (p67) carrying the same recessive mutation as patient 49.

Isolation of peripheral blood mononuclear cells and phenotyping of lymphocytes

Peripheral blood mononuclear cells (PBMC) were obtained from patients, family members and healthy donors by Ficoll density gradient separation. PBMC were stored in liquid nitrogen until analysis. Thawed PBMC were stained with the following fluorochrome-labeled antibodies against the indicated cell surface antigen: CD3 (clone #UCHT1) and CD4 (#13B8.2) (Beckman-Coulter); CD8 (#SK1), CD19 (#SJ25C1), CD20 (#L27) CD27 (#L128), CD28 (#L293) and IgM (#G20-127) (BD Biosciences); CCR7 (#150503) (R&D Systems); IgD (rabbit F(ab')₂) (DAKO); CD45RA (#MEM-56) (Invitrogen Life Technologies). DAPI (4',6-diamidino-2-phenylindole) was added to discriminate between live and dead cells. Samples were analyzed on a BD Biosciences LSR II flowcytometer with DIVA software.

In vitro B-cell stimulation and analysis of IgG and IgA production

PBMC (0.25 x 10⁶/well) were cultured in a flatbottom 96-well plate in AIM-V medium supplemented with 5% FCS ultra-low IgG, penicillin/streptomycin (100 IU/mL/100 mg/mL; Life Technologies), 0.05 mg/mL transferrin and 5 mg/mL insulin (Sigma-Aldrich). Added stimuli were: MAB89 (aCD40; 0.5 mg/mL; Beckman-Coulter), aIgM (1 mg/mL; Jackson Immunoresearch), CpG (ODN2006; 1 mg/mL; Invivogen) and IL-21 (20 ng/mL; Peprotech). Supernatants were harvested at day 7 and analyzed for IgG and IgA levels by sandwich ELISA using goat anti-human IgG or IgA (Life Technologies) for coating of the 96-well microtiter plates and alkaline phosphatase conjugated goat anti-human IgG or IgA (Life Technologies) for detection.

Immunoglobulin heavy chain (IgH) repertoire analysis using next generation sequencing

The VH-JH rearrangements, C α and C γ transcripts were amplified from post-ficoll PBMC in a multiplex PCR using the VH1-6 FR1 and JH consensus BIOMED-2 primers (van Dongen et al. 2003) or a consensus C α (IGHA-R; 5'-CTTTCGCTCCAGGTCCACTGAG-3') and C γ primer (3'C γ -CH1 (Tiller et al., 2008)). The primers were adapted for 454 sequencing by adding the forward A or reverse B adaptor, the 'TCAG' key and multiplex identifier (MID) adaptor. PCR products were purified by gel extraction (Qiagen) and Agencourt AMPure XP beads (Beckman Coulter). DNA concentration was measured using the Quant-it Picogreen dsDNA assay (Invitrogen, Carlsbad, CA). Purified PCR products were sequenced on the 454 GS junior instrument (Roche) according to the manufacturer's recommendations, using the GS Junior Titanium emPCR (Lib-A), GS Junior Titanium sequencing and PicoTiterPlate kits for the VH-JH rearrangements, and the GS Junior+ emPCR (Lib-A), GS Junior sequencing XL+ and PicoTiterPlate kits for the C α and C γ transcripts. Using the IGGalaxy Tool (Moorhouse et al. 2014) sequences were demultiplexed based on their MID sequence and quality checked. FASTA files were uploaded in IMG T HighV-Quest (www.imgt.org). Further analysis of the data was done using the IGGalaxy tool. Uniqueness of sequences was defined by V, D and J gene usage and nucleotide sequence of the CDR3 region for the VH-JH rearrangements, and V gene usage, amino acid sequence of the CDR3 region and C gene usage for the C α

and C_γ transcripts. Only unique, productive sequences were used for the analysis and the frequency of mutated nucleotides in the VH gene was calculated from CDR1 until FR3.

Sequencing of switch recombination junctions

Amplification, cloning and sequencing of the Sm-Sa or Sm-Sg fragments derived from PBMC was performed using a previously described PCR strategy (Pan-Hammarstrom et al. 2005). The CSR junctions were determined by aligning the switch fragment sequences with the reference Sm, Sa or Sg sequences. Analysis of the repair pattern of the CSR junctions was performed based on the suggested guidelines (Stavnezer et al. 2010).

Cell culture

U2OS, HEK293, HEK293T and VH10-SV40-immortalized fibroblast cells were grown in DMEM (Gibco) containing 10% FCS (Bodinco BV) and 1% penicillin/ streptomycin unless stated otherwise. U2OS 2–6–3 cells containing 200 copies of a LacO-containing cassette (~4 Mbp) were gifts from Dr. J. Lukas and Dr. S. Janicki (Doil et al. 2009; Shanbhag et al. 2010) and were used to establish U2OS 2-6-3 cell lines stably expressing GFP-tagged XRCC4 using puromycin selection (1 µg/ml). U2OS 2-6-3 cells stably expressing ER-mCherry-LacR-FokI-DD, which were a gift from Dr. R. Greenberg (Tang et al. 2013), were induced for 5 h by 1 µM Shield-1 (Clontech) and 1 µM 4-OHT (Sigma).

Plasmids

The full-length cDNA of human ZBTB24 was obtained by RT-PCR and flanking restriction sites for conventional cloning (BglII/SalI) were introduced using a nested PCR on the cDNA. The obtained PCR product was subsequently cloned into pEGFP-C1 and pEGFP-N1 (both Clontech) using the BglII and SalI restriction sites. The GST-ZBTB24 expression vector was generated by cloning the ZBTB24 ORF from pEGFP-C1-ZBTB24 as a BglII/ EcoRI fragment into BamHI/EcoRI-digested pGEX-6p-3 (GE Healthcare). The Myc-ZBTB24 expression vector was obtained by exchanging GFP, using the AgeI and BglII restriction sites, for a single Myc tag (EQKLISEEDL) by oligo annealing in the pEGFP-ZBTB24 construct. Deletion constructs were generated by amplifying the specified regions using internal primers containing BglII (forward) or EcoRI (reverse) and subsequent exchange of the deletion fragments for the full length cDNA. All ZBTB24 expression constructs were verified using Sanger sequencing. mCherry-PARG wt/cd were kindly provided by Michael Hendzel (Ismail et al., 2012) and GFP-PARP1 was obtained from Valerie Schreiber (Mortusewicz et al. 2007).

An IRES-Puro cassette was amplified by PCR and inserted into EGFP-C1 (Addgene). The XRCC4 cDNA, a generous gift of P. Jeggo (Girard et al. 2004), was inserted into EGFP-C1-IRES-Puro. Single U2OS clones stably expressing EGFP-XRCC4 were isolated after selection on puromycin (1 mg/ml). Immunoblotting with anti-GFP antibody showed that the XRCC4 fusion proteins were expressed at the expected molecular weight.

Transfections and RNA interference

siRNA and plasmid transfections were performed using Lipofectamine RNAiMAX (Invitrogen), Lipofectamine 2000 (Invitrogen), and JetPEI (Polyplus Transfection), respectively, according to the manufacturer's instructions. siRNA sequences are listed in Table S5. Cells were transfected twice with siRNAs (40 or 80 nM) within 24 h and examined further 48 h after the second transfection unless stated otherwise. PARP inhibitor (KU-0058948) was a gift from Mark O'Connor and was used at a concentration of 10 µM. The DNA-PK inhibitor (NU7026,

EMD Biosciences) was used at a concentration of 10 μ M.

Non-homologous end-joining assay

HEK293 cell lines containing a stably integrated copy of the EJ5-GFP reporter were used to measure the repair of I-SceI-induced DSBs or NHEJ (Pierce et al. 1999; Bennardo et al. 2008). Briefly, 48 h after siRNA transfection, cells were transfected with the I-SceI expression vector pCBASce and a mCherry expression vector. 48 h later the fraction of GFP-positive cells among the mCherry-positive cells was determined by FACS on a BD LSRII flow cytometer (BD Bioscience) using FACSDiva software version 5.0.3. Quantifications were performed using Flowing software 2.5.1 (by Perttu Terho in collaboration with Turku Bioimaging).

Plasmid integration assay

Upon siRNA mediated knockdown of the indicated genes, U2OS cells were transfected with XhoI/BamHI-linearized pEGFP-C1 plasmid DNA. After overnight transfection, a fraction of cells was used to determine transfection efficiency, as measured by the amount of GFP positive cells using the ArrayScan high content analysis reader (Thermo Scientific) using the target activation protocol. In parallel cells were seeded on 14 cm plates at a density of 10.000 and 2.000 cells per plate for determination of the cloning efficiency with and without G418 (0.5 mg/ml, Gibco) selection respectively. After 10 days, cells were washed in 0.9% NaCl and stained with methylene blue. NHEJ efficiency was calculated as follows: (cloning efficiency G418 selection) / ((cloning efficiency without selection) x (transfection efficiency)) and subsequently normalized to the luciferase control.

Cell cycle profiling

For cell cycle analysis cells were treated as described in figure legends and fixed in 70% ethanol, followed by DNA staining with 50 μ g/ml propidium iodide in the presence of RNase A (0.1 mg/ml). Cell sorting was performed on a flow cytometer (LSRII; BD) using FACSDiva software (version 5.0.3; BD). Quantification was performed using Flowing software 2.5.1.

Cell survival assay

VH10-SV40 cells were transfected with siRNAs, trypsinized, seeded at low density, and exposed to IR at indicated doses. Seven days later cells were washed with 0.9% NaCl and stained with methylene blue. Colonies of more than 10 cells were counted and relative survival compared to the untreated sample was calculated.

RNA expression analysis by RT-qPCR and RNA sequencing

Gene expression analysis using quantitative realtime PCR was carried out as described before (Helfricht et al. 2013). Briefly, RNA isolation was done using the miRNeasy minikit (Qiagen) and subsequently polydT primed cDNA was generated using the RevertAid first strand cDNA synthesis kit (Thermo scientific) according to manufacturer's instructions. Realtime qPCR was performed in duplicate on the CFX96/384 system using SYBR green master mix (Bio-Rad). Primers, which are listed in Table 5S, were designed using Primer3Plus software (<http://primer3plus.com>). Relative expression levels were obtained with the CFX manager (version 3.0), correcting for primer efficiencies and using GAPDH and GUSB as reference genes. For RNA sequencing, the RNA 6000 Nano kit (Agilent technologies) was used to confirm RNA integrity before the RNA was subjected to poly(A) enrichment. cDNA synthesis, library preparation and sequencing were carried out using the Ion Total RNA-Seq

kit V2, the Ion PI Template OT2 200 Kit v3 and the Ion Sequencing 200 kit v3, respectively, according to the manufacturer's instructions (Thermo Fisher Scientific). RNA was sequenced on an Ion Proton System at a depth of approximately 20 million reads per sample, with a median read length of 90bp. Sequence files obtained in the bam format were converted to fastq using the bam2fastq conversion utility from the bedtools package. Reads were aligned to the human genome build GRCh37 - Ensembl using Tophat2 (Version 2.0.10). In a second alignment step, Bowtie2 (Version 2-2.10) was used in the local, very sensitive mode to align remaining un-aligned reads. HTSeq-Count (Version 0.6.1) was used with default settings to quantify gene expression. Finally, DESeq (Version 1.2.10) was used to generate a list of genes differentially expressed between ZBTB24-depleted and control cells (Table S2).

Sample preparation and mass spectrometry

For stable isotope labeling by amino acids in cell culture (SILAC), U2OS cells were cultured for 14 days in light (L) ([12C6,14N2]lysine/[12C6,14N4]arginine) or heavy (H) ([13C6,15N2]lysine/[13C6,15N4]arginine) SILAC medium. SILAC-labeled cells were transiently transfected with either GFP-PARP1 or GFP-ZBTB24 (H) and an empty vector (L). Equal amounts of H and L cells were lysed separately in EBC-150 buffer (50 mM Tris-HCl pH 7.5, 150 mM NaCl, 0.5% NP-40, 1 mM EDTA) supplemented with protease and phosphatase inhibitor cocktails. The lysed cell suspension was sonicated 6 times for 10s on ice and subsequently incubated with 500 U Benzoyl-DL-arginine hydrochloride for 1 hour under rotation. The NaCl concentration was increased to 300 mM and the cleared lysates were subjected to GFP immunoprecipitation with GFP Trap beads (Chromotek). The beads were then washed 2 times with EBC-300 buffer (50 mM Tris, pH 7.5, 300 mM NaCl, 0.5% NP-40, 1 mM EDTA) and 2 times with 50 mM (NH₄)₂CO₃ followed by overnight digestion using 2.5 µg trypsin at 37°C under constant shaking. Peptides of the H and L precipitates were mixed and desalted using a Sep-Pak tC18 cartridge by washing with 0.1 % acetic acid. Finally, peptides were eluted with 0.1 % acetic acid/60 % acetonitrile and lyophilized. Samples were analyzed by nanoscale LC-MS/MS using an EASY-nLC system (Proxeon) connected to a Q-Exactive Orbitrap (Thermo). Peptides were separated in a 13 cm analytical column with inner-diameter of 75 µm, in-house packed with 1.8 µm C18 beads (ReproSpher, Dr. Maisch). The gradient length was 120 minutes with a flow rate of 200nL/minutes. Data dependent acquisition was used with a top 10 method. Full-scan MS spectra were acquired at a target value of 3 x 10⁶ and a resolution of 70,000, and the Higher-Collisional Dissociation (HCD) tandem mass spectra (MS/MS) were recorded at a target value of 1 x 10⁵ and with resolution of 17,500 with a normalized collision energy (NCE) of 25%. The precursor ion masses of scanned ions were dynamically excluded (DE) from MS/MS analysis for 60 sec. Ions with charge 1, and greater than 6 were excluded from triggering MS² events (Hendriks et al. 2014). Analysis of raw data was performed using MaxQuant software (Cox and Mann 2008).

Protein interaction studies

To study ZBTB24 interactions, cells expressing the indicated GFP fusion proteins were lysed in 1 ml EBC buffer (50 mM Tris, pH 7.3, 150 mM NaCl, 0.5% NP-40, 2.5 mM MgCl) supplemented with protease and phosphatase inhibitor cocktails (Roche). Lysis and protein extraction were enhanced by 6 x 10" sonication in a sonicator bath (Bioruptor UCD-20, Diagenode, Liège, Belgium) followed by 1 hour incubation with 500 units benzoyl-DL-arginine hydrochloride (Novagen) on ice. Upon centrifugation, cleared lysates were subjected to immunoprecipitation with GFP Trap beads (Chromotek) for 1.5 h at 40C top over top. Beads were washed 6 times with cold EBC buffer,

boiled in Laemmli buffer and interacting proteins were visualized using western blot analysis.

Western blot analysis

Protein extracts were generated by direct lysis of cells in 2x Laemmli buffer and boiled for 10' at 95°C. Proteins were size separated using Novex 4-12% Bis-Tris mini gels (Invitrogen) or 4–12% Criterion XT Bis-Tris gels (Bio-rad) in 1x MOPS buffer (Invitrogen) and transferred to PVDF membranes, which were blocked in 4% milk for at least 30 minutes and incubated with the indicated antibodies overnight. Several wash steps before and after 1 h incubation with secondary antibodies rabbit-anti-700 and mouse-anti-800 (Sigma) were executed. Protein bands were visualized using the Odyssey infrared imaging system or the C-Digit blot scanner (both Licor) according to manufacturer's instructions.

Laser micro-irradiation

Multiphoton laser micro-irradiation was performed on a Leica SP5 confocal microscope equipped with an environmental chamber set to 37°C and 5% CO₂ as described (Helfricht et al. 2013). Briefly, U2OS cells were grown on 18 mm glass coverslips and media was replaced with colorless DMEM or CO₂-independent Leibovitz L15 medium, both supplemented with 10% FCS and pen/strep. Cells were placed in a Chamlide TC-A live-cell imaging chamber before imaging and were kept at 37°C. DSB-containing tracks (1 or 1.5 μm width) were generated with a Mira modelocked Ti:Sapphire laser ($\lambda = 800$ nm, pulselength = 200 fs, repetition rate = 76 MHz, output power = 80 mW). Typically, cells were micro-irradiated with 1 iteration per pixel using LAS-AF software. For live cell imaging, confocal images were recorded before and after laser irradiation at different time intervals. For UV-A laser micro-irradiation U2OS cells were sensitized with 10 μM 5-bromo-2-deoxyuridine (BrdU) for 24 h, as described (Helfricht et al. 2013). For micro-irradiation, the cells were placed on the stage of a Leica DM IRBE widefield microscope stand (Leica) integrated with a pulsed nitrogen laser (Micropoint Ablation Laser System, Photonic Instruments, Inc; 16 Hz, 364 nm), which was directly coupled to the epifluorescence path of the microscope and focused through a Leica 40× HCX PLAN APO 1.25–0.75 oil-immersion objective. The laser output power was set to 78 to generate strictly localized sub-nuclear DNA damage and images were taken before and after micro-irradiation at the indicated time-points or after immunofluorescent labeling using Andor IQ software.

Immunofluorescent labeling

Immunofluorescent labeling of γ H2AX and XRCC4 was performed as described previously (Helfricht et al. 2013). Briefly, cells were grown on glass coverslips and treated as indicated in the figure legends. Subsequently, cells were washed with PBS, fixed with 4% formaldehyde for 15 min and treated with 0.25% Triton X-100 in PBS for 5 min. Cells were rinsed with PBS and equilibrated in WB (PBS containing 5 g BSA/L, 1.5 g glycine/L) prior to immunostaining. Detection was done using goat anti-mouse or goat anti-rabbit IgG coupled to Alexa 488, 555 or 647 (Invitrogen Molecular probes). Samples were incubated with 0.1 μg/ml DAPI and mounted in Polymount.

Microscopy analysis

Images of fixed samples were acquired on a Zeiss AxioImager M2 or D2 widefield fluorescence microscope equipped with 40×, 63×, and 100× PLAN APO (1.4 NA) oil-immersion objectives (Zeiss) and an HXP 120 metal-halide lamp used for excitation. Fluorescent probes were

detected using the following filters: DAPI (excitation filter: 350/50 nm, dichroic mirror: 400 nm, emission filter: 460/50 nm), GFP/Alexa 488 (excitation filter: 470/40 nm, dichroic mirror: 495 nm, emission filter: 525/50 nm), mCherry (excitation filter: 560/40 nm, dichroic mirror: 585 nm, emission filter: 630/75 nm), Alexa 555 (excitation filter: 545/25 nm, dichroic mirror: 565 nm, emission filter: 605/70 nm), Alexa 647 (excitation filter: 640/30 nm, dichroic mirror: 660 nm, emission filter: 690/50 nm). Images recorded after multi-photon- and UV-A-laser micro-irradiation and immunofluorescence stainings were analyzed using ImageJ. The average pixel intensity of laser tracks induced by either the multi-photon- or the UV-A laser system was measured within the locally irradiated area (I_{damage}), in the nucleoplasm outside the locally irradiated area (I_{nucleoplasm}) and in a region not containing cells in the same field of view (I_{background}) using ImageJ. The relative level of accumulation expressed relative to the protein level in the nucleoplasm was calculated as follows: $((I_{\text{damage}} - I_{\text{background}})/(I_{\text{nucleoplasm}} - I_{\text{background}}) - 1)$. The accumulation in the control cells transfected with siLUC within each experiment was normalized to 100%. Images obtained from live cell imaging after multi-photon micro-irradiation were analyzed using LAS-AF software. Fluorescence intensities were subtracted by the pre-bleach values and normalized to the first data point, which was set to 0, to obtain relative fluorescence units (RFU). The average reflects the quantification of between 50–150 cells from 2–3 independent experiments.

Antibodies

Immunofluorescence and western blot analysis were performed using antibodies against GFP (1:1000, #11814460001, Roche), PARP1 (1:1000, #9542, Cell Signaling, Alexis), Myc (1:1000, 9E10, SC-40, Santa Cruz), γ H2AX (1:1000, #07-164, Millipore), α -Tubulin (Sigma), DNA-PKcs (1:500, ab1832, Abcam), LIG4 (1:1000, #80514, Abcam), XRCC4 (1:500, gift from Mauro Modesti), Histone H3 (1:2000, #1791, Abcam), GST (1:2000, Amersham), PARP1 (1:1000, #9542S, Cell Signaling), PARP2 (1:500, #C3956, Sigma), PAR (1:1000, #4336-BPC-100, Trevigen; used in Fig. 5A-B) and PAR monoclonal 10H, which was purified from the culture medium of 10H hybridoma obtained from Dr. Miwa through the Riken cell ban (Kawamitsu et al. 1984).

GST protein purification

For GST purifications 50 ml cultures of *E. coli* BL21 cells containing pGEX or pGEX-ZBTB24 plasmid were grown to an OD₆₀₀ of 0.6 absorbance units. 2 mM IPTG was added and cells were incubated overnight at 20 °C. After centrifugation cell pellets were frozen and stored at -80 °C. For protein purification cell pellets were lysed at room temperature for 30 minutes in 2.5 ml lysis buffer (125 mM Tris-HCl pH 8, 150 mM NaCl, 1 mM MgCl₂, 5 mM DTT, 0.1 volume BugBuster 10x (Novagen-Merck), 2500 units rLysozyme (Novagen-Merck), 62.5 units benzonase (Novagen-Merck), Protease Inhibitor Cocktail EDTA-free (Sigma-Aldrich)). The lysate was centrifuged at 4 °C in a table centrifuge for 10 minutes at full speed. Supernatant was taken and incubated with 500 μ l Glutathione Superflow Agarose beads (Life Technologies) for 2 hrs at 4 °C. The Agarose beads were packed in a column and loaded on an ÄKTA chromatography system (GE Healthcare Biosciences). The column was rinsed using a wash buffer (125 mM Tris-HCl pH8, 150 mM NaCl, 10 mM β -mercaptoethanol) and eluted using wash buffer supplemented with 10 mM reduced glutathione (Sigma-Aldrich). Fractions with purified protein were collected and concentrated using 50kD Vivaspin ultrafiltration cups (Sartorius). Finally, the buffer was changed in ultrafiltration cups to 125

mM Tris-HCl pH8, 150 mM NaCl, 10% glycerol, and purified proteins were frozen in liquid nitrogen and stored at -80 °C.

Analysis of protein PARylation

Cells were washed with ice-cold PBS supplemented with PARG inhibitor (PARGi; 400 nM Tannic acid), scraped in a small volume of PBS with PARGi and transferred to low binding tubes, followed by high speed centrifugation at 4°C. Cells were lysed in RIPA buffer (10 mM Tris-HCl (pH 8), 1% Triton X-100, 0.1% deoxycholate, 0.1% SDS, 100 µM Tannic acid) supplemented with protease and phosphatase inhibitor cocktails (Roche) comprising a NaCl-concentration of 450 mM. After centrifugation, cleared lysates were subjected to immunoprecipitation with GFP Trap beads (Chromotek) for 2 hours on a rotating wheel in the presence of 150 mM NaCl. Beads were washed 6 times with RIPA buffer containing increasing NaCl concentrations (150 mM and 1 M) followed by 2 washes with TBS-T buffer (20x TBS, 0.1% Tween, 100 µM Tannic acid). After boiling in Laemmli buffer the interacting proteins were visualized using western blot analysis.

Production of radiolabeled PAR

PARP1 activation assays were carried out as described earlier (Shah et al. 2011) with minor modifications. To prepare radiolabeled PAR, purified bovine PARP1 was activated at 30°C for 30 min in 900 µl reaction mix (100 mM Tris-HCl pH 8.0, 10mM MgCl₂, 10 % glycerol, 10 mM DTT, 500 µM cold NAD, 250 µCi of 32P-NAD (350 nM), 10% ethanol and 23 µg activated calf thymus DNA). Auto-PARylated PARP1 was precipitated on ice for at least 30 min by addition of 100 µl 3 M Na-acetate pH 5.2 and 700 µl isopropanol. After centrifugation, pellet was washed twice with ethanol, air-dried and dissolved (1M KOH, 50 mM EDTA), while heating at 60°C for 1 h. Upon addition of AAGE9 (250 mM NH₄OAc, 6 M guanidine-HCl, 10 mM EDTA), pH was adjusted to 9.0 and solution was loaded onto DHBB resin in Econocolumns (BioRad). Resin was washed with AAGE9 and NH₄-acetate pH 9.0. The polymer was eluted with water at 37°C in separate fractions and stored at -30°C till usage in southwestern assays.

Southwestern assay

The southwestern assay was carried out as described (Robu et al. 2013). Briefly, IP samples were resolved on 8% denaturing PAGE gels along with purified human PARP1 (Aparptosis) as a positive control. Gels were incubated for 1 h with gentle agitation in SDS-PAGE running buffer (20-30 ml 25 mM Tris 7.5, 192 mM glycine, 5 % β-mercaptoethanol, 0.1% SDS) followed by protein transfer to a nitrocellulose membrane at 4°C. Membrane were rinsed three times with TST buffer (10 mM Tris pH 7.5, 150 mM NaCl, 0.05 % Tween) and incubated in 20 ml TST buffer supplemented with 250 nM radioactive PAR polymer on a shaker at room temperature for 1 h, followed by three washes with TST and one wash with TST buffer containing 500 mM NaCl. After a final wash with regular TST, membranes were dried and either exposed to a film or a phosphorimager screen to detect radioactivity. Afterwards membranes were blocked in 5 % milk containing 0.1 % Tween and probed for PARP and GFP with the indicated antibodies.

PARP1 activation assays

To examine the stimulatory effect of ZBTB24 on the catalytic activity of PARP1, PARP1 activation reactions were carried out in a 20 µl assay volume with 0.4 pmol of PARP1, 160 ng activated DNA and 100 µM unlabeled NAD at 30°C for 10 min with no other protein (control)

or varying molar ratios of GST-ZBTB24 or GST over PARP1. The reactions were stopped by the addition of equal volumes of 2x Laemmli buffer. Aliquots from each sample were resolved on 6 or 10 % SDS-PAGE followed by immunoblotting for PAR, PARP1 and GST.

PAR protection assays

To examine the effect of ZBTB24 on PAR protection, PARP1 activation reactions were carried out in a 15 μ l assay volume with 4 pmol of PARP1, 3 μ g of activated and 100 μ M unlabeled NAD at 30°C for 30 min to allow the formation of autoPARylated PARP1. The reaction was stopped by the addition of 1 μ l of 1 mM PARPi (PJ-34). 1/10th of the reaction mixes containing 0.4 pmols of PARP1 were reacted for 15 min with no other protein (control) or varying molar ratios of GST-ZBTB24 or GST over PARP1. All samples were reacted at 30°C for 15 min in the PARG-assay buffer (50 mM Tris-Cl pH 7.5 containing 50 mM KCl, 1.5 mM DTT, 0.1 mg/ml BSA, 2.5 mM EDTA) with 5 ng PARG (Sigma), whereas the undigested PAR samples were mock-treated with PARG assay buffer. The reactions were stopped by the addition of equal volumes of 2X Laemmli buffer. Aliquots from each sample were resolved on 6 or 10 % SDS-PAGE followed by immunoblotting for PAR, PARP1 and GST.



SUPPLEMENTAL REFERENCES

1. Bennardo N, Cheng A, Huang N, Stark JM. 2008. Alternative-NHEJ is a mechanistically distinct pathway of mammalian chromosome break repair. *PLoSGenet* 4: e1000110.
2. Cox J, Mann M. 2008. MaxQuant enables high peptide identification rates, individualized p.p.b.-range mass accuracies and proteome-wide protein quantification. *NatBiotechnol* 26: 1367-1372.
3. Doil C, Mailand N, Bekker-Jensen S, Menard P, Larsen DH, Pepperkok R, Ellenberg J, Panier S, Durocher D, Bartek J et al. 2009. RNF168 binds and amplifies ubiquitin conjugates on damaged chromosomes to allow accumulation of repair proteins. *Cell* 136: 435-446.
4. Girard PM, Kysela B, Harer CJ, Doherty AJ, Jeggo PA. 2004. Analysis of DNA ligase IV mutations found in LIG4 syndrome patients: the impact of two linked polymorphisms. *HumMolGenet* 13: 2369-2376.
5. Helfricht A, Wiegant WW, Thijssen PE, Vertegaal AC, Luijsterburg MS, van Attikum H. 2013. Remodeling and spacing factor 1 (RSF1) deposits centromere proteins at DNA double-strand breaks to promote non-homologous end-joining. *Cell Cycle* 12: 3070-3082.
6. Hendriks IA, D'Souza RC, Yang B, Verlaan-de VM, Mann M, Vertegaal AC. 2014. Uncovering global SUMOylation signaling networks in a site-specific manner. *NatStructMolBiol* 21: 927-936.
7. Kawamitsu H, Hoshino H, Okada H, Miwa M, Momoi H, Sugimura T. 1984. Monoclonal antibodies to poly(adenosine diphosphate ribose) recognize different structures. *Biochemistry* 23: 3771-3777.
8. Moorhouse MJ, van ZD, Ijspeert H, Hiltemann S, Horsman S, van der Spek PJ, van der Burg M, Stubbs AP. 2014. ImmunoGlobulin galaxy (IGGalaxy) for simple determination and quantitation of immunoglobulin heavy chain rearrangements from NGS. *BMCImmunol* 15: 59.
9. Mortusewicz O, Ame JC, Schreiber V, Leonhardt H. 2007. Feedback-regulated poly(ADP-ribosyl)ation by PARP-1 is required for rapid response to DNA damage in living cells. *Nucleic Acids Res* 35: 7665-7675.
10. Murray JE, van der Burg M, Ijspeert H, Carroll P, Wu Q, Ochi T, Leitch A, Miller ES, Kysela B, Jawad A et al. 2015. Mutations in the NHEJ component XRCC4 cause primordial dwarfism. *AmJHumGenet* 96: 412-424.
11. Pan-Hammarstrom Q, Jones AM, Lahdesmaki A, Zhou W, Gatti RA, Hammarstrom L, Gennery AR, Ehrenstein MR. 2005. Impact of DNA ligase IV on nonhomologous end joining pathways during class switch recombination in human cells. *JExpMed* 201: 189-194.
12. Pierce AJ, Johnson RD, Thompson LH, Jasin M. 1999. XRCC3 promotes homology-directed repair of DNA damage in mammalian cells. *Genes Dev* 13: 2633-2638.
13. Robu M, Shah RG, Petittler N, Brind'Amour J, Kandan-Kulangara F, Shah GM. 2013. Role of poly(ADP-ribose) polymerase-1 in the removal of UV-induced DNA lesions by nucleotide excision repair. *ProcNatlAcadSciUSA* 110: 1658-1663.
14. Shah GM, Kandan-Kulangara F, Montoni A, Shah RG, Brind'Amour J, Vodenicharov MD, Affar eB. 2011. Approaches to detect PARP-1 activation in vivo, in situ, and in vitro. *Methods MolBiol* 780: 3-34.
15. Shanbhag NM, Rafalska-Metcalf IU, Balane-Bolivar C, Janicki SM, Greenberg RA. 2010. ATM-dependent chromatin changes silence transcription in cis to DNA double-strand breaks. *Cell* 141: 970-981.
16. Stavnezer J, Bjorkman A, Du L, Cagigi A, Pan-Hammarstrom Q. 2010. Mapping of switch recombination junctions, a tool for studying DNA repair pathways during immunoglobulin class switching. *AdvImmunol* 108: 45-109.
17. Tang J, Cho NW, Cui G, Manion EM, Shanbhag NM, Botuyan MV, Mer G, Greenberg RA. 2013. Acetylation limits 53BP1 association with damaged chromatin to promote homologous recombination. *Nat Struct Mol Biol* 20: 317-325.
18. van Dongen JJ, Langerak AW, Bruggemann M, Evans PA, Hummel M, Lavender FL, Delabesse E, Davi F, Schuurink E, Garcia-Sanz R et al. 2003. Design and standardization of PCR primers and protocols for detection of clonal immunoglobulin and T-cell receptor gene recombinations in suspect lymphoproliferations: report of the BIOMED-2 Concerted Action BMH4-CT98-3936. *Leukemia* 17: 2257-2317.
19. Weemaes CM, van Tol MJ, Wang J, van Ostaijen-ten Dam MM, van Eggermond MC, Thijssen PE, Aytekin C, Brunetti-Pierri N, van der Burg M, Graham DE et al. 2013. Heterogeneous clinical presentation in ICF syndrome: correlation with underlying gene defects. *EurJHumGenet* 21: 1219-1225.

SUPPLEMENTAL FIGURES

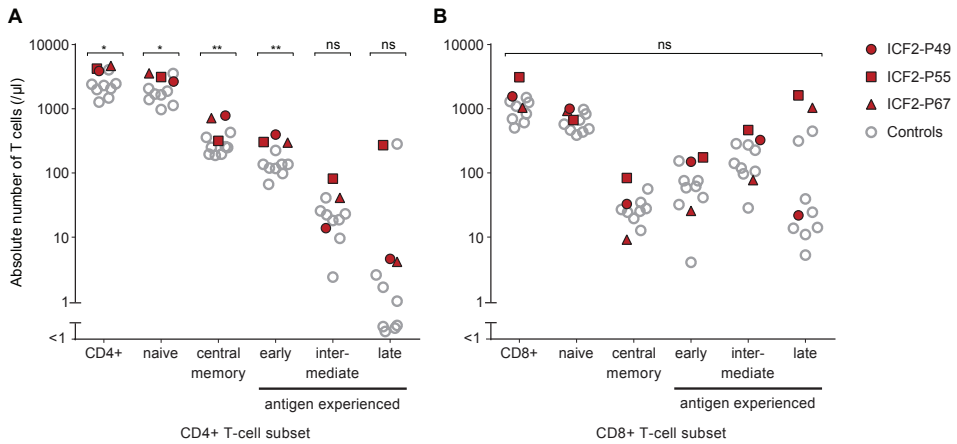
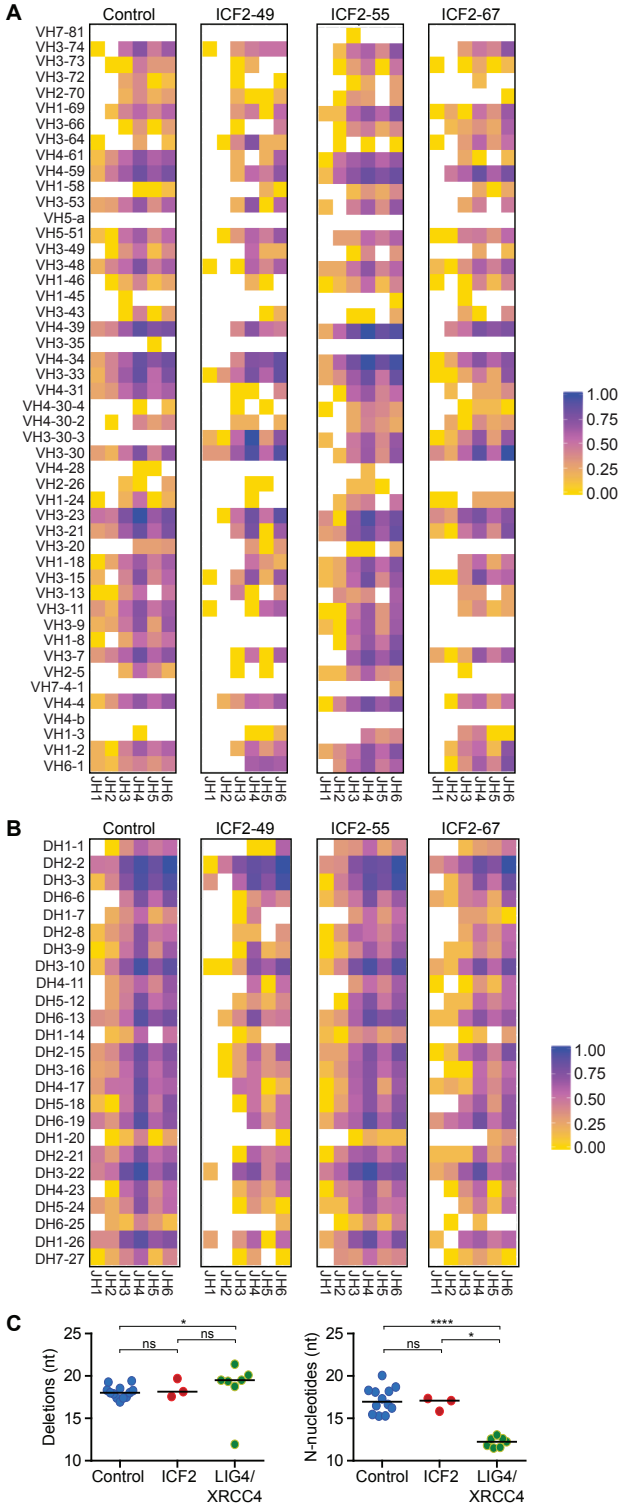


Figure S1. T-cell differentiation in ICF2 patients (related to Fig. 1). Absolute numbers (per μL) of the peripheral blood CD3+CD4+ T-cell subset (A) and CD3+CD8+ T-cell subset (B) and the indicated differentiation stages in both subsets were determined in the ICF2 patients P49, P55 and P67 (closed red symbols) and eight healthy age-matched controls (open grey circles, age range 0.8 to 4.3 years) by flow cytometry. These studies were performed with patient PBMC obtained at the age of 0.9, 0.8 and 3.6 years, respectively. Phenotypic definitions: naïve T cells: CD45RA+CCR7+; central memory T cells: CD45RA-CCR7+; antigen experienced CD4+ T cells CD45RA-/+CCR7-: early CD28+CD27+; intermediate CD28+CD27-; late CD28-CD27-; antigen experienced CD8+ T cells CD45RA-/+CCR7-: early CD28+CD27+; intermediate CD28-CD27+; late CD28-CD27-.



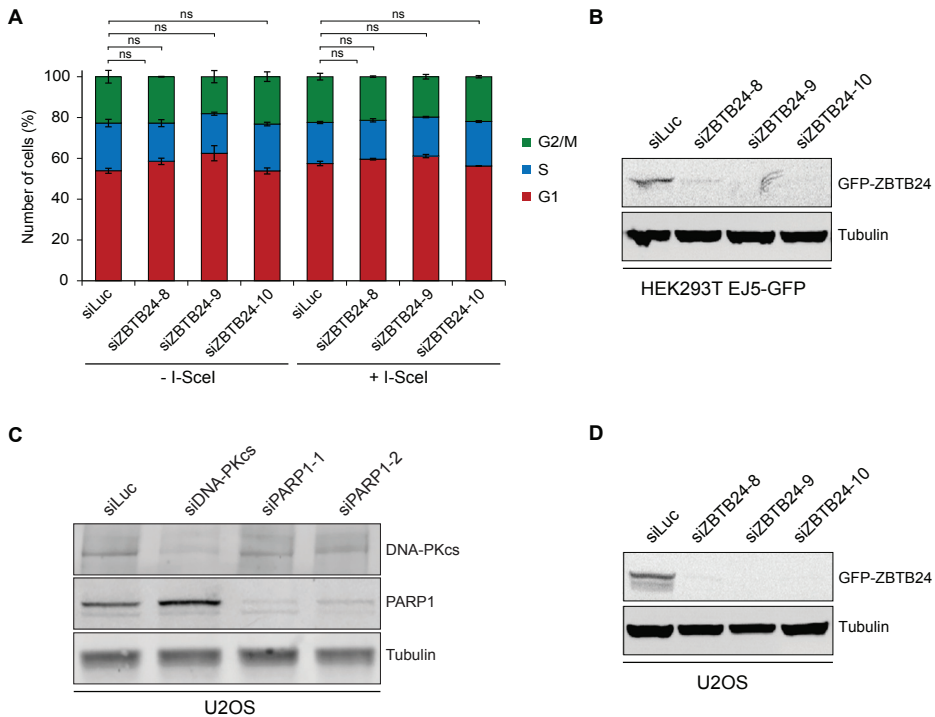


Figure S3. Knockdown of ZBTB24 does not affect cell cycle progression (related to Fig. 2). (A) HEK293T cells containing the EJ5-GFP reporter were transfected with the indicated siRNAs. 48 h later cells were transfected with a control vector or the I-SceI expression vector (pCBASce). After an additional 24 h cells were subjected to propidium iodide staining followed by flow cytometry analysis. The percentage of cells in G1 (red bar), S (blue bar) and G2/M (green bar) phase is presented. (B) HEK293T EJ5-GFP cells were treated with the indicated siRNAs. 48 h later, cells were transiently transfected with GFP-ZBTB24. WCEs were prepared 24 h later and subjected to western blot analysis for GFP. Tubulin is a loading control. (C) U2OS cells were treated with the indicated siRNAs. WCEs were prepared 48 h later and subjected to western blot analysis for DNA-PKcs and PARP1. Tubulin is a loading control. (D) As in B, except that U2OS cells were used.

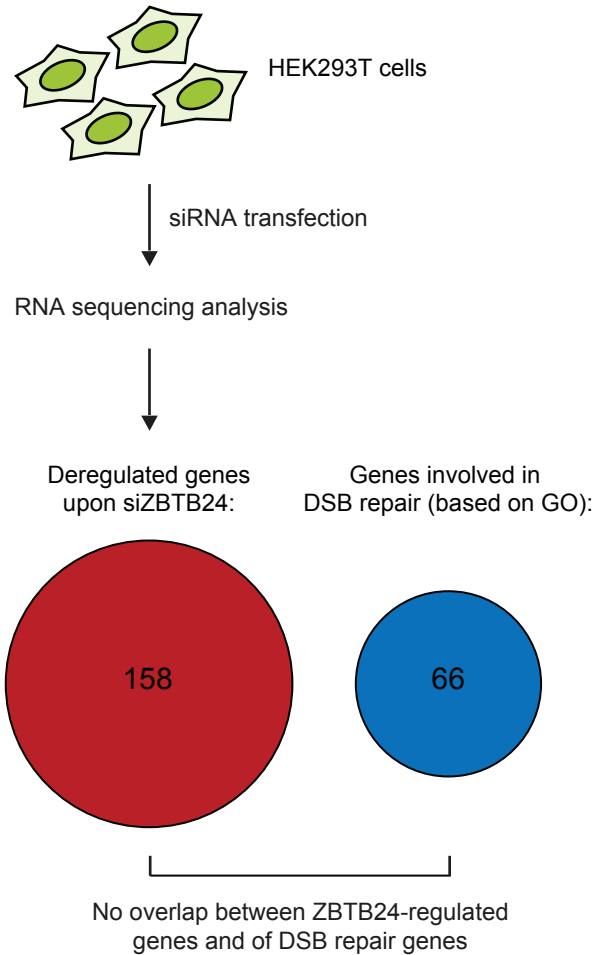


Figure S4. ZBTB24 does not regulate the expression of genes involved in DSB repair (related to Fig. 2). HEK293T cells were treated with control siRNAs against Luciferase or 3 different siRNAs against ZBTB24. Four days later RNA was isolated and subjected to RNA sequencing analysis. The number of genes found to be commonly misregulated following ZBTB24-depletion with each of the siRNAs is presented (FDR < 0.05). Importantly, GO-term analysis (0006302; DSB repair) did not reveal the presence of DSB repair genes among the misregulated genes.

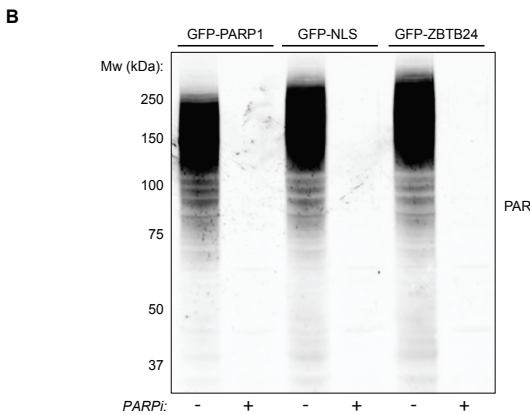
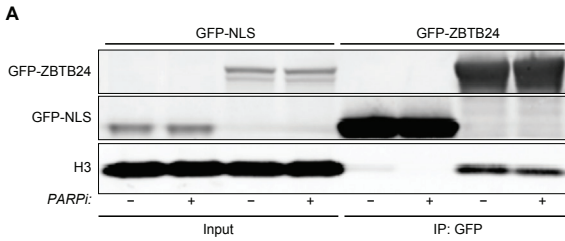


Figure S5. ZBTB24 interacts with histone H3 (related to Fig. 3). (A) U2OS cells transiently expressing GFP-ZBTB24 or GFP-NLS were either treated with DMSO (Mock) or with PARPi. WCEs were subjected to GFP-IP followed by western blot analysis of the indicated proteins. (B) U2OS cells transfected with the indicated GFP-tagged proteins were either treated with DMSO (Mock) or PARPi. WCEs were prepared and subjected to western blot analysis to assess total PAR levels.

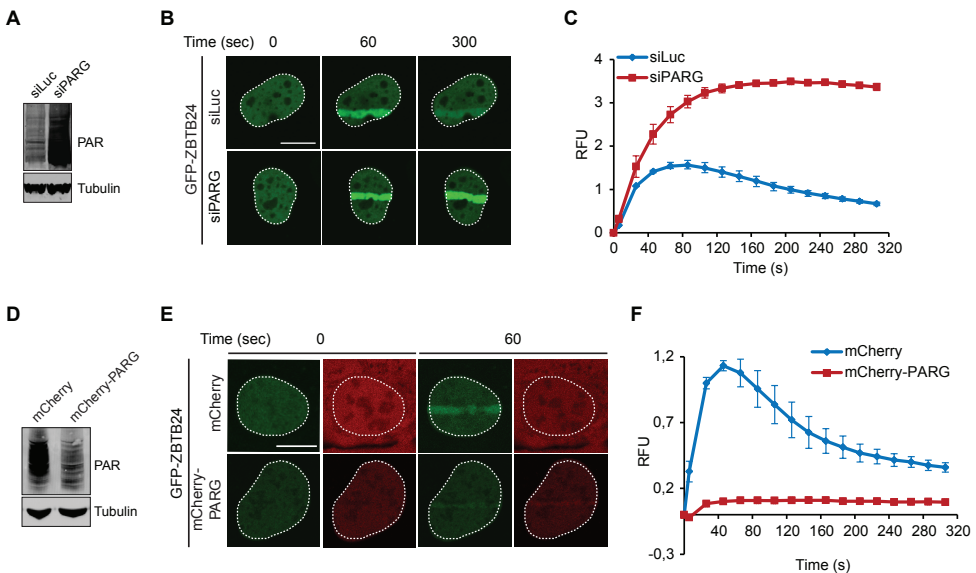


Figure S6. PARG-dependent turnover of PAR chains modulates the accumulation of ZBTB24 at sites of DNA damage (related to Fig. 3). (A) Western blot analysis showing total PAR levels in U2OS cells transfected with the indicated siRNAs and transiently expressing GFP-ZBTB24. Tubulin is loading control. (B) GFP-ZBTB24 accumulation as monitored at the indicated time points after laser micro-irradiation in cells from A. (C) Quantification of the results from B. RFU is Relative Fluorescent Units. (D) As in A, except that cells were co-transfected with a GFP-ZBTB24 and either a mCherry or mCherry-PARG expression vector were used. (E) As in B, expect that cells from D were used. (F) Quantification of the results from E. Scale bar 10 μ m.

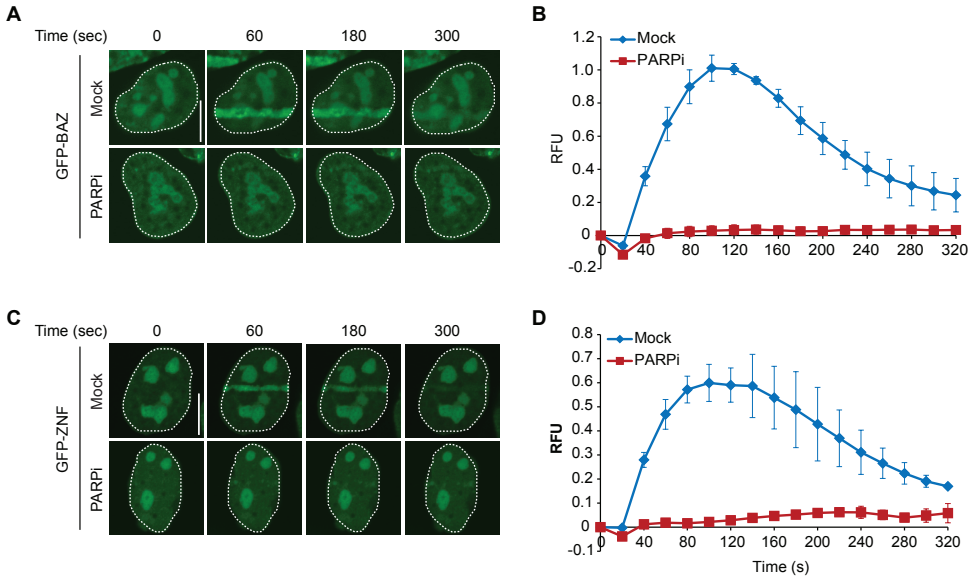


Figure S7. The ZNF domain of ZBTB24 accumulates at sites of DNA damage in a PARP-dependent manner (related to Fig. 4). (A) U2OS cells transiently expressing GFP-tagged BAZ domains of ZBTB24 were treated with DMSO (Mock) or PARPi, and subjected to laser micro-irradiation to follow GFP-BAZ accumulation at sites of DNA damage at the indicated time points after irradiation. Representative images are shown. RFU is Relative Fluorescence Units. Scale bar 10 μ m. (B) Quantification of A. (C) As in A, except for the GFP-tagged ZNF domain of ZBTB24 (GFP-ZNF). (D) Quantification of C.

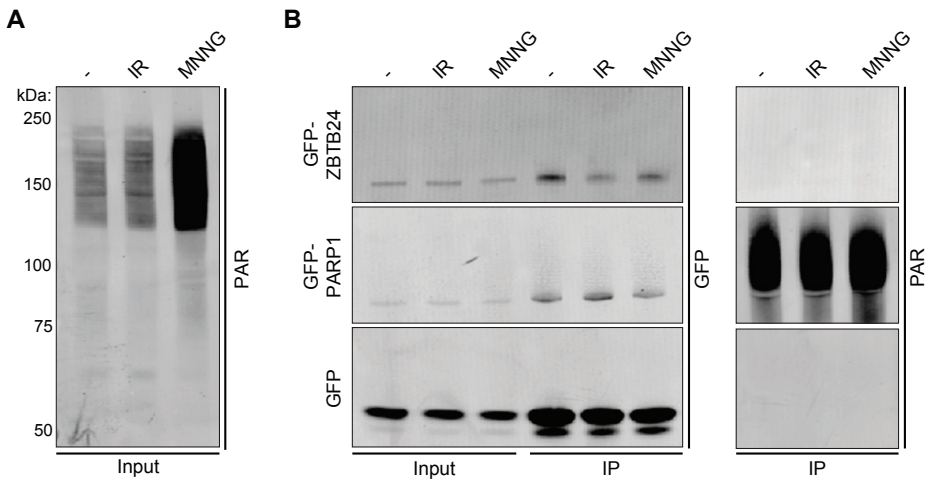


Figure S8. ZBTB24 is not PARylated following DNA damage induction (related to Fig. 4). (A) U2OS cells expressing GFP were left untreated, or treated with IR or MNNG. WCE were prepared and subjected to western blot analysis for global PAR levels. (B) WCE extracts from A and from cells expressing GFP-ZBTB24 or GFP-PARP1 were subjected to GFP-IP. Washes were performed under high-salt conditions to remove interacting proteins. Western blot analysis was done for the indicated proteins and PAR. The experiment was performed 2 times for PARP1 and 4 times for ZBTB24. Blots from a representative experiment are show.

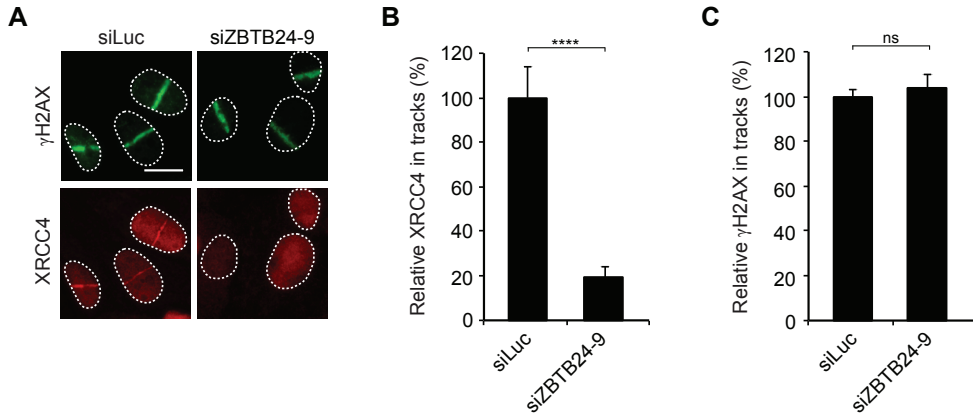


Figure S9. ZBTB24 promotes the recruitment of endogenous XRCC4 to sites of DNA damage (related to Fig. 6). (A) Accumulation of γ H2AX and endogenous XRCC4 at sites of laser-inflicted DNA damage. U2OS cells were treated with the indicated siRNAs, subjected to laser micro-irradiation and 10 minutes later fixed and immunostained for γ H2AX and endogenous XRCC4. (B) Quantification of endogenous XRCC4 levels in laser tracks from A. (C) As in B, except for γ H2AX. Scale bar 10 μ m.

Table S1: Serum Ig isotype concentrations at first analysis

Patient	Age (m)	IgG (g/L)	Normal range	IgM (g/L)	Normal range	IgA (g/L)	Normal range
ICF2-P49	6 66	1.15 n.d.	3.16-11.48	n.d. <0.04	0.65-2.82	n.d. <0.06	0.34-3.39
ICF2-P55	6 24	1.45 n.d.	3.16-11.48	n.d. <0.04	0.63-2.51	n.d. <0.06	0.23-1.23
ICF2-P67	9	<0.33	3.16-11.48	<0.04	0.47-2.04	<0.07	0.13-0.69

The range of age-dependent normal values (g/L) represents the 5th and 95th percentiles, respectively (Kanariou et al., 1995). m: month, n.d.: not detectable.

Table S2: List of ZBTB24-regulated genes identified by RNA-seq

HEK293T cells were transfected with siRNAs against Luciferase or ZBTB24 (siZBTB24-8, siZBTB24-9 or siZBTB24-10) and subjected to RNA-seq. Genes whose expression was affected following treatment with each of the siRNAs against ZBTB24 are shown.

Ensembl.Gene.ID	Associated Gene Name	Fold Change	log2 Fold Change	pval	padj
ENSG00000100292	HMOX1	0.242319408	-2.045018134	2.83908E-05	0.018667905
ENSG000000005102	MEOX1	0.323998217	-1.625942223	3.65729E-07	0.001132639
ENSG00000145721	LIX1	0.340926569	-1.552467058	1.61882E-05	0.014854662
ENSG00000230171	RPL22P18	0.356349218	-1.488636337	2.18977E-05	0.016693086
ENSG00000248979	LAMTOR3P2	0.398942805	-1.325746168	6.25567E-05	0.029242879
ENSG00000232027	RP11-275F13.3	0.406609005	-1.298285928	3.71884E-05	0.021937162
ENSG00000271113	RP11-159H10.4	0.416214274	-1.264801652	5.0755E-07	0.00147939
ENSG00000112365	ZBTB24	0.421111515	-1.24772577	1.88817E-20	9.35608E-16
ENSG00000120675	DNAJC15	0.4545578	-1.137464341	4.32056E-05	0.023526151
ENSG00000123480	RP11-364P2.2	0.484195745	-1.046337694	5.86427E-09	4.37278E-05
ENSG00000256940	RP11-783K16.5	0.52099793	-0.940650455	0.000116923	0.04316744
ENSG00000236015	AC011290.5	0.52630168	-0.926038095	0.000000287	0.001016514
ENSG00000224274	ENSAF1	0.53524199	-0.901736796	2.67935E-05	0.018439527
ENSG00000165507	C10orf10	0.54564478	-0.873966047	1.02742E-08	6.36372E-05
ENSG00000254910	RP11-326C3.7	0.548888257	-0.86541562	0.000138315	0.045997476
ENSG00000220494	YAP1P1	0.558208854	-0.841123087	7.82227E-05	0.033340721
ENSG00000130066	SAT1	0.564614975	-0.824660701	2.14387E-05	0.016598569
ENSG00000260563	RP13-516M14.1	0.566027439	-0.821056104	1.48213E-06	0.002937647
ENSG00000247095	MIR210HG	0.571981543	-0.805959501	5.76607E-05	0.028288584
ENSG00000236182	RP11-297K7.1	0.575450831	-0.797235432	2.43288E-05	0.01753826
ENSG00000225770	AC092933.3	0.582534838	-0.779583763	6.17736E-09	4.37278E-05
ENSG00000167733	HSD11B1L	0.583448174	-0.777323583	2.78074E-05	0.018620084
ENSG00000143847	PPFIA4	0.584092594	-0.775731004	5.41691E-07	0.001491185
ENSG00000145293	ENOPH1	0.585854597	-0.771385448	2.87203E-07	0.001016514
ENSG00000229083	PSMA6P2	0.590486762	-0.760023378	0.0006528	0.029950838
ENSG00000230224	PHBP9	0.603938741	-0.727525875	0.000117608	0.04316744
ENSG00000186897	C1QL4	0.614348374	-0.702871109	9.62855E-05	0.038168359
ENSG00000254506	RP11-748H22.1	0.619001977	-0.691984077	4.62144E-05	0.024532999
ENSG00000232380	ZDHHC20P4	0.622162252	-0.684637229	1.60488E-05	0.014854462
ENSG00000176788	BASP1	0.623449344	-0.681655752	2.44221E-05	0.01753826
ENSG00000228986	RP13-228J13.8	0.624530743	-0.679155504	2.96195E-06	0.00456816
ENSG00000244153	WWP1P1	0.625151169	-0.677230003	9.31647E-07	0.002098365
ENSG00000142227	EMP3	0.626777792	-0.673974032	0.000001602	0.00305313
ENSG00000139921	TMX1	0.628377	-0.670297719	7.83921E-07	0.001849717
ENSG00000213290	PGK1P2	0.634386151	-0.656566818	4.91773E-05	0.024846568
ENSG00000237801	AMD1P1	0.639994148	-0.643869382	5.48222E-06	0.006596589
ENSG00000131389	SLC6A6	0.64229385	-0.638694612	0.000000967	0.002126309
ENSG00000090054	SPTLC1	0.646719963	-0.628786952	4.71065E-06	0.005835434
ENSG00000230870	FBXW11P1	0.648540377	-0.624731698	0.000112513	0.042558399
ENSG00000236686	BZW1P1	0.651711446	-0.617694761	0.000151113	0.048621906
ENSG00000121966	CXCR4	0.65512456	-0.610158861	4.04265E-06	0.00527151
ENSG00000272520	CTD-2044J15.2	0.656889602	-0.606277165	0.000123013	0.043717729
ENSG00000122203	KIAA1191	0.663631161	-0.591546464	1.96077E-05	0.015596156
ENSG00000198406	BZW1P2	0.663736204	-0.591318126	3.52198E-05	0.021453568
ENSG00000254406	RP11-215D10.1	0.664082175	-0.59056632	1.89685E-05	0.015596156
ENSG00000026682	UBL5P2	0.664657609	-0.589316752	4.38366E-06	0.005569605
ENSG00000254682	RP11-660L16.2	0.665024554	-0.588520486	6.34857E-05	0.029399819
ENSG00000248015	AC005329.7	0.665050876	-0.588463385	0.000075332	0.03274365
ENSG00000169242	EFNA1	0.669841996	-0.578107265	4.08778E-05	0.022802697
ENSG00000141425	RPRD1A	0.672548701	-0.572289355	5.72511E-07	0.001493079
ENSG00000231549	USMG5P1	0.676331869	-0.564196759	2.63535E-05	0.018392137
ENSG00000232801	SDCBP3	0.679462884	-0.55753335	0.000125842	0.04390957
ENSG00000214121	TDPX2	0.680475654	-0.555384548	1.98292E-05	0.015596156
ENSG00000261612	SUB1P3	0.683524585	-0.548934866	0.000137557	0.045997476
ENSG00000160408	ST6GALNAC6	0.688644251	-0.538169207	6.91152E-05	0.030853386
ENSG00000173674	EIF1AX	0.689250253	-0.536900202	6.15708E-05	0.029240244
ENSG00000249286	CTD-2210P15.2	0.693848208	-0.527308014	0.000114945	0.042824457
ENSG00000258445	RP11-307P22.1	0.693964876	-0.52706545	9.03382E-05	0.036994623
ENSG00000103449	SALL1	0.69616196	-0.522505111	5.27786E-05	0.026152313
ENSG00000270553	RP11-15E18.5	0.69719548	-0.520364879	0.000139701	0.046148875
ENSG00000157514	TSC22D3	0.697842351	-0.51902694	0.000029906	0.018998379
ENSG00000180730	SHISA2	0.698902817	-0.516836234	0.000121026	0.043514535
ENSG00000110218	PANX1	0.700723706	-0.513082391	0.00012818	0.044107264
ENSG00000221988	PPT2	0.701357405	-0.511778279	0.000124609	0.043790708
ENSG00000213409	RP11-658F2.3	0.701489017	-0.511507579	0.000111999	0.042558399
ENSG00000213684	LDHBP2	0.708015124	-0.498147917	0.000100621	0.038952261
ENSG00000006831	ADIPOR2	0.708029432	-0.498118763	8.82767E-05	0.036757985
ENSG00000130522	JUND	0.711466486	-0.491132295	2.95435E-05	0.018998379
ENSG00000257923	CUX1	1.365449977	0.449374642	0.000158375	0.049957002
ENSG00000133059	DSTYK	1.375898777	0.460374336	0.000123519	0.043717729
ENSG00000142156	COL6A1	1.38834809	0.473369329	0.000126719	0.04390957
ENSG00000116260	QSOX1	1.395197484	0.480469343	0.000121035	0.043514535
ENSG00000130363	RSPH3	1.42211213	0.508035222	0.000130535	0.044607681
ENSG00000196562	SULF2	1.422165478	0.508089341	0.000092847	0.037403769
ENSG00000183741	CBX6	1.425280114	0.511245483	1.41245E-05	0.01398908
ENSG00000241360	PDXP	1.425722878	0.511693588	0.000159295	0.049957002

Table S3: Proteins identified as ZBTB24 interactors by SILAC MS ordered by H/L

Label	Cell line			
Light (L)	UZOS-GFP			
Heavy (H)	UZOS-GFP-ZBTB24			
Proteins with increased (SILAC ratio H/L ≥ 4) enrichment with at least 2 unique peptides				
Protein names	Gene names	Fasta headers	Peptides	Ratio H/L
Zinc finger and BTB domain-containing protein 24	ZBTB24	>sp Q43167 ZBT2	30	13.94
Zinc finger and BTB domain-containing protein 11	ZBTB11	>sp O95625 ZBT1	2	11.32
Heat shock 70 kDa protein 1A/1B	HSPA1A	>sp P08107 HSP7	25	7.57
60S ribosome subunit biogenesis protein NIP7 homolog	NIP7	>sp Q9Y221 NIP7	4	7.31
Pentatricopeptide repeat domain-containing protein 3, mitochondrial	PTCD3	>sp Q96EY7 PTC3	11	7.22
Probable rRNA-processing protein EBP2	EBNA1BP2	>sp Q99848 EBP2	9	7.06
Phospholipase DDHD1	DDHD1	>sp Q8NEL9 DDH	22	6.98
Nucleolar complex protein 3 homolog	NOC3L	>tr F6H677 F5H67	2	6.81
Guanine nucleotide-binding protein-like 3	GNL3	>sp Q95VP2-2 GN3	5	6.79
ATP-dependent RNA helicase DDX54	DDX54	>sp Q81TD1 DDX	4	6.65
Putative ribosomal RNA methyltransferase NOP2	NOP2	>sp P46087-2 NOC1	11	6.36
Ribosome production factor 2 homolog	RPF2	>sp Q9H7B2 RPF2	2	6.34
28S ribosomal protein S29, mitochondrial	DAP3	>sp P51398-2 RT2	11	6.23
Pumilio domain-containing protein KIAA0020	KIAA0020	>sp Q15397 K0020	7	6.22
Putative helicase MOV-10	MOV10	>tr Q5JR04 Q5JRC	2	6.21
ATP-dependent RNA helicase DDX24	DDX24	>tr F5GYL3 F5GY1	2	6.04
SHC SH2 domain-binding protein 1	SHCBP1	>sp Q8NEM2 SHC	2	6.03
Ribosomal L1 domain-containing protein 1	RSL1D1	>sp Q76021 RL1D	15	6.00
Histone H3.2;Histone H3.1;Histone H3;Histone H3.1t;Histone H3.3;Histone H3.3C	HIST2H3A;HIST1H3A;H3F3B;H3F3A;HIST3H3;	>sp Q71D3 H32_1	7	5.98
Ribosome biogenesis protein BRX1 homolog	BRX1	>sp Q81DN6 BRX	5	5.97
Ankyrin repeat domain-containing protein 17;Ankyrin repeat and KH domain-containing protein 17	ANKRD17;ANKHD1	>sp Q75179-6 ANI	4	5.86
Serine/threonine-protein phosphatase 6 regulatory subunit 3	PPP6R3	>tr H7BK2H H7BK	6	5.84
Histone H2A.V;Histone H2A.Z;Histone H2A	H2AFV;H2AFZ	>sp Q71UI9 H2AV	3	5.83
Core histone macro-H2A.1	H2AFY	>sp Q75367-2 H2A	8	5.83
Procollagen-lysine,2-oxoglutarate 5-dioxygenase 3	PLOD3	>sp Q60568 PLO3	6	5.73
Histone H2B type 1-L;Histone H2B type 1-N;Histone H2B type 1-H;Histone H2B type 1-K	HIST1H2BL;HIST1H2BN;HIST1H2BH;HIST1H2S	>sp Q99880 H2B1	7	5.72
RRP12-like protein	RRP12	>sp Q5J7H9-2 RRR	6	5.69
Protein mago nashi homolog 2;Protein mago nashi homolog	MAGOHB;MAGOH	>tr A9NEC0 A9NE	3	5.66
Cytoskeleton-associated protein 4	CKAP4	>sp Q07065 CKAF	22	5.63
Methylome protein 50	WDR77	>tr B4DP38 B4DP	2	5.59
Histone H1.1;Histone H1t	HIST1H1A;HIST1H1T	>sp Q02539 H11_1	6	5.59
Histone H1.4;Histone H1.2;Histone H1.3	HIST1H1E;HIST1H1C;HIST1H1D	>sp P10412 H14_1	9	5.59
Procollagen-lysine,2-oxoglutarate 5-dioxygenase 1	PLOD1	>sp Q02809 PLO1	14	5.58
mRNA turnover protein 4 homolog	MRT04	>sp Q9UKD2 MRT	2	5.57
Protein KR11 homolog	KR11	>tr H0YFD2 H0YFI	2	5.56
Histone H4	HIST1H4A	>sp P62805 H4_H	11	5.52
Tripartite motif-containing protein 58	TRIM58	>sp Q8M06 TRIS	3	5.52
Ribonucleases P/MRP protein subunit POP1	POP1	>sp Q99575 POP1	2	5.48
Growth arrest and DNA damage-inducible proteins-interacting protein 1	GADD45GIP1	>sp Q81AE8 G45I1	2	5.45
BAG family molecular chaperone regulator 2	BAG2	>sp Q95816 BAG2	3	5.45
Protein SET	SET	>sp Q01105-3 SE1	2	5.43
Ribosome biogenesis regulatory protein homolog	RRS1	>sp Q15050 RRS1	2	5.41
Nucleolar protein 16	NOP16	>tr D6R1C3 D6R1C	2	5.39
E3 ubiquitin-protein ligase HERC2	HERC2	>sp Q95714 HERC	2	5.39
Heat shock cognate 71 kDa protein	HSPA8	>sp P11142 HSP71	27	5.36
Bystin	BYSL	>sp Q13895 BYST	7	5.36
Importin subunit alpha-3	KPNA3	>sp Q00505 IMA4	3	5.33
YTH domain-containing protein 1	YTHDC1	>sp Q96MU7-2 YTT	3	5.32
pre-rRNA processing protein FTSJ3	FTSJ3	>sp Q8H181 SPB1	10	5.29
Histone H2B type 2-E;Histone H2B type 1-O;Histone H2B type 1-J;Histone H2B type 1-K	HIST2H2BE;HIST1H2BO;HIST1H2BJ;HIST3H2E	>sp Q16778 H2B2	7	5.28
Periodic tryptophan protein 1 homolog	PWP1	>tr B4DJ15 B4DJ1	4	5.28
Guanine nucleotide-binding protein subunit beta-2-like 1	GNB2L1	>sp P63244 GBLP	11	5.27
Metastasis-associated protein MTA2	MTA2;DKFZp686F2281	>sp Q94776 MTA2	7	5.26
Melanoma-associated antigen B2	MAGEB2	>sp Q15479 MAGB	2	5.25
Poly (ADP-ribose) polymerase 1	PARP1	>sp P09874 PARP	7	5.23
Prolow-density lipoprotein receptor-related protein 1;Low-density lipoprotein receptor-related protein 1	LRP1	>sp Q07954 LRP1	7	5.23
DnaJ homolog subfamily C member 9	DNAJC9	>sp Q8WXX5 DNJ	2	5.15
Histone H2A type 2-B	HIST2H2AB	>sp Q81UE8 H2A2	4	5.13
Serine/threonine-protein kinase Nek7;Serine/threonine-protein kinase Nek6	NEK7;NEK6	>sp Q81DX7 NEK	2	5.08
Probable ubiquitin carboxyl-terminal hydrolase FAF-X	USP9X	>sp Q83008-1 US9	21	5.08
Histone H2A type 1-J;Histone H2A type 1-H;Histone H2A.J;Histone H2A type 2-C;Histone H2A.K;Histone H2A.H;H2AFJ;HIST2H2AC;Histone H2A.L	HIST1H2AJ;HIST1H2AH;H2AFJ;HIST2H2AC;HIST1H2AL	>sp Q99878 H2A1	6	5.07
Ankyrin repeat and SAM domain-containing protein 2	ANKS3	>tr D3DUE4 D3DU	3	5.05
Putative ATP-dependent RNA helicase DHX30	DHX30	>sp Q7L2E3-3 DH	17	5.02
RNA-binding protein 8A	RBM8A	>sp Q9Y5S9 RBM	4	4.99
Chromobox protein homolog 3	CBX3	>sp Q13185 CBX3	2	4.98
Protein AATF	AATF	>sp Q9N9Y1 AATF	2	4.97
Eukaryotic initiation factor 4A-III	EIF4A3	>sp P38919 IF4A3	8	4.95
Histone-binding protein RBBP4;Histone-binding protein RBBP7	RBBP4;RBBP7	>sp Q09029-3 RBB	6	4.94
RNA-binding protein 34	RBM34	>tr A2A2V2 A2A2	3	4.93
Heterogeneous nuclear ribonucleoproteins C1/C2;Heterogeneous nuclear ribonucleoprotein C1	HNRNPC;HNRNPCL1	>tr G3VAW0 G3VA	10	4.92
Nucleolar RNA helicase 2	DDX21	>sp Q9NR30-2 DD	11	4.89
78 kDa glucose-regulated protein	HSPA5	>sp P11021 GRP7	23	4.87
Heterogeneous nuclear ribonucleoprotein U	HNRNPU	>sp Q00839 HNRU	12	4.86
RNA-binding protein NOB1	NOB1	>tr H3BUR4 H3BU	3	4.85
Y-box-binding protein 3	YBX3	>sp P16989-3 YBC	9	4.83
Oxysterol-binding protein-related protein 3	OSBPL3	>sp Q9H4L5-2 OS	2	4.77
N-acetyltransferase 10	NAT10	>sp Q9H0A0 NAT1	8	4.76
Serine/threonine-protein phosphatase 6 regulatory ankyrin repeat subunit C	ANKRD52	>sp Q8N846 ANR	4	4.76
Leucine-rich repeat-containing protein 1;Protein scribble homolog	LRR1;SCRIB	>sp Q96TT6 LRR1	2	4.75
Serine/threonine-protein phosphatase 6 regulatory ankyrin repeat subunit A	ANKRD28	>sp Q15084-2 ANI	3	4.73
Histone H1.0	H1FO	>sp P07305 H10_1	7	4.68
Melanoma-associated antigen C1	MAGEC1	>tr A0PK03 A0PK	2	4.68
Dedicator of cytokinesis protein 6	DOCK6	>sp Q96HP0 DOC	15	4.67
Histone H1x	H1FX	>sp Q92522 H1X	3	4.66
Ribosome biogenesis protein BOP1	BOP1;KM-PA-2	>tr E9PIF8 E9PIF	2	4.64
Pinin	PNN	>sp Q9H307 PINI	6	4.59
Protein arginine N-methyltransferase 5;Protein arginine N-methyltransferase 5, N-terminal	PRMT5	>sp Q14744-2 ANI	6	4.55
RNA-binding protein PNO1	PNO1	>sp Q9NRX1 PNO	4	4.54
Protein LTV1 homolog	LTV1	>sp Q96GA3 LTV1	3	4.48
Heterogeneous nuclear ribonucleoprotein M	HNRNPM	>sp P52272-2 HNF	6	4.45
Transformer-2 protein homolog beta	TRA2B	>sp P62995 TRA2	7	4.43
Serine/arginine-rich splicing factor 6;Serine/arginine-rich splicing factor 4	SRSF6;SRSF4	>sp Q13247-3 SR	3	4.43

Table S4: Proteins identified as PARP1 interactors by SILAC MS ordered by H/L

Label	Cell line			
Light (L)	U2OS-GFP			
Heavy (H)	U2OS-GFP-PARP1			
Proteins with increased (SILAC ratio H/L ≥ 2) enrichment with at least 2 unique peptides				
Protein names	Gene names	Fasta headers	Peptides	Ratio H/L
Zinc finger and BTB domain-containing protein 24	ZBTB24	>sp O43167 ZBTB24_HU	2	10.02
Poly (ADP-ribose) polymerase 1	PARP1	>sp P09874 PARP1_HU	68	8.92
DNA polymerase beta	POLB	>tr E7EW18 E7EW18_f	3	8.83
Bifunctional polynucleotide phosphatase/kinase;Polynucleotide 3-phosphatase;Polynu	PNKP	>tr MOR3C8 MOR3C8_f	4	7.06
DNA repair protein XRCC1	XRCC1	>tr F5H8D7 F5H8D7_H	5	6.15
DNA ligase 3	LIG3	>sp P49916 DNLJ3_HU	20	5.88
Chromodomain-helicase-DNA-binding protein 1-like	CHD1L	>sp Q8WJ1-2 CHD1L_	3	5.85
Core histone macro-H2A.1	H2AFY	>sp O73367-2 H2AFY_H	5	5.48
Histone H2B type 1-L;Histone H2B type 1-N;Histone H2B type 1-H;Histone H2B type 1-J;Histone H2B type 1-K;Histone H2B type 1-L	HIST1H2B;HIST1H2BN;HIST1H2C	>sp Q99880 H2B1L_HU	5	5.14
Histone H2A.V;Histone H2A.Z;Histone H2A	H2AFV;H2AFZ	>sp Q71U H2AFV_HUM	4	5.02
Histone H4	HIST1H4A	>sp P62805 H4_HUMAN	9	4.92
Histone H3.2;Histone H3.1;Histone H3;Histone H3.1t;Histone H3.3;Histone H3.3C	HIST2H3A;HIST1H3A;H3F3B;H3F	>sp Q71D H32_HUM	5	4.83
Histone H2B type 2-E;Histone H2B type 1-O;Histone H2B type 1-J;Histone H2B type 1-K;Histone H2B type 1-L	HIST2H2BE;HIST1H2BO;HIST1H	>sp Q16778 H2BE2_HL	6	4.74
Histone H2A type 2-B	HIST2H2AB	>sp Q8IU66 H2A2B_HL	3	4.70
Histone H2A type 1-J;Histone H2A type 1-H;Histone H2A.J;Histone H2A type 2-C;Hist	HIST1H2AJ;HIST1H2AH;H2AFJ;H	>sp Q99878 H2A1J_HU	4	4.40
Inosine-5-monophosphate dehydrogenase 2	IMPDH2	>tr H0Y4R1 H0Y4R1_H	6	4.30
Heat shock 70 kDa protein 1A/1B	HSPA1A	>sp P08107 HSP71_HU	14	3.51
DNA topoisomerase 2;DNA topoisomerase 2-alpha;DNA topoisomerase 2-beta	TOP2B;TOP2A	>tr E9PCY5 E9PCY5_H	2	2.99
Ubiquitin-60S ribosomal protein L40;Ubiquitin;60S ribosomal protein L40;Ubiquitin-40	UBB;RPS27A;UBC;UBA52;UBBP	>tr J3Q539 J3Q539_HU	2	2.83
Heat shock cognate 71 kDa protein	HSPA9	>sp P11442 HSP70_HU	16	2.76
Nuclease-sensitive element-binding protein 1	YBX1	>sp P67809 YBOX1_HL	4	2.33
78 kDa glucose-regulated protein	HSPA5	>sp P11021 GRP78_HL	13	2.32
Nucleolin	NCL	>sp P19338 NCL_HU	5	1.94
Heterogeneous nuclear ribonucleoproteins C1/C2;Heterogeneous nuclear ribonucleo	HNRNPC;HNRNPCL1	>tr G3V4W0 G3V4W0_f	2	1.94
Guanine nucleotide-binding protein subunit beta-2-like 1	GNB2L1	>sp P63244 GNBL_HU	4	1.92
Tubulin beta-4B chain	TUBB4B	>sp P68371 TBB4B_HU	9	1.50
Tubulin alpha-1B chain;Tubulin alpha-1C chain	TUBA1B;TUBA1C	>sp P68363 TBA1B_HU	8	1.23
Heterogeneous nuclear ribonucleoprotein U	HNRNPU	>sp Q00839 HNRPU_H	2	1.21
Tubulin beta chain	TUBB	>tr Q5JP53 Q5JP53_HL	10	1.17
ADP/ATP translocase 3	SLC25A6	>sp P12236 ADT3_HU	2	1.17
Tubulin alpha-3C/D chain;Tubulin alpha-3E chain	TUBA3C;TUBA3E	>sp Q13748 TBA3C_HL	9	1.15
ADP/ATP translocase 2;ADP/ATP translocase 1	SLC25A5;SLC25A4	>sp P05141 ADT2_HU	2	1.13
Pyruvate kinase isozymes M1/M2;Pyruvate kinase	PKM;PKM2	>sp P14618 PKYM_HU	6	1.10
Claudin heavy chain 1	CLTC	>sp Q00610-2 CLH1_H	2	1.03
Nucleophosmin	NPM1	>sp P06748-2 NPM_HU	2	1.03
Galectin-1	LGALS1	>sp P09382 LEG1_HU	2	1.02
Heat shock protein beta-1	HSPB1	>sp P04792 HSPB1_HL	2	0.97
Vimentin	VIM	>sp P08670 VIME_HU	10	0.91
LanC-like protein 2	LANCL2	>sp Q9NS86 LANC2_H	2	0.90
Elongation factor 1-delta	EEF1D	>sp P29692-3 EF1D_HL	2	0.86
DNA replication licensing factor MCM3	MCM3	>sp P25205 MCM3_HU	5	0.83
Annexin A2;Annexin;Putative annexin A2-like protein	ANXA2;ANXA2P2	>sp P07355 ANXA2_HL	15	0.80
Cystatin-B	CS1B	>sp P04080 CYTB_HU	2	0.80
Filamin-A	FLNA	>tr Q5HY44 Q5HY44_H	2	0.80
ATP-dependent RNA helicase DDX3X;ATP-dependent RNA helicase DDX3Y	DDX3X;DDX3Y	>sp Q00571-2 DDX3X_f	3	0.79
Melanoma-associated antigen 4;Melanoma-associated antigen 8	MAGEA4;MAGEA8	>sp P43358 MAGEA4_H	2	0.78
Heterogeneous nuclear ribonucleoprotein H;Heterogeneous nuclear ribonucleoprotein	HNRNPH1	>sp P31943 HNRH1_HL	3	0.77
Endoplasmic reticulum resident protein 44	ERP44	>sp Q9S266 ERP44_HL	3	0.77
Glyceraldehyde-3-phosphate dehydrogenase	GAPDH	>sp P04406-2 G3P_HU	2	0.77
Profilin	PFN2	>tr C9J0J7 C9J0J7_HU	4	0.77
Peroxisiredoxin-1	PRDX1	>sp Q06830 PRDX1_HL	9	0.76
Phenylalanine--tRNA ligase beta subunit	FARSB	>sp Q9NSD9 SYFB_HU	3	0.75
Cysteine and glycine-rich protein 2	CSR2P	>sp Q16527 CSR2P_H	5	0.74
Probable ATP-dependent RNA helicase DDX17	DDX17	>sp Q92841-1 DDX17_f	4	0.74
Filamin-C	FLNC	>sp Q14315-2 FLNC_H	3	0.74
Crk-like protein	CRKL	>sp P46109 CRKL_HU	4	0.72
Putative elongation factor 1-alpha-like 3;Elongation factor 1-alpha 1	EEF1A1P5;EEF1A1	>sp Q5VTE0 EF1A3_HL	8	0.72
CTP synthase 1	CTPS1	>sp P17812 PYRG1_HL	6	0.72
Heat shock protein HSP 90-beta	HSP90AB1	>sp P08238 H90B_HU	5	0.71
Myosin-9	MYH9	>sp P35579 MYH9_HU	3	0.68
Probable ATP-dependent RNA helicase DDX5	DDX5	>sp P17844 DDX5_HU	5	0.65
Actin, cytoplasmic 2;Actin, cytoplasmic 2, N-terminally processed;Actin, cytoplasmic 1	ACTG1;ACTB;ACTA1;ACTC1;ACT	>sp P63261 ACTG_HU	12	0.65
Peptidyl-prolyl cis-trans isomerase A;Peptidyl-prolyl cis-trans isomerase	PPIA	>sp P62937 PPIA_HU	2	0.63
Cofilin-1	CFL1	>sp P23528 COF1_HU	4	0.62
Histone deacetylase 6	HDAC6	>sp Q9UBN7 HDAC6_H	4	0.61
U2 small nuclear ribonucleoprotein A	SNRPA1	>sp P09661 RU2A_HU	5	0.58
Prohibitin-2	PFB2	>tr F5GY37 F5GY37_H	2	0.57
Protein RCC2	RCC2	>sp Q9P258 RCC2_HU	2	0.50
Ketosamine-3-kinase	FN3KRP	>tr SLZ333 SLZ333_HU	2	0.42
Thioredoxin	TXN	>sp P10599-2 THIO_HL	2	0.41
Heterogeneous nuclear ribonucleoprotein A1;Heterogeneous nuclear ribonucleoprotein	HNRNPA1;HNRNPA1L2	>sp P09651-3 R0A1_H	3	0.32
Tubulin beta-3 chain	TUBB3	>sp Q13509 TBB3_HU	8	0.25
LanC-like protein 1	LANCL1	>tr E9PHS0 E9PHS0_H	2	0.24
Keratin, type I cytoskeletal 17	KRT17	>sp Q04695 K1C17_HU	4	0.21
Hornerin	HRNR	>sp Q86Y23 HORN_HU	5	0.19
Keratin, type II cytoskeletal 5	KRT5	>sp P13647 K2C5_HU	8	0.11
Keratin, type I cytoskeletal 14	KRT14	>sp P02533 K1C14_HU	10	0.09
Keratin, type II cytoskeletal 6C;Keratin, type II cytoskeletal 6B;Keratin, type II cytoskele	KRT6C;KRT6B;KRT6A	>sp P48668 K2C6C_HU	12	0.06
Keratin, type I cytoskeletal 16	KRT16	>sp P08779 K1C16_HU	7	0.03
Keratin, type I cytoskeletal 9	KRT9	>sp P35527 K1C9_HU	7	0.03
Keratin, type I cytoskeletal 2 epidermal	KRT2	>sp P35908 K2E_HU	13	0.03
Keratin, type I cytoskeletal 10	KRT10	>sp P13645 K1C10_HU	18	0.02
Keratin, type II cytoskeletal 1	KRT1	>sp P04264 K2C1_HU	22	0.02

5
 LOSS OF ZBTB24 IMPAIRS CLASS-SWITCH-RECOMBINATION IN ICF SYNDROME



PERSPECTIVES

6

PERSPECTIVES

Introduction

Since the genetic information in our cells is constantly threatened by a large variety of DNA damage-inducing agents, the detection and accurate repair of DNA lesions is vital to preserve genome stability. Among the most devastating types of DNA damage are DNA double strand breaks (DSBs). DSBs can be generated endogenously by physiological processes, for instance upon replication stress or during meiotic recombination. Additionally, DSBs can be inflicted exogenously by physical agents such as ionizing radiation (IR) or by chemicals such as chemotherapeutic drugs. Cells respond to DSBs by sensing the DNA damage and initiating a cascade of signaling events that are capable to activate DNA repair and cell cycle checkpoints (Smeenk and van Attikum, 2013). This intricate network of defense mechanisms towards DNA damage is termed the DNA damage response (DDR). The signaling of DSBs is driven by posttranslational modifications (PTMs) (primarily phosphorylation and ubiquitylation) of proteins that function as DNA damage sensors or signal transducers. Ultimately this cascade of events regulates effector proteins that facilitate DNA damage repair and control cell cycle progression. Since chromatin often forms a barrier for DNA repair proteins to access the damaged DNA, the cellular response to DNA damage demands accurate and timely changes in chromatin structure to allow efficient protection against DNA damage. Chromatin modifiers and remodelers are capable to level this barrier by changing nucleosomal organization in the vicinity of DSBs and modulating PTMs on for example histones. This leads to a temporal increase in the accessibility of the chromatin surrounding the lesion (Smeenk and van Attikum, 2013). Hence chromatin modifiers and remodelers are considered to be key players in the DSB response and their loss can have severe effects on genome stability and consequently the development and health of an organism. Perhaps not surprisingly, genetic defects in these chromatin factors are frequently found in human disorders. Interestingly, such disorders have a number of common clinical characteristics like developmental defects, neurological degeneration, immunodeficiency and cancer predisposition. In order to identify the molecular origin of these diseases, it is essential to determine the function of chromatin factors involved in development and maintenance of genome stability.

In this study we characterized and deciphered the function of three chromatin factors EHMT1, RSF1 and ZBTB24 in the cellular response to DSBs. The histone methyltransferase EHMT1 was identified as a possible negative regulator of 53BP1 recruitment to DSBs that promotes DSB repair via non-homologous end-joining (NHEJ) and homologous recombination (HR) (Helfricht et al., 2013) (chapter 2). Remodeling and Spacing Factor 1 (RSF1), on the other hand, deposits centromeric proteins at DSBs. These proteins appeared to be critical for the RSF1-dependent recruitment of the important NHEJ-factor XRCC4 to DSBs. Interestingly besides NHEJ, RSF1 is also involved in the efficient repair of DSBs via HR (Helfricht et al., 2013) (chapter 3) and the function of RSF1 during both DSB repair pathways might be dependent on SUMOylation (chapter IV). Moreover, in **chapter 5** we discovered a role for ZBTB24 during classical NHEJ by means of promoting PARP1 activity and stabilizing PARP1-associated PAR-chains, thereby facilitating the PARP1/PARYlation-dependent assembly of NHEJ complexes at DSBs. Moreover, we found ZBTB24's role in NHEJ to be critical for class-switch recombination (CSR), providing an explanation for the immunological phenotype of ZBTB24-deficient ICF2 patients (chapter 5). In conclusion, these findings contribute to our current understanding of the chromatin alterations taking place during the signaling and

repair of DSBs, and raise several questions regarding their link to human diseases, which are discussed in the following sections.

EHMT1 involved in intellectual disability syndrome and the DDR

Epigenetic processes such as DNA methylation are fundamental for (neuronal) development and cognitive functioning (Day and Sweatt, 2011). Consequently, the disruption of the methylation machinery can cause cognitive disorders (Miller et al., 2010) such as Kleeftstra syndrome (KS) (OMIM #610253). KS is caused by haploinsufficiency of the histone methyltransferase EHMT1 due to loss-of-function mutations or deletions in the encoding gene at chromosome 9q34.3. The clinical core features of KS patients are developmental delay/intellectual disability, (childhood) hypotonia and characteristic facial features such as disproportional shortness of the head, synophrys, midface hypoplasia, unusual shape of the lips, protruding tongue and prognathism (Willemsen et al., 2012). Defective learning and memory phenotypes were also observed in an EHMT mutant in *Drosophila melanogaster*. Interestingly, these phenotypes were rescued upon restoration of EHMT expression in adult flies, indicating that cognitive defects are reversible in EHMT mutants (Kramer et al., 2011). Moreover, since homozygous *Ehmt1* deficiency leads to embryonic lethality between E9.5 and E12.5 in mice, heterozygous *Ehmt1*^{+/-} mouse models were employed. *Ehmt1* protein levels were strongly reduced in heterozygous *Ehmt1*^{+/-} cells, indicative of haploinsufficiency of *Ehmt1* (Balemans et al., 2013). In line with these findings, *Ehmt1*^{+/-} mice phenocopied the KS core features observed in the *Drosophila* EHMT mutant and haploinsufficient KS patients (Balemans et al., 2010; Balemans et al., 2014). Hence *Ehmt1*^{+/-} mice can be used as a model for KS to investigate whether learning and memory formation can also be restored by the expression of functional *Ehmt1*. In addition, since mice and humans show 95% similarity in their genes, *Ehmt1*^{+/-} mice provide a model for KS that is more closely related to the human situation compared to the *Drosophila* EHMT mutant. The *Ehmt1*^{+/-} mice can also be used to define the exact role of EHMT1 in cellular processes, most notably in transcription and the DDR.

Gene expression analysis of heterozygous *Ehmt1*^{+/-} mice already revealed a significant upregulation of bone tissue related genes, which likely results from decreased *Ehmt1*-induced H3K9me2 levels in the promoter region of these genes. This altered gene expression most likely contributes to the cranial dysmorphic features of KS (Balemans et al., 2014). In addition, our functional studies on the role of EHMT1 suggests that EHMT1 is a factor involved in the DDR that may act as a negative regulator of 53BP1 accrual at DSBs. EHMT1 also functions in DSB repair: in **chapter 2** we showed that EHMT1 promotes DSB repair via both NHEJ and HR. Whether EHMT1 functions directly in DSB repair or mediates DSB repair via promoting the recruitment of DDR signaling proteins such as 53BP1 requires further investigation. To this end, it would be interesting to further study EHMT1's interactors as these could be potential substrates for methylation. Substrates of EHMT1 and EHMT2 have already been identified using SILAC combined with quantitative MS on proteins captured with an engineered mono- or dimethylation-binding domain from normal and EHMT1/2 inhibitor treated cells (Moore et al., 2013). 23 proteins were appointed as EHMT1/2 substrates amongst which are known EHMT1/2 methylation targets like WIZ, the adaptor protein that stabilizes EHMT1/EHMT2 complex formation. Other potentially relevant substrates are DNA ligase 1 (LIG1), the chromatin remodeler SMARCA5 and the NHEJ factor DNA-PKcs (Moore et al., 2013). SMARCA5 and DNA-PKcs are both involved in DSB repair and could potentially provide a causal link for the observed decrease in DSB repair efficiency

upon EHMT1-depletion in cells containing the NHEJ or HR reporter (chapter 2). It would be relevant to map the methylation site(s) in these proteins and generate non-methylatable mutants. By using complementation studies the effect of their expression on DSB repair could be determined in order to assess the role of EHMT1/2-mediated methylation of these proteins in DSB repair.

Studies with mouse or human cells may reveal the relevance of results from genetic interaction studies in *Drosophila* that investigated changes in vein formation in the *Drosophila* wing upon modulating the expression of EHMT alone or with other factors simultaneously. This study described a functional link between EHMT1 and several epigenetic regulators including the histone H3K4 methyltransferase KMT2C, the heterochromatin binding protein MBD5 and the nuclear receptor NR1I3. Mutations in these genes and the core-component of the hSWI/SNF chromatin remodeling complex SMARCB1 were identified in human individuals with severe intellectual disability that comprise features closely resembling those of KS patients. KMT2C, MBD5 and NR1I3 cooperate with EHMT1, whereas SMARCB1 directly interacts with KMT2C. These findings lead to the proposal of a putative conserved epigenetic network that underlies cognitive disorders and as such a tight epigenetic control of higher brain function (Kleefstra et al., 2012). Whether this network of chromatin modifiers is equally relevant for human cells or if EHMT1 is the only factor of this network that participates in regulating the DDR remains to be investigated. Ultimately, examination of protein levels and recruitment of relevant DDR factors to DNA damage is required to shed light on the mechanisms by which EHMT1 regulates DSB repair.

Dissecting the role of RSF1 in DNA repair

RSF1 protects cells from the harmful effects of genotoxic agents such as IR (Helfricht et al., 2013; Min et al., 2014), most likely by contributing to the repair of IR-induced DSBs via HR and NHEJ (chapter 3). RSF1 is recruited to laser-induced DNA damage and site-specific DSBs in an ATM-dependent manner (Min et al., 2014) and deposits the centromere proteins CENP-S and CENP-X at DSBs (Helfricht et al., 2013) (chapter 3). This role of RSF1 may require its DNA damage-induced SUMOylation (chapter 4), but surprisingly does not rely on the presence of its binding partner SMARCA5 (Helfricht et al., 2013) (chapter 3). Remarkably, we found that CENP-S and CENP-X exclusively stimulate DSB repair through NHEJ by promoting the recruitment of XRCC4, a factor critical for the final ligation step of this repair process (Helfricht et al., 2013) (chapter 3). However, the exact role(s) of these centromere proteins in NHEJ have yet to be determined.

The assessment of a putative role of RSF1 in the signaling of DSBs revealed that RSF1, in contrast to its binding partner SMARCA5 (Helfricht et al., 2013; Smeenk et al., 2013), is dispensable for the RNF8/RNF168-mediated ubiquitin signaling cascade (Helfricht et al., 2013) (chapter 3). In contrast to our findings, however, another report showed the analysis of nuclear foci (γ H2AX, MDC1 and 53BP1) induced by the radiomimetic agent phleomycin and revealed a reduction in foci formation in RSF1-depleted U2OS cells (Min et al., 2014) favoring a role of RSF1 in the signaling of DSBs. Whether these contradictory results reflect the nature of the DNA damaging agent, the acute versus chronic genotoxic exposure or the timing of foci analysis after DNA damage induction remains elusive and requires further investigation.

Another important function of RSF1 is the maintenance of centromeric chromatin. This function involves the incorporation of the histone H3 variant centromere protein A (CENP-A) and its positioning along the centromeric chromatin (Perpelescu et al., 2009). Similar to RSF1,

CENP-A was shown to be recruited to DSBs (Zeitlin et al., 2009). However, unexpectedly only CENP-S and CENP-X were recruited to sites of laser-induced DNA damage in our experimental set-up in a manner strictly dependent on RSF1 (Helfricht et al., 2013) (chapter 3). Moreover, CENP-S and CENP-X have been shown to form an evolutionary conserved complex with the Fanconi anaemia (FA) complementation group M (FANCM) protein that is required for the repair of DNA interstrand crosslinks (ICLs) and genome stability maintenance (Singh et al., 2010; Yan et al., 2010). FA is a rare genetic disease that affects 1 in 160,000 individuals worldwide. It is characterized by physical abnormalities, bone marrow failure as well as cancer predisposition and is caused by a genetic defect in one of the FA group proteins. RSF1 could possibly facilitate ICL repair through the loading of the CENP-S and CENP-X proteins at sites of ICLs. This subsequently promotes or coordinates the accrual of other FA proteins and might implicate RSF1 as a yet unknown FA gene. It is evident that more work is required to unravel the exact role of RSF1 in ICL repair and other cellular processes. For instance, its contribution to ICL repair, recruitment to ICLs and functional interplay with known FA proteins should be studied using a combination of cell biology, biochemistry and microscopy approaches.

CENP-N, CENP-U and CENP-T have also been shown to be recruited to sites of laser-induced DNA damage (Zeitlin et al., 2009). However, whether these CENP proteins, similar to CENP-S and CENP-X, rely on RSF1 for their recruitment is unclear. Moreover, their recruitment to sites of DNA damage raises the question as to whether RSF1 is involved in the formation of a CENP complex at DSBs. Particularly, is this complex if present at DSBs comparable to the one that is formed at kinetochores (Perpelescu and Fukagawa, 2011)? On the other hand, we also lack understanding of how RSF1 recruits CENP proteins and to what extent the accrual of RSF1 and CENP proteins induces structural changes in DSB-flanking chromatin that makes it amenable to DNA repair. RSF1-induced chromatin structural changes should therefore be studied in response to DNA damage, for instance by examining nucleosome occupancy and compaction at site-specific DSBs by ChIP-seq and MNase-based assays. Alternatively, the effect of recombinant CENP proteins on the compaction of reconstituted nucleosomal arrays could be studied by biophysical approaches *in vitro*.

In addition, recombinant CENP proteins could be investigated for their effect on chromatin folding *in vitro* by monitoring chromatin fiber composition in biophysical experiments. Finally, it would be interesting to know whether CENP proteins undergo PTMs upon DNA damage induction. Interestingly, CENP-S was recently shown to be ubiquitylated upon exposure to IR (Elia et al., 2015), but whether this PTM is important for its function at DSBs remains elusive.

Currently, the mechanism by which RSF1 executes its role in DSB repair is vague. Intriguingly, RSF1 itself does not display any enzymatic activity, yet it is able to load CENP proteins at sites of DNA damage (Helfricht et al., 2013) (chapter 3). A step towards understanding the mechanistic role of RSF1 in DSB repair is to elucidate whether RSF1 acts individually, with SMARCA5 as part of the RSF complex or even as a member of another complex. One approach to address this key question is to perform DSB repair experiments in RSF1- and/or SMARCA5-depleted cells and monitor whether RSF1 and SMARCA5 act epistatically or synergistically. Additionally, interactors of RSF1 could be identified by SILAC-based MS analysis following DNA damage induction and their interplay with RSF1 in DSB repair should be studied.

ICF1-4 ... is there a common mechanism?

ICF patients have been categorized into four subgroups (ICF1, 2, 3 and 4; causally linked to mutations in DNMT3b, ZBTB24, CDCA7 and HELLS, respectively) dependent on their genotype. Interestingly, a few ICF cases do not have mutations in one of the four ICF genes, which means that at least one additional gene can be identified as ICF-disease gene. In spite of this remarkable genetic heterogeneity of the ICF syndrome, the clinical phenotypes of ICF patients are substantially overlapping. This raises the question whether analogously to ZBTB24, the ICF-causing genes DNMT3B, CDCA7 and HELLS also play a role during NHEJ and CSR. This is an intriguing question as to our knowledge DNMT3B, ZBTB24, CDCA7 and HELLS do not share enzymatic activities, whereas all four genes affect CpG methylation. ZBTB24 and CDCA7 were described to maintain CpG methylation whereas DNMT3B has a role in establishing methylated CpGs (Okano et al., 1999). HELLS on the other hand functions in both processes (Thijssen et al., 2015; Zhu et al., 2006). A key goal of future research is to reach mechanistic understanding of how the four hitherto identified ICF genes DNMT3B, ZBTB24, CDCA7 and HELLS cause ICF syndrome. A variety of assays focusing on DSB repair, immunoglobulin serum levels and CSR in control and patient material of all ICF subtypes could shed light on the above-mentioned question. DNMT3B and HELLS have already been implicated to function in DSB repair, but their precise roles in NHEJ and/or CSR still remain to be resolved (Burrage et al., 2012; O'Hagan et al., 2008).

One of the phenotypes of ICF patients is DNA hypomethylation especially at centromeric repeats. DNA methyltransferase 1 (DNMT1) maintains DNA methylation during DNA replication and has been shown to bind non-covalently to PARylated PARP1, which leads to DNMT1 inactivation and subsequently to DNA hypomethylation (Reale et al., 2005). Whether DNMT3B also binds to (PARylated) PARP1 to become inactivated, requires further investigation. One possibility is that DNMT3B and ZBTB24 compete for the binding of PAR chains. In the case of ICF2 patients, the established PAR chains might become available for DNMT3B binding due to ZBTB24 loss, leading to the observed DNA hypomethylation phenotype. However, there is currently no obvious mechanism that could explain the DNA hypomethylation phenotype of ICF3 and ICF4 patients carrying mutations in CDCA7 or HELLS, respectively. No function has yet been described for CDCA7, while mouse Hells/Lsh has been reported to associate with Dnmt3a or Dnmt3b, but not with Dnmt1, and to aid in the establishment of de novo methylation (Zhu et al., 2006). To investigate the possible roles of CDCA7 and HELLS particularly in relation the DDR, cell biology, microscopy and mass spectrometry based approaches should be employed. These will help to unravel whether these proteins localize to sites of DNA damage, what their mode of action is in which biochemical context they operate at DNA lesions is.

Chromatin modifiers in cancer

Recent studies have indicated that human cancers exhibit global epigenetic abnormalities as well as genetic alterations (Jones and Baylin, 2007). In contrast to the latter, epigenetic changes are reversible and can be enzymatically restored to their non-disease state. Therefore, more and more studies focus on understanding chromatin modifiers and the PTMs they induce in various pathways to identify novel targets for cancer therapy.

Somatic mutations in many of the histone modifying and chromatin remodeling genes are associated with cancer development (Shih et al., 2012) (chapter 1, Table1). In addition, the overexpression of chromatin remodeling proteins is often linked to a poor prognosis for cancer patients and can therefore serve as a prognostic tumor marker (Guan et al., 2014; Lee

et al., 2014; Li et al., 2014; Xie et al., 2014). The chromatin modifying proteins EHMT1, RSF1 and ZBTB24 studied in this thesis, have been linked to cancer and are therefore discussed in the following sections.

While reduced EHMT1 activity leads to KS, the overexpression of EHMT1 seems to promote cancer development, for instance in the case of esophageal squamous cell carcinomas (Guan et al., 2014). The overexpression of EHMT1 leads to an increase in the repressive H3K9me1/2 chromatin marks in general and more specifically at promoter regions of genes frequently silenced in cancer (Yoo and Jones, 2006). As a conceivable hypothesis, increased EHMT1 expression might also alter the DDR and might lead to impaired DSB repair. The proposed hypothesis could straightforwardly be addressed using DSB repair assays in cells transiently overexpressing EHMT1.

Also RSF1 has been linked to tumorigenesis and as much as 191 unique somatic mutations have been identified in various cancers listed in the catalogues of somatic mutations in cancer (COSMIC). Whether these mutations affect RSF1 expression and/or function and influence DNA repair levels in cancer is an important question. Intriguingly, RSF1 was also found to be overexpressed in various types of cancer with a frequency of 55% in ovarian carcinomas, 50% in colon cancer tissues and 45% in prostate cancer specimens, and this phenotype correlates with a poor prognosis for the length of patient survival (Davidson et al., 2006; Liu et al., 2012; Shih et al., 2005). Interestingly, siRNA-mediated knockdown of RSF1 in cells with high endogenous RSF1 expression remarkably decreased cell proliferation and colony formation (Li et al., 2014). Furthermore, the overexpression of RSF1 is likely to increase DNA damage levels as evidenced by increased γ H2AX levels and chromosomal aberrations in ovarian cancer cells (Sheu et al., 2010). Hence it is tempting to speculate that increased RSF1 expression negatively impacts on DNA damage repair and ultimately leads to chromosomal instability in tumor cells. Accordingly, the question raises as to what extend the equilibrium of SMARCA5-containing complexes might be disturbed through RSF1 overexpression. One way to discover an imbalance in SMARCA5-containing complexes and their putative impact on DSB repair is to assess their composition by mass spectrometry and perform quantitative DSB repair assays in cells transiently overexpressing RSF1. The latter should also clarify whether increased levels of RSF1 in cancer cells affect the equilibrium between DSB repair via HR and NHEJ. A change in the balance between these two repair pathways is important and critical for the choice of therapy as this might sensitize cancer cells to certain drugs. For instance PARP inhibitors could be applied during therapy in the case that altered expression of RSF1 renders cells HR deficient (see also section on PARP inhibitor-based cancer therapy). In conclusion, given RSF1's critical role in DSB repair and its link with carcinogenesis, it may serve as an important marker and/or therapeutic target in personalized cancer therapy.

We discovered that ICF2 patients with mutations in ZBTB24 display defects in CSR, which is the immunoglobulin (Ig) gene-diversification process occurring in B-cells (chapter 5), explaining the immunodeficiency phenotype of these patients. During CSR, recombination events between different switch (S) regions within the heavy chain Ig (IgH) locus occur upon DSB induction by the cytidine deaminase (AID) (chapter 1, Fig. 5). Under normal conditions CSR mediates the removal of a DNA segment between switch regions on one chromosome, whereas defects in CSR can also lead to NHEJ-mediated translocations between two different chromosomes. Several chromosomal breakpoints have been found in the IgH switch regions in a number of different translocations in lymphoma, leukemia and myeloma. The common location of these chromosomal translocation breakpoints strongly suggests their occurrence

to originate from mistakes in CSR, which links CSR to tumorigenesis (Bergsagel et al., 1996; Janz, 2006; Kuppers and Dalla-Favera, 2001). Unfortunately, ICF patients die at a young age usually in the first or second decade of life mostly from the disastrous consequences of severe, opportunistic and recurrent infections (Weemaes et al., 2013). Hence, it is rather difficult to assess the effect of ZBTB24 on IgH translocations and cancer development in these patients. ZBTB24 knockout mice would therefore be extremely helpful to investigate the role of ZBTB24 in translocation formation and cancer development. However, attempts to generate ZBTB24 knockout mice indicated that complete loss of ZBTB24 leads to embryonic lethality (unpublished data). Thus, a conditional ZBTB24 knock-out mouse would be desired now, which could for instance allow the study of ZBTB24 loss on translocation formation in B-cells specifically.

Interestingly, already 78 unique somatic mutations have been identified in ZBTB24 in various cancers listed within the COSMIC database. Despite the young age of 4 up to 19 years, a few ICF patients have been diagnosed with different cancers such as myelodysplastic syndrome, classical Hodgkin lymphoma (Hagleitner et al., 2008; Schuetz et al., 2007) and adrenocortical adenoma (Kubota et al., 2004). The Hodgkin lymphoma was diagnosed in a 4 year old ICF2 patient (Weemaes et al., 2013), while the other detected cancers not certainly originated from ICF2 patients. Another case reported on the death of a 21 year old ICF1 patient from complications of a metastatic angiosarcoma of the liver (van den Brand et al., 2011). Since angiosarcoma is utterly rare at such a young age, this could suggest a link between tumorigenesis and defective DNA methylation caused by a mutation in DNMT3B in this ICF1 patient. However, so far we can only speculate about what exactly leads to tumorigenesis in those four described ICF patients and whether ICF patients in general are predisposed to develop cancer.

Chromatin modifier-defects and therapy options

Cancer is a disease that is driven by genomic instability, a feature that can arise from a defective DDR. Currently, the established approach to treat cancer is to kill tumor cells through the induction of DNA damage via chemotherapy or radiation, but this strategy also targets healthy cells for cell death. Thus, alternative therapy methodologies that specifically target cancer cells are to be found. One promising approach to enhance the efficacy of cancer therapy is the use of specific inhibitors that target DDR factors in cancer cells to disable certain DNA repair pathways (Jackson and Bartek, 2009). The DDR is therefore intensely investigated to identify novel (chromatin-modifying) factors that are suitable anti-drug targets in anti-cancer regimes.

PARP inhibitors for instance are effective in cells comprising a defect in HR; HR-deficient BRCA1/2 tumors therefore display high sensitivity towards PARP inhibitors, providing an example of a synthetic lethal relation (Bryant et al., 2005; Farmer et al., 2005). Remarkably, the treatment of siRSF1-depleted U2OS cells with the PARP inhibitor Olaparib resulted in reduced cell survival (Pessina and Lowndes, 2014). This suggests that tumors with decreased expression of RSF1 are likely to be sensitive to PARP inhibitors. Whether the latter can also provide an efficient therapy for malignancies that comprise altered expression levels of EHMT1 or ZBTB24 is not known and will require further investigations. However, it is promising that our research implicates all three factors in the repair of DSBs via HR (chapter 2, 3, 5), a requisite for an effective PARP inhibitor treatment. However, EHMT1, RSF1 and ZBTB24 also promote NHEJ (chapter 2, 3, 5) and hence, NHEJ might also be defective in cancer cells missing functional EHMT1, RSF1 or ZBTB24. This could be a disadvantage for

a PARP inhibitor-based therapy, since loss of the NHEJ-promoting factor 53BP1 or REV7 (a factor acting downstream of 53BP1 in blocking HR), has been shown to diminish the PARP inhibitor cytotoxicity in HR-deficient cells (Bouwman et al., 2010; Bunting et al., 2010; Xu et al., 2015). PARP1 inhibition induces the formation of lethal radial chromosomes in HR-deficient cells that likely result from mis-rejoined DSBs. This is prevented by 53BP1 deletion (Lottersberger et al., 2013), suggesting that combined loss of HR and NHEJ may compromise an effective PARP inhibitor treatment. Surprisingly, however, despite the role of RSF1 in NHEJ, RSF1-depleted cells were sensitive to PARP inhibition (Pessina and Lowndes, 2014). In order to obtain direct proof for a possible sensitivity towards PARP inhibitors, cell killing (e.g. measured by clonogenic survival) of EHMT1- or ZBTB24-knockdown cells and EHMT1-, RSF1- or ZBTB24-overexpressing cells should be assessed. In addition, further genetic screening for other synthetic lethality combinations in cells containing a defect in DDR factors will be of great importance for the development of additional therapy opportunities for personalized cancer treatments in the future. Administering chemical compounds in the framework of personalized medicine that are tailored to the (epi)genetic defects of a tumor will possibly lead to an increase in treatment success rates for patients with genetic alterations in chromatin factors, as is the case for the majority of tumors comprising mutations in BRCA1 or BRCA2 (Bao et al., 2015).

Also the development of specific inhibitors that restrain the activity of overexpressed chromatin factors in cancer cells might lead back to a non-disease state. For instance reversing the epigenetic changes induced by aberrant EHMT1 activity due to its overexpression in certain cancers by means of EHMT1/2 inhibition, might lead to the re-expression of genes that had been silenced through an increase in EHMT1/2-mediated H3K9me1/2 marks. Efforts have been made to develop small-molecule inhibitors for EHMT1 and EHMT2. A few of these inhibitors have recently been proven to provide a way to counteract EHMT1 activity in breast cancer, esophageal squamous carcinoma and leukemia cells (Liu et al., 2013). Thus, EHMT inhibitors may ultimately improve the poor survival prognosis of patients with aberrant EHMT1 expression in the future (Curry et al., 2015; Guan et al., 2014; Pappano et al., 2015).

ICF patients suffer from severe respiratory and opportunistic infections caused by their immunodeficiency. Current therapeutic opportunities for ICF patients mainly concentrate on counteracting these severe infections. In 4 out of 5 ICF patients hematopoietic stem cell (HSC) transplantations have been successfully performed to restore their immunity. Interestingly, HSC transplantations have so far never been performed in ICF2 patients (Weemaes et al., 2013), which could be linked to the generally more pronounced humoral immunodeficiency in ICF1 patients. In any case, an early diagnose of ICF syndrome is of great importance, since early immunoglobulin supplementation can improve the course of the disease. A drawback of this method is however the availability of a compatible donor. Therefore, gene therapy might form a potent alternative and employs the transfer of a transgene via for instance viral infection to patient-derived HSCs. These cells are subsequently transplanted back into the patient. Notably, this form of gene therapy already became available for patients with specific types of severe combined immunodeficiency (Mukherjee and Thrasher, 2013). Another approach to restore gene function could be gene correction, where the mutated DNA sequence is replaced by a wildtype DNA sequence using for instance CRISPR/Cas9-based genome editing. Such an experimental approach might not only be beneficial for ICF patients but could also provide an interesting strategy for the development of therapies for KS patients if applicable in humans in the future.

REFERENCES

1. Balemans, M.C., Ansar, M., Oudakker, A.R., van Caam, A.P., Bakker, B., Vitters, E.L., van der Kraan, P.M., de Bruijn, D.R., Janssen, S.M., Kuipers, A.J., Huibers, M.M., Maliepaard, E.M., Walboomers, X.F., Benevento, M., Nadif, K.N., Kleefstra, T., Zhou, H., Van der Zee, C.E., and van, B.H. (2014). Reduced Euchromatin histone methyltransferase 1 causes developmental delay, hypotonia, and cranial abnormalities associated with increased bone gene expression in Kleefstra syndrome mice. *Dev. Biol.* 386, 395-407.
2. Balemans, M.C., Huibers, M.M., Eikelenboom, N.W., Kuipers, A.J., van Summeren, R.C., Pijpers, M.M., Tachibana, M., Shinkai, Y., van, B.H., and Van der Zee, C.E. (2010). Reduced exploration, increased anxiety, and altered social behavior: Autistic-like features of euchromatin histone methyltransferase 1 heterozygous knockout mice. *Behav. Brain Res.* 208, 47-55.
3. Balemans, M.C., Kasri, N.N., Kopanitsa, M.V., Afinowi, N.O., Ramakers, G., Peters, T.A., Beynon, A.J., Janssen, S.M., van Summeren, R.C., Eeftens, J.M., Eikelenboom, N., Benevento, M., Tachibana, M., Shinkai, Y., Kleefstra, T., van, B.H., and Van der Zee, C.E. (2013). Hippocampal dysfunction in the Euchromatin histone methyltransferase 1 heterozygous knockout mouse model for Kleefstra syndrome. *Hum. Mol. Genet.* 22, 852-866.
4. Bao, Z., Cao, C., Geng, X., Tian, B., Wu, Y., Zhang, C., Chen, Z., Li, W., Shen, H., and Ying, S. (2015). Effectiveness and safety of poly (ADP-ribose) polymerase inhibitors in cancer therapy: A systematic review and meta-analysis. *Oncotarget.*
5. Bergsagel, P.L., Chesi, M., Nardini, E., Brents, L.A., Kirby, S.L., and Kuehl, W.M. (1996). Promiscuous translocations into immunoglobulin heavy chain switch regions in multiple myeloma. *Proc. Natl. Acad. Sci. U. S. A.* 93, 13931-13936.
6. Bouwman, P., Aly, A., Escandell, J.M., Pieterse, M., Bartkova, J., van der Gulden, H., Hiddingh, S., Thanasoula, M., Kulkarni, A., Yang, Q., Haffty, B.G., Tommiska, J., Blomqvist, C., Drapkin, R., Adams, D.J., Nevanlinna, H., Bartek, J., Tarsounas, M., Ganesan, S., and Jonkers, J. (2010). 53BP1 loss rescues BRCA1 deficiency and is associated with triple-negative and BRCA-mutated breast cancers. *Nat. Struct. Mol. Biol.* 17, 688-695.
7. Bryant, H.E., Schultz, N., Thomas, H.D., Parker, K.M., Flower, D., Lopez, E., Kyle, S., Meuth, M., Curtin, N.J., and Helleday, T. (2005). Specific killing of BRCA2-deficient tumours with inhibitors of poly(ADP-ribose) polymerase. *Nature* 434, 913-917.
8. Bunting, S.F., Callen, E., Wong, N., Chen, H.T., Polato, F., Gunn, A., Bothmer, A., Feldhahn, N., Fernandez-Capetillo, O., Cao, L., Xu, X., Deng, C.X., Finkel, T., Nussenzweig, M., Stark, J.M., and Nussenzweig, A. (2010). 53BP1 inhibits homologous recombination in Brca1-deficient cells by blocking resection of DNA breaks. *Cell* 141, 243-254.
9. Burrage, J., Termanis, A., Geissner, A., Myant, K., Gordon, K., and Stancheva, I. (2012). The SNF2 family ATPase LSH promotes phosphorylation of H2AX and efficient repair of DNA double-strand breaks in mammalian cells. *J. Cell Sci.* 125, 5524-5534.
10. Curry, E., Green, I., Chapman-Rothe, N., Shamsaei, E., Kandil, S., Cherblanc, F.L., Payne, L., Bell, E., Ganesh, T., Srirongkolpithak, N., Caron, J., Li, F., Uren, A.G., Snyder, J.P., Vedadi, M., Fuchter, M.J., and Brown, R. (2015). Dual EZH2 and EHMT2 histone methyltransferase inhibition increases biological efficacy in breast cancer cells. *Clin. Epigenetics.* 7, 84.
11. Davidson, B., Trope, C.G., Wang, T.L., and Shih, I. (2006). Expression of the chromatin remodeling factor Rsf-1 is upregulated in ovarian carcinoma effusions and predicts poor survival. *Gynecol. Oncol.* 103, 814-819.
12. Day, J.J. and Sweatt, J.D. (2011). Epigenetic mechanisms in cognition. *Neuron* 70, 813-829.
13. Elia, A.E., Boardman, A.P., Wang, D.C., Huttlin, E.L., Everley, R.A., Dephoure, N., Zhou, C., Koren, I., Gygi, S.P., and Elledge, S.J. (2015). Quantitative Proteomic Atlas of Ubiquitination and Acetylation in the DNA Damage Response. *Mol. Cell* 59, 867-881.
14. Farmer, H., McCabe, N., Lord, C.J., Tutt, A.N., Johnson, D.A., Richardson, T.B., Santaros, M., Dillon, K.J., Hickson, I., Knights, C., Martin, N.M., Jackson, S.P., Smith, G.C., and Ashworth, A. (2005). Targeting the DNA repair defect in BRCA mutant cells as a therapeutic strategy. *Nature* 434, 917-921.
15. Guan, X., Zhong, X., Men, W., Gong, S., Zhang, L., and Han, Y. (2014). Analysis of EHMT1 expression and its correlations with clinical significance in esophageal squamous cell cancer. *Mol. Clin. Oncol.* 2, 76-80.
16. Hagleitner, M.M., Lankester, A., Maraschio, P., Hulten, M., Fryns, J.P., Schuetz, C., Gimelli, G., Davies, E.G., Gennery, A., Belohradsky, B.H., de, G.R., Gerritsen, E.J., Mattina, T., Howard, P.J., Fasth, A., Reisl, I., Furthner, D., Slatter, M.A., Cant, A.J., Cazzola, G., van Dijken, P.J., van, D.M., de Greef, J.C., van der Maarel, S.M., and Weemaes, C.M. (2008). Clinical spectrum of immunodeficiency, centromeric instability and facial dysmorphism (ICF syndrome). *J. Med. Genet.* 45, 93-99.
17. Helfricht, A., Wiegant, W.W., Thijssen, P.E., Vertegaal, A.C., Luijsterburg, M.S., and van Attikum, H. (2013). Remodeling and spacing factor 1 (RSF1) deposits centromere proteins at DNA double-strand breaks to promote non-homologous end-joining. *Cell Cycle* 12, 3070-3082.
18. Jackson, S.P. and Bartek, J. (2009). The DNA-damage response in human biology and disease. *Nature* 461, 1071-1078.
19. Janz, S. (2006). Myc translocations in B cell and plasma cell neoplasms. *DNA Repair (Amst)* 5, 1213-1224.
20. Jones, P.A. and Baylin, S.B. (2007). The epigenomics of cancer. *Cell* 128, 683-692.
21. Kleefstra, T., Kramer, J.M., Neveling, K., Willemsen, M.H., Koemans, T.S., Vissers, L.E., Wissink-Lindhout, W., Fencckova, M., van den Akker, W.M., Kasri, N.N., Nillesen, W.M., Prescott, T., Clark, R.D., Devriendt, K., van Rieuwijk, J., de Brouwer, A.P., Gilissen, C., Zhou, H., Brunner, H.G., Veltman, J.A., Schenck, A., and van Bokhoven, H. (2012). Disruption of an EHMT1-associated chromatin-modification module causes intellectual disability. *Am. J. Hum. Genet.* 91, 73-82.
22. Kramer, J.M., Kochinke, K., Oortveld, M.A., Marks, H., Kramer, D., de Jong, E.K., Asztalos, Z., Westwood, J.T., Stunnenberg, H.G.,

- Sokolowski,M.B., Keleman,K., Zhou,H., van Bokhoven,H., and Schenck,A. (2011). Epigenetic regulation of learning and memory by *Drosophila* EHMT/G9a. *PLoS. Biol.* 9, e1000569.
22. Kubota,T., Furuumi,H., Kamoda,T., Iwasaki,N., Tobita,N., Fujiwara,N., Goto,Y., Matsui,A., Sasaki,H., and Kajii,T. (2004). ICF syndrome in a girl with DNA hypomethylation but without detectable DNMT3B mutation. *Am. J. Med. Genet. A* 129A, 290-293.
 - Kuppers,R. and Dalla-Favera,R. (2001). Mechanisms of chromosomal translocations in B cell lymphomas. *Oncogene* 20, 5580-5594.
 23. Lee,H.E., Han,N., Kim,M.A., Lee,H.S., Yang,H.K., Lee,B.L., and Kim,W.H. (2014). DNA damage response-related proteins in gastric cancer: ATM, Chk2 and p53 expression and their prognostic value. *Pathobiology* 81, 25-35.
 24. Li,H., Zhang,Y., Zhang,Y., Bai,X., Peng,Y., and He,P. (2014). Rsf-1 overexpression in human prostate cancer, implication as a prognostic marker. *Tumour. Biol.* 35, 5771-5776.
 25. Liu,F., Barsyte-Lovejoy,D., Li,F., Xiong,Y., Korboukh,V., Huang,X.P., Allali-Hassani,A., Janzen,W.P., Roth,B.L., Frye,S.V., Arrowsmith,C.H., Brown,P.J., Vedadi,M., and Jin,J. (2013). Discovery of an in vivo chemical probe of the lysine methyltransferases G9a and GLP. *J. Med. Chem.* 56, 8931-8942.
 26. Liu,S., Dong,Q., and Wang,E. (2012). Rsf-1 overexpression correlates with poor prognosis and cell proliferation in colon cancer. *Tumour. Biol.* 33, 1485-1491.
 27. Lotterberger,F., Bothmer,A., Robbiani,D.F., Nussenzweig,M.C., and de,L.T. (2013). Role of 53BP1 oligomerization in regulating double-strand break repair. *Proc. Natl. Acad. Sci. U. S. A* 110, 2146-2151.
 28. Miller,C.A., Gavin,C.F., White,J.A., Parrish,R.R., Honasoge,A., Yancey,C.R., Rivera,I.M., Rubio,M.D., Rumbaugh,G., and Sweatt,J.D. (2010). Cortical DNA methylation maintains remote memory. *Nat. Neurosci.* 13, 664-666.
 29. Min,S., Jo,S., Lee,H.S., Chae,S., Lee,J.S., Ji,J.H., and Cho,H. (2014). ATM-dependent chromatin remodeler Rsf-1 facilitates DNA damage checkpoints and homologous recombination repair. *Cell Cycle* 13, 666-677.
 30. Moore,K.E., Carlson,S.M., Camp,N.D., Cheung,P., James,R.G., Chua,K.F., Wolf-Yadlin,A., and Gozani,O. (2013). A general molecular affinity strategy for global detection and proteomic analysis of lysine methylation. *Mol. Cell* 50, 444-456.
 31. Mukherjee,S. and Thrasher,A.J. (2013). Gene therapy for PIDs: progress, pitfalls and prospects. *Gene* 525, 174-181.
 32. O'Hagan,H.M., Mohammad,H.P., and Baylin,S.B. (2008). Double strand breaks can initiate gene silencing and SIRT1-dependent onset of DNA methylation in an exogenous promoter CpG island. *PLoS. Genet.* 4, e1000155.
 33. Okano,M., Bell,D.W., Haber,D.A., and Li,E. (1999). DNA methyltransferases Dnmt3a and Dnmt3b are essential for de novo methylation and mammalian development. *Cell* 99, 247-257.
 34. Pappano,W.N., Guo,J., He,Y., Ferguson,D., Jagadeeswaran,S., Osterling,D.J., Gao,W., Spence,J.K., Pliushchev,M., Sweis,R.F., Buchanan,F.G., Michaelides,M.R., Shoemaker,A.R., Tse,C., and Chiang,G.G. (2015). The Histone Methyltransferase Inhibitor A-366 Uncovers a Role for G9a/GLP in the Epigenetics of Leukemia. *PLoS. One.* 10, e0131716.
 35. Perpelescu,M. and Fukagawa,T. (2011). The ABCs of CENPs. *Chromosoma* 120, 425-446.
 36. Perpelescu,M., Nozaki,N., Obuse,C., Yang,H., and Yoda,K. (2009). Active establishment of centromeric CENP-A chromatin by RSF complex. *J. Cell Biol.* 185, 397-407.
 37. Pessina,F. and Lowndes,N.F. (2014). The RSF1 histone-remodelling factor facilitates DNA double-strand break repair by recruiting centromeric and Fanconi Anaemia proteins. *PLoS. Biol.* 12, e1001856.
 38. Reale,A., De Matteis,G., Galleazzi,G., Zampieri,M., and Caiapa,P. (2005). Modulation of DNMT1 activity by ADP-ribose polymers. *Oncogene* 24, 13-19.
 39. Rudra,S. and Skibbens,R.V. (2013). Chl1 DNA helicase regulates Scc2 deposition specifically during DNA-replication in *Saccharomyces cerevisiae*. *PLoS. One.* 8, e75435.
 40. Schuetz,C., Barbi,G., Barth,T.F., Hoenig,M., Schulz,A., Moeller,P., Smeets,D., de Greef,J.C., van der Maarel,S.M., Vogel,W., Debatin,K.M., and Friedrich,W. (2007). ICF syndrome: high variability of the chromosomal phenotype and association with classical Hodgkin lymphoma. *Am. J. Med. Genet. A* 143A, 2052-2057.
 41. Sheu,J.J., Guan,B., Choi,J.H., Lin,A., Lee,C.H., Hsiao,Y.T., Wang,T.L., Tsai,F.J., and Shih,I. (2010). Rsf-1, a chromatin remodeling protein, induces DNA damage and promotes genomic instability. *J. Biol. Chem.* 285, 38260-38269.
 42. Shih,A.H., Abdel-Wahab,O., Patel,J.P., and Levine,R.L. (2012). The role of mutations in epigenetic regulators in myeloid malignancies. *Nat. Rev. Cancer* 12, 599-612.
 43. Shih,J., Sheu,J.J., Santillan,A., Nakayama,K., Yen,M.J., Bristow,R.E., Vang,R., Parmigiani,G., Kurman,R.J., Trope,C.G., Davidson,B., and Wang,T.L. (2005). Amplification of a chromatin remodeling gene, Rsf-1/HBXAP, in ovarian carcinoma. *Proc. Natl. Acad. Sci. U. S. A* 102, 14004-14009.
 44. Singh,T.R., Saro,D., Ali,A.M., Zheng,X.F., Du,C.H., Killen,M.W., Sachpatzidis,A., Wahengbam,K., Pierce,A.J., Xiong,Y., Sung,P., and Meetei,A.R. (2010). MHF1-MHF2, a histone-fold-containing protein complex, participates in the Fanconi anemia pathway via FANCM. *Mol. Cell* 37, 879-886.
 45. Smeenk,G. and van Attikum,H. (2013). The chromatin response to DNA breaks: leaving a mark on genome integrity. *Annu. Rev. Biochem.* 82, 55-80.
 46. Smeenk,G., Wiegant,W.W., Marteiijn,J.A., Luijsterburg,M.S., Sroczynski,N., Costelloe,T., Romeijn,R.J., Pastink,A., Mailand,N., Vermeulen,W., and van Attikum,H. (2013). Poly(ADP-ribosyl)ation links the chromatin remodeler SMARCA5/SNF2H to RNF168-

- Sokolowski,M.B., Keleman,K., Zhou,H., van Bokhoven,H., and Schenck,A. (2011). Epigenetic regulation of learning and memory by *Drosophila* EHMT/G9a. *PLoS. Biol.* 9, e1000569.
47. Kubota,T., Furuumi,H., Kamoda,T., Iwasaki,N., Tobita,N., Fujiwara,N., Goto,Y., Matsui,A., Sasaki,H., and Kajii,T. (2004). ICF syndrome in a girl with DNA hypomethylation but without detectable DNMT3B mutation. *Am. J. Med. Genet. A* 129A, 290-293.
 - Kuppers,R. and Dalla-Favera,R. (2001). Mechanisms of chromosomal translocations in B cell lymphomas. *Oncogene* 20, 5580-5594.
 48. Lee,H.E., Han,N., Kim,M.A., Lee,H.S., Yang,H.K., Lee,B.L., and Kim,W.H. (2014). DNA damage response-related proteins in gastric cancer: ATM, Chk2 and p53 expression and their prognostic value. *Pathobiology* 81, 25-35.
 49. Li,H., Zhang,Y., Zhang,Y., Bai,X., Peng,Y., and He,P. (2014). Rsf-1 overexpression in human prostate cancer, implication as a prognostic marker. *Tumour. Biol.* 35, 5771-5776.
 50. Liu,F., Baryste-Lovejoy,D., Li,F., Xiong,Y., Korboukh,V., Huang,X.P., Allali-Hassani,A., Janzen,W.P., Roth,B.L., Frye,S.V., Arrowsmith,C.H., Brown,P.J., Vedadi,M., and Jin,J. (2013). Discovery of an in vivo chemical probe of the lysine methyltransferases G9a and GLP. *J. Med. Chem.* 56, 8931-8942.
 51. Liu,S., Dong,Q., and Wang,E. (2012). Rsf-1 overexpression correlates with poor prognosis and cell proliferation in colon cancer. *Tumour. Biol.* 33, 1485-1491.
 52. Lotterberger,F., Bothmer,A., Robbiani,D.F., Nussenzweig,M.C., and de,L.T. (2013). Role of 53BP1 oligomerization in regulating double-strand break repair. *Proc. Natl. Acad. Sci. U. S. A* 110, 2146-2151.
 53. Miller,C.A., Gavin,C.F., White,J.A., Parrish,R.R., Honasoge,A., Yancey,C.R., Rivera,I.M., Rubio,M.D., Rumbaugh,G., and Sweatt,J.D. (2010). Cortical DNA methylation maintains remote memory. *Nat. Neurosci.* 13, 664-666.
 54. Min,S., Jo,S., Lee,H.S., Chae,S., Lee,J.S., Ji,J.H., and Cho,H. (2014). ATM-dependent chromatin remodeler Rsf-1 facilitates DNA damage checkpoints and homologous recombination repair. *Cell Cycle* 13, 666-677.
 55. Moore,K.E., Carlson,S.M., Camp,N.D., Cheung,P., James,R.G., Chua,K.F., Wolf-Yadlin,A., and Gozani,O. (2013). A general molecular affinity strategy for global detection and proteomic analysis of lysine methylation. *Mol. Cell* 50, 444-456.
 56. Mukherjee,S. and Thrasher,A.J. (2013). Gene therapy for PIDs: progress, pitfalls and prospects. *Gene* 525, 174-181.
 57. O'Hagan,H.M., Mohammad,H.P., and Baylin,S.B. (2008). Double strand breaks can initiate gene silencing and SIRT1-dependent onset of DNA methylation in an exogenous promoter CpG island. *PLoS. Genet.* 4, e1000155.
 58. Okano,M., Bell,D.W., Haber,D.A., and Li,E. (1999). DNA methyltransferases Dnmt3a and Dnmt3b are essential for de novo methylation and mammalian development. *Cell* 99, 247-257.
 59. Pappano,W.N., Guo,J., He,Y., Ferguson,D., Jagadeeswaran,S., Osterling,D.J., Gao,W., Spence,J.K., Pliushchev,M., Sweis,R.F., Buchanan,F.G., Michaelides,M.R., Shoemaker,A.R., Tse,C., and Chiang,G.G. (2015). The Histone Methyltransferase Inhibitor A-366 Uncovers a Role for G9a/GLP in the Epigenetics of Leukemia. *PLoS. One.* 10, e0131716.
 60. Perpelescu,M. and Fukagawa,T. (2011). The ABCs of CENPs. *Chromosoma* 120, 425-446.
 61. Perpelescu,M., Nozaki,N., Obuse,C., Yang,H., and Yoda,K. (2009). Active establishment of centromeric CENP-A chromatin by RSF complex. *J. Cell Biol.* 185, 397-407.
 62. Pessina,F. and Lowndes,N.F. (2014). The RSF1 histone-remodelling factor facilitates DNA double-strand break repair by recruiting centromeric and Fanconi Anaemia proteins. *PLoS. Biol.* 12, e1001856.
 63. Reale,A., De Matteis,G., Galleazzi,G., Zampieri,M., and Caiafa,P. (2005). Modulation of DNMT1 activity by ADP-ribose polymers. *Oncogene* 24, 13-19.
 64. Rudra,S. and Skibbens,R.V. (2013). Chl1 DNA helicase regulates Scc2 deposition specifically during DNA-replication in *Saccharomyces cerevisiae*. *PLoS. One.* 8, e75435.
 65. Schuetz,C., Barbi,G., Barth,T.F., Hoenig,M., Schulz,A., Moeller,P., Smeets,D., de Greef,J.C., van der Maarel,S.M., Vogel,W., Debatin,K.M., and Friedrich,W. (2007). ICF syndrome: high variability of the chromosomal phenotype and association with classical Hodgkin lymphoma. *Am. J. Med. Genet. A* 143A, 2052-2057.
 66. Sheu,J.J., Guan,B., Choi,J.H., Lin,A., Lee,C.H., Hsiao,Y.T., Wang,T.L., Tsai,F.J., and Shih,I. (2010). Rsf-1, a chromatin remodeling protein, induces DNA damage and promotes genomic instability. *J. Biol. Chem.* 285, 38260-38269.
 67. Shih,A.H., Abdel-Wahab,O., Patel,J.P., and Levine,R.L. (2012). The role of mutations in epigenetic regulators in myeloid malignancies. *Nat. Rev. Cancer* 12, 599-612.
 68. Shih,I., Sheu,J.J., Santillan,A., Nakayama,K., Yen,M.J., Bristow,R.E., Vang,R., Parmigiani,G., Kurman,R.J., Trope,C.G., Davidson,B., and Wang,T.L. (2005). Amplification of a chromatin remodeling gene, Rsf-1/HBXAP, in ovarian carcinoma. *Proc. Natl. Acad. Sci. U. S. A* 102, 14004-14009.
 69. Singh,T.R., Saro,D., Ali,A.M., Zheng,X.F., Du,C.H., Killen,M.W., Sachpatzidis,A., Wahengbam,K., Pierce,A.J., Xiong,Y., Sung,P., and Meetei,A.R. (2010). MHF1-MHF2, a histone-fold-containing protein complex, participates in the Fanconi anemia pathway via FANCM. *Mol. Cell* 37, 879-886.
 70. Smeenk,G. and van Attikum,H. (2013). The chromatin response to DNA breaks: leaving a mark on genome integrity. *Annu. Rev. Biochem.* 82, 55-80.
 71. Smeenk,G., Wiegant,W.W., Marteiijn,J.A., Luijsterburg,M.S., Sroczynski,N., Costelloe,T., Romeijn,R.J., Pastink,A., Mailand,N., Vermeulen,W., and van Attikum,H. (2013). Poly(ADP-ribosyl)ation links the chromatin remodeler SMARCA5/SNF2H to RNF168-

- dependent DNA damage signaling. *J. Cell Sci.* 126, 889-903.
72. Thijsen,P.E., Ito,Y., Grillo,G., Wang,J., Velasco,G., Nitta,H., Unoki,M., Yoshihara,M., Suyama,M., Sun,Y., Lemmers,R.J., de Greef,J.C., Gennery,A., Picco,P., Kloeckener-Gruissem,B., Gungor,T., Reisli,I., Picard,C., Kebaili,K., Roquelaure,B., Iwai,T., Kondo,I., Kubota,T., van Ostaijen-Ten Dam MM, van Tol,M.J., Weemaes,C., Francastel,C., van der Maarel,S.M., and Sasaki,H. (2015). Mutations in CDCA7 and HELLS cause immunodeficiency-centromeric instability-facial anomalies syndrome. *Nat. Commun.* 6, 7870.
 73. van den Brand,M., Flucke,U.E., Bult,P., Weemaes,C.M., and van,D.M. (2011). Angiosarcoma in a patient with immunodeficiency, centromeric region instability, facial anomalies (ICF) syndrome. *Am. J. Med. Genet. A* 155A, 622-625.
 74. Weemaes,C.M., van Tol,M.J., Wang,J., van Ostaijen-Ten Dam MM, van Eggermond,M.C., Thijsen,P.E., Aytekin,C., Brunetti-Pierri,N., van der Burg,M., Graham,D.E., Ferster,A., Furthner,D., Gimelli,G., Gennery,A., Kloeckener-Gruissem,B., Meyn,S., Powell,C., Reisli,I., Schuetz,C., Schulz,A., Shugar,A., van den Elsen,P.J., and van der Maarel,S.M. (2013). Heterogeneous clinical presentation in ICF syndrome: correlation with underlying gene defects. *Eur. J. Hum. Genet.* 21, 1219-1225.
 75. Willemsen,M.H., Vulto-van Silfhout,A.T., Nillesen,W.M., Wissink-Lindhout,W.M., van Bokhoven,H., Philip,N., Berry-Kravis,E.M., Kini,U., van Ravenswaaij-Arts,C.M., Delle,C.B., Innes,A.M., Houge,G., Kosonen,T., Cremer,K., Fannemel,M., Stray-Pedersen,A., Reardon,W., Ignatius,J., Lachlan,K., Mircher,C., Helderma van den Eenden,P.T., Mastebroek,M., Cohn-Hokke,P.E., Yntema,H.G., Drunat,S., and Kleefstra,T. (2012). Update on Kleefstra Syndrome. *Mol. Syndromol.* 2, 202-212.
 76. Xie,C., Fu,L., Xie,L., Liu,N., and Li,Q. (2014). Rsf-1 overexpression serves as a prognostic marker in human hepatocellular carcinoma. *Tumour Biol.* 35, 7595-7601.
 77. Xu,G., Chapman,J.R., Brandsma,I., Yuan,J., Mistrik,M., Bouwman,P., Bartkova,J., Gogola,E., Warmerdam,D., Barazas,M., Jaspers,J.E., Watanabe,K., Pieterse,M., Kersbergen,A., Sol,W., Celie,P.H., Schouten,P.C., van den Broek,B., Salman,A., Nieuwland,M., de,R., I, de,R.J., Jalink,K., Boulton,S.J., Chen,J., van Gent,D.C., Bartek,J., Jonkers,J., Borst,P., and Rottenberg,S. (2015). REV7 counteracts DNA double-strand break resection and affects PARP inhibition. *Nature* 521, 541-544.
 78. Yan,Z., Delannoy,M., Ling,C., Daege,D., Osman,F., Muniandy,P.A., Shen,X., Oostra,A.B., Du,H., Steltenpool,J., Lin,T., Schuster,B., Decaillet,C., Stasiak,A., Stasiak,A.Z., Stone,S., Hoatlin,M.E., Schindler,D., Woodcock,C.L., Joenje,H., Sen,R., de Winter,J.P., Li,L., Seidman,M.M., Whitby,M.C., Myung,K., Constantinou,A., and Wang,W. (2010). A histone-fold complex and FANCM form a conserved DNA-remodeling complex to maintain genome stability. *Mol. Cell* 37, 865-878.
 79. Zeitlin,S.G., Baker,N.M., Chapados,B.R., Soutoglou,E., Wang,J.Y., Berns,M.W., and Cleveland,D.W. (2009). Double-strand DNA breaks recruit the centromeric histone CENP-A. *Proc. Natl. Acad. Sci. U. S. A* 106, 15762-15767.
 80. Zhu,H., Geiman,T.M., Xi,S., Jiang,Q., Schmidtmann,A., Chen,T., Li,E., and Muegge,K. (2006). Lsh is involved in de novo methylation of DNA. *EMBO J.* 25, 335-345.



APPENDIX



ENGLISH SUMMARY

The human body consists of a variety of cell types, which all contain the same genetic information that is encoded in the DNA. The DNA is structured into specific regions, called genes, and each gene contains the building information for a particular protein. All the different functions of proteins together facilitate cellular mechanisms required for life. In order for cells to survive in a healthy manner, it is crucial to keep their genetic information intact and transmit it unaltered to daughter cells. However, each day our DNA is exposed to various damaging agents originating from the environment, like UV light, ionizing radiation or cigarette smoke, or from chemical reactions taking place inside cells such as oxygen free radicals. Scientists estimated that between 1.000 and 10.000 DNA lesions per cell arise each day from such DNA damage-inducing assaults. Fortunately, our cells are equipped with sophisticated DNA signaling and repair mechanisms, commonly termed the DNA damage response (DDR), that can detect and repair different types of DNA lesions. If DNA damage is not (correctly) repaired, alterations in the basic units of the DNA, the nucleotides, can occur. These are generally referred to as mutations and can potentially give rise to cancer. Although the general steps of the different DNA repair pathways are known, novel proteins involved in the response to DNA damage are still frequently identified. In addition, more and more cancer-causing mutations are found in genes that encode DDR proteins. Thus, it is of great importance to investigate the role of DDR proteins and use this knowledge for the development of innovative anti-cancer therapies.

The research described in this thesis focusses on the cellular response to DNA Double-Strand Breaks (DSBs). This type of lesion causes the disruption of both DNA strands and therefore can be potentially deleterious. In **chapter 1** of my thesis, I provide the reader with a detailed introduction on the mechanisms involved in the signaling and repair of DSBs. Additionally, I explain the link between the DDR and human diseases, like cancer, and its relevance for therapy development.

In **chapter 2**, I present the results obtained from an siRNA screen I performed to identify novel chromatin-modifying proteins involved in the signaling of DSBs. As a read-out, I monitored the accumulation of the DNA damage signaling markers γ H2AX and 53BP1 in cells after exposure to ionizing radiation (IR). Euchromatic histone-lysine N-methyltransferase 1 (EHMT1) was a prominent hit and appeared to be a negative regulator of 53BP1 recruitment. In follow-up experiments, I observed recruitment of EHMT1 to laser-induced DNA damage and found EHMT1 to be involved in the two DSB repair pathways, Non-Homologous End-Joining (NHEJ) and Homologous Recombination (HR).

In **chapter 3**, my findings reveal a novel role of Remodeling and Spacing Factor 1 (RSF1) in the DSB response. RSF1 facilitates the assembly and incorporation of the centromere proteins CENP-S and CENP-X at DSBs, which in turn facilitates the recruitment of the NHEJ factor XRCC4 to damaged chromatin and promotes NHEJ-mediated DSB repair. RSF1 is also required for efficient DSB repair via HR. However, since CENP-S and CENP-X are dispensable for HR, this function of RSF1 is independent from these centromeric proteins. Surprisingly, I found that RSF1's role in DSB repair is also independent from its binding partner SMARCA5. My study on the effect of post-translational modification of RSF1 by the small ubiquitin-like modifier (SUMO) on the role of RSF1 in DSB repair is presented in **chapter 4**. 21 SUMO-acceptor lysines in RSF1 have been identified and their SUMOylation strongly increases after IR-induced DNA damage. In addition, I show that a SUMOylation-deficient mutant (SUMO Δ) of RSF1 is still efficiently recruited to laser-induced DSBs. However, while wildtype RSF1 can

recruit XRCC4 to DSBs, the RSF1 SUMO Δ mutant was no longer capable of doing so. In **chapter 5**, I summarize our findings on the Zinc finger and BTB (bric-a-bric, tramtrack, broad complex) containing 24 (ZBTB24) protein. Mutations in ZBTB24 have been shown to cause the Immunodeficiency, Centromeric instability and Facial anomalies (ICF) syndrome type 2. I demonstrate that the loss of ZBTB24 impairs class-switch recombination by NHEJ during immunoglobulin switching in B cells from ICF2 patients. This leads to impaired immunoglobulin production and an imbalance in immunoglobulin subtype formation in these patients. In addition, mechanistic studies revealed that the zinc finger in ZBTB24 interacts with poly(ADP-ribose) polymerase 1 (PARP1)-associated poly(ADP-ribose) chains and is required for the PARP1-dependent transient recruitment of ZBTB24 to laser-induced DNA damage. The protective binding of ZBTB24 to poly(ADP-ribose) chains counteracts their degradation by poly(ADP-ribose) glycohydrolase (PARG) and enhances the poly(ADP-ribose)-mediated interaction of PARP1 and the NHEJ complex LIG4/XRCC4, thereby promoting DSB repair via NHEJ.

Finally in **chapter 6**, I discuss the discovered roles of the investigated chromatin-modifying proteins EHMT1, RSF1 and ZBTB24 within a broader context. Since all three proteins are linked to cancer and other human diseases, I also evaluate their potential application in existing and novel disease therapies.



NEDERLANDSE SAMENVATTING

Het menselijk lichaam bestaat uit een groot aantal verschillende soorten cellen, die allemaal dezelfde genetische informatie bevatten. Deze informatie ligt in ons DNA, in specifieke regio's die we de genen noemen. Elk gen bevat een bouwplan voor een bepaald eiwit met een of meerdere specifieke functies. De functies van alle eiwitten samen faciliteren de processen in onze cellen, die voor het leven noodzakelijk zijn. Om gezond te kunnen leven is het van belang dat elke cel de genomische informatie intact houdt, en deze onveranderd doorgeeft aan de dochtercellen. Ons DNA wordt echter elke dag blootgesteld aan een diversiteit van schadelijke stoffen die uit de omgeving op ons inwerken, zoals UV licht, ioniserende straling en sigarettenrook. Ook ontstaan er schadelijke stoffen tijdens chemische reacties binnen onze cellen, zoals bijvoorbeeld oxidatieve radicalen. Wetenschappers hebben berekend dat er door de blootstelling aan DNA-schade-inducerende stoffen elke dag tussen de 1000 en 10.000 DNA schades per cel ontstaan. Gelukkig zijn onze cellen uitgerust met een geraffineerd signaleringssysteem en verschillende herstel mechanismen, die allerlei types DNA schade kunnen detecteren en repareren. Maar, als de schades in het DNA niet of onzorgvuldig gerepareerd worden, kunnen veranderingen ontstaan in de basiseenheden van het DNA, de nucleotiden. Dergelijke veranderingen worden mutaties genoemd en kunnen kanker veroorzaken. De manier waarop cellen verschillende vormen van DNA schade repareren is globaal in kaart gebracht. Toch worden er nog regelmatig nieuwe eiwitten geïdentificeerd die een rol spelen tijdens het herstel van DNA schade. Studies naar het functioneren van deze eiwitten leveren nog steeds nieuwe inzichten over het verloop van DNA schade herstel. Bovendien worden er meer en meer kanker-veroorzakende mutaties in patiënten gevonden in genen die voor DNA schadeherstel eiwitten coderen. Recent onderzoek heeft uitgewezen dat kennis over DNA reparatie belangrijk is voor het ontwikkelen van nieuwe kankertherapieën. Daarom is het van groot belang de rol van (nieuwe) DNA schadeherstel eiwitten te onderzoeken en deze kennis te gebruiken voor de mogelijke ontwikkeling van nieuwe behandelingen.

Het onderzoek beschreven in dit proefschrift richt zich op de reactie van cellen op DNA dubbelstrengbreuken (DSBs). Dit is een zeer schadelijke vorm van DNA schade waarbij beide strengen van het DNA doorbroken worden. In **hoofdstuk 1** van mijn proefschrift voorzie ik de lezer van een uitgebreide inleiding over DSB signalering en herstel. Ook ga ik in op de link tussen fundamenteel mechanistisch onderzoek van DNA schadeherstel, menselijke ziekten zoals kanker en therapiemogelijkheden.

De verkregen resultaten van een siRNA screen, die ik heb uitgevoerd om nieuwe eiwitten met een rol in de signalering van DSB te identificeren, worden gepresenteerd in **hoofdstuk 2**. Hier heb ik de ophoping van de DNA schade-signalerings-eiwitten γ H2AX en 53BP1 op DNA breuken in cellen na blootstelling aan ioniserende straling (IS) bestudeerd. Door middel van RNA interferentie technologie heb ik systematisch chromatine-modificerende eiwitten uitgeschakeld om het effect daarvan op de accumulatie van γ H2AX en 53BP1 te bestuderen. Euchromatic histone-lysine N-methyltransferase 1 (EHMT1) kwam als een prominente hit uit de screen; het eiwit bleek de 53BP1 ophoping te controleren. In vervolgonderzoek heb ik gevonden dat EHMT1 naar laser-geïnduceerde DNA schade gerekruteerd wordt en betrokken is bij de twee belangrijke DSB herstel routes, 'Non-Homologous End-Joining' (NHEJ) en 'Homologous Recombination' (HR).

In **hoofdstuk 3** leggen mijn bevindingen een nieuwe rol voor 'Remodeling and Spacing Factor 1' (RSF1) in het NHEJ-herstelmechanisme bloot. RSF1 faciliteert het ophopen en inbouwen

van de centromerische eiwitten CENP-S en CENP-X op DSB. Dat heeft als gevolg, dat de NHEJ factor XRCC4 naar beschadigd chromatine gerekruteerd wordt en DSB met behulp van NHEJ gerepareerd worden. RSF1 is echter ook noodzakelijk voor het efficiënte herstel van DSBs door middel van HR, maar omdat CENP-S en CENP-X overbodig bleken voor de HR route, lijkt de functie van RSF1 tijdens HR onafhankelijk te zijn van de twee centromerische eiwitten. Tegen de verwachting in bleek de rol van RSF1 in DSB herstel ook onafhankelijk te zijn van de interactie partner SMARCA5.

Het effect van post-translationale modificatie van RSF1 door small ubiquitin-like modifier (SUMO) op de DSB herstel-gerelateerde rol van RSF1 is beschreven in **hoofdstuk 4**. Er zijn 21 lysines in de aminozuursequentie van RSF1 geïdentificeerd die door SUMO gemodificeerd kunnen worden. De SUMO-afhankelijke modificatie van RSF1 neemt duidelijk toe na de inductie van DNA schade door middel van IS. Verder bleek, dat een niet-SUMO-modificeerbare vorm (SUMO Δ) van RSF1 nog steeds op laser-geïnduceerde DSBs ophoopt. Echter, terwijl wildtype RSF1 XRCC4 naar DSBs kan rekruteren, was de RSF1 SUMO Δ mutant hiertoe niet langer in staat.

In **hoofdstuk 5** vat ik onze bevindingen samen over het Zinc finger and BTB (bric-a-bric, tramtrack, broad complex) containing 24 (ZBTB24) eiwit, waarvoor is aangetoond dat genetische defecten het Immunodeficiency, Centromeric instability and Facial anomalies (ICF) syndroom type 2 veroorzaken. Ik laat zien dat, in cellen van ICF2 patiënten die geen werkend ZBTB24 hebben, NHEJ tijdens immunoglobuline class switching niet naar behoren functioneert. Dat leidt tot verminderde immunoglobuline productie en een onbalans in de immunoglobuline subtype formatie in deze patiënten. Verder onderzoek wees uit dat de zinc finger van ZBTB24 en poly(ADP-ribose) polymerase 1 (PARP1)-associeerde poly(ADP-ribose) ketens met elkaar interacteren. De zinc finger is dan ook noodzakelijk voor de PARP1-afhankelijke accumulatie van ZBTB24 op laser-geïnduceerde DNA schade. De beschermende binding van ZBTB24 aan poly(ADP-ribose) ketens werkt hun afbraak door poly(ADP-ribose) glycohydrolase (PARG) tegen, en verbetert de poly(ADP-ribose)-gemedieerde interactie van PARP1 en het NHEJ complex LIG4/XRCC4, hetgeen DSB herstel via NHEJ bevordert.

Tot slot voer ik in **hoofdstuk 6** discussie over de ontdekte functies van de bestudeerde chromatine-modificerende eiwitten EHMT1, RSF1 en ZBTB24, in DNA schade herstel. Omdat deze drie eiwitten te maken hebben met kanker en andere menselijke ziekten evalueer ik ook hoe de vergaarde kennis over deze eiwitten gebruikt kan worden voor de ontwikkeling van nieuwe therapieën.



DEUTSCHE ZUSAMMENFASSUNG

Der menschliche Körper besteht aus einer Vielzahl an verschiedenen Zellsorten, welche alle die gleiche genetische Information enthalten. Diese Information ist auf der DNA in spezifischen Regionen, den Genen, codiert. Jedes Gen beinhaltet den Bauplan für ein bestimmtes Protein und alle Proteinfunktionen gemeinsam regulieren lebenswichtige zelluläre Mechanismen. Um auf eine gesunde Art und Weise zu überleben, ist es wichtig für Zellen, die DNA intakt zu halten und unverändert von der Mutterzelle zu vererben. Unsere DNA wird jedoch täglich mit verschiedenen DNA-schädigenden Reagenzien konfrontiert, die entweder aus unsere Umgebung stammen, wie UV-Licht, ionisierende Strahlung und Zigarettenrauch, oder ihren Ursprung haben im Inneren unserer Zellen, wie z.B. Produkte chemischer Reaktionen. Nach wissenschaftlichen Schätzungen entstehen zwischen 1.000 und 10.000 DNA-Schäden pro Zelle pro Tag als Folge von solchen Angriffen. Glücklicherweise sind unsere Zellen mit anspruchsvollen DNA-Signal- und Reparaturmechanismen ausgestattet, die verschiedene Arten von DNA-Schäden erkennen als auch reparieren können. Diese Mechanismen werden unter dem Nenner ‚DNA damage response‘ zusammengefasst. Wenn DNA-Schäden nicht (richtig) repariert werden, können Veränderungen in der Basiseinheit der DNA, den Nukleotiden, auftreten. Solche Veränderungen werden auch ‚Mutationen‘ genannt und können potenziell zur Entwicklung von Krebs führen. Die grundlegenden Schritte der verschiedenen DNA-Reparaturmechanismen sind bereits bekannt. Trotzdem werden noch immer regelmäßig neue Proteine identifiziert, die während der zellulären Reaktion auf DNA-Schäden eine Rolle spielen. Außerdem werden mehr und mehr Mutationen in Genen von Krebspatienten gefunden, die für DNA-damage-response-Proteine codieren. Deshalb ist es sehr wichtig, die Rolle dieser besonderen Proteine zu erforschen und dieses Wissen für die Entwicklung von innovativen Anti-Krebstherapien anzuwenden.

Die Forschungsergebnisse, die in dieser Dissertation beschrieben werden, fokussieren sich auf die zelluläre Reaktion auf DNA-Doppelstrangbrüche (DSBs). Diese Art von DNA-Schaden verursacht das Auseinanderbrechen von beiden DNA-Strängen und ist deswegen potenziell sehr schädlich. In **Kapitel 1** meiner Dissertation biete ich dem Leser eine ausführliche Einleitung in die Signalmechanismen und die Reparatur von DSBs. Zusätzlich erkläre ich den Zusammenhang zwischen der Grundlagenforschung zur Aufklärung der Mechanismen in der DNA damage response und menschlicher Krankheiten, wie z.B. Krebs, und möglicher Therapieentwicklungen.

Die Resultate eines siRNA-Screens, mit dem ich noch unbekannte Proteine identifizieren wollte, die an der Signaltransduktion von DSBs beteiligt sind, werden in **Kapitel 2** präsentiert. Ich habe die Akkumulation der DNA-Schaden-Signalisierungsmarker γ H2AX und 53BP1 in Abwesenheit von Chromatin-modifizierenden Proteinen in Zellen untersucht, die mit ionisierender Strahlung (IS) behandelt wurden. Euchromatic histone-lysine N-methyltransferase 1 (EHMT1) zeigte sich dabei als prominenter Hit für einen negativen Regulator der 53BP1-Rekrutierung zu IS-induzierten DNA-Brüchen. Zudem habe ich die Rekrutierung von EHMT1 zu Laser-induzierten DNA-Schäden zeigen können und bewiesen, dass EHMT1 in beiden DSB- Reparaturmechanismen, Non-Homologous End-Joining (NHEJ) als auch Homologous Recombination (HR), eine Rolle spielt.

In **Kapitel 3** implizieren meine Observationen eine bisher unbeschriebene Rolle des Remodeling and Spacing Factor 1 (RSF1) in der zellulären Reaktion auf DSBs. RSF1 fördert das Ansammeln und den Einbau der centromeren Proteine CENP-S und CENP-X an DSBs,



was letztendlich die Rekrutierung des NHEJ-Proteins XRCC4 ins geschädigte Chromatin bewirkt und somit die Reparatur von DSBs mit Hilfe von NHEJ unterstützt. RSF1 ist außerdem erforderlich für die Reparatur von DSBs mittels HR. Da aber, laut meiner Resultate, CENP-S und CENP-X für HR nicht benötigt werden, hat RSF1 wahrscheinlich eine andere Funktion während der HR. Wieder Erwartens scheint die Rolle von RSF1 während der Reparatur von DSBs auch unabhängig vom Interaktionspartner SMARCA5 zu sein.

Die Ergebnisse zum Effekt der posttranslationalen Modifikation durch small ubiquitin-like modifier (SUMO) auf die Funktion von RSF1 in der Reparatur von DSBs werden in **Kapitel 4** präsentiert. Es wurden 21 SUMO-modifizierte Lysine in RSF1 identifiziert. Ich konnte zeigen, dass die SUMOylierung von RSF1 nach der Induktion von DNA-Schäden mit IS deutlich zunimmt. Eine nicht-SUMOylierbare Mutante (SUMO Δ) von RSF1 wurde noch immer zu Laser-induzierten DSBs rekrutiert. Aber während Wildtyp-RSF1 XRCC4 zu DSBs befördern kann, war RSF1 SUMO Δ dazu nicht länger in der Lage.

In **Kapitel 5** fasse ich unsere Forschungsergebnisse bezüglich des Zinc finger and BTB (bric-a-bric, tramtrack, broad complex) containing 24 (ZBTB24) Gens, in dem Mutationen Immunodeficiency, Centromeric instability and Facial anomalies (ICF) Syndrom Typ 2-verursachenden, zusammen. Wir zeigen, dass NHEJ in ICF2-Patienten während des Isotypenwechsels in B-Zellen durch den Verlust von ZBTB24 beeinträchtigt ist. Dies führt zu einer fehlerhaften Immunglobulin-Produktion und einem gestörten Gleichgewicht in der Bildung der verschiedenen Antikörper-Isotypen bei diesen Patienten. Bei weiteren Untersuchungen der mechanistischen Details haben wir eine Interaktion zwischen ZBTB24 und den Poly(ADP-ribose) Polymerase 1 (PARP1)-assoziierten Poly(ADP-ribose)-Ketten entdeckt. Diese sind erforderlich für die transiente Rekrutierung von ZBTB24 zu Laser-induzierten DNA-Schäden. Die schützende Bindung der Poly(ADP-ribose)-Ketten durch ZBTB24 wirkt deren Abbau durch Poly(ADP-ribose) Glycohydrolase (PARG) entgegen und verstärkt die Poly(ADP-ribose)-abhängige Bindung von ZBTB24 zu PARP1 und dem NHEJ-Komplex LIG4/XRCC4, was wiederum die DSB-Reparatur durch NHEJ begünstigt.

Abschließend diskutiere ich in **Kapitel 6** über die neu-entdeckten Funktionen der untersuchten Chromatin-modifizierenden Proteine EHMT1, RSF1 und ZBTB24 anhand kürzlich publizierter Literatur. Da alle drei Proteine in Zusammenhang mit Krebs oder anderen menschlichen Krankheiten stehen, evaluiere ich auch, wie die neugewonnenen Erkenntnisse bezüglich dieser Proteine eingesetzt werden können, um neue Therapieformen zu entwickeln.



CURRICULUM VITAE

Angela Helfricht was born on the 28th of December 1984 in Dresden, Germany. After obtaining her diploma from the German Gymnasium in 2003, she continued her studies with a Bachelor in Life Science and Technology at Leiden University and the Technical University in Delft, both in the Netherlands. She conducted her Bachelor internship in the group of Dr. Nora Goosen at the Leiden University in 2007. During this internship, she worked on a project entitled 'The road to the lesion for the E.coli NER proteins UvrA and UvrB'. She then completed her master education in Life Science and Technology with a particular focus on Functional Genomics at Leiden University, which included a company internship of 3 month at ProteoNic in Leiden in 2008 and a final research internship. She undertook the latter in 2009 at the Department of Human Genetics in the FSHD group of Prof. Dr. Silvère van der Maarel at the Leiden University Medical Center (LUMC), where she spent 8 months investigating how chromatin is organized at the nuclear lamina during human myoblast differentiation. In October 2009, she joined the laboratories of Dr. Haico van Attikum at the Department of Human Genetics and Dr. Alfred C. O. Vertegaal at the Department of Molecular Cell Biology in the LUMC to start her PhD and identify novel chromatin factors involved in the response to DNA double-strands breaks. During her occupation as a PhD student, she participated in organizing the 2012 edition of the MGC PhD student workshop in Düsseldorf, Germany. After the completion of the practical part of her PhD project, she continued her carrier in the laboratory of Prof. Dr. Wim Vermeulen under the supervision of Dr. Hannes Lans at the Erasmus Medical Center in Rotterdam in the Netherlands. There she is currently investigating the role of chromatin factors in response to DNA damage induced by UV light.



LIST OF PUBLICATIONS

Helfricht,A.*, Thijssen,P.E.*, Ijspeert,H., Shah,R.G., van Ostaijen-ten Dam,M.M., Luijsterburg,M.S., Stoepker,C., Jak,R., Grootaers,G., Wang,J., Rao,P., Vertegaal,A.C.O., van Tol,M.J.D., Pan-Hammarström,Q., Shah,G.M., van der Burg,M., van der Maarel, S.M. and van Attikum,H. (2016). Loss of ZBTB24, a novel non-homologous end-joining protein, impairs class-switch recombination in ICF syndrome. * equal contribution. *In preparation for publication*.

Pfeiffer,A., Luijsterburg,M.S., Acs,K., Wiegant,W.W., **Helfricht,A.**, Herzog,L.K., Minoia,M., Böttcher,C., Salomons,F.A., van Attikum,H., Dantuma,N.P. (2016). Ataxin-3 is a SUMO-targeted deubiquitylation enzyme that consolidates the MDC1-dependent DNA double-strand break response. *Under review at EMBO*.

Typas,D., Luijsterburg,M.S., Wiegant,W.W., Diakatou,M., **Helfricht,A.**, Thijssen,P.E., van de Broek,B., Mullenders,L.H., and van Attikum,H. (2015). The de-ubiquitylating enzymes USP26 and USP37 regulate homologous recombination by counteracting RAP80. *Nucleic Acids Research*. 43. 6916-6933.

Helfricht,A. and van Attikum,H. (2014). Remodeling and spacing factor 1 (RSF1): a rising star in DNA repair. *Epigenomics*. 6, 261-265.

Helfricht,A., Wiegant,W.W., Thijssen,P.E., Vertegaal,A.C., Luijsterburg,M.S., and van Attikum,H. (2013). Remodeling and spacing factor 1 (RSF1) deposits centromere proteins at DNA double-strand breaks to promote non-homologous end-joining. *Cell Cycle*. 12, 3070-3082.

Vyas,R., Kumar,R., Clermont,F., **Helfricht,A.**, Kalev,P., Sotiropoulou,P., Hendriks,I.A., Radaelli,E., Hochepped,T., Blanpain,C., Sablina,A., van,A.H., Olsen,J.V., Jochemsen,A.G., Vertegaal,A.C., and Marine,J.C. (2013). RNF4 is required for DNA double-strand break repair in vivo. *Cell Death and Differentiation*. 20, 490-502.

Neumayer,G., **Helfricht,A.**, Shim,S.Y., Le,H.T., Lundin,C., Belzil,C., Chansard,M., Yu,Y., Lees-Miller,S.P., Gruss,O.J., van Attikum,H., Helleday,T., and Nguyen,M.D. (2012). Targeting protein for xenopus kinesin-like protein 2 (TPX2) regulates gamma-histone 2AX (gamma-H2AX) levels upon ionizing radiation. *Journal of Biological Chemistry*. 287, 42206-42222.



ACKNOWLEDGEMENTS

Here it is: my thesis. For years I worked towards this point and I am proud and relieved that I have reached the finish line. It's been a more than interesting journey during which I learned a lot, not only about molecular cell biology but also about myself. I feel grateful for the opportunities I got and like to thank all the people, I met along the way and who made valuable contributions to this thesis in one way or another.

During my Master internship in Silvère's FSHD group, I got caught by your enthusiasm for scientific work, Peter. You convinced me that doing a PhD would not be a bad idea, since I would actually get payed for the same work I was already doing as a student. Who would have known by that time that we would end up working so closely side by side on the same project? The lack of hierarchy and very enjoyable conversations made work more feel like spending time with a good friend. I could learn a lot from you and am very lucky with having you as a colleague and paranymp.

But to start a PhD, one need an actual position, to which I was kindly patched through by Silvère. After accepting me for my Master internship you eventually also became my promotor. Thank you for guiding me towards the subject I found most interesting to work on and for your support.

Haico, I am thankful for the opportunity to explore science within your group, your frankness and everything that I could pick-up from working with you. Your thoroughness and eye for detail taught me to always think of the right controls before starting an experiment, and I became almost as picky about lining out figures. I realized that scientific success means hard work, and I appreciate every publication we achieved and will achieve in the near future.

Alfred, I would like to thank you for the chance to let me get more familiar with biochemical experiments and with SUMO. I enjoyed the time I got to work in your lab and would also like to thank you for your support.

Leon, I again would like to express my gratitude for your efforts during the last stages of writing my thesis. With your own words you kept on motivating me similar to Angela Merkel's 'Wir schaffen das!' and indeed we did.

Next, I would like to thank my office roomies: first of all Wouter. Unfortunately, the beadle did not allow me to have three paranymp, but you would have undoubtedly deserved this honor too. Right from the start you let me benefit from your experimental expertise and I would like to thank you for everything you taught me, which is actually too much to mention here! Thank you for everything including the great surprise on my officially last day in the lab! Cees, Ron and Anton thanks for trying to answer all my questions and helping out, but also for all the distraction in the office and not taking work too serious.

I would like to thankfully acknowledge my former lab partners for sharing our every day (scientific) struggles, discussions and successes: Su Ming, Thomas, Martijn, Albert, Leonie, Jenny, Aude, Erik and Godelieve. Pierre, thank you for introducing me to French ChIPping as well. In addition, I would like to especially thank my two Master students Gwendolynn and Rianca. You two have done a great job and worked dedicated to push the ZBTB24 project into the right direction.

The benefit of working in two labs at the same time is having even more great colleagues. One, who deserves an incredible huge thank you, is my other paranymp Karolin. Mit deinem unvergänglichen Lachen hast du mir neben verschiedenen IP-Protokollen auch ein paar Wörter wissenschaftliches Deutsch beibringen können. Du warst immer für mich da, wenn ich Fragen hatte oder jemanden zum Reden brauchte. Damit warst du sprichwörtlich

‘Mein Fels in der Brandung’ und ich hätte unzählige Einträge in ‘Mein liebes Tagebuch’ schreiben können über unsere für gewöhnlich lustige Treffen. Ich möchte dir danken für alles, was du in mein (PhD-)Leben gebracht hast!

Other great colleagues that have been very helpful in scientific matters and much fun to be surrounded by are Joost, Ivo and Matty. I would also like to thank all employees of the former department of Toxicogenetics, especially Sophie, Maartje, Nuria, Robin, Dimitris, Bennie, Wouter, Ivo, Alex, Mark and Agata. Ingrid, without your help I would have been lost trying to meet all the regulations: thank you so much! Joop, Annelies and Willem: thank you for your help within the MCB microscopy facility as well as for coping with a somewhat frustrated version of myself when there were problems with the usage of the multiphoton laser. In addition, I truly appreciate the contributions of collaborators from the Toxicology department of Leiden University: Bob, Erik, Ram and Bram; but especially Louise, Jordi and Lisa: I am very fortunate to also have become friends with you.

Moreover, I like to express my gratitude to Wim and Hannes for their patience during the writing of my thesis and the mental encouragement from every member of the Vermeulen lab.

Besides my colleagues, I need to thank a couple of very dear friends. Linda en Paul, zonder het nodige zetje van jullie was ik nooit aan een academische loopbaan begonnen: ontzettend veel dank daarvoor. Sandra en Mark, Ewelina en Jorim, Denice en Shuaib, Fleur en Henk, Edmee en Ray, Stephanie en Sven, Sabine en Jurrán, Milena: dank dat jullie er allemaal voor mij waren en mij regelmatig uit de promotieachtbaan hebben gehaald! Jane und Franz, vielen Dank fürs Zuhören und die Motivation. Anna, thanks for the countless runs after work, for listening and your friendship.

Off course I would not have been in the Netherlands doing a PhD without a supporting family. Mama und Papa, ich möchte euch danken, das ihr mich so selbstlos meinen eigenen Weg gehen lassen habt. Ohne euer Vertrauen und eure Unterstützung hätte ich es nicht bis hierhin geschafft! Kay, der Rolle als großer Bruder bist du immer gerecht geworden und ich weiß die mentale Unterstützung von dir und Ricci sehr zu schätzen! Das beste Anti-Stressmittel waren für mich unsere lustigen Familien-wanderungen in den Bergen.

Met veel interesse hebben ook jullie, Cia, Pieter en Tino steeds naar de verloop van mijn promotie gevraagd. Ontzettend bedankt voor jullie steun en aanmoedigende worden.

And then last but for sure not least, Seger. Wat ben ik blij dat jij in mijn leven bent en dat ik altijd op jouw steun kan rekenen. Bedankt dat je me steeds weer in contact hebt gebracht met de rest van de wereld en voor alle mooie dingen, die we samen hebben gedaan naast mijn promotie.



